

**GEOCHEMICAL SIGNATURES OF WEATHERING AND
SURFACE WATER CHEMISTRY IN THE LATE ARCHEAN**

by
Jihua Hao

A dissertation submitted to Johns Hopkins University in conformity with the
requirements for the degree of Doctor of Philosophy

Baltimore, Maryland

December, 2016

© 2016 Jihua Hao
All Rights Reserved

Abstract

Earth's Archean surface environment was important for the origin and evolution of life. Here, it is proposed that the $pH_{2,g}$ controlled the redox state of the Archean atmosphere, consistent with the stabilities of detrital minerals, such as pyrite, siderite, and uraninite. In the marine environment, greenalite, siderite, and hematite, or amorphous precursors, were primary minerals. Magnetite was formed during diagenesis and metamorphism. Fluctuations of $pH_{2,g}$ or pH could oxidize elements such as Mo and Re. Organic acids were metastable in the surface waters at high $pH_{2,g}$ values, possibly stimulating biologic activity and the formation of organic hazes in the atmosphere.

Reaction path models were used to simulate rainwater, weathering, and river water chemistry under present-day and late Archean conditions. The thermodynamic properties of ferrous iron and other end-member minerals important on the early Earth were estimated using an extended Linear Free Energy Relationship. Modeling of the present-day weathering of basalt + calcite produced hematite, kaolinite, Na-Mg-saponite, and chalcedony, and world average river water (WARW) after destruction of 10^{-4} moles kg^{-1} H_2O . Late Archean weathering of olivine basalt + calcite produced kaolinite, chalcedony, and Fe(II)-rich clays, and WARW with low pH, and high HCO_3^- and Fe.

The behavior of P, Mn, Cr, and Cu during late Archean weathering was investigated during weathering of olivine basalt. Apatite and Mn-olivine dissolved, producing high phosphate and Mn(II) in Archean WARW. Insoluble $\text{MnO}_{2,\text{cr}}$ and hematite formed during whiff of oxidants. Chromite hardly dissolved but $\text{Cr}(\text{OH})_{3,\text{am}}$ dissolved completely, forming high Cr(III) waters. Weathering of chalcopyrite produced

chalcocite and bornite, but whiffs of oxidants produced native copper, chalcocite, bornite, and hematite, and high dissolved Cu.

Aqueous Cr^{2+} could be stable in hydrothermal solutions and a dominant species even with Cr(III)-Cl complexation whereas higher pressure favors Cr(III). For example, at 5 GPa and 1000 °C, Cr^{2+} is the dominant species at geologically reasonable pH and log $f\text{O}_2$ values. However, at 5 GPa and 600 °C, Cr^{3+} and Cr^{2+} might coexist. It appears likely that Cr(II) could play a significant role in low pressure hydrothermal fluids and in subduction zone fluids.

First reader (thesis advisor): Dimitri A. Sverjensky

Second reader: Robert M. Hazen.

Acknowledgments

This work has been supported by many people both within and outside of the Department of Earth and Planetary Sciences at Johns Hopkins University (JHU-EPS) and the Geophysical Laboratory at Carnegie Institution of Washington (CIW-GL). I would like to specially thank my advisor, Professor Dimitri Sverjensky, for his remarkable support and help throughout my whole PhD program. He created a beneficial and enjoyable learning environment with great patience since the beginning of my PhD when I had little background in geochemistry. I also greatly appreciate his forgiveness and comfort when I made mistakes and complaints. He told me that everyone makes mistakes and that's how people grow up, which relieved me greatly during the periods of depression. He is also very inspiring and encouraging when I initially raised naïve questions or ideas. He always takes every responsibility but gives all credits to his students.

In addition, I want to acknowledge Dr. Robert Hazen as my mentor at the Geophysical Laboratory and the second reader of my proposal and thesis. Bob was very generously supportive during my experimental studies and at conferences. I also benefited a lot from his recommendations to other distinguished scientists. His creative ideas and views on origin of life, mineral evolution, and mineral ecology greatly enlightened me and opened my eyes to a bigger vision of the early Earth system.

I would also like to thank my colleagues in Johns Hopkins University. Professors John Ferry, Naomi Levin, Linda Hinnov, Kevin Lewis, Anand Gnanadesikan in the Department of Earth and Planetary Sciences, and Professors Alan Stone and Ciaran Harman in the Department of Environmental Health and Engineering have kindly served

as my committee members and provided insightful feedback to my study and research. Professor Darrell Strobel and Sarah Hörst offered valuable advice and help on the early atmosphere of planetary bodies. Professor David Veblen provided help learning of mineralogy and generously shared some software resources. Professor Katalin Szlavecz offered her inspiring suggestions on weathering and soil chemistry. This work also benefited from helpful discussion with Professor Emmy Smith.

Since the summer of 2013, I conducted experimental studies in Geophysical Laboratory as a predoctoral associate. I met wonderful people there who greatly helped my research and life. Dr. George Cody provided helpful guidance in the analytical facilities and discussions about my results. Dr. Dionysis Foustoukos supervised hydrothermal experimental techniques with great patience. Dr. Bjorn Mysen generously offered his welding lab and provided helpful guidance. Dr. John Armstrong helped analyze mineral surfaces with the TEM. Dr. Timothy Strobel helped me with X-ray diffraction analysis.

Furthermore, I would like to thank all of my friends who helped and accompanied me during these years. Specially, Fang Huang, Coiby Xu, Dongdong Tian, Dongdong Yao, Zehui Xia, Yuanyuan Xu, Qiaoting Lou are friends since our undergraduate days and have persistently supported me for more than eight years. Dr. Cécile Feuille, Dr. Charlene Estrada, and Dr. Namhey Lee are former students and postdoctoral associates of Dimitri's and they provided numerous help with my study and research. Dr. Irena Mamajanov helped prepare and analyze my samples. Dr. Xiaoming Liu and Dr. Chao Liu are postdocs in GL and they provided helpful suggestions on my PhD research and career development plan. Merri Wolf, Shaun Hardy, Gefei Qian, and others as supporting staff

at Broad Branch Road have shown remarkable kindness to me during my visit. All of the other colleagues and friends are also acknowledged here.

I also want to thank all of the funding agencies for the financial support I received during my PhD, specifically, the JHU EPS Fellowship, JHU Teaching Assistant opportunities, the W.M. Keck foundation for my tuition and stipend. A grant from the US Department of Energy, The Robert and Margaret Hazen Foundation, and the Deep Carbon Observatory also supported my lab expenses. The Deep Carbon Observatory, NASA, and the Elliott Field Fund also provided financial support for my conference and field trip travel.

Lastly, I want to thank my parents, brother, and extended families who gave their selfless love to me. I also thank my girlfriend Chunmiao Ye for her beautiful support of me.

Some of the chapters were the product of collaborative work. The acknowledgements are provided after the manuscripts.

Table of Contents

Abstract.....	ii
Acknowledgments	iv
List of Tables	xii
List of Figures.....	xiv
 1. Introduction.....	 1
Reference	11
 2. Importance of atmospheric H_{2,g} in surficial environments of the Archean.....	 21
1. Redox states on the surface of the Archean Earth	24
2. Importance of H _{2,g} as the redox indicator before the GOE	25
2.1 Redox indicators in the near-surface environments: O _{2,g} or H _{2,g} ?	26
2.2 H _{2,g} -world on the Archean Earth surface	27
3. Importance of H _{2,g} as the redox indicator before the GOE	30
3.1 Mobility of trace elements during weathering due to ‘whiffs of oxygenation’ before the GOE	30
3.2 Possible connections between haze formation and whiffs of H _{2,g} in late Archean near-surface waters.....	33
3.3 Mineralogy in the marine environment.....	36
4. Summary and concluding remarks.....	37
Acknowledgments.....	38
References.....	40

3. An extended linear free energy relationship for predicting ΔG_f° of crystalline solids	55
1. Introduction.....	57
2. Linear Free Energy Relations for predicting standard free energies of formation	57
3. Conclusion	64
4. References.....	66
 4. A model for late Archean chemical weathering and world average river water ...	80
1. Introduction.....	83
2. Theoretical modeling approach and assumptions	86
2.1 Modeling approach	86
2.2 Thermodynamic data used in the calculations	89
3. Initial conditions for the modeling.....	89
3.1 Rainwater models: present-day and the late Archean.....	89
3.2 Initial rock types: present-day and the late Archean.....	91
4. Present-day weathering model results	92
4.1 Weathering of basalt + calcite	92
4.2 Weathering of granite + calcite.....	94
4.3 Comparison with present-day world-average river water (WARW) ...	94
5. Late Archean weathering model results.....	96
5.1 Weathering of olivine basalt + calcite	96

5.2 Weathering of tonalite–trondhjemite–granodiorite (TTG) + calcite ...	98
6. Implications for interpretations of the Archean near-surface environment	98
6.1 A model for late Archean world-average river water	98
6.2 Detrital mineral records	101
6.3 Paleosols	102
6.4 Possible connections between haze formation and organic species in near-surface waters	103
7. Summary and concluding remarks.....	104
Acknowledgments.....	107
References.....	108

5. Mobility of nutrients and trace metals during weathering in the late Archean...130

1. Introduction.....	134
2. Factors affecting the dissolution of trace elements during the weathering.....	137
2.1 Redox level of the atmosphere.....	137
2.2 pH of near-surface waters	138
2.3 Accessory source minerals in the rocks	140
2.4 Formation of secondary minerals during weathering	140
3. Theoretical modeling approach and assumptions.....	141
3.1 Late Archean rainwater chemistry	141
3.2 Initial rock type: olivine basalt plus accessory minerals	142
3.3 Model for trace element behavior during weathering.....	143

4. Model results for late Archean weathering of olivine basalt and trace elements	144
4.1 Behavior of phosphorus	144
4.2 Behavior of manganese	145
4.3 Behavior of chromium	147
4.4 Behavior of copper	148
5. Discussion and Implications for the Late Archean Environment	149
5.1 Riverine transport of phosphorus and the Great Oxidation Event	149
5.2 Manganese and chromium during weathering: whiffs of oxidant or not?	152
5.3 Trace Cu-minerals as signatures of the surface environment and mineral evolution	154
6. Conclusions	155
Acknowledgments	159
References	160

6. Chromium Redox Equilibria in Aqueous Fluids Under Hydrothermal and

Subduction-zone Conditions	180
1. Introduction	184
2. Theoretical calculation approach and assumptions	187
2.1 Calculation approach	187
2.2 Assumptions for hydrothermal and subduction-zone conditions	188

3. Predicted behavior of aqueous chromium at elevated temperatures and pressures.....	189
3.1 Chromium redox equilibria in low-pressure hydrothermal systems..	189
3.2 Chromium redox equilibria in high pressure-temperature fluids.....	191
3.3 Solubility of $\text{Cr}_2\text{O}_{3,\text{cr}}$ at high temperature and pressure.....	194
4. Discussions and implications.....	196
4.1 The sedimentary banded iron formation record of chromium geochemistry	196
4.2 Behavior of chromium in hydrothermal and subduction-zone fluids	198
5. Concluding remarks	200
References.....	203
 7. Conclusions.....	218
Reference	226
 Curriculum Vitae.....	227

List of Tables

Chapter 3

Table 1. Summary of regression parameters for oxide, hydroxide, carbonate, and silicate mineral families generated by regression with Eqn. (1) and plotted in Fig. 1.....	70
Table 2. Comparison of the standard Gibbs free energies of formation of minerals ($\Delta G_{f,M_vX}^\circ$) from three different thermodynamic databases used to calculate a_{M_vX} values of orthopyroxene, olivine, and biotite in this study.....	71
Table 3. Summary of estimated and regression parameters for Berman minerals used in Eqns. (1) & (2).	72
Table 4. Summary of estimated and regression parameters for Helgeson minerals used in Eqns. (1) & (2).	73
Table 5. Summary of estimated and regression parameters for Holland & Powell minerals used in Eqns. (1) & (2).	74
Table 6. Predicted standard Gibbs free energies of formation of divalent metal silicate families using Eqn. (1), the parameters in Table 3 and the ionic radii and thermodynamic data for aqueous cations listed below.	75

Chapter 4

Table 1. Summary of the compositions adopted for world-average present day rainwater (Berner and Berner, 2012) and late Archean rainwater (see text). Full details of the aqueous speciation of all the elements are given in the initial step of the model weathering results.	121
---	------------

Table 2. Major constituents of fluids from present-day weathering of basalt or granite plus calcite and Archean weathering of olivine basalt or TTG plus calcite (at $\log \xi = -4.0$) compared with modern and Archean world-average river water (WARW).....	122
--	------------

Chapter 5

Table 1. Sources of trace elements in the weathering model expressed as amounts of accessory minerals in olivine basalt estimated from elemental upper continental crust abundances.....	172
---	------------

Table 2. Potential mineral products that might form during weathering and that were in the thermodynamic data file used for the modeling.....	173
--	------------

Chapter 6

Table 1. Thermodynamic properties of chromium aqueous species and minerals used in this study.	211
--	------------

List of Figures

Chapter 2

- Figure 1.** Stability of minerals in Fe-S-C-O system as functions of log fugacity of a. $O_{2,g}$ or b. $H_{2,g}$ and $S_{2,g}$ at 25 °C, 1 bar.51
- Figure 2.** Correlation between log fugacity of $H_{2,g}$ of the volcanic gases with the temperature of the volcanoes (Symonds *et al.*, 1994).52
- Figure 3.** Stability of minerals and aqueous species in Mo-Re-S-O-H system at 25 °C and 1 bar.53
- Figure 4.** (a) Metastability of carboxylic acids in the aqueous environments on the Earth surface. Suggested boundary of $pH_{2,g}$ (bold green line) above which carboxylic acids will be metastable in the aqueous environments on the Earth surface. (b) Equilibrium phase diagram of proposed primary Fe minerals in the shallow marine environment.54

Chapter 3

- Figure 1.** Graphic representation of Eqn. (4) for minerals with same cation coordination number.76
- Figure 2.** Linear correlation between normalized a (a values divided by number of metal atoms, a_{M_vX}/v) and stoichiometry index (total number of tetrahedral sites divided by total number of oxygen atoms, $(v_{Al,t}+v_{Si,t})/v_O$). Thermodynamic properties of mineral groups are from Berman (1988).77
- Figure 3.** Linear correlation between normalized a (a values divided by number of metal atoms, a_{M_vX}/v) and stoichiometry index (total number of tetrahedral sites divided by total

number of oxygen atoms, $(v_{Al,t} + v_{Si,t})/v_O$). Thermodynamic properties of mineral groups are from Helgeson (1978).78

Figure 4. Linear correlation between normalized a (a values divided by number of metal atoms, $a_{M,X}/v$) and stoichiometry index (total number of tetrahedral sites divided by total number of oxygen atoms, $(v_{Al,t} + v_{Si,t})/v_O$). Thermodynamic properties of mineral groups are from Holland & Powell (1998).79

Chapter 4

Figure 1. Modeling results of basaltic weathering under present-day atmospheric conditions.123

Figure 2. Modeling results of granitic weathering under present-day atmospheric conditions.124

Figure 3. Predicted river water chemistry during present-day weathering of basalt and granite plus calcite compared with present-day world-average river water (WARW) composition.125

Figure 4. The distribution of weathering rates calculated with riverine runoff and dissolved Si concentration.126

Figure 5. Modeling results of olivine-basaltic weathering under Archean atmospheric conditions.127

Figure 6. Modeling results of trondjemite-tonalite-granodiorite (TTG) weathering under Archean atmospheric conditions.128

Figure 7. Predicted river water chemistry during Archean weathering of olivine basalt and TTG plus calcite compared with present-day world-average river water (WARW) composition.	129
--	------------

Chapter 5

Figure 1. Equilibrium diagrams in the Fe-S-N-O-H system as a function of pH and a. $pO_{2,g}$ or b. $pH_{2,g}$	174
Figure 2. Proposed ranges of pH values of late Archean rainwater and river water as a function of atmospheric $pCO_{2,g}$	175
Figure 3. a. Destruction of 5.5×10^{-7} moles primary apatite during weathering of olivine basalt under the standard Archean atmospheric conditions. b. Evolution of aqueous phosphate during the weathering.	176
Figure 4. a. & b. Destruction of Mn-bearing olivine during the weathering of olivine basalt: (a) The standard Archean atmospheric conditions; (b) Whiff of $O_{2,g}$. The upper parts of the figures show the changes of $\log pH_{2,g}$ during the weathering; (c) & (d) Evolution of dissolved manganese during weathering during the addition of O_2 or HNO_3 , respectively.	177
Figure 5. a. Destruction of $Cr(OH)_{3,am}$, stability of chromite ($FeCr_2O_4$) and formation of secondary minerals during the weathering of olivine basalt under the Archean atmospheric conditions. b. Evolution of dissolved chromium during weathering.	178
Figure 6. Destruction of chalcopyrite ($CuFeS_2$) and formation of secondary minerals during the weathering of olivine basalt under (a) the standard Archean atmospheric	

conditions and (b) Whiff of $O_{2,g}$ (10^{-6} mole $O_{2,g}$ kg^{-1} H_2O). c. Evolution of dissolved copper during weathering.	179
---	-----

Chapter 6

Figure 1. Equilibrium diagram of Cr-O-H system at 25 °C and 1 bar. Equal activities of aqueous species or activities of Cr(aq) equal to 10^{-8} define the stability boundaries.	212
--	-----

Figure 2. Predicted speciation of aqueous Cr under hydrothermal conditions: (a) 100 °C, $P_{sat.}$; (b) 250 °C, $P_{sat.}$	213
--	-----

Figure 3. Equilibrium boundaries for equal activities between Cr^{2+} and $CrCl^{2+}$ at 250 °C, $P_{sat.}$	214
--	-----

Figure 4. Effects of temperature and pressure on the equilibrium constant relating aqueous Cr^{2+} to Cr^{3+}	215
--	-----

Figure 5. Predicted speciation of aqueous chromium under conditions relevant to subduction-zones: (a) 1 GPa, 200 °C; (b) 1 GPa, 600 °C; (c) 5 GPa, 600 °C; (d) 5 GPa, 1000 °C.	216
--	-----

Figure 6. Effect of Cr-Cl complexation on the solubility of $Cr_2O_{3,cr}$ at conditions relevant to subduction-zone environments: (a) 600 °C, 0.5 GPa; (b) 1000 °C, 5 GPa.....	217
--	-----

Chapter 1

Introduction

Life on Earth may well have originated during the Archean (Arndt and Nisbet, 2012; Cleaves et al., 2012; Hazen, 2005; Valley, 2006). Consequently, the geochemical environments on the Archean Earth, including the atmosphere, surface water chemistry, and the minerals and rocks exposed at the surface, play a central role in theories of the origin and evolution of life (Hazen and Sverjensky, 2010; Kasting and Catling, 2003; Jelen et al., 2016). Consequently, numerous studies have been carried out to attempt to unravel the nature of different parts of the near-surface early Earth system.

The abundance of atmospheric $O_{2,g}$ at present, its importance for life on Earth since the Great Oxidation Event (GOE) at about 2.33 Ga (Farquhar et al., 2000; Luo et al., 2016), and the subsequent increase of atmospheric $O_{2,g}$ in the early Cambrian (Berner, 1999; Canfield et al., 2007; Canfield & Teske, 1996; Marais et al., 1992; Och & Shields-Zhou, 2012) has led to enormous interest in the oxidation state of the ancient atmosphere. Unlike the present-day oxidizing atmosphere, the Archean atmosphere is thought to be anoxic with trace amounts of $O_{2,g}$. Based on non-equilibrium atmospheric models, the Archean atmosphere has been described as anoxic ($pO_{2,g} \sim 10^{-11}$ bar or less) but with moderately high concentrations of $H_{2,g}$ ($pH_{2,g} \sim 10^{-3}$ to 10^{-6} bar or less) (Catling and

Claire, 2005; Kasting, 1993, 2014; Kasting et al., 2001; Kharecha et al., 2005). Sulfur isotopic studies have further established that the atmosphere was anoxic prior to 2.33 Ga (Farquhar et al., 2000; Luo et al., 2016). Combined sulfur and carbon isotopic studies, and atmospheric models, have documented the likely importance of global organic-rich hazy atmospheres alternating with periods of no haze in the Neoarchean from 2.7-2.5 Ga (Izon et al., 2015; Zerkle et al., 2012). Under these circumstances, whether $O_{2,g}$ is an important gas controlling redox state of the atmosphere is particularly important for geochemical modeling of the Archean surface processes, such as weathering and chemistry of surface waters.

It is also expected that many important aspects of weathering and surficial water chemistry in the late Archean were very different from the present-day. On the late Archean continents, paleosol studies have inferred the leaching of iron during weathering caused by the mobility of aqueous Fe^{2+} -species in the near-surface weathering environment (Rye and Holland, 1998). Detrital mineral records suggested preservation of uraninite, siderite, pyrite, and ferrous clay minerals during late Archean weathering and riverine transport (Frimmel, 2005; Hessler and Lowe, 2006; Johnson et al., 2014; Rasmussen and Buick, 1999). Moreover, mineral evolution studies reported that episodic deposition and diversification of mineral distribution and species were consistent with major changes in the near-surface environment (Hazen et al., 2014). It has been suggested that the oceans were probably rich in dissolved silica (Siever, 1992), low in sulfate (Crowe et al., 2014), and contained redox-sensitive elements in their reduced forms, for example $H_2S(aq)$, Fe^{2+} and NH_4^+ (Catling and Claire, 2005; Holland, 1984; Lyons et al., 2014). Late Archean shallow marine sediments, represented by banded iron formations,

might consist of greenalite, hematite, and siderite as the primary minerals, but whether magnetite is primary or not is controversial (Bekker et al., 2014; Klein, 2005; Rosing et al., 2010). Furthermore, little is really known about the potential linkages between the atmosphere, the water chemistry during weathering and riverine transport, and the mineralogic records.

The availability of bio-essential nutrients and trace metals in the surface environment were critical factors for the origin and evolution of life throughout Earth history (Anbar, 2008; Anbar & Knoll, 2002; Morel, 2008; Pasek et al., 2015; Saito et al., 2003; Williams et al., 2003; Zerkle et al., 2006). However, large uncertainties still exist in estimation of the levels of nutrients and trace elements. For example, in the case of phosphate, Archean productivity was first thought to be limited by low dissolved phosphate in the seawater due to adsorption onto iron oxides deposited as banded iron formations (Bjerrum and Canfield, 2002), but in a subsequent study it was pointed out that the high concentration of dissolved silica expected in Archean seawater would effectively block phosphate adsorption sites on iron oxides and therefore dissolved phosphate might be higher than previously suggested (Konhauser et al., 2007; Planavsky et al., 2010). Such disputes mainly focused on the removal of phosphate from seawater and did not address the important role of weathering and riverine transport, which was the dominant influx of phosphate to the early oceans. The importance of this role has been emphasized for the Phanerozoic (Guidry and Mackenzie, 2000).

In the case of trace metals, the redox-sensitive trace metals, such as Cr, Cu, U, Mo, and Re, and their isotopic fractionations recorded in various sedimentary records are now widely used to infer fluctuations in the redox history of Earth's surface environment

(Anbar and Rouxel, 2007; Farquhar et al., 2014; Tribovillard et al., 2006). The atmosphere before the Great Oxidation Event (GOE) is widely accepted to have been anoxic with a relatively high $p\text{H}_{2,\text{g}}$. Consequently, during normal weathering processes in the late Archean, elements such as Cr, Cu, U, Mo, and Re would have been immobile, and the solubilities of Fe and Mn would have been much higher than in present-day surface waters. However, recent studies reported enrichments of several trace metals (e.g. Mo, Re, Cr) and variability of isotopic fractionations in some sedimentary records that have been interpreted as evidence of “whiffs of molecular oxygen” in the Archean atmosphere (Anbar et al., 2007; Frei et al., 2009). This interpretation currently contradicts the overall picture of an anoxic Archean atmosphere as described above suggested by the mass independent fractionation of S isotopes, the Fe-loss from paleosols, and the preservation of detrital minerals unstable in the presence of molecular oxygen. Nevertheless, the exact conditions under which trace metals and their isotopes might have been mobilized have not been examined in a comprehensive framework of weathering simulations that link trace metals and their potential sources, major elements and rock-forming minerals, and perturbations of an anoxic late Archean environment.

One metal that has received a lot of attention as a potential recorder of fluctuations in the Archean environment is chromium - a trace element in the continental crust but enriched in ultramafic and mafic rocks. Chromium has three common redox states: Cr(II), Cr(III), and Cr(VI). Under ambient conditions, Cr(II) requires very reducing conditions and is not stable in water. Under anoxic to reducing conditions, Cr(III) is stable. If the surface water is acidic ($\text{pH} < 5.5$), the solubility of Cr(III) is high and Cr^{3+} is the major aqueous species; otherwise, $\text{Cr}(\text{OH})_{3,\text{am}}$ will precipitate and limit the

solubility of chromium. Oxidation of Cr(III) in the surface environment relies on the catalysis of strong oxidants, e.g. $\text{MnO}_{2,\text{cr}}$ or H_2O_2 (Oze et al., 2007). If somehow these oxidants are present, Cr(III) can be oxidized to Cr(VI) which greatly increases the solubility of chromium. These processes facilitate riverine transport of chromium to the ocean where Cr(VI) can again be reduced and sequestered into sediments. Based on studies of present-day chromium weathering and riverine transport, recent studies have utilized the chemical profiles of chromium recorded in ancient marine sediments to reconstruct the evolutionary history of atmosphere $\text{O}_{2,\text{g}}$. For example, high concentrations of chromium in banded iron formations were interpreted to indicate the appearance of molecular $\text{O}_{2,\text{g}}$ in the early atmosphere before the Great Oxidation Event (Frei et al., 2009). Besides the question of whether the oxidation of Cr(III) requires molecular $\text{O}_{2,\text{g}}$ or not, all early sedimentary records have experienced diagenesis and low to high-grade metamorphism which might potentially modify the original geochemical signatures. For this reason, the aqueous geochemistry of chromium at elevated temperatures and pressures was investigated in the present study.

At elevated temperature and pressure, previous studies have suggested that low valence states of trace metals such as Fe(II), Eu(II), and Cu(I) are thermodynamically favorable to predominate in aqueous solutions due to the large differences of entropy between ions with a difference valence state (e.g. Sverjensky, 1984). If this principle also applies to chromium, then Cr(II) might be expected in aqueous fluids once the temperature is increased during advanced diagenesis or low to high-grade metamorphism. Reduction of Cr(III) to Cr(II) would be expected to increase the solubility of chromium in aqueous fluids. In this case, the original depositional isotopic signature of chromium may

not be preserved. However, until now, no experimental investigations or theoretical simulations addressed this possibility.

Overall, the rich record of clues about the nature of the near-surface environment on early Earth offers a tantalizing, if not confusing, picture that is marked by numerous uncertainties and outright disagreements. However, the consistency of all these lines of evidence has not been examined with the aid of geochemical theory. Quantitative geochemical models of rainwater, river water, the oceans, and water-rock interactions could, in principle, be applied to early Earth, but have rarely been used (Alfimova et al., 2014; Fabre et al., 2011; González-Álvarez and Kerrich, 2012; Lafon and Mackenzie, 1974; Schmitt, 1999; Sverjensky and Lee, 2010). Nor has there been any attempt to link such models to the long literature on models of the early Earth atmosphere (e.g. Claire et al., 2014; Kurzweil et al., 2013). With one exception (Alfimova et al., 2014) involving paleosols on basalts, the application of quantitative models of chemical weathering that include the chemical speciation of surface waters on the continents and the chemical speciation and state of saturation with respect to minerals in the shallow and deep oceans have not been addressed for the late Archean. The lack of quantitative chemistry prevents construction of an internally consistent, quantitative picture of the evolution of the near-surface environment of early Earth through deep time. Moreover, the possibility that diagenesis and/or metamorphism involving hydrous fluids could modify the original geochemical signatures of the sedimentary archives could be examined with thermodynamic modeling tools but has never been done yet.

Water-rock interactions over wide range of temperatures and pressures generally generate solid solutions of secondary minerals. One specific example is the replacement

of Ca(II) in the calcite crystal structure by other divalent cations such as Mg, Mn(II), and Fe(II) during diagenesis and hydrothermal alteration. Precipitation of these mineral solid solutions usually controls the solubility of trace elements in the fluids. In turn, the chemical signatures of trace metals recorded in secondary minerals that form solid solutions might reflect the concentrations of trace elements in the aquatic environment. This principle has been widely applied to infer the availability of trace elements in the early ocean and is a key theme of studies of the co-evolution of the geosphere and biosphere. Examples include the speciation of trace elements in sulfides in black shale (Gregory et al., 2015; Large et al., 2014, 2015), Re in molybdenite ($\text{MoS}_{2,\text{cr}}$) (Golden et al., 2013), and Zn, Fe in marine carbonates (Canfield, 2005; Liu et al., 2016). Compared with the bulk analysis of trace elements in whole-rocks, the concentrations of trace elements in mineral solid solutions potentially provide a more detailed record. In order to quantitatively examine these signatures, it is necessary to build a thermodynamic model of speciation of the trace elements in solid solutions. However, this research is currently hampered by a lack of thermodynamic properties of mineral end-members hosting trace elements, particularly secondary silicate minerals.

Based on the concerns and unknowns described above, this study was designed to apply thermodynamic modeling methods to answer four questions:

- I. Was $\text{O}_{2,\text{g}}$ important in the Archean surface environment?
- II. Are different lines of evidence on geochemical properties of the late Archean surface environment consistent with each other?
- III. What were the behaviors of trace elements during the Archean weathering and the influence of fluctuations of atmospheric redox state?

IV. How did diagenesis and metamorphism affect the original signatures of chromium in sediments?

In this work, I firstly examined the relative importance of $O_{2,g}$ and $H_{2,g}$ in reflecting the redox state of the Archean atmosphere based on the stability relations of iron minerals as functions of redox states ($pO_{2,g}$ or $pH_{2,g}$) and sulfur concentration ($pS_{2,g}$). Iron minerals because iron is geologically abundant and pyrite and siderite are proposed to be detrital minerals stably preserved during the Archean weathering and riverine transport (Johnson et al., 2014; Rasmussen et al., 1999). As a dominant source of reducing gases on the Archean Earth, volcanic outgassing was also investigated in terms of effects of tectonic settings on its gas compositions, especially $pH_{2,g}$. Furthermore, implications of fluctuations of $pH_{2,g}$ in the late Archean on the mobility of trace elements and haze formation were also explored with the aid of thermodynamic modeling tools. Finally, the relative stability of proposed primary minerals of BIFs in the proposed Archean atmosphere and seawater chemistry were tested.

A weathering study was designed to build a quantitative linkage between the results of atmospheric modeling of early Earth, the chemistry of surface waters on the continents, and the associated mineral weathering products that might be preserved in the geologic record. This work focuses on water chemistry and the mineralogic record of change in the near-surface environment. It was proposed that ferrous clay minerals could be an important weathering product in the late Archean anoxic atmosphere (Hazen et al., 2013). However, there are few reported thermodynamic properties of Fe(II)-clay minerals that can be used in the thermodynamic modeling study. This work proposed an extended linear free energy relationship for predicting the ΔG_f° values of crystalline solids based on

a generalization of a method proposed previously ([Sverjensky and Molling, 1992](#)). Specifically, estimation methods for key parameters characteristic of the structure were explored by this work which enabled the estimation of the ΔG_f° values of ferrous clays from a known ΔG_f° of another compositional end-member with the same crystal structure.

With the predicted thermodynamic properties of ferrous clay minerals, I applied theoretical geochemical models of aqueous speciation, solubility, and chemical mass transfer to weathering on early Earth during the late Archean (3.0 - 2.5 Ga). This time period was chosen because of the reported occurrences of unusual detrital minerals in rocks interpreted to represent the sediments from riverine systems ([Frimmel, 2005](#); [Hessler and Lowe, 2006](#); [Johnson et al., 2014](#); [Rasmussen and Buick, 1999](#)) and the formation of major continents and therefore weathering and riverine transport ([Taylor & McLennan, 2009](#)). Similar approaches have focused previously on chemical weathering processes on Mars ([Catalano, 2013](#)) and on perturbations of early Earth's atmosphere that might affect weathering ([Sverjensky and Lee, 2010](#)), but these emphasized $pO_{2,g}$ in the early atmosphere. Here, I focused on the simulation of weathering processes with a steady-state atmosphere defined by atmospheric models in which the role of $H_{2,g}$ is emphasized. An overall goal was to build a chemical model of the connection between weathering and late Archean world-average river water (WARW). This model will serve as a framework for examining the potential mobility of trace metals and nutrients during weathering processes and is also a first step towards developing a geochemical model for the late Archean oceans.

Based on the recently developed weathering model ([Hao et al., 2017](#)), I further simulated the dissolution of minerals that are hosting the nutrient P and the trace metals

Mn, Cr, Cu during weathering of olivine basalt and the mobility of these trace elements in late Archean (3.0-2.5 Ga) surface waters. Again, this time period is selected because life probably originated in the Archean ([Arndt and Nisbet, 2012](#)) and a supply of nutrients and trace metals is vitally important for the habitability and evolution of early life ([Anbar, 2008](#)). Geochemical modeling, which considers many environmental factors simultaneously, can approximate the major chemical reactions involved in weathering consistent with present-day world average river water ([Hao et al., 2017](#)). The goal of this project was to calculate the dissolution and speciation of these four elements during Archean weathering and riverine transport. Additionally, the influence of whiffs of oxidants, e.g. $O_{2,g}$ or HNO_3 , on the behaviors of trace elements were investigated.

To reveal the behaviors of chromium during diagenesis and metamorphism, this study applied the recently developed Deep Earth Water (DEW) Model ([Sverjensky et al., 2014](#)) to calculate the speciation and solubility of chromium in aqueous solutions over a wide range of temperatures and pressures covering hydrothermal, subduction-zone, and upper mantle conditions. In addition, the effects of redox state, pH, and complexation with possible ligands on the behavior of chromium were investigated. The goal of this project was to use theoretical thermodynamic calculations to explore the possible behavior of chromium in aqueous fluids as a guide to future experiments and as an aid to the interpretation of the chromium concentrations in minerals.

References:

- Anbar, A.D., Duan, Y., Lyons, T.W., Arnold, G.L., Kendall, B., Creaser, R.A., Kaufman, A.J., Gordon, G.W., Scott, C., Garvin, J., Buick, R., 2007. A whiff of oxygen before the great oxidation event? *Science* 317, 1903–1906. doi:10.1126/science.1140325
- Anbar, A.D., Rouxel, O., 2007. Metal stable isotopes in paleoceanography. *Annu. Rev. Earth Planet. Sci.* 35, 717–746. doi:10.1146/annurev.earth.34.031405.125029
- Anbar, A.D., 2002. Proterozoic Ocean Chemistry and Evolution: A Bioinorganic Bridge? *Science* 297, 1137–1142. doi:10.1126/science.1069651
- Anbar, A.D., 2008. Elements and Evolution. *Science* 322, 1481–1483. doi:10.1126/science.1163100
- Arndt, N.T., Nisbet, E.G., 2012. Processes on the Young Earth and the Habitats of Early Life. *Annu. Rev. Earth Planet. Sci.* Vol 40 40, 521–549. doi:10.1146/annurev-earth-042711-105316
- Bekker, A., Planavsky, N.J., Krapež, B., Rasmussen, B., Hofmann, A., Slack, J.F., Rouxel, O.J., Konhauser, K.O., 2014. 9.18 - Iron Formations: Their Origins and Implications for Ancient Seawater Chemistry A2 - Holland, Heinrich D, in: Turekian, K.K. (Ed.), *Treatise on Geochemistry (Second Edition)*. Elsevier, Oxford, pp. 561–628. doi:10.1016/B978-0-08-095975-7.00719-1
- Berner, R.A., 1999. Atmospheric oxygen over Phanerozoic time. *Proc. Natl. Acad. Sci.* 96, 10955–10957. doi:10.1073/pnas.96.20.10955

- Bjerrum, C.J., Canfield, D.E., 2002. Ocean productivity before about 1.9 Gyr ago limited by phosphorus adsorption onto iron oxides. *Nature* 417, 159–162.
doi:10.1038/417159a
- Canfield, D.E., 2005. The early history of atmospheric oxygen: Homage to Robert A. Garrels. *Annu. Rev. Earth Planet. Sci.* 33, 1–36.
doi:10.1146/annurev.earth.33.092203.122711
- Canfield, D.E., Poulton, S.W., Narbonne, G.M., 2007. Late-Neoproterozoic deep-ocean oxygenation and the rise of animal life. *Science* 315, 92–95.
doi:10.1126/science.1135013
- Canfield, D.E., Teske, A., 1996. Late Proterozoic rise in atmospheric oxygen concentration inferred from phylogenetic and sulphur-isotope studies. *Nature* 382, 127–132.
- Catalano, J.G., 2013. Thermodynamic and mass balance constraints on iron-bearing phyllosilicate formation and alteration pathways on early Mars. *J. Geophys. Res. Planets* 118, 2124–2136. doi:10.1002/jgre.20161
- Catling, D.C., Claire, M.W., 2005. How Earth's atmosphere evolved to an oxic state: A status report. *Earth Planet. Sci. Lett.* 237, 1–20. doi:10.1016/j.epsl.2005.06.013
- Claire, M.W., Kasting, J.F., Domagal-Goldman, S.D., Stüeken, E.E., Buick, R., Meadows, V.S., 2014. Modeling the signature of sulfur mass-independent fractionation produced in the Archean atmosphere. *Geochim. Cosmochim. Acta* 141, 365–380.
doi:10.1016/j.gca.2014.06.032

- Cleaves 2nd, H.J., Michalkova Scott, A., Hill, F.C., Leszczynski, J., Sahai, N., Hazen, R.,
2012. Mineral-organic interfacial processes: potential roles in the origins of life.
Chem Soc Rev 41, 5502–5525. doi:10.1039/c2cs35112a
- Crowe, S.A., Paris, G., Katsev, S., Jones, C., Kim, S.-T., Zerkle, A.L., Nomosatryo, S.,
Fowle, D.A., Adkins, J.F., Sessions, A.L., Farquhar, J., Canfield, D.E., 2014. Sulfate
was a trace constituent of Archean seawater. Science 346, 735–739.
doi:10.1126/science.1258966
- E., J., Johnson, A., Gerpheide, P., M., Lamb, Fischer, W.W., 2014. O₂ constraints from
Paleoproterozoic detrital pyrite and uraninite. Bull. Geol. Soc. Am. 126, 813–830.
doi:10.1130/B30949.1
- Fabre, S., Berger, G., Nédélec, A., 2011. Modeling of continental weathering under high-
CO₂ atmospheres during Precambrian times. Geochemistry, Geophys. Geosystems
12, Q10001. doi:10.1029/2010GC003444
- Farquhar, J., Zerkle, A.L., Bekker, A., 2014. 6.4 - Geologic and Geochemical Constraints
on Earth's Early Atmosphere A2 - Holland, Heinrich D, in: Turekian, K.K. (Ed.),
Treatise on Geochemistry (Second Edition). Elsevier, Oxford, pp. 91–138.
doi:http:10.1016/B978-0-08-095975-7.01304-8
- Farquhar, J., Bao, H., Thiemens, M., 2000. Atmospheric Influence of Earth's Earliest
Sulfur Cycle. Science 289, 756–758. doi:10.1126/science.289.5480.756
- Frei, R., Gaucher, C., Poulton, S.W., Canfield, D.E., 2009. Fluctuations in Precambrian
atmospheric oxygenation recorded by chromium isotopes. Nature 461, 250–253.
doi:10.1038/nature08266

- Frimmel, H.E., 2005. Archaean atmospheric evolution: evidence from the Witwatersrand gold fields, South Africa. *Earth-Science Rev.* 70, 1–46.
doi:10.1016/J.Earscirev.2004.10.003
- Golden, J., McMillan, M., Downs, R.T., Hystad, G., Goldstein, I., Stein, H.J., Zimmerman, A., Sverjensky, D.A., Armstrong, J.T., Hazen, R.M., 2013. Rhenium variations in molybdenite (MoS₂): Evidence for progressive subsurface oxidation. *Earth Planet. Sci. Lett.* 366, 1–5. doi:10.1016/j.epsl.2013.01.034
- González-Álvarez, I., Kerrich, R., 2012. Weathering intensity in the Mesoproterozoic and modern large-river systems: A comparative study in the Belt-Purcell Supergroup, Canada and USA. *Precambrian Res.* 208–211, 174–196.
doi:10.1016/j.precamres.2012.04.008
- Gregory, D.D., Large, R.R., Halpin, J.A., Baturina, E.L., Lyons, T.W., Wu, S., Danyushevsky, L., Sack, P.J., Chappaz, A., Maslennikov, V. V, Bull, S.W., 2015. Trace Element Content of Sedimentary Pyrite in Black Shales. *Econ. Geol.* 110, 1389–1410. doi:10.2113/econgeo.110.6.1389
- Guidry, M.W., Mackenzie, F.T., 2000. Apatite weathering and the Phanerozoic phosphorus cycle. *Geology*, 7, 631–634. doi:10.1130/0091-7613(2000)028<0631:Awatpp>2.3.Co;2
- Hao, J., Sverjensky, D.A., Hazen, R.M., 2017. A model for late Archean chemical weathering and world average river water. *Earth Planet. Sci. Lett.* 457, 191–203.
doi:10.1016/j.epsl.2016.10.021
- Hazen, R.M., Liu, X.M., Downs, R.T., Golden, J., Pires, A.J., Grew, E.S., Hystad, G., Estrada, C., Sverjensky, D.A., 2014. Mineral Evolution: Episodic Metallogenesis,

- the Supercontinent Cycle, and the Coevolving Geosphere and Biosphere. *Build. Explor. Capab. 21st Century* 1–15.
- Hazen, R.M., Sverjensky, D.A., 2010. Mineral Surfaces, Geochemical Complexities, and the Origins of Life. *Cold Spring Harb. Perspect. Biol.* 2.
doi:10.1101/cshperspect.a002162
- Hazen, R.M., Sverjensky, D.A., Azzolini, D., Bish, D.L., Elmore, S.C., Hinnov, L., Milliken, R.E., 2013. Clay mineral evolution. *Am. Mineral.* 98, 2007–2029.
doi:10.2138/Am.2013.4425
- Hazen, R., 2005. *Genesis: The Scientific Quest for Life's Origins*. National Academies Press.
- Hessler, A.M., Lowe, D.R., 2006. Weathering and sediment generation in the Archean: An integrated study of the evolution of siliciclastic sedimentary rocks of the 3.2 Ga Moodies Group, Barberton Greenstone Belt, South Africa. *Precambrian Res.* 151, 185–210. doi:10.1016/j.precamres.2006.08.008
- Holland, H.D., 1984. *The chemical evolution of the atmosphere and oceans*. Princeton University Press.
- Izon, G., Zerkle, A.L., Zhelezinskaia, I., Farquhar, J., Newton, R.J., Poulton, S.W., Eigenbrode, J.L., Claire, M.W., 2015. Multiple oscillations in Neoarchean atmospheric chemistry. *Earth Planet. Sci. Lett.* 431, 264–273.
doi:10.1016/j.epsl.2015.09.018
- Jelen, B.I., Giovannelli, D., Falkowski, P.G., 2016. The Role of Microbial Electron Transfer in the Coevolution of the Biosphere and Geosphere. *Annu Rev Microbiol* 70, 45–62. doi:10.1146/annurev-micro-102215-095521

- Johnson, J.E., Gerpheide, A., Lamb, M.P., Fischer, W.W., 2014. O₂ constraints from Paleoproterozoic detrital pyrite and uraninite. *Geol. Soc. Am. Bull.*
doi:10.1130/B30949.1
- Kasting, J.F., 2014. 6.6 - Modeling the Archean Atmosphere and Climate, in: Holland, H.D., Turekian, K.K. (Eds.), *Treatise on Geochemistry (Second Edition)*. Elsevier, Oxford, pp. 157–175. doi:10.1016/B978-0-08-095975-7.01306-1
- Kasting, J.F., 1993. Earth's Early Atmosphere. *Science* 259, 920–926.
doi:10.1126/science.11536547
- Kasting, J.F., Catling, D., 2003. Evolution of a habitable planet. *Annu. Rev. Astron. Astrophys.* 41, 429–463. doi:10.1146/Annurev.Astro.41.071601.170049
- Kasting, J.F., Pavlov, A.A., Siefert, J.L., 2001. A coupled ecosystem-climate model for predicting the methane concentration in the Archean atmosphere. *Orig. Life Evol. Biosph.* 31, 271–285. doi:10.1023/a:1010600401718
- Kharecha, P., Kasting, J., Siefert, J., 2005. A coupled atmosphere–ecosystem model of the early Archean Earth. *Geobiology* 3, 53–76. doi:10.1111/j.1472-4669.2005.00049.x
- Klein, C., 2005. Some Precambrian banded iron-formations (BIFs) from around the world: Their age, geologic setting, mineralogy, metamorphism, geochemistry, and origin. *Am. Mineral.* 90, 1473–1499. doi:10.2138/Am.2005.1871
- Konhauser, K.O., Lalonde, S. V, Amskold, L., Holland, H.D., 2007. Was there really an Archean phosphate crisis? *Science* 315, 1234. doi:10.1126/science.1136328

- Kurzweil, F., Claire, M., Thomazo, C., Peters, M., Hannington, M., Strauss, H., 2013. Atmospheric sulfur rearrangement 2.7 billion years ago: Evidence for oxygenic photosynthesis. *Earth Planet. Sci. Lett.* 366, 17–26. doi:10.1016/j.epsl.2013.01.028
- Lafon, G.M., Mackenzie, F.T., 1974. Early Evolution of the Oceans—A Weathering Model.
- Large, R.R., Halpin, J.A., Danyushevsky, L. V, Maslennikov, V. V, Bull, S.W., Long, J.A., Gregory, D.D., Lounejeva, E., Lyons, T.W., Sack, P.J., McGoldrick, P.J., Calver, C.R., 2014. Trace element content of sedimentary pyrite as a new proxy for deep-time ocean-atmosphere evolution. *Earth Planet. Sci. Lett.* 389, 209–220. doi:10.1016/j.epsl.2013.12.020
- Large, R.R., Halpin, J.A., Lounejeva, E., Danyushevsky, L. V, Maslennikov, V. V, Gregory, D., Sack, P.J., Haines, P.W., Long, J.A., Makoundi, C., Stepanov, A.S., 2015. Cycles of nutrient trace elements in the Phanerozoic ocean. *Gondwana Res.* 28, 1282–1293. doi:10.1016/j.gr.2015.06.004
- Liu, X.M., Kah, L.C., Knoll, A.H., Cui, H., Kaufman, A.J., Shahar, A., Hazen, R.M., 2016. Tracing Earth's O₂ evolution using Zn/Fe ratios in marine carbonates. *Geochemical Perspect. Lett.* 2, 24–34. doi:10.7185/geochemlet.1603
- Luo, G., Ono, S., Beukes, N.J., Wang, D.T., Xie, S., Summons, R.E., 2016. Rapid oxygenation of Earth's atmosphere 2.33 billion years ago. *Sci. Adv.* 2, e1600134–e1600134. doi:10.1126/sciadv.1600134
- Lyons, T.W., Reinhard, C.T., Planavsky, N.J., 2014. The rise of oxygen in Earth's early ocean and atmosphere. *Nature* 506, 307–15. doi:10.1038/nature13068

- Marais, D.J. Des, Strauss, H., Summons, R.E., Hayes, J.M., 1992. Carbon isotope evidence for the stepwise oxidation of the Proterozoic environment. *Nature* 359, 605–609.
- Morel, F.M.M., 2008. The co-evolution of phytoplankton and trace element cycles in the oceans. *Geobiology* 6, 318–324. doi:10.1111/j.1472-4669.2008.00144.x
- Och, L.M., Shields-Zhou, G.A., 2012. The Neoproterozoic oxygenation event: Environmental perturbations and biogeochemical cycling. *Earth-Science Rev.* 110, 26–57. doi:10.1016/J.Earscirev.2011.09.004
- Oze, C., Bird, D.K., Fendorf, S., 2007. Genesis of hexavalent chromium from natural sources in soil and groundwater. *Proc Natl Acad Sci U S A* 104, 6544–6549. doi:10.1073/pnas.0701085104
- Pasek, M., Herschy, B., Kee, T.P., 2015. Phosphorus: a case for mineral-organic reactions in prebiotic chemistry. *Orig. Life Evol. Biosph.* 45, 207–18. doi:10.1007/s11084-015-9420-y
- Planavsky, N.J., Rouxel, O.J., Bekker, A., Lalonde, S. V, Konhauser, K.O., Reinhard, C.T., Lyons, T.W., 2010. The evolution of the marine phosphate reservoir. *Nature* 467, 1088–1090. doi:10.1038-nature09485
- Rasmussen, B., Buick, R., 1999. Redox state of the Archean atmosphere: Evidence from detrital heavy minerals in ca. 3250-2750 Ma sandstones from the Pilbara Craton, Australia. *Geology* 27, 115–118. doi:10.1130/0091-7613(1999)027<0115:RSOTAA>2.3.CO
- Rosing, M.T., Bird, D.K., Sleep, N.H., Bjerrum, C.J., 2010. No climate paradox under the faint early Sun. *Nature* 464, 744–747. doi:10.1038/Nature08955

- Rye, R., Holland, H.D., 1998. Paleosols and the evolution of atmospheric oxygen: a critical review. *Am J Sci* 298, 621–672. doi:10.2475/ajs.298.8.621
- Saito, M.A., Sigman, D.M., Morel, M.M., 2003. The bioinorganic chemistry of the ancient ocean : the co-evolution of cyanobacterial metal requirements and biogeochemical cycles at the Archean-Proterozoic boundary ? *Inorganica Chim. Acta* 356, 308–318. doi:10.1016/S0020-1693(03)00442-0
- Schmitt, J.M., 1999. Weathering, Rainwater and Atmosphere Chemistry: Example and Modelling of Granite Weathering in Present Conditions in a CO₂-Rich, and in an Anoxic Palaeoatmosphere, in: *Palaeoweathering, Palaeosurfaces and Related Continental Deposits: Special Publication of the IAS. The International Association of Sedimentologists.*, pp. 21–41.
- Siever, R., 1992. The Silica Cycle in the Precambrian. *Geochim. Cosmochim. Acta* 56, 3265–3272. doi:10.1016/0016-7037(92)90303-Z
- Sverjensky, D.A., Lee, N., 2010. The Great Oxidation Event and Mineral Diversification. *Elements* 6, 31–36. doi:10.2113/gselements.6.1.31
- Sverjensky, D.A., Molling, P.A., 1992. A Linear Free-Energy Relationship for Crystalline Solids and Aqueous Ions. *Nature* 356, 231–234. doi:10.1038/356231a0
- Sverjensky, D.A., Harrison, B., Azzolini, D., 2014. Water in the deep Earth: The dielectric constant and the solubilities of quartz and corundum to 60 kb and 1200 °C. *Geochim. Cosmochim. Acta* 129, 125–145. doi:10.1016/j.gca.2013.12.019
- Sverjensky, D.A., 1984. Europium redox equilibria in aqueous solution. *Earth Planet. Sci. Lett.* 67, 70–78. doi:10.1016/0012-821X(84)90039-6

- Taylor, S.R., McLennan, S., 2009. Planetary crusts: their composition, origin and evolution. Cambridge University Press.
- Tribovillard, N., Algeo, T.J., Lyons, T., Riboulleau, A., 2006. Trace metals as paleoredox and palaeoproductivity proxies: an update. *Chem. Geol.* 232, 12–32.
doi:10.1016/j.chemgeo.2006.02.012
- Valley, J.W., 2006. Early Earth. *Elements* 2, 201–204. doi:10.2113/Gselements.2.4.201
- Williams, R.J.P., Da Silva, J.J.R.F., 2003. Evolution was chemically constrained. *J. Theor. Biol.* 220, 323–343. doi:10.1006/jtbi.2003.3152
- Zerkle, A.L., Claire, M., Domagal-Goldman, S.D., Farquhar, J., Poulton, S.W., 2012. A bistable organic-rich atmosphere on the Neoproterozoic Earth. *Nat. Geosci.* 5, 359–363.
doi:10.1038/Ngeo1425
- Zerkle, A.L., House, C.H., Cox, R.P., Canfield, D.E., 2006. Metal limitation of cyanobacterial N₂ fixation and implications for the Precambrian nitrogen cycle. *Geobiology* 4, 285–297. doi:10.1111/j.1472-4669.2006.00082.x

Chapter 2

Importance of Atmospheric $H_{2,g}$ in Surficial Environments of the Archean

The Archean atmosphere is widely recognized as anoxic with negligible $pO_{2,g}$ and moderately high $pH_{2,g}$ despite recent studies suggesting occasional whiffs of oxygen and oscillatory haze formation. Here we emphasize that $pO_{2,g}$ is too low to control the redox state of the Archean surface environment; however, $pH_{2,g}$ is high enough to control the redox state and plays important roles in various biogeochemical processes.

For example, under Archean $pO_{2,g}$ boundary conditions, hematite is thermodynamically stable, inconsistent with detrital mineral records. In contrast, within the proposed range of Archean $pH_{2,g}$, siderite and pyrite are thermodynamically stable, consistent with detrital mineral records. Therefore, $pH_{2,g}$ rather than $pO_{2,g}$ is the more useful redox indicator for Archean surface environments. Furthermore, $pH_{2,g}$ in present-day volcanic gases varies greatly with different temperatures and the tectonic settings of the volcanoes. Thus, the effects of temperature and tectonic setting of volcanoes on outgassing flux of $H_{2,g}$ should be considered to estimate Archean $pH_{2,g}$. Moreover, early biological activity could greatly affect $pH_{2,g}$.

A transient drop in $p\text{H}_{2,\text{g}}$, or increase of pH, could cause oxidation and mobility of the trace elements Mo and Re without $\text{O}_{2,\text{g}}$. At high $p\text{H}_{2,\text{g}}$ ($\sim 10^{-4}$ bar or greater), modeling of Archean rainwater shows no thermodynamic driving force to destroy simple aqueous organic compounds such as formate or acetate. This result implies a possible riverine transport of aqueous organic C species, and may contribute to haze formation by feeding methanogens in marginal marine systems. Furthermore, in Archean shallow marine environments where $\text{SiO}_{2,\text{aq}}$ might be in equilibrium with solid amorphous silica, a new estimation of the relative thermodynamic stabilities in the system $\text{FeO-SiO}_2\text{-H}_2\text{O-CO}_2\text{-H}_2$ suggests that greenalite, siderite, or hematite should be the primary minerals precipitated in banded iron formations. Magnetite has no stability field and therefore cannot be used to constrain atmospheric $p\text{CO}_{2,\text{g}}$ or $p\text{O}_{2,\text{g}}$.

This paper is currently under review in Geobiology

Authors: Jihua Hao, Dimitri A. Sverjensky, and Robert M. Hazen

1. Redox States on the Surface of the Archean Earth

The abundance of atmospheric $O_{2,g}$ at present, its importance for life on Earth since the Great Oxidation Event (GOE) at about 2.33 Ga (Farquhar *et al.*, 2000; Luo *et al.*, 2016), and the subsequent increase of atmospheric $O_{2,g}$ in the early Cambrian (Berner, 1999; Canfield *et al.*, 2007; Canfield & Teske, 1996; Marais *et al.*, 1992; Och & Shields-Zhou, 2012) has led to enormous interest in the oxidation state of the ancient atmosphere. Unlike the present-day oxidizing atmosphere, $O_{2,g}$ is thought to be a trace constituent in the Archean atmosphere, but the actual level is poorly known. One estimate for $pO_{2,g}$ in the prebiotic near-surface atmosphere in the early Archean is 10^{-11} to 10^{-17} bars or less, based on a photochemical model providing an $H_{2,g}$ concentration determined by a balance between the average present-day outgassing rate of volcanic $H_{2,g}$ and a diffusion-limited escape rate of H atoms to space (Catling & Claire, 2005; Kasting, 1993, 2014). In the late Archean, after the advent of oxygenic photosynthesis, an upper limit for near-surface $pO_{2,g}$ is $< 10^{-6}$ bars, based on evidence from mass-independent fractionation (MIF) of sulfur isotopes (Farquhar *et al.*, 2000; Pavlov & Kasting, 2002). Along with these fragmentary pieces of evidence, additional studies have suggested “whiffs” of molecular $O_{2,g}$ existed in the Meso- and Neo- Archean (3.0 - 2.4 Ga) atmosphere, based on spikes in isotopic and trace elemental abundances in the geological record (Anbar *et al.*, 2007; Crowe *et al.*, 2013; Frei *et al.*, 2009; Gregory *et al.*, 2015; Kaufman *et al.*, 2007; Large *et al.*, 2014; Stüeken *et al.*, 2015). Overall, the implication of all these studies is that the $O_{2,g}$ level in the Archean atmosphere is somehow an important indicator of the redox state of the near-surface environment.

The purpose of this communication is to assert that $O_{2,g}$ levels of 10^{-6} to 10^{-11} bars or less are not significant for understanding the evolution of the redox state of the near-surface environment. The fundamental reason is that such levels of $O_{2,g}$ are so low that they are not capable of participating in significant chemical mass transfer in surficial geochemical environments involving mineral-water interactions. Instead, we believe that attention should be focused on the more abundant reducing gas $H_{2,g}$ in order to further unravel the evolution of the redox state of the near-surface environment in the Archean. In the prebiotic atmosphere of the early Archean it has been estimated that $pH_{2,g}$ was about 10^{-3} to 10^{-4} bars, based on the approach discussed above. After the origin of life, it is likely that the steady state partial pressure of $H_{2,g}$ was lower, but still higher than that of $O_{2,g}$. We show below that such H_2 levels make more geochemical sense than using the $O_{2,g}$ estimates when trying to understand weathering processes in the geologic record of the late Archean. Furthermore, the steady state volcanic and metamorphic fluxes of $H_{2,g}$ to the atmosphere likely influenced the near surface environment in a way that contributed to an anoxic state for the atmosphere (Catling, 2014; Catling & Claire, 2005). We also show that non-steady state variations in the volcanic flux of $H_{2,g}$, both increases and decreases, are to have been expected. In summary, although most previous studies agree with the concept of an anoxic Archean atmosphere, the redox states on the surface of the Archean Earth are still not well constrained and the attention focused on $O_{2,g}$ as an indicator of redox state may be unwarranted, especially when trying to understand the evolution of the near-surface environment with time.

2. Importance of $H_{2,g}$ as the Redox Indicator Before the GOE

2.1 Redox indicators in the near-surface environments: $O_{2,g}$ or $H_{2,g}$?

Here, we examine which gas is the more useful for understanding redox changes on the early Earth. First, we examine $O_{2,g}$ as a redox indicator. Fig. 1a is an equilibrium diagram showing the stability of minerals in the Fe-S-C-O system as functions of the logarithms of the partial pressures of $O_{2,g}$ and $S_{2,g}$ at 25 °C and 1 bar. With $pO_{2,g}$ in the range 10^{-6} to 10^{-11} bars or below suggested by atmospheric models and isotopic studies, hematite is the stable mineral and siderite and pyrite are predicted to be unstable. This result is not consistent with our general understanding of the late Archean geologic record in which detrital siderite and pyrite were preserved during weathering and riverine transport (Frimmel, 2005; Hessler & Lowe, 2006; Rasmussen & Buick, 1999). Previous studies have applied kinetic models to explain the preservation of these detrital minerals with redox controlled by $pO_{2,g}$ (Johnson *et al.*, 2014; Reinhard *et al.*, 2013). However, the amount of $O_{2,aq}$ in aqueous solution in equilibrium with less than 10^{-6} to 10^{-11} bars of $O_{2,g}$ is completely negligible. There is just not enough $O_{2,aq}$ to participate in any chemical reactions. Therefore, when $pO_{2,g}$ is this low, $O_{2,g}$ or $O_{2,aq}$ are no longer important constituents of the near surface environment. Moreover, with $O_{2,g}$ levels of 10^{-6} to 10^{-11} bars or less there are thermodynamic driving forces to oxidize pyrite or siderite to hematite with available oxidants, such as H_2O . Microbes could utilize this thermodynamic driving force to gain energy while facilitating oxidation of pyrite and siderite. But hematite is not believed to be either a weathering product or a detrital mineral in the late Archean. Thus, $pO_{2,g}$ is not a useful redox parameter when it comes to understanding the near-surface environments of the Archean Earth.

In contrast, $H_{2,g}$ is a useful redox parameter for the Archean. Using $H_{2,g}$ as the indicator of near-surface redox states is consistent with the detrital mineral records. For example, [Fig. 1b](#) shows the stability of minerals in the Fe-S-C-O system as functions of $H_{2,g}$ and $S_{2,g}$. With $pH_{2,g}$ values in the prebiotic range of 10^{-3} to 10^{-4} bars, and even down to at least 10^{-5} bars, pyrite and siderite are thermodynamically stable phases under a wide range of $pCO_{2,g}$ conditions. In other words, there is no thermodynamic driving force for the oxidation of pyrite and siderite during Archean weathering and riverine transport, consistent with the detrital mineral records. Furthermore, compared with $O_{2,g}$ ($pO_{2,g} < 10^{-11}$ bar), $H_{2,g}$ is abundant enough in the Archean atmosphere ($pH_{2,g} = 10^{-3}$ to 10^{-4} bar) to participate in reactions under Earth surface conditions ([Walker, 1978](#)). More importantly, compared with $O_{2,g}$, $H_{2,g}$ is 15 times lighter and can diffuse much faster between different chemical conditions to mediate redox conditions ([Krupp *et al.*, 1994](#)). Even though the atmospheric model is not an equilibrium model, we assume that H_2 dissolves from the atmosphere into rainwater at equilibrium. It is then available for weathering reactions, during which we assume that equilibrium exists between dissolved H_2 and most, but not all, aqueous species and minerals ([Hao *et al.*, 2017](#)). It is therefore more sensible, and practical, to use $pH_{2,g}$ rather than $pO_{2,g}$ as a redox parameter for geochemical calculations under early Earth conditions. Consequently, we advocate using $pH_{2,g}$ for monitoring the redox state of early Earth surface environments.

2.2 $H_{2,g}$ -world on the Archean Earth surface

As indicated above, the partial pressure of $H_{2,g}$ is usually estimated by the balance between the fluxes of an $H_{2,g}$ source and sink in the Archean. Volcanic outgassing is

widely assumed to have been the most significant source of $H_{2,g}$ and other gases into the Archean atmosphere. Most modern studies have approximated an Archean volcanic flux based on an average present-day outgassing rate estimated by Holland (Holland, 2002, 2009). Holland took an average value of the ratio of $\Sigma C/H_2O = (0.03 \pm 0.02)$ in present-day volcanic gases from Symonds *et al.* (1994) and Giggenbach (1996), and used a total C flux of 6×10^{12} mol/yr to calculate a flux for H_2O of $2.0 \pm 1.5 \times 10^{14}$ mol/yr from volcanic outgassing. He then assumed that the equilibrium oxidation state of volcanic gases in the subsurface was controlled by the reaction



and calculated an $H_{2,g}$ flux from the water flux and the equilibrium constant for the above reaction.

We would like to emphasize that a single value for the flux of $H_{2,g}$ estimated in this way for the whole Archean is unrealistic. First, it is solely a volcanic flux. Yet there must be a substantial metamorphic flux as well, e.g., from serpentinization reactions in ultramafic rocks, which were more abundant in the Archean than in the Proterozoic (Taylor & McLennan, 2009). Second, as mentioned in Holland (2002), volcanoes from different tectonic settings have highly variable gas compositions. For example, it can be seen in Fig. 2 that $\log pH_{2,g}$ in volcanic gases depends strongly on the tectonic setting and temperature of last equilibrium. The total range of $\log pH_{2,g}$ is about 1.8 units. There is also clearly a positive correlation between $\log pH_{2,g}$ and the temperature for convergent plate environments. Moreover, divergent-plate and hot-spot environments have volcanoes producing the highest values of $pH_{2,g}$. Clearly, tectonic setting and the temperature of equilibration could greatly affect the estimation of volcanic outgassing fluxes of $H_{2,g}$ and

therefore must be considered in the estimation of $p\text{H}_{2,\text{g}}$ in the Archean. Such considerations raise interesting possibilities for the temporal evolution of the Archean near-surface environment.

One can expect that before subduction began some type of plume activity might be widespread (Condie & Benn, 2013; Van Kranendonk, 2010; Wyman & Hollings, 1998). And the relevant temperatures might have been greater (Arndt & Nisbet, 2012). In this case, hot spot volcanoes would be the relevant analogue for the present day. Consequently, the $\text{H}_{2,\text{g}}$ partial pressures in the volcanic gases might be much higher than the present-day, supporting a higher $\text{H}_{2,\text{g}}$ atmosphere in the Archean than previously suggested. With higher volcanic outgassing rates and slower escape of $\text{H}_{2,\text{g}}$, mixing ratios of $\text{H}_{2,\text{g}}$ might be as high as 0.1 in the early Archean (Tian *et al.*, 2005). Such an atmosphere is thought to be relevant for the atmospheric abiotic synthesis and stability of various organic molecules that are the building blocks of life (Trainer, 2013).

After life originated and spread in the Archean, it would have strongly affected the atmospheric composition (Walker, 1977). $\text{H}_{2,\text{g}}$ is one of the most readily available electron donors in the Archean, consequently most metabolisms are thought to have been H_2 -based (Canfield *et al.*, 2006; Kasting, 2014; Kharecha *et al.*, 2005). For example, laboratory culture of methanogens using $\text{H}_{2,\text{g}}$ and $\text{CO}_{2,\text{g}}$ to produce $\text{CH}_{4,\text{g}}$ showed that methanogenesis can draw $p\text{H}_{2,\text{g}}$ down to $\sim 10^{-5}$ bar (Kral *et al.*, 1998). A coupled ecosystem-climate model of the late Archean atmosphere reported that burial of organic carbon from methanogenesis could reduce $p\text{H}_{2,\text{g}}$ down to $\sim 10^{-6}$ bar (Kasting *et al.*, 2001). Both evolutionary and isotopic evidence suggested that methanogens were probably present and prospered in the Archean (Battistuzzi *et al.*, 2004; Canfield *et al.*, 2006; Ueno

et al., 2006). Apart from methanogens, anoxygenic photosynthesis has also been proposed to use $H_{2,g}$ as electron donor to reduce $CO_{2,g}$, competing with methanogens for the use of atmospheric H_2 (Kasting *et al.*, 2001; Kharecha *et al.*, 2005), and therefore further drawing down $pH_{2,g}$ (Catling & Claire, 2005). Right now, due to a lack of understanding of anoxygenic photosynthesis, especially with $H_{2,g}$ as the electron donor, more experimental and modeling studies are still needed to be able to estimate how low $pH_{2,g}$ could go in the late Archean.

3. Implications of the $H_{2,g}$ World

3.1 Mobility of trace elements during weathering due to 'whiffs of oxygenation' before the GOE

Numerous recent studies of the isotopic and trace element composition of the late Archean sedimentary record have reported non-steady state fluctuations in the redox state of the near-surface environment at least 50 Ma prior to the beginning of the GOE. These studies have been interpreted as "whiffs" or pulses of atmospheric $O_{2,g}$ in the Meso- and Neo- Archean. The interpretation of "whiffs" of atmospheric $O_{2,g}$ is based on anomalies in the concentrations of redox-sensitive elements such as Mo and Re and isotopic records (e.g. S, N, and Se) in late Archean marine shale deposits (Anbar *et al.*, 2007; Garvin *et al.*, 2009; Godfrey & Falkowski, 2009; Kaufman *et al.*, 2007; Kendall *et al.*, 2010; Reinhard *et al.*, 2009; Stüeken *et al.*, 2015), Cr isotopes in BIFs (Frei *et al.*, 2009) and paleosols (Crowe *et al.*, 2013), and the trace element compositions of sedimentary pyrites (Gregory *et al.*, 2015; Large *et al.*, 2014).

The oxidation of elements such as Mo, Re, and Cr has been suggested to result in the production of the more mobile oxyanions of these elements during weathering, followed by transport in rivers to the oceans, where subsequent reduction and preservation in shales or banded iron formations preserved the anomalous abundances of these elements. However, the continuous presence of the MIF signal of sulfur isotopes and the presence of detrital minerals unstable in the presence of molecular O₂ certainly make it difficult to understand how molecular O₂ could circulate to any significant extent in the Archean atmosphere and hydrosphere. One solution to this conundrum is that the molecular O₂ responsible for the mobility of trace elements may only exist under mats of cyanobacterial activity, and it didn't actually get into the atmosphere (Lalonde & Konhauser, 2015), i.e. no "whiffs" of O_{2,g}. However, without the UV-protective ozone layer, microbial activity was probably limited on the continents despite various protection mechanisms (Bishop *et al.*, 2006; Dillon & Castenholz, 1999; Gauger *et al.*, 2015). Global runoff of the rivers in the Archean was probably larger due to the large area ratio of ocean to land and no vegetation on the continents (Hao *et al.*, 2017). A stagnant riverine transport coated by microbial mats was probably unlikely or unimportant in the Archean. In addition, reduction of the oxyanions such as CrO₄²⁻, MoO₄²⁻, and ReO₄⁻ has been suggested to be very rapid in presence of Fe(II) aqueous cations or minerals (Eary & Rai, 1989; Fendorf & Li, 1996). If Cr, Mo and Re were oxidized in some local oxidizing environments covered by microbial mats, they might be reduced quickly during riverine transport and not be preserved in marine sediments.

Here we show that the issue of trace element mobility can be examined with the aid of stability diagrams that indicate the conditions required for oxidation of elements

such as Mo, Re, Cr, U, S, and N. Fig. 3 shows the relative stabilities of the reduced and oxidized forms of Mo, Re, and S as functions of $p\text{H}_{2,\text{g}}$ and pH. These are compared with the ranges of $p\text{H}_{2,\text{g}}$ and pH inferred in the present study for the steady-state levels in the Archean near-surface environment. Under the latter conditions, it can be seen that aqueous S would be present in its reduced forms, and that no mobility of Mo and Re can be expected. Non-steady state transient perturbations of the atmosphere are indeed required for oxidation of these elements. Such perturbations are indicated by arrows in the figures. It can be seen that with lower $p\text{H}_{2,\text{g}}$ values, H_2S could be oxidized to sulfate, but this still takes place under reducing conditions. There is certainly no molecular O_2 present in such solutions. Therefore, the occurrence of SO_4^{2-} in the near-surface environment does not require any molecular O_2 , despite frequent literature references to the contrary (Bao, 2015; Canfield, 2005; Stüeken *et al.*, 2012).

Similarly, with lower $p\text{H}_{2,\text{g}}$ values, less than about 10^{-10} bars, $\text{MoS}_{2,\text{cr}}$ and $\text{ReS}_{2,\text{cr}}$ in continental rocks could be weathered to the more mobile MoO_4^{2-} and ReO_4^{2-} respectively. Again, this can take place in the complete absence of molecular O_2 . Only fluctuations in $\text{H}_{2,\text{g}}$ in the atmosphere, sediments, or weathering zone are needed. These fluctuations could arise from a variety of causes, for example, the consumption of $\text{H}_{2,\text{g}}$ by microbial activity, quiescent periods of volcanism, or a change in the predominant style of volcanism. Therefore, pulses in the redox state of the near surface environment as recorded in the sedimentary records may reflect changes in $p\text{H}_{2,\text{g}}$. Similar reasoning may also be applicable to the presence of methanotrophy in the late Archean inferred from carbon isotopic studies (Hayes, 1994; Hayes & Waldbauer, 2006; Rasmussen *et al.*, 2009; Rye & Holland, 2000; Schidlowski *et al.*, 1983).

It can also be seen in Fig. 3 that, apart from fluctuations of $\log p\text{H}_{2,\text{g}}$, increases of pH of natural waters can also solubilize and oxidize molybdenite and rhenium sulfide. The pH of dilute (non-marine) surface waters is mainly controlled by equilibrium with acidic atmosphere gases, such as $\text{CO}_{2,\text{g}}$, and the stage of weathering achieved. Late Archean rainwater and river water have model pH values ranging from about 5.0 to 7.0 based on weathering models at $p\text{CO}_{2,\text{g}} = 10^{-1.5}$ bar (Hao *et al.*, 2017). However, the pH range would be different given different levels of $p\text{CO}_{2,\text{g}}$, i.e., low pH at high $p\text{CO}_{2,\text{g}}$ and high pH at low $p\text{CO}_{2,\text{g}}$. A high pH environment could form when very alkaline fluids (pH ~ 10) from ultramafic rock-water interaction flow through the sediments (Barnes *et al.*, 1967; Bruni *et al.*, 2002; Neal & Stanger, 1983). In another example, decreasing pH caused by oxidation of sulfide has been suggested as one possible mechanism for the mobility and enrichment of Cr and its isotopic fractionation recorded in banded iron formations (Konhauser *et al.*, 2011; Stüeken *et al.*, 2012). Therefore, pH changes in surface waters can also cause the mobility of trace elements and fractionation of their isotopes without the appearance of $\text{O}_{2,\text{g}}$.

3.2 Possible connections between haze formation and whiffs of $\text{H}_{2,\text{g}}$ in late Archean near-surface waters

Multiple episodes of organic haze formation in the late Archean atmosphere (2.7 to 2.5 Ga) have recently been inferred based on sulfur and carbon isotopic analyses and atmospheric models (Izon *et al.*, 2015; Zerkle *et al.*, 2012). It has also been suggested that organic compounds could be deposited at the surface from a reducing Archean atmosphere (Kasting, 1990; Kasting & Brown, 1998; Pinto *et al.*, 1980; Trainer, 2013;

Trainer *et al.*, 2004; Trainer *et al.*, 2006; Ueno & Ito, 2015) or could form by photo-oxidation of Fe(II)-compounds in early waters (Joe *et al.*, 1986). Under present-day oxidizing conditions, simple organic compounds in surface waters are not stable and usually have lifetimes from several to tens of days (Berner & Berner, 2012). However, in the Archean surface environments, much longer lifetime might be expected given the anoxic atmosphere. All of the above lines of evidence suggest that organic molecules may have played a significant role in the surficial environment of the Archean. We examine this suggestion next.

Here, we applied a rainwater model (Hao *et al.*, 2017) to explore the stability of simple aqueous organic species under the atmospheric conditions discussed above, i.e., $p\text{CO}_{2,\text{g}} = 10^{-2.5 \text{ to } 1.0}$ bars and $p\text{H}_{2,\text{g}} = 10^{-3.0 \text{ to } -5.0}$ bars (Catling & Claire, 2005; Haqq-Misra *et al.*, 2008; Kasting, 1993 & 2014; Kasting *et al.*, 2001; Kharecha *et al.*, 2005; von Paris *et al.*, 2008). Rainwater speciation and weathering calculations with these parameters indicate that aqueous organic carbon species such as acetate and formate could be thermodynamically metastable in the rainwater and other surficial waters in the late Archean. This situation arises in the models when the formation of hydrocarbons (e.g. $\text{CH}_{4,\text{aq}}$, $\text{C}_2\text{H}_{6,\text{aq}}$) is suppressed in the aqueous speciation model for kinetic reasons. This situation permits metastable equilibria amongst a variety of aqueous organic species including formate and acetate (Manning *et al.*, 2013). One way of interpreting this result is that carboxylic acids incorporated in rainwater through microbial activity or photochemical reactions could persist metastably in the rainwater and other surface waters in contact with the atmosphere. In other words, there would be no thermodynamic driving force for them to be destroyed during weathering and/or riverine transport. They

could be transported to the oceans and once there they could provide food supporting Archean methanogens.

The higher the $p\text{H}_{2,\text{g}}$ for a given value of $p\text{CO}_{2,\text{g}}$, the higher the predicted ratio of metastable organic carbon to total carbon. For example, at $p\text{H}_{2,\text{g}} > 10^{-3.5} - 10^{-4.6}$ bars, the dissolved organic carbon species in the rainwater is predicted to exceed 50% of the total dissolved carbon. Assuming this level as a basis for calculations, we investigated the effects of different $p\text{H}_{2,\text{g}}$ and $p\text{CO}_{2,\text{g}}$ levels to determine an upper limit of $p\text{H}_{2,\text{g}}$ as shown in Fig. 4a. Our limit for $p\text{H}_{2,\text{g}}$ is $10^{-3.5} - 10^{-4.6}$ bars during the Archean, which is a bit higher than the lower limit set by methanogenesis (Kasting *et al.*, 2001; Kharecha *et al.*, 2005; Kral *et al.*, 1998).

Levels of $p\text{H}_{2,\text{g}}$ of 10^{-4} bars or higher can be easily achieved by flood basalt volcanism in the late Archean. In more recent Earth history, it is estimated that flood basalts typically erupt magma and volcanic gases 100 ~ 1000 times faster than normal basaltic volcanism (Self *et al.*, 2014; Self *et al.*, 2005). Furthermore, it could be expected that the gases released during flood basalt eruption are plume-like in their chemistry (Fig. 2), with high relative concentrations of $\text{H}_{2,\text{g}}$. Consequently, the intensely volcanic activity could have increased $p\text{H}_{2,\text{g}}$ rapidly in the late Archean, disturbing a period when methanogens had thrived and kept $p\text{H}_{2,\text{g}}$ at a much lower level ($\sim 10^{-5}$ bars) with the steady state volcanic outgassing rate (Kasting *et al.*, 2001; Kharecha *et al.*, 2005; Kral *et al.*, 1998). As discussed above, with high $p\text{H}_{2,\text{g}}$, simple organic compounds become thermodynamically stable and could provide food for the early methanogens to form organic hazes. A coupled geosphere-biosphere model of haze formations during the flood basalt volcanisms will be greatly helpful for understanding these possibilities.

3.3 Mineralogy in the marine environment

In addition to the possible formation of rainwater and continental surface waters containing metastable aqueous organic species, indicated by the boundary in [Fig. 4a](#), the mineral stability relations shown in [Fig. 4b](#) have interesting implications for the Fe-bearing minerals that could be expected to form in an Archean marine environment. The stability relations shown in the figure for greenalite ($\text{Fe}_3\text{Si}_2\text{O}_5(\text{OH})_4$), siderite (FeCO_3), and hematite (Fe_2O_3) refer specifically to 25 °C and 1 bar and equilibrium with solid amorphous silica. The standard Gibbs free energy of formation of greenalite used in the present study was taken from a linear free energy correlation approach ([Hao *et al.*, 2017](#)). One assumption that the water is in equilibrium with amorphous silica is appropriate for an Archean ocean as it has long been recognized that silica concentrations at that time would have likely been limited only by the precipitation of amorphous silica, provided that the temperature is low enough that quartz is kinetically inhibited from forming ([Maliva *et al.*, 2005](#); [Siever, 1992](#)).

Under the conditions shown in [Fig. 4b](#), it can be seen that there is no stability field for magnetite. Consequently, it cannot be expected that magnetite is a primary mineral in rocks originating from chemical precipitation from Archean seawater, consistent with the result of petrographic studies ([LaBerge, 1964](#); [Ewers & Morris, 1981](#)). Thermodynamic calculations show that magnetite can only be stable at lower silica concentrations if quartz precipitates, and/or at higher temperatures. [Fig. 4b](#) is quantitatively consistent with experimental results for the formation of poorly crystalline greenalite relative to siderite ([Posth *et al.*, 2008](#)), which supports our linear free energy correlation approach used to

estimate the standard Gibbs free energy of formation of greenalite. However, it contradicts the assumption made in interpreting the mineral assemblage magnetite + hematite + quartz in banded iron formations as a primary chemical precipitate (Rosing *et al.*, 2010).

4. Summary and concluding remarks

The present study has focused on examining the quantification of $O_{2,g}$ and $H_{2,g}$ as redox indicators of Archean surficial environments based on evidence from atmospheric models, detrital mineral records, isotopic signals, and abnormal enrichment of trace metals in sediments. This effort represents a first step towards a more fundamental understanding of the redox history of Archean surface environments. We carried out aqueous speciation and mineral solubility calculations to provide insights into preservation of detrital minerals, mobility of trace elements, and the metastable presence of simple organic compounds in surface waters during the Archean.

Our main conclusions are as follows:

(1) Using $pO_{2,g}$ as the redox indicator of the Archean surface environment is not consistent with detrital mineral records and therefore not appropriate or useful. However, $pH_{2,g}$ is much higher than $pO_{2,g}$ in the Archean atmosphere. Using $pH_{2,g}$ as the redox indicator gives consistent results with detrital minerals. Therefore, $pH_{2,g}$ is a more sensible and practical redox indicator of Archean surface environments.

(2) Volcanic outgassing of $H_{2,g}$ is significantly affected by the tectonic settings and temperatures of the volcanoes. Before subduction began, $pH_{2,g}$ might be much higher than previous estimates, which is very favorable for the origin of life.

(3) After life appeared and prospered on the Earth, early metabolisms would use $H_{2,g}$ as an important electron donor and therefore draw down $pH_{2,g}$ probably to $< 10^{-5}$ bar in the atmosphere.

(4) Fluctuations of $pH_{2,g}$ and/or pH in the Archean surface environments might be the major reasons for the abnormal enrichment of trace elements and their isotopic fractionations recorded in the sediments before the GOE.

(5) Simple organic compounds such as acetate and formate, could metastably persist in Archean rainwater and river water, which would provide sources of food for early methanogens, and support haze formation in the Archean. Our Archean rainwater model predicted an upper limit of $pH_{2,g}$ of $10^{-3.5}$ to $10^{-4.6}$ bars above which more than 50% of total C in the waters could be organic present metastably. Intense pulses of volcanic activity, e.g. flood basalt eruptions, could easily increase $pH_{2,g}$ to 10^{-4} bars or higher and trigger hazy atmospheres.

(6) In the Archean marine environment, where it is likely that high concentrations of silica are set by equilibrium with solid amorphous silica, it is predicted that magnetite does not have a stability field. Instead, in the $H_{2,g}$ world, either greenalite or siderite should form, depending on the $pCO_{2,g}$.

Acknowledgments

This research was supported by a Johns Hopkins Graduate Fellowship (J. H. H.) and the W.M. Keck Foundation (D. A. S. and R. M. H.). We gratefully acknowledge the help and support of the Johns Hopkins University and the Geophysical Laboratory of the Carnegie Institution for Science. We thank S. D. Domagal-Goldman, M. W. Claire, G. N.

Arney, B. Jelen, E. Moore, P. G. Falkowski, F. Huang, F. Tian, D. F. Strobel, and A. Gnanadesikan for discussions.

References:

- Anbar AD, Duan Y, Lyons TW, Arnold GL, Kendall B, Creaser RA, Kaufman AJ, Gordon GW, Scott C, Garvin J, Buick R (2007) A whiff of oxygen before the great oxidation event? *Science* **317**, 1903-1906.
- Arndt NT, Nisbet EG (2012) Processes on the young Earth and the habitats of early life. *Annual Review of Earth and Planetary Sciences* **40**, 521-549.
- Bao H (2015) Sulfate: A time capsule for Earth's O₂, O₃, and H₂O. *Chemical Geology* **395**, 108-118.
- Barnes I, Lamarche VC, Jr., Himmelberg G (1967) Geochemical evidence of present-day serpentinization. *Science* **156**, 830-832.
- Battistuzzi FU, Feijao A, Hedges SB (2004) A genomic timescale of prokaryote evolution: insights into the origin of methanogenesis, phototrophy, and the colonization of land. *BMC Evolutionary Biology* **4**, 1-14.
- Berner RA (1999) Atmospheric oxygen over Phanerozoic time. *Proceedings of the National Academy of Sciences* **96**, 10955-10957.
- Berner EK, Berner RA (2012) *Global environment: water, air, and geochemical cycles*, Princeton University Press.
- Bishop JL, Louri SK, Rogoff DA, Rothschild LJ (2006) Nanophase iron oxides as a key ultraviolet sunscreen for ancient photosynthetic microbes. *International Journal of Astrobiology* **5**, 1-12.
- Bruni J, Canepa M, Chiadini G, Cioni R, Cipolli F, Longinelli A, Marini L, Ottonello G, Vetuschi Zuccolini M (2002) Irreversible water-rock mass transfer accompanying

- the generation of the neutral, Mg–HCO₃ and high-pH, Ca–OH spring waters of the Genova province, Italy. *Applied Geochemistry* **17**, 455-474.
- Canfield DE (2005) The early history of atmospheric oxygen: Homage to Robert A. Garrels. *Annual Review of Earth and Planetary Sciences* **33**, 1-36.
- Canfield DE, Poulton SW, Narbonne GM (2007) Late-Neoproterozoic deep-ocean oxygenation and the rise of animal life. *Science* **315**, 92-95.
- Canfield DE, Rosing MT, Bjerrum C (2006) Early anaerobic metabolisms. *Philosophical Transactions of the Royal Society of London B: Biological Sciences* **361**, 1819-1836.
- Canfield DE, Teske A (1996) Late Proterozoic rise in atmospheric oxygen concentration inferred from phylogenetic and sulphur-isotope studies. *Nature* **382**, 127-132.
- Catling DC (2014) 6.7 - The Great Oxidation Event Transition. In: *Treatise on Geochemistry (Second Edition)* (eds Holland HD, Turekian KK). Elsevier, Oxford, pp. 177-195.
- Catling DC, Claire MW (2005) How Earth's atmosphere evolved to an oxic state: A status report. *Earth and Planetary Science Letters* **237**, 1-20.
- Condie KC, Benn K (2013) Archean geodynamics: similar to or different from modern geodynamics? In: *Archean Geodynamics and Environments* (eds Benn K, Mareschal J, Condie KC). American Geophysical Union, pp. 47-59.
- Crowe SA, Dossing LN, Beukes NJ, Bau M, Kruger SJ, Frei R, Canfield DE (2013) Atmospheric oxygenation three billion years ago. *Nature* **501**, 535-538.

- Dillon JG, Castenholz RW (1999) Scytonemin, a cyanobacterial sheath pigment, protects against UVC radiation: Implications for early photosynthetic life. *Journal of Phycology* **35**, 673-681.
- Eary LE, Rai D (1989) Kinetics of chromate reduction by ferrous ions derived from hematite and biotite at 25 °C. *American Journal of Science* **289**, 180-213.
- Ewers WE, Morris RC (1981) Studies of the Dales Gorge Member of the Brockman Iron Formation, Western Australia. *Economic Geology* **76**, 1929-1953.
- Farquhar J, Bao H, Thiemens M (2000) Atmospheric influence of Earth's earliest sulfur cycle. *Science* **289**, 756-758.
- Fendorf SE, Li G (1996) Kinetics of chromate reduction by ferrous iron. *Environmental Science & Technology* **30**, 1614-1617.
- Frei R, Gaucher C, Poulton SW, Canfield DE (2009) Fluctuations in Precambrian atmospheric oxygenation recorded by chromium isotopes. *Nature* **461**, 250-253.
- Frimmel HE (2005) Archaean atmospheric evolution: evidence from the Witwatersrand gold fields, South Africa. *Earth-Science Reviews* **70**, 1-46.
- Garvin J, Buick R, Anbar AD, Arnold GL, Kaufman AJ (2009) Isotopic evidence for an aerobic nitrogen cycle in the latest Archean. *Science* **323**, 1045-1048.
- Gauger T, Konhauser K, Kappler A (2015) Protection of phototrophic iron(II)-oxidizing bacteria from UV irradiation by biogenic iron (III) minerals: Implications for early Archean banded iron formation. *Geology* **43**, 1067-1070.
- Giggenbach WF (1996) Chemical composition of volcanic gases. In: *Monitoring and Mitigation of Volcano Hazards*. Springer Berlin Heidelberg, Berlin, Heidelberg, pp. 221-256.

- Godfrey LV, Falkowski PG (2009) The cycling and redox state of nitrogen in the Archaean ocean. *Nature Geoscience* **2**, 725-729.
- Gregory DD, Large RR, Halpin JA, Baturina EL, Lyons TW, Wu S, Danyushevsky L, Sack PJ, Chappaz A, Maslennikov VV, Bull SW (2015) Trace element content of sedimentary pyrite in black shales. *Economic Geology* **110**, 1389-1410.
- Hao J, Sverjensky DA, Hazen RM (2017). A model for late Archean chemical weathering and world average river water. *Earth and Planetary Science Letters* **457**, 191-203.
- Haqq-Misra JD, Domagal-Goldman SD, Kasting PJ, Kasting JF (2008) A revised, hazy methane greenhouse for the Archean Earth. *Astrobiology* **8**, 1127-1137.
- Hayes J (1994) Global methanotrophy at the Archean-Proterozoic transition. *Early life on Earth* **84**, 220-236.
- Hayes JM, Waldbauer JR (2006) The carbon cycle and associated redox processes through time. *Philosophical Transactions of the Royal Society of London B: Biological Sciences* **361**, 931-950.
- Hessler AM, Lowe DR (2006) Weathering and sediment generation in the Archean: An integrated study of the evolution of siliciclastic sedimentary rocks of the 3.2 Ga Moodies Group, Barberton Greenstone Belt, South Africa. *Precambrian Research* **151**, 185-210.
- Holland HD (2002) Volcanic gases, black smokers, and the Great Oxidation Event. *Geochimica et Cosmochimica Acta* **66**, 3811-3826.
- Holland HD (2009) Why the atmosphere became oxygenated: A proposal. *Geochimica et Cosmochimica Acta* **73**, 5241-5255.

- Izon G, Zerkle AL, Zhelezinskaia I, Farquhar J, Newton RJ, Poulton SW, Eigenbrode JL, Claire MW (2015) Multiple oscillations in Neoarchaeon atmospheric chemistry. *Earth and Planetary Science Letters* **431**, 264-273.
- Joe H, Kuma K, Paplawsky W, Rea B, Arrhenius G (1986) Abiotic photosynthesis from ferrous carbonate (siderite) and water. *Origins of Life and Evolution of Biospheres* **16**, 369-370.
- Johnson JE, Gerpheide A, Lamb MP, Fischer WW (2014) O₂ constraints from Paleoproterozoic detrital pyrite and uraninite. *Geological Society of America Bulletin* **126**, 813-830.
- Kasting JF (1990) Bolide impacts and the oxidation state of carbon in the Earth's early atmosphere. *Origins of Life and Evolution of Biospheres* **20**, 199-231.
- Kasting JF (1993) Earth's early atmosphere. *Science* **259**, 920-926.
- Kasting JF (2014) 6.6 - Modeling the Archean Atmosphere and Climate. In: *Treatise on Geochemistry (Second Edition)* (eds Holland HD, Turekian KK). Elsevier, Oxford, pp. 157-175.
- Kasting JF, Brown LL (1998) The early atmosphere as a source of biogenic compounds. In: *The Molecular Origins of Life* (eds Brack A). Cambridge University Press, pp. 35-56.
- Kasting JF, Pavlov AA, Siefert JL (2001) A coupled ecosystem-climate model for predicting the methane concentration in the Archean atmosphere. *Origins of Life and Evolution of Biospheres* **31**, 271-285.

- Kaufman AJ, Johnston DT, Farquhar J, Masterson AL, Lyons TW, Bates S, Anbar AD, Arnold GL, Garvin J, Buick R (2007) Late Archean biospheric oxygenation and atmospheric evolution. *Science* **317**, 1900-1903.
- Kendall B, Reinhard CT, Lyons TW, Kaufman AJ, Poulton SW, Anbar AD (2010) Pervasive oxygenation along late Archean ocean margins. *Nature Geoscience* **3**, 647-652.
- Kharecha P, Kasting J, Siefert J (2005) A coupled atmosphere–ecosystem model of the early Archean Earth. *Geobiology* **3**, 53-76.
- Konhauser KO, Lalonde SV, Planavsky NJ, Pecoits E, Lyons TW, Mojzsis SJ, Rouxel OJ, Barley ME, Rosiere C, Fralick PW, Kump LR, Bekker A (2011) Aerobic bacterial pyrite oxidation and acid rock drainage during the Great Oxidation Event. *Nature* **478**, 369-373.
- Kral TA, Brink KM, Miller SL, Mckay CP (1998) Hydrogen consumptions by methanogens on the early earth. *Origins of Life and Evolution of Biospheres* **28**, 311-319.
- Krupp R, Oberthur T, Hirdes W (1994) The early Precambrian atmosphere and hydrosphere: Thermodynamic constraints from mineral deposits. *Economic Geology* **89**, 1581-1598.
- Kump LR (2008) The rise of atmospheric oxygen. *Nature* **451**, 277-278.
- LaBerge GL (1964) Development of magnetite in iron formations of the Lake Superior region. *Economic Geology* **59**, 1313-1342.

- Lalonde SV, Konhauser KO (2015) Benthic perspective on Earth's oldest evidence for oxygenic photosynthesis. *Proceedings of the National Academy of Sciences* **112**, 995-1000.
- Large RR, Halpin JA, Danyushevsky LV, Maslennikov VV, Bull SW, Long JA, Gregory DD, Lounejeva E, Lyons TW, Sack PJ, Mcgoldrick PJ, Calver CR (2014) Trace element content of sedimentary pyrite as a new proxy for deep-time ocean-atmosphere evolution. *Earth and Planetary Science Letters* **389**, 209-220.
- Luo G, Ono S, Beukes NJ, Wang DT, Xie S, Summons RE (2016) Rapid oxygenation of Earth's atmosphere 2.33 billion years ago. *Science Advance* **2**.
- Lyons TW, Reinhard CT, Planavsky NJ (2014) The rise of oxygen in Earth's early ocean and atmosphere. *Nature* **506**, 307-315.
- Maliva RG, Knoll AH, Simonson BM (2005) Secular change in the Precambrian silica cycle: Insights from chert petrology. *Geological Society of America Bulletin* **117**, 835-845.
- Manning CE, Shock EL, Sverjensky DA (2013) The chemistry of carbon in aqueous fluids at crustal and upper-mantle conditions: Experimental and theoretical constraints. *Reviews in Mineralogy & Geochemistry* **75**, 109-148.
- Marais DJD, Strauss H, Summons RE, Hayes JM (1992) Carbon isotope evidence for the stepwise oxidation of the Proterozoic environment. *Nature* **359**, 605-609.
- Neal C, Stanger G (1983) Hydrogen generation from mantle source rocks in Oman. *Earth and Planetary Science Letters* **66**, 315-320.

- Och LM, Shields-Zhou GA (2012) The Neoproterozoic oxygenation event: Environmental perturbations and biogeochemical cycling. *Earth-Science Reviews* **110**, 26-57.
- Pavlov AA, Kasting JF (2002) Mass-independent fractionation of sulfur isotopes in Archean sediments: strong evidence for an anoxic Archean atmosphere. *Astrobiology* **2**, 27-41.
- Pinto JP, Gladstone GR, Yung YL (1980) Photochemical production of formaldehyde in Earth's primitive atmosphere. *Science* **210**, 183-185.
- Posth NR, Hegler F, Konhauser KO, Kappler A (2008) Alternating Si and Fe deposition caused by temperature fluctuations in Precambrian oceans. *Nature Geoscience* **1**, 703-708.
- Rasmussen B, Blake TS, Fletcher IR, Kilburn MR (2009) Evidence for microbial life in synsedimentary cavities from 2.75 Ga terrestrial environments. *Geology* **37**, 423-426.
- Rasmussen B, Buick R (1999) Redox state of the Archean atmosphere: Evidence from detrital heavy minerals in ca. 3250–2750 Ma sandstones from the Pilbara Craton, Australia. *Geology* **27**, 115.
- Reinhard CT, Lalonde SV, Lyons TW (2013) Oxidative sulfide dissolution on the early Earth. *Chemical Geology* **362**, 44-55.
- Reinhard CT, Raiswell R, Scott C, Anbar AD, Lyons TW (2009) A late Archean sulfidic sea stimulated by early oxidative weathering of the continents. *Science* **326**, 713-716.

- Rosing MT, Bird DK, Sleep NH, Bjerrum CJ (2010) No climate paradox under the faint early Sun. *Nature* **464**, 744-747.
- Rye R, Holland HD (2000) Life associated with a 2.76 Ga ephemeral pond?: Evidence from Mount Roe #2 paleosol. *Geology* **28**, 483-486.
- Schidlowski M, Hayes J, Kaplan I (1983) Isotopic inferences of ancient biochemistries: Carbon, sulfur, hydrogen, and nitrogen. In: *Earth's Earliest Biosphere* (ed Schopf JW). Princeton University Press.
- Self S, Schmidt A, Mather TA (2014) Emplacement characteristics, time scales, and volcanic gas release rates of continental flood basalt eruptions on Earth. *Geological Society of America Special Papers* **505**, 319-337.
- Self S, Thordarson T, Widdowson M (2005) Gas fluxes from flood basalt eruptions. *Elements* **1**, 283-287.
- Siever R (1992) The silica cycle in the Precambrian. *Geochimica et Cosmochimica Acta* **56**, 3265-3272.
- Stüeken EE, Buick R, Anbar AD (2015) Selenium isotopes support free O₂ in the latest Archean. *Geology* **43**, 259-262.
- Stüeken EE, Catling DC, Buick R (2012) Contributions to late Archaean sulphur cycling by life on land. *Nature Geoscience* **5**, 722-725.
- Symonds RB, Rose WI, Bluth GJS, Gerlach TM (1994) Volcanic gas studies: Methods, results, and applications. *Reviews in Mineralogy and Geochemistry* **30**, 1-66.
- Taylor SR, McLennan S (2009) *Planetary crusts: their composition, origin and evolution*, Cambridge University Press.

- Tian F, Toon OB, Pavlov AA, De Sterck H (2005) A hydrogen-rich early Earth atmosphere. *Science* **308**, 1014-1017.
- Trainer MG (2013) Atmospheric prebiotic chemistry and organic hazes. *Current Organic Chemistry* **17**, 1710-1723.
- Trainer MG, Pavlov AA, Curtis DB, McKay CP, Worsnop DR, Delia AE, Toohey DW, Toon OB, Tolbert MA (2004) Haze aerosols in the atmosphere of early Earth: manna from heaven. *Astrobiology* **4**, 409-419.
- Trainer MG, Pavlov AA, Dewitt HL, Jimenez JL, Mckay CP, Toon OB, Tolbert MA (2006) Organic haze on Titan and the early Earth. *Proceedings of the National Academy of Sciences* **103**, 18035-18042.
- Ueno Y, Ito S (2015) Supply of organic compounds from early atmosphere into hydrosphere. *Goldschmidt Abstracts* 3201.
- Ueno Y, Yamada K, Yoshida N, Maruyama S, Isozaki Y (2006) Evidence from fluid inclusions for microbial methanogenesis in the early Archaean era. *Nature* **440**, 516-519.
- Van Kranendonk MJ (2010) Two types of Archean continental crust: Plume and plate tectonics on early Earth. *American Journal of Science* **310**, 1187-1209.
- von Paris P, Rauer H, Lee Grenfell J, Patzer B, Hedelt P, Stracke B, Trautmann T, Schreier F (2008) Warming the early earth—CO₂ reconsidered. *Planetary and Space Science* **56**, 1244-1259.
- Walker JCG (1977) Evolution of the atmosphere. New York: Macmillan, and London: Collier Macmillan.

- Walker JCG (1978) Early history of oxygen and ozone in the atmosphere. *Pure and Applied Geophysics* **117**, 498-512.
- Wyman D, Hollings P (1998) Long-lived mantle-plume influence on an Archean protocontinent: Geochemical evidence from the 3 Ga Lumby Lake greenstone belt, Ontario, Canada. *Geology* **26**, 719-722.
- Zerkle AL, Claire M, Domagal-Goldman SD, Farquhar J, Poulton SW (2012) A bistable organic-rich atmosphere on the Neoarchaeon Earth. *Nature Geoscience* **5**, 359-363.

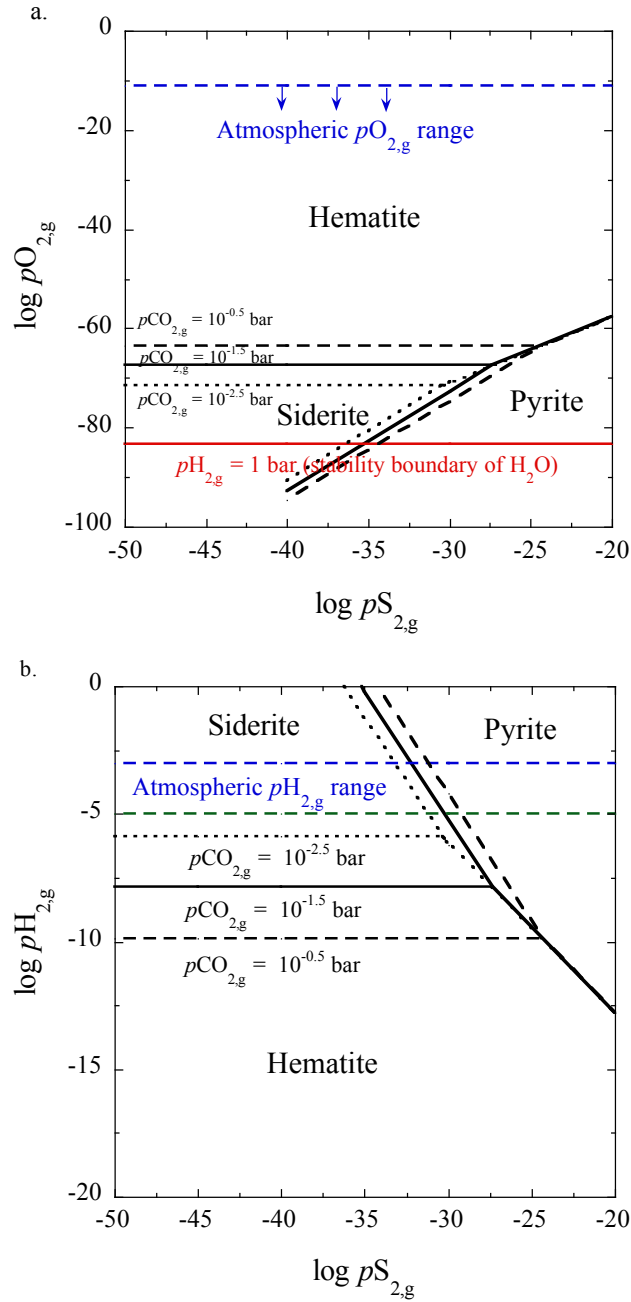


Figure 1. Stability of minerals in Fe-S-C-O system as functions of log fugacity of a. $O_{2,g}$ or b. $H_{2,g}$ and $S_{2,g}$ at 25 °C, 1 bar. The dashed and solid black lines correspond to the boundaries for equilibrium between two minerals under different $pCO_{2,g}$ conditions. Blue lines show the Archean atmosphere boundary condition from classical atmospheric modeling studies (Catling & Claire, 2005; Kasting, 1993, 2014). Green line corresponds to the lower limit of $pH_{2,g}$ formed by methanogenesis (Kral *et al.*, 1998).

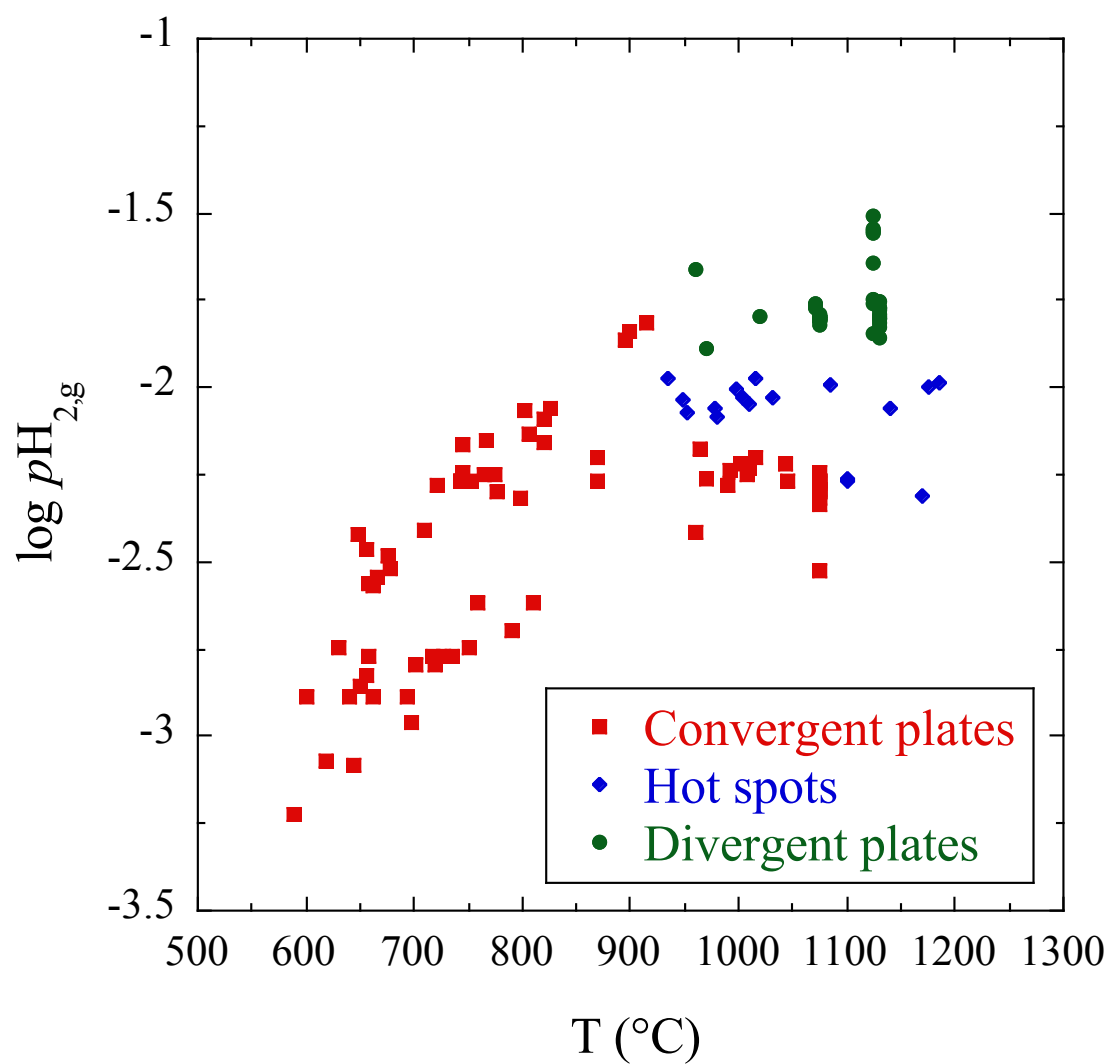


Figure 2. Correlation between log fugacity of $H_{2,g}$ of the volcanic gases with the temperature of the volcanoes (Symonds *et al.*, 1994).

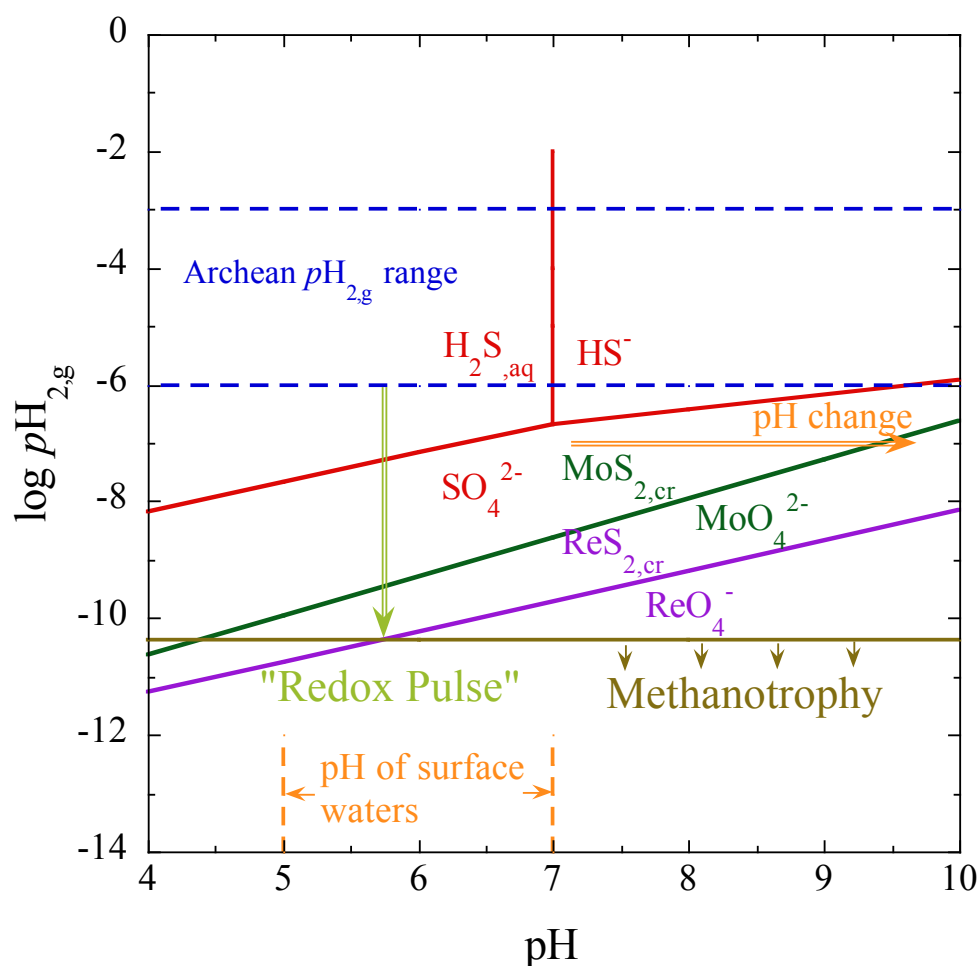


Figure 3. Stability of minerals and aqueous species in Mo-Re-S-O-H system at 25 °C and 1 bar. Blue dashed lines represent the range of $pH_{2,g}$ in the Archean atmosphere according to atmospheric modeling studies and methanogenesis culture study (Catling & Claire, 2005; Kasting, 2014; Kasting, 1993; Kasting *et al.*, 2001; Kharecha *et al.*, 2005; Kral *et al.*, 1998). The red, green, and purple solid lines correspond to the boundaries for equilibria between two aqueous species or between a mineral and an aqueous species by assuming that all aqueous species have equal concentrations as 10^{-6} M. Source of thermodynamic data: $MoS_{2,cr}$ and $ReS_{2,cr}$ came from Mills (1974), MoO_4^{2-} from Minubayeva & Seward (2010), others from Shock *et al.* (1997). The brown line represents the maximum level of $\log pH_{2,g}$ for the methanotrophy ($CH_{4,g} + 2 H_2O \rightarrow CO_{2,g} + 4 H_{2,g}$) when $\log (pCO_{2,g}/pCH_{4,g}) = 3$. Yellow dashed lines represent the range of pH of rainwater and river water in the later Archean (Authors, in press). Yellow arrow shows dissolution and oxidation of $MoS_{2,cr}$ caused by change of environmental pH.

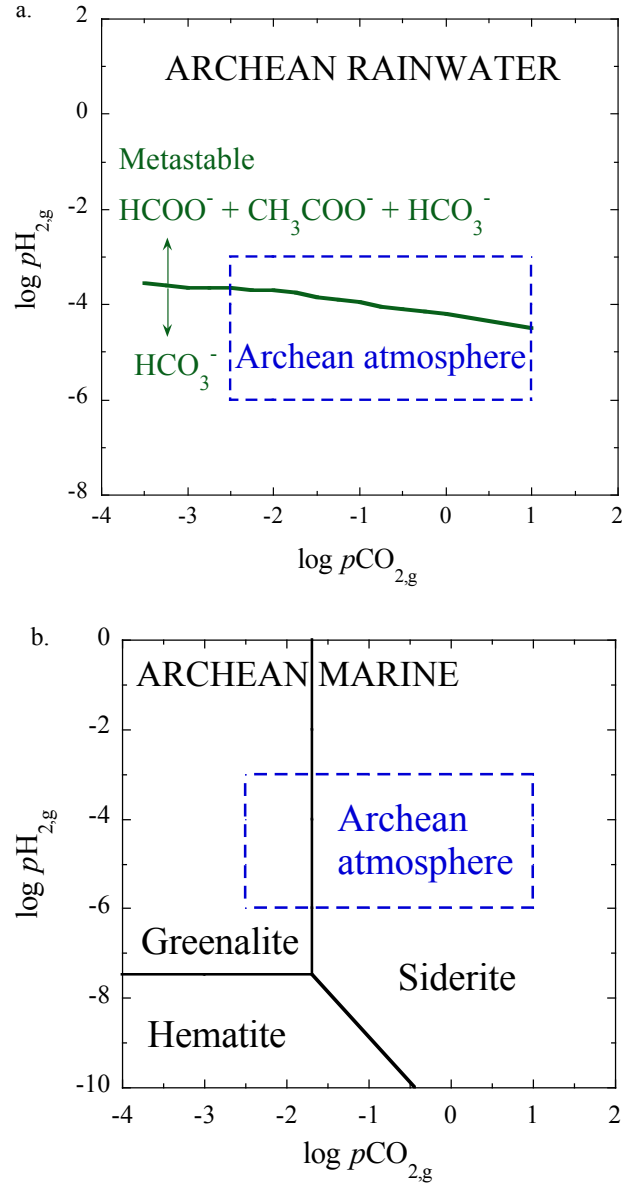


Figure 4. (a) Metastability of carboxylic acids in the aqueous environments on the Earth surface. Suggested boundary of $p\text{H}_{2,g}$ (bold green line) above which carboxylic acids will be metastable in the aqueous environments on the Earth surface. (b) Equilibrium phase diagram of proposed primary Fe minerals in the shallow marine environment. The black lines show equilibrium boundaries between Fe minerals (hematite, siderite, and greenalite) at 25 °C and 1 bar with $\text{SiO}_{2,\text{aq}}$ set by equilibrium with amorphous-silica. The dashed blue box shows the classic atmospheric modeling and methanogenesis activity constraints for the Archean atmosphere (Catling & Claire, 2005; Haqq-Misra *et al.*, 2008; Kasting, 2014; Kral *et al.*, 1998; von Paris *et al.*, 2008).

Chapter 3

An extended linear free energy relationship for predicting ΔG_f° of crystalline solids

The distribution of trace elements during water-rock interactions is usually controlled by the precipitation of secondary mineral solid solutions. Quantitatively modeling of the behavior of trace elements in water-rock systems is currently hampered by a lack of thermodynamic properties of compositional endmembers hosting trace elements. In this study, we improved the Linear Free Energy Relationship (LFER) for predicting the Gibbs free energy of formation (ΔG_f°) of crystalline solids ([Sverjensky and Molling, 1992](#)) by proposing an estimation method for a key parameter β . Specifically, experimental β values are shown to have a correlation with oxygen numbers and coordination numbers, representing the stoichiometry of mineral families and the coordination environment of the cation. The LFER method was applied to estimate the ΔG_f° of isostructural end-members hosting a wide range of divalent cations. The method and thermodynamic data proposed in this study have important implications for the thermodynamic modeling of the speciation and solubility of trace metals during surface weathering, the deposition of marine sediments and their diagenesis, hydrothermal alteration, and mantle metasomatic processes involving aqueous fluids.

Authors: Dimitri A. Sverjensky and Jihua Hao

1. Introduction

Water-rock interactions over wide range of temperatures and pressures generally generate solid solutions of secondary minerals. One specific example is the replacement of Ca(II) in the calcite crystal structure by other divalent cations such as Mg, Mn(II), and Fe(II) during diagenesis and hydrothermal alteration. Precipitation of these mineral solid solutions usually controls the solubility of trace elements in the fluids. In turn, the chemical signatures of trace metals recorded in secondary minerals which could form solid solutions might reflect the concentrations of trace elements in the aquatic environment. This principle has been widely applied to infer the availability of trace elements in the early ocean which is one key theme of the co-evolution of geosphere and biosphere. Examples include the speciation of trace elements in sulfides in black shale (Gregory et al., 2015; Large et al., 2014, 2015), Re in molybdenite ($\text{MoS}_{2,\text{cr}}$) (Golden et al., 2013), and Zn, Fe in marine carbonates (Canfield, 2005; Liu et al., 2016). Compared with the bulk analysis of trace elements in whole-rocks, the concentrations of trace elements in mineral solid solutions potentially provide a more detailed record. In order to quantitatively examine these signatures, it is necessary to build a thermodynamic model of speciation of the trace elements in solid solutions. However, this research is currently hampered by a lack of thermodynamic properties of mineral end-members hosting trace elements, particularly secondary silicate minerals.

Numerous methods for estimating the standard Gibbs free energies or enthalpies of formation of crystalline solids at 25°C and 1 bar have been proposed. The most general of these are based on one of two approaches. In the first approach, the derived properties of fictive polyhedra are summed to give the properties of a specific mineral

based on the polyhedra in its crystal structure (Chermak and Rimstidt, 1989, 1990; Hazen, 1988). In the second approach, a correlation is developed between mineral thermodynamic properties and aqueous ions for a specific chemical stoichiometry, but different structures with the same stoichiometry are all grouped in the same correlation (Gaboreau and Vieillard, 2004; Mathieu and Vieillard, 2010; Tardy and Garrels, 1976, 1977; Vieillard and Tardy, 1988). The uncertainties associated with these estimation techniques are typically at least $\pm 2,000 \text{ cal} \cdot \text{mole}^{-1}$ (Sverjensky and Molling, 1992), based on the scatter of the known standard Gibbs free energies or enthalpies used to construct the predictive methods. This large uncertainty is likely owing to the fact that different crystal structures are mixed in a given estimation approach.

In contrast, if the predictive approach is built on consideration of a family of crystalline solids with the same crystal structure, it is less general but much more accurate (Sverjensky, 1984, 1985; Sverjensky and Molling, 1992; Sverjensky, 1992). In this approach, the different crystalline solids differ only in the identity of a single cation. The standard Gibbs free energies of the end-member crystalline solids correlate very closely with the corresponding standard Gibbs free energies of formation of the aqueous cations corrected for differences of radius in the solid and in the aqueous states. The uncertainties associated with this estimation technique are typically $< 1,000 \text{ cal} \cdot \text{mole}^{-1}$ (Sverjensky and Molling, 1992).

The greater accuracy of the above approach is related to the consideration of only one crystal structure at a time. It is closely analogous in approach and accuracy to the widely used Hammett Linear Free Energy Relationship (LFER) for organic species (Sverjensky and Molling, 1992). In Hammett LFERs the thermodynamic or kinetic

properties of a given organic structure with exchangeable functional groups is correlated with the corresponding aqueous protonation constants of the functional groups. For crystalline solids, the exchange of cations from a given crystal structure is analogous to the exchange of organic functional groups in a given organic structure.

2. Linear Free Energy Relations for predicting standard free energies of formation

The LFER approach for minerals and aqueous ions has been applied to MO oxides with the halite and zincite structures (where M represents a family of cations), $M(OH)_2$ and MCl_2 with the $CdCl_2$ structure, MF_2 with the fluorite and rutile structures, $CaCO_3$ with the calcite and aragonite structures, MSO_4 with the barite structure, M_2SiO_4 with the olivine and phenakite structures (Sverjensky and Molling, 1992; Sverjensky, 1993). Additional applications have been made to surface precipitation (Zhu, 2002) and to nuclear waste-related compounds (Xu and Wang, 1999a, b, c, d). In all of these examples, the standard Gibbs free energies of at least three end-members of each crystal structure were known from experimental studies. In the present study, the LFER for minerals and aqueous ions has been generalized in order to facilitate the prediction of the standard Gibbs free energies of formation of additional crystal structures for which only one end-member was known, typically the Mg-end-member.

The LFER used in the present study represents the compositional end-members of an isostructural family of solids by the formula M_vX , where M represents a cation and X represents the remainder of the composition of the solid and is generally polyatomic. Although we focus below mainly on M^{2+} cations, M can be a cation of any charge. The general equation relating the standard Gibbs free energies of formation ($\Delta G_{f, M_vX}^\circ$) to the

standard Gibbs free energy of formation of the corresponding divalent cation M^{2+} is given by

$$\Delta G_{f, M_vX}^{\circ} = a_{M_vX} \Delta G_{n, M^{2+}}^{\circ} + b_{M_vX} + \beta_{M_vX} r_{M^{2+}} \quad (1)$$

where $\Delta G_{n, M^{2+}}^{\circ}$ represents the non-solvation Gibbs free energy of the aqueous cation. It is a radius-based correction to the standard Gibbs free energy of formation of the aqueous cation M ($\Delta G_{f, M^{2+}}^{\circ}$) calculated using

$$\Delta G_{n, M^{2+}}^0 = \Delta G_{f, M^{2+}}^0 - \Delta G_{s, M^{2+}}^0 \quad (2)$$

In [Eqn. \(2\)](#), $\Delta G_{s, M^{2+}}^{\circ}$ represents the solvation free energy of the aqueous cation calculated from the conventional Born solvation coefficients ($\omega_{M^{2+}}$) using

$$\Delta G_{s, M^{2+}}^{\circ} = \omega_{M^{2+}} \left(\frac{1}{\epsilon} - 1 \right) \quad (3)$$

In [Eqn. \(1\)](#) the coefficients a_{M_vX} , b_{M_vX} , and β_{M_vX} were previously obtained by regression of the standard Gibbs free energies of formation and are characteristic of the particular crystal structure (M_vX); $r_{M^{2+}}$ is the Shannon-Prewitt radius (in Å) of M in a given coordination state. This regression method is only possible and reliable when we have at least three values of $\Delta G_{f, M_vX}^{\circ}$ with the same crystal structure, and M refers at least three cations with a wide range of radius and free energies of the aqueous cations. For many families of isostructural silicate minerals, experimentally derived standard Gibbs free energies for at least three end-member minerals are not known. Under these circumstances, we show here that it is possible to estimate values of both a_{M_vX} and β_{M_vX} for a given composition and crystal structure. By making these estimations, it is possible to use [Eqn. \(1\)](#) and the standard Gibbs free energy of formation of a single solid (e.g. the

Mg end-member) to obtain a value for the parameter b_{M_vX} and then to estimate many other end-members with the same crystal structure.

It can be seen in [Table 1](#) that the parameter β_{M_vX} depends strongly on the stoichiometry of the chemical formula and the coordination number of the cation in the crystal structure as well. In this study, we use the β values given in [Table 1](#) to propose an estimation method to calculate β_{M_vX} values using the empirical equation

$$\log \frac{\beta_{M_vX}}{v} = a' * (O_{x,\#}) + b' + a'' * \log (CN) \quad (4)$$

where $O_{x,\#}$ represents the stoichiometry of a family of isostructural solids calculated from the equation

$$O_{x,\#} = (v_O / v_M) * (2/Z) \quad (5)$$

and v_O and v_M represent the number of moles of oxygen and metal atoms, respectively, per formula unit, Z represents the charge on the metal M , and CN represents the coordination number of M . Regression of the data in [Table 1](#) gave the values $a' = -0.0812459$, $b' = 2.48392$, and $a'' = -0.4200737$. The fit of [Eqn. \(4\)](#) to a wide variety of crystal structures and stoichiometries is shown in [Fig. 1](#). It can be seen that close agreement exists between the calculated curves and the β_{M_vX} values from [Table 1](#), all of which were derived from independent regression of free energy data using [Eqns. \(1\), \(4\) and \(5\)](#) were then used to predict values of β_{M_vX} that could be used in turn to develop a method for estimation of the a_{M_vX} parameter.

In contrast to the β_{M_vX} parameter, which depends on structure, it was previously demonstrated that the parameter a_{M_vX} depends only on the chemistry and stoichiometry of a family of crystalline solids and is independent of the coordination number of the

cation M^{2+} (Sverjensky and Molling, 1992). For example, a_{MCO_3} is the same within uncertainties for the calcite (0.9694 ± 0.0026) structure and for the aragonite (0.9601 ± 0.0038) structure. For this reason, we can refer to a_{M_vX} as a stoichiometry parameter for the composition M_vX . A similar conclusion was reached for the differences between the enthalpies of formation of Mg and Fe end-members of major silicate and oxide families (Helgeson et al., 1978). Indeed, the latter study demonstrated a remarkably close correlation between these enthalpy differences and a simple coefficient expressing the stoichiometry of complex silicates. We build on this relationship below.

Using β_{M_vX} values predicted with Eqns. (4) and (5), Eqn. (1) can be rewritten for the Mg- and Fe-end-members of an isostructural family of crystalline solids in the form

$$a_{M_vX} \left(\Delta G_{n, M_1^{2+}}^\circ - \Delta G_{n, M_2^{2+}}^\circ \right) = (\Delta G_{f, M_1, vX}^\circ - \Delta G_{f, M_2, vX}^\circ) - \beta_{M_vX} (r_{M_1^{2+}} - r_{M_2^{2+}}) \quad (6)$$

Eqn. (6) enables pairs of standard Gibbs free energies of Mg- and Fe-end-members of isostructural families to be used with the predicted β_{M_vX} values to calculate values of a_{M_vX} . Standard Gibbs free energies of formation of orthopyroxene, olivine and biotite from three different sources of thermodynamic data are given in Table 2. These data together with predicted values of β_{M_vX} were used in Eqn. (6) to obtain the a_{M_vX} values for orthopyroxene, olivine and biotite in Tables 3, 4, and 5. The same approach was used for serpentine, talc, chlorite, and smectite (Tables 2 and 3). The end-member clay minerals Mg-saponite and Mg-beidellite from Vidal and Dubacq (2009) are consistent with Berman (1988). However, because the cations in beidellite are in the interlayer, and probably highly solvated and very weakly coordinated, we assumed there is no specific coordination number for them. In this instance, we regressed ΔG_f° of Ca- and Mg-

beidellite to obtain an estimate of the β_{M_vX} value (Table 3). This approach expands considerably the number of known values of the parameter a_{M_vX} for a variety of silicate structures, particularly those of interest for early Earth weathering calculations.

Because the parameter a_{M_vX} is a stoichiometry parameter, we can expect that it will correlate with the stoichiometry index for silicates and oxides developed previously for enthalpies (Helgeson, 1978). Accordingly we investigated the application of the equation

$$a_{MX}/v_M = k_{MX}(v_{Al,t} + v_{Si,t})/v_O \quad (7)$$

where $v_{Al,t}$ and $v_{Si,t}$ represent the number of moles of tetrahedrally coordinated Al and Si per formula unit and k_{MX} represents a constant for oxygen bearing solids. It can be seen in Figs. 2 - 4 that the values of a_{M_vX} from Tables 3 - 5 correlate very closely with the stoichiometry index $(v_{Al,t}+v_{Si,t})/v_O$ regardless of the source of thermodynamic data. However, it can be seen in Fig. 2 that the correlation has the highest value for data from Berman (1988). The success of Eqn. (7) strongly suggests that values of a_{M_vX} can be estimated in a way that will be useful for geochemical modeling purposes. Overall, Eqns. (1) - (7) indicate that with estimated values of a_{M_vX} and it becomes possible to use one experimentally derived standard Gibbs free energy of formation of an isostructural series (e.g. for a Mg-end-member) to estimate the free energies of all the other divalent cation end-members of the same isostructural series of crystalline solids.

With the aid of Eqns. (1) - (7), we calculated the $\Delta G_{f,M_vX}^\circ$ of M-silicates for a variety of mineral families of interest geochemically. The predicted ΔG_f° values are given in Table 6. These values are consistent with Berman (1988). It should be noted that the

end-member clay minerals Mg-saponite and Mg-beidellite from [Vidal & Dubacq \(2009\)](#) are also consistent with [Berman \(1988\)](#). Consequently, we used these values to estimate ΔG_f° of Na-Fe(II)-saponite and Fe(II)-beidellite which were probably common clay minerals before the Great Oxidation Event (GOE) and therefore incorporated into the late Archean weathering models ([Hao et al., 2017](#)). The thermodynamic properties of end-member solids hosting trace elements could also be used to model the behavior of trace elements during surface weathering. For example, Mn is mainly hosted as solid solution in ultramafic and mafic minerals such as olivine. Weathering models including Mn in the olivine solid solution have been used to simulate the geochemical behaviors of Mn during weathering and riverine transport ([Hao et al., in preparation](#)).

3. Conclusions

Overall, this study proposed an extended linear free energy relationship for predicting ΔG_f° of crystalline solids with same crystal structure. Specifically, it is now possible to estimate the parameters necessary to estimate the ΔG_f° values of all the divalent cation end-members of a given crystal structure, based on knowing only the ΔG_f° of the Mg end-member solid. The key parameters characteristic of each structure β and a ([Sverjensky and Molling, 1992](#)) were shown to be predictable from correlations of experimentally derived β values with the stoichiometry and cation coordination properties of the silicate mineral families.

Using the LFER approach, the thermodynamic properties of the end-member solids for eighteen different divalent cations were predicted for crystal structures corresponding to those of common silicates, including orthopyroxene, olivine, garnet, biotite, serpentine, chlorite, talc, saponite and beidellite. These predicted standard Gibbs

free energies of formation can be used to predict trace element distribution between silicates and aqueous solutions at 25 °C and 1 bar. Together with predicted values of the entropies, volumes, and heat capacities, the results of the present study could also be applied to predict trace element distribution at elevated temperatures and pressures. The results of our study should have considerable practical application to modeling the behavior of trace during water-rock interactions in geological processes.

References:

- Berman, R.G., 1988. Internally-consistent thermodynamic data for minerals in the system $\text{Na}_2\text{O-K}_2\text{O-CaO-MgO-FeO-Fe}_2\text{O}_3\text{-Al}_2\text{O}_3\text{-SiO}_2\text{-TiO}_2\text{-H}_2\text{O-CO}_2$. *J. Petrol.* 29, 445–522. doi: 10.1093/petrology/29.2.445
- Chermak, J.A., Rimstidt, J.D., 1989. Estimating the thermodynamic properties (ΔG_f° and ΔH_f°) of silicate minerals at 298 K from the sum of polyhedral contributions. *Am. Mineral.* 74, 1023–1031.
- Chermak, J.A., Rimstidt, J.D., 1990. Estimating the free energy of formation of silicate minerals at high temperatures from the sum of polyhedral contributions. *Am. Mineral.* 75, 1376–1380.
- Cox, J.D., Wagman, D.D., Medvedev, V.A., 1989. CODATA key values for thermodynamics. *Chem/Mats-Sci/E*.
- Gaboreau, S. P. & Vieillard, P. 2004. Prediction of Gibbs free energies of formation of minerals of the alunite supergroup. *Geochim. Cosmochim. Acta* 68, 3307-3316. doi: 10.1016/j.gca.2003.10.040
- Glushko, V.P. 1965-1981. Thermal Constants of Substances: Handbook. Ed., Moscow: VINITI Vols. 1-10.
- Hao, J., Sverjensky, D.A., Hazen, R.M., 2017. A model for late Archean chemical weathering and world average river water. *Earth Planet. Sci. Lett.* 457, 191–203. doi:<http://dx.doi.org/10.1016/j.epsl.2016.10.021>
- Hao, J., Sverjensky, D.A., Hazen, R.M. in preparation. Mobility of nutrients and trace metals during weathering in the late Archean.

- Hazen, R.M., 1988. A useful fiction: polyhedral modeling of mineral properties. *Am. J. Sci.* 288, 242–269.
- Holland, T.J.B., Powell, R., 1998. An internally consistent thermodynamic data set for phases of petrological interest. *J. Metamorph. Geol.* 16, 309–343. doi:10.1111/j.1525-1314.1998.00140.x
- Helgeson, H.C., Delany, J.M., Nesbitt, H.W., Bird, D.K., 1978. Summary and Critique of the Thermodynamic Properties of Rock-Forming Minerals. *Am. J. Sci.* 278, 1–229.
- Mathieu, R., Vieillard, P., 2010. A predictive model for the enthalpies of formation of zeolites. *Microporous Mesoporous Mater.* 132, 335–351. doi: 10.1016/j.micromeso.2010.03.011
- Shannon, R.D., Prewitt, C.T., 1969. Effective ionic radii in oxides and fluorides. *Acta Crystallogr. Sect. B* 25, 925–946. doi:10.1107/S0567740869003220
- Shock, E.L., Helgeson, H.C., 1988. Calculation of the thermodynamic and transport-properties of aqueous species at high-pressures and temperatures - Correlation algorithms for ionic species and equation of state predictions to 5 kb and 1000 °C. *Geochim. Cosmochim. Acta* 52, 2009–2036. doi: 10.1016/0016-7037(88)90181-0
- Sverjensky, D.A., 1984. Prediction of Gibbs free energies of calcite-type carbonates and the equilibrium distribution of trace elements between carbonates and aqueous solutions. *Geochim. Cosmochim. Acta* 48, 1127–1134. doi: 10.1016/0016-7037(84)90203-5
- Sverjensky, D.A., 1985. The distribution of divalent trace elements between sulfides, oxides, silicates and hydrothermal solutions: I. Thermodynamic basis. *Geochim. Cosmochim. Acta* 49, 853–864. doi: 10.1016/0016-7037(85)90177-2

- Sverjensky, D.A., 1992. Linear free energy relations for predicting dissolution rates of solids. *Nature* 358, 310–313. doi: 10.1038/358310a0
- Sverjensky, D.A., Molling, P.A., 1992. A linear free-energy relationship for crystalline solids and aqueous ions. *Nature* 356, 231–234. doi: 10.1038/356231a0
- Tardy, Y., Garrels, R.M., 1976. Prediction of Gibbs energies of formation—I. Relationships among Gibbs energies of formation of hydroxides, oxides and aqueous Ions. *Geochim. Cosmochim. Acta* 40, 1051–1056. doi: 10.1016/0016-7037(76)90046-6
- Tardy, Y., Garrels, R.M., 1977. Prediction of Gibbs energies of formation of compounds from elements—II. Monovalent and divalent metal silicates. *Geochim. Cosmochim. Acta* 41, 87–92. doi: 10.1016/0016-7037(77)90189-2
- Vidal, O., Dubacq, B., 2009. Thermodynamic modelling of clay dehydration, stability and compositional evolution with temperature, pressure and H₂O activity. *Geochim. Cosmochim. Acta* 73, 6544–6564. doi: 10.1016/J.Gca.2009.07.035
- Vieillard, P., Tardy, Y., 1988. Estimation of enthalpies of formation of minerals based on their refined crystal structures. *Am. J. Sci.* 288, 997–1040. doi:10.2475/ajs.288.10.997
- Wagman, D.D., Evans, W.H., Parker, V.B., Schumm, R.H., Halow, I., 1982. The NBS tables of chemical thermodynamic properties. Selected values for inorganic and C₁ and C₂ organic substances in SI units. DTIC Document.
- Xu, H., Wang, Y., L. Barton, L., 1999. Application of a linear free energy relationship to crystalline solids of MO₂ and M(OH)₄. *J. Nucl. Mater.* 273, 343–346. doi: 10.1016/S0022-3115(99)00092-6

- Xu, H., Wang, Y., 1999. Use of linear free energy relationship to predict Gibbs free energies of formation of zirconolite phases (MZrTi_2O_7 and MHfTi_2O_7). J. Nucl. Mater. 275, 211–215. doi: 10.1016/S0022-3115(99)00190-7
- Xu, H., Wang, Y., 1999. Use of linear free energy relationship to predict Gibbs free energies of formation of pyrochlore phases (CaMTi_2O_7). J. Nucl. Mater. 275, 216–220. doi: 10.1016/S0022-3115(99)00189-0
- Xu, H., Wang, Y. 1999. Use of linear free energy relationship to predict Gibbs free energies of formation of MUO_4 phases. Radiochimica Acta 87, 37-40. doi: 10.1524/ract.1999.87.12.37
- Zhu, C., 2002. Estimation of surface precipitation constants for sorption of divalent metals onto hydrous ferric oxide and calcite. Chem. Geol. 188, 23–32. doi:10.1016/S0009-2541(02)00060-8

Table 1. Summary of regression parameters for oxide, hydroxide, carbonate, and silicate mineral families generated by regression with Eqn. (1) and plotted in Fig. 1.

Isostructural Type (M _v X)	Structure	Metal Coord. Number (CN)	Oxygen number ^a	n(M)	a _{M_vX}	b _{M_vX} ^b	β _{M_vX} ^c
M ₂ O	Na ₂ O	4	1	2	5.4358 ^d	-206.92 ^d	286.04 ^d
MO	Zincite	4	1	1	0.8756 ^e	-277.02 ^e	141.75 ^e
MO	Halite	6	1	1	0.8756 ^f	-254.21 ^f	199.10 ^f
M ₂ O ₃	Hematite	6	1	2	1.7536 ^g	-790.36 ^g	237.30 ^g
M(OH) ₂	CdCl ₂	6	2	1	0.9169 ^f	-302.84 ^f	97.67 ^f
MCO ₃	Calcite	6	3	1	0.9694 ^f	-339.92 ^f	80.46 ^f
MCO ₃	Aragonite	9	3	1	0.9601 ^f	-326.12 ^f	66.64 ^f
MSiO ₃	Orthopyroxene	6	3	1	0.9408 ^x	-442.26 ^x	81.9 ^y
M ₂ SiO ₄	Olivine	6	2	2	1.8422 ^x	-701.46 ^x	197.5 ^y
M ₃ Al ₂ Si ₃ O ₁₂	Garnet	8	4	3	2.7719 ^z	-1656.12 ^z	187.34 ^z

^aO_{x, #} defined by Eqn. (5), refers to the oxygen/metal ratio and the cation charge

^bkcal·mol⁻¹.

^ckcal·Å⁻¹.

^dBased on regression of ΔG_{f, M₂O}^o for Li₂O (-134.135), Na₂O (-89.898), and Rb₂O (-71.697) in kcal·mole⁻¹ from Glushko et al. (1981) and values of ΔG_{f, M⁺}^o (Shock and Helgson, 1988), and r_{x, M⁺} (Shannon and Prewitt, 1969).

^eSverjensky (1992).

^fSverjensky & Molling (1992).

^gBased on regression of ΔG_{f, M₂O₃}^o for Al₂O₃ (-378.15; Berman, 1988), Fe₂O₃ (-177.74; Berman, 1988), and Ga₂O₃ (-238.60; Wagman et al., 1982) in kcal·mole⁻¹ and values of ΔG_{f, M³⁺}^o for Al³⁺ (CODATA), Fe³⁺ (Shock and Helgeson, 1989), and Ga³⁺ (Glushko et al., 1971), and r_{x, M³⁺} (Shannon and Prewitt, 1969).

^xRegression of Mg and Fe end-member minerals.

^yPredicted with Eqn. (4).

^zRegression of Mg, Fe, and Ca end-member minerals.

Table 2. Comparison of the standard Gibbs free energies of formation of minerals ($\Delta G_{f,M_vX}^\circ$) from three different thermodynamic databases used to calculate a_{M_vX} values of orthopyroxene, olivine, and biotite in this study.

Mineral Type	Name	$\Delta G_{f,M_vX}^\circ$ (kcal·mole ⁻¹)		
		Berman	Helgeson	Holland & Powell
Orthopyroxene	Enstatite	-348.51 ^a	-348.93 ^b	-348.41 ^c
	Ferrosilite	-267.08 ^a	-267.59 ^b	-267.03 ^c
Olivine	Forsterite	-491.16 ^a	-491.56 ^b	-490.62 ^c
	Fayalite	-329.86 ^a	-330.23 ^b	-329.58 ^c
Biotite	Phlogopite	-1395.08 ^a	-1396.19 ^b	-1395.18 ^c
	Annite	-1147.24 ^a	-1147.16 ^b	-1146.28 ^c
Na-saponite	Na-Mg-saponite	-1740.36 ^d		
	Na-Fe(II)-saponite	-1494.04 ^e		
Beidellite	Mg-beidellite	-1679.78 ^d		
	Fe(II)-beidellite	-1667.47 ^e		
	Ca-beidellite	-1683.84 ^d		
	Na-beidellite	-1683.01 ^d		
	K-beidellite	-1681.27 ^d		

^aBerman (1988).

^bHelgeson et al. (1978).

^cHolland & Powell (1998).

^dVidal & Dubacq (2009), Mg-beidellite modified by +2.05 kcal·mole⁻¹.

^eEstimated using method proposed by Sverjensky & Molling (1992).

Table 3. Summary of estimated and regression parameters for Berman minerals used in [Eqns. \(1\) & \(2\)](#).

Isostructural Type (M_vX)	Structure	Stoichiometry Index ^a	a_{M_vX}	$n(M)$	$a_{M_vX}/n(M)$	b_{M_vX} ^b	β_{M_vX} ^c
MO	NaCl	0	0.8756 ^d	1	0.8756	-254.21 ^d	199.1 ^d
MSiO ₃	Orthopyroxene	0.33	0.9408 ^x	1	0.9408	-442.26 ^x	81.9 ^y
M ₂ SiO ₄	Olivine	0.25	1.8422 ^x	2	0.9211	-701.46 ^x	197.5 ^y
M ₃ Al ₂ Si ₃ O ₁₂	Garnet	0.25	2.7719 ^z	3	0.9240	-1656.12 ^z	187.34 ^z
KM ₃ AlSi ₃ O ₁₀ (OH) ₂	Biotite	0.40	2.8911 ^x	3	0.9637	-1648.7 ^x	203.76 ^y
M ₃ Si ₂ O ₅ (OH) ₄	Serpentine	0.40	2.8727	3	0.9576 ^u	-1247.59 ^v	245.71 ^y
M ₃ Si ₄ O ₁₀ (OH) ₂	Talc	0.40	2.8727	3	0.9576 ^u	-1571.68 ^v	203.79 ^y
M ₅ Al(AlSi ₃)O ₁₀ (OH) ₈	Clinochlore	0.40	4.7878	5	0.9576 ^u	-2412.48 ^v	366.04 ^y
Na _{0.3} M ₃ (Al _{0.3} Si _{3.7})O ₁₀ ·7H ₂ O	Na-saponite.3w	0.40	2.8727	3	0.9576 ^u	-1993.27 ^v	203.76 ^y
M _{0.15} Al ₂ (Al _{0.3} Si _{3.7})O ₁₀ (OH) ₂ ·7H ₂ O	Beidellite.3w	0.40	0.1436	0.15	0.9576 ^u	-1692.31 ^v	10.03 ^w

^a($v_{Al,t} + v_{Si,t}$)/ v_O defined by [Helgeson \(1978\)](#), refers to the ratio of the number of tetrahedral sites to the number of moles of oxygen (other than that in OH⁻).

^bkcal·mol⁻¹.

^ckcal·Å⁻¹.

^d[Sverjensky & Molling \(1992\)](#).

^xRegression of Mg and Fe end-member minerals.

^yPredicted with [Eqn. \(4\)](#).

^uPredicted using the equation in [Figure 2](#).

^vCalculated with [Eqn. \(1\)](#) using ΔG_f° of Mg-end member minerals and predicted a and β values.

^wRegression of Ca and Mg end-member minerals.

Table 4. Summary of regression parameters for Helgeson minerals used in [Eqns. \(1\) & \(2\)](#).

Isostructural Type (M _v X)	Structure	Stoichiometry Index ^a	a _{M_vX}	n(M)	a _{M_vX} /n(M)	b _{M_vX} ^b	β _{M_vX} ^c
MO	NaCl	0	0.8756 ^d	1	0.8756	-254.21 ^d	199.1 ^d
MSiO ₃	Orthopyroxene	0.33	0.9397 ^x	1	0.9397	-442.64 ^x	81.9 ^y
M ₂ SiO ₄	Olivine	0.25	1.8425 ^x	2	0.9213	-701.88 ^x	197.5 ^y
M ₃ Al ₂ Si ₃ O ₁₂	Garnet	0.25	2.7719 ^z	3	0.9240	-1656.12 ^z	187.34 ^z
KM ₃ AlSi ₃ O ₁₀ (OH) ₂	Biotite	0.40	2.9056 ^x	3	0.9685	-1650.3 ^x	203.76 ^y

^a(v_{Al,t} + v_{Si,t})/v_O defined by [Helgeson \(1978\)](#), refers to the ratio of the number of tetrahedral sites to the number of moles of oxygen (other than that in OH⁻).

^bkcal·mol⁻¹.

^ckcal·Å⁻¹.

^d[Sverjensky & Molling \(1992\)](#).

^xRegression of Mg and Fe end-member minerals.

^yPredicted with [Eqn. \(4\)](#).

^zRegression of Mg, Fe, and Ca end-member minerals.

Table 5. Summary of regression parameters for Holland & Powell minerals used in [Eqns. \(1\) & \(2\)](#).

Isostructural Type (M_vX)	Structure	Stoichiometry Index ^a	a_{M_vX}	$n(M)$	$a_{M_vX}/n(M)$	b_{M_vX} ^b	β_{M_vX} ^c
MO	NaCl	0	0.8756 ^d	1	0.8756	-254.21 ^d	199.1 ^d
MSiO ₃	Orthopyroxene	0.33	0.9402 ^x	1	0.9402	-442.14 ^x	81.9 ^y
M ₂ SiO ₄	Olivine	0.25	1.8314 ^x	2	0.9157	-697.93 ^x	197.5 ^y
M ₃ Al ₂ Si ₃ O ₁₂	Garnet	0.25	2.7719 ^z	3	0.9240	-1656.12 ^z	187.34 ^z
KM ₃ AlSi ₃ O ₁₀ (OH) ₂	Biotite	0.40	2.9041 ^x	3	0.9680	-1658.9 ^x	203.76 ^y

^a $(v_{Al,t} + v_{Si,t})/v_O$ defined by [Helgeson \(1978\)](#), refers to the ratio of the number of tetrahedral sites to the number of moles of oxygen (other than that in OH⁻).

^b kcal·mol⁻¹.

^c kcal·Å⁻¹.

^d [Sverjensky & Molling \(1992\)](#).

^x Regression of Mg and Fe end-member minerals.

^y Predicted with [Eqn. \(4\)](#).

^z Regression of Mg, Fe, and Ca end-member minerals.

Table 6. Predicted standard Gibbs free energies of formation of divalent metal silicate families using Eqn. (1), the parameters in Table 3 and the ionic radii and thermodynamic data for aqueous cations listed below.

M	$r_{M^{2+}}^a$ Å	$\Delta G_{n, M^{2+}}^\circ$ kcal·mole ⁻¹	Ortho- pyroxene ^b	Olivine ^c	Garnet ^d	Biotite ^e	Serpentine ^f	Chlorite ^g	Talc ^h	Saponite ⁱ	Beidellite ^j
Be	0.45	85.23	-325.22	-455.57	-1335.57	-1310.6	-892.18	-1839.70	-1235.13	-1656.74	-1675.56
Mg	0.72	36.97	-348.51	-491.16	-1418.88	-1395.08	-964.48	-1971.93	-1318.75	-1740.36	-1679.78
Ca	1	-10.83	-370.55	-523.91	-1498.8	-1476.25	-1032.99	-2098.29	-1399.00	-1820.62	-1683.84
Mn	0.82	81.26	-298.65	-389.81	-1277.26	-1246.69	-812.67	-1723.27	-1171.14	-1592.75	-1672.42
Fe	0.77	119.17	-267.08	-329.86	-1181.52	-1147.24	-716.05	-1560.07	-1072.42	-1494.04	-1667.47
Co	0.735	131.35	-258.49	-314.32	-1154.34	-1119.19	-689.66	-1514.56	-1044.57	-1466.18	-1666.08
Ni	0.7	136.85	-256.18	-311.1	-1145.65	-1110.42	-682.46	-1501.04	-1035.90	-1457.51	-1665.64
Cu	0.73	160.38	-231.59	-261.83	-1074.8	-1036.28	-607.50	-1377.40	-962.19	-1383.80	-1661.96
Zn	0.745	108.23	-279.42	-354.94	-1216.55	-1184	-753.62	-1621.60	-1108.94	-1530.56	-1669.30
Sr	1.16	-24.41	-370.22	-517.33	-1506.47	-1482.91	-1032.69	-2104.74	-1405.41	-1827.03	-1684.18
Cd	0.95	106.74	-264.03	-317.2	-1182.27	-1146.53	-707.53	-1553.69	-1071.45	-1493.07	-1667.45
Sn	1.11	106.28	-251.36	-286.45	-1153.58	-1115.26	-669.54	-1497.33	-1040.16	-1461.79	-1665.91
Ba	1.36	-36.73	-365.43	-500.52	-1503.15	-1477.78	-1018.94	-2090.52	-1400.04	-1821.67	-1683.94
Eu	1.17	-20.5	-365.72	-508.15	-1493.76	-1469.57	-1019.00	-2082.36	-1392.14	-1813.76	-1683.52
Hg	1.02	159.07	-209.07	-206.97	-1024.11	-980.98	-540.01	-1277.52	-906.85	-1328.47	-1659.24
Pb	1.18	102.1	-249.56	-280.32	-1152.05	-1113.08	-664.35	-1491.72	-1037.91	-1459.53	-1665.81
Ra	1.39	-40.06	-366.11	-500.73	-1506.76	-1481.29	-1021.13	-2095.48	-1403.49	-1825.12	-1684.12
UO ₂	0.754	-85.15	-460.62	-709.41	-1750.89	-1741.24	-1306.94	-2544.17	-1662.63	-2084.25	-1696.97

^a Sverjensky & Molling (1992); ^b MSiO₃; ^c M₂SiO₄; ^d M₃Al₂Si₃O₁₂; ^e KM₃AlSi₃O₁₀(OH)₂; ^f M₃Si₂O₅(OH)₄; ^g M₅Al(AlSi₃)O₁₀(OH)₈; ^h M₃Si₄O₁₀(OH)₂; ⁱ Na_{0.3}M₃(Al_{0.3}Si_{3.7})O₁₀·7H₂O; ^j M_{0.15}Al₂(Al_{0.3}Si_{3.7})O₁₀(OH)₂·7H₂O.

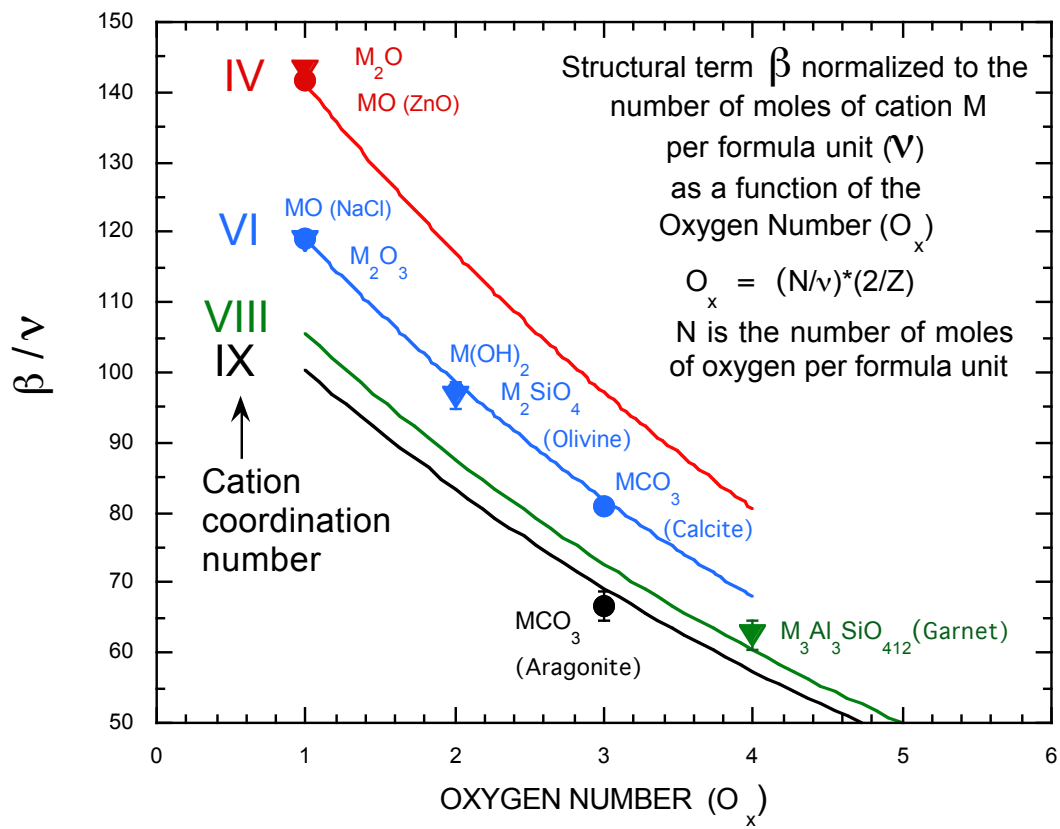


Figure 1. Graphic representation of Eqn. (4) for minerals with same cation coordination number. The symbols represent experimentally derived values of β , divided by number of metal atoms (v).

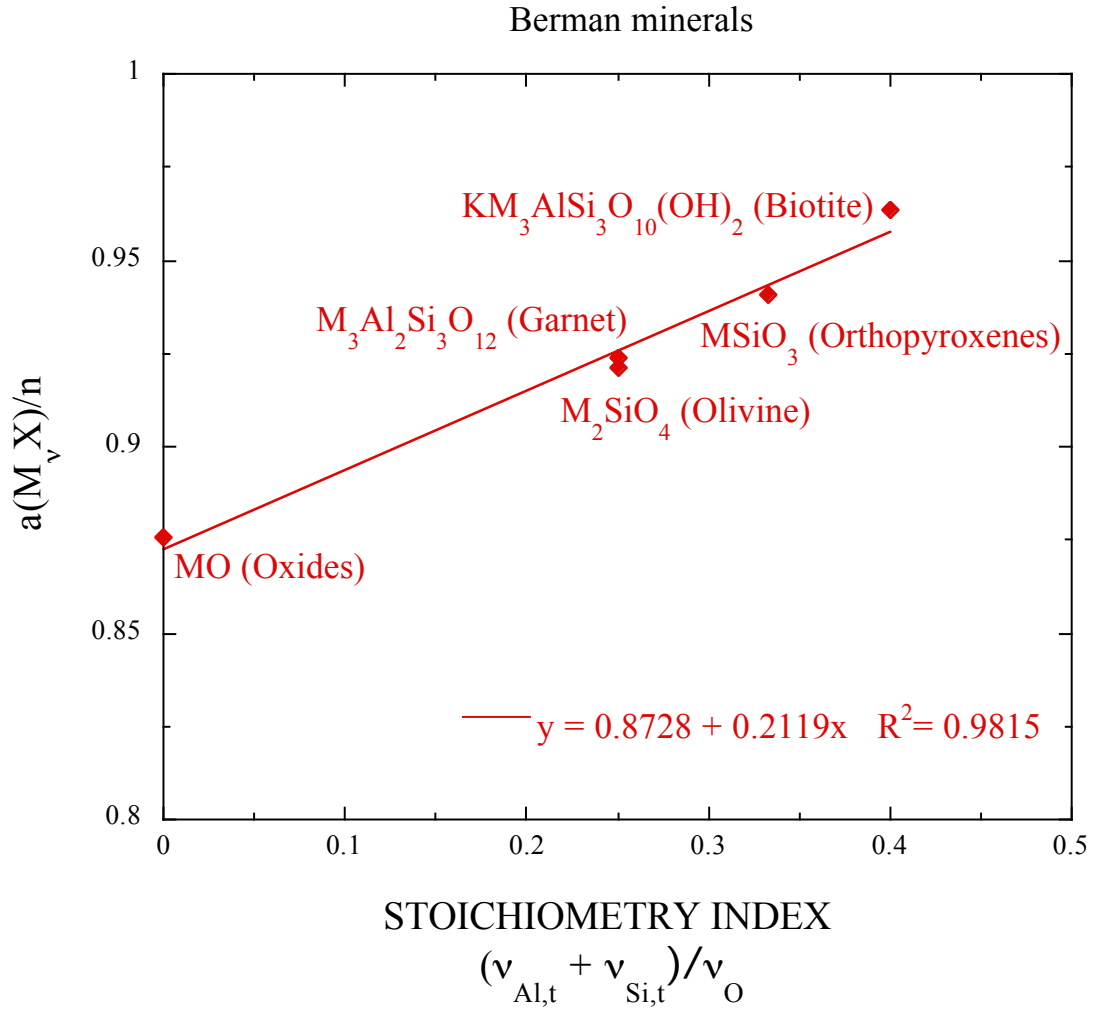


Figure 2. Linear correlation between normalized a (a values divided by number of metal atoms, a_{M_vX}/v) and stoichiometry index (total number of tetrahedral sites divided by total number of oxygen atoms, $(v_{Al,t} + v_{Si,t})/v_O$). Thermodynamic properties of mineral groups are from [Berman \(1988\)](#).

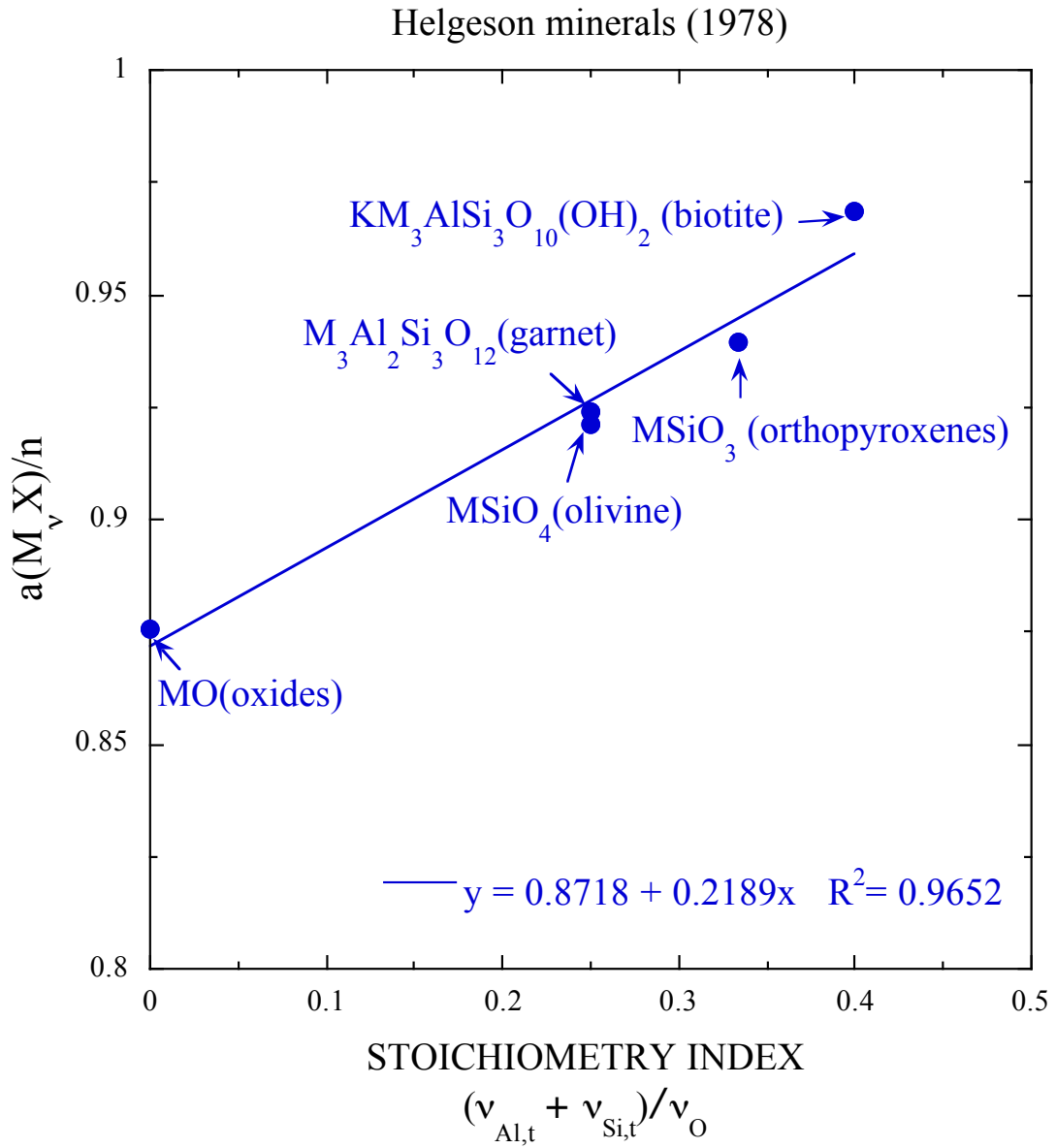


Figure 3. Linear correlation between normalized a (a values divided by number of metal atoms, a_{M_vX}/v) and stoichiometry index (total number of tetrahedral sites divided by total number of oxygen atoms, $(v_{Al,t} + v_{Si,t})/v_O$). Thermodynamic properties of mineral groups are from Helgeson (1978).

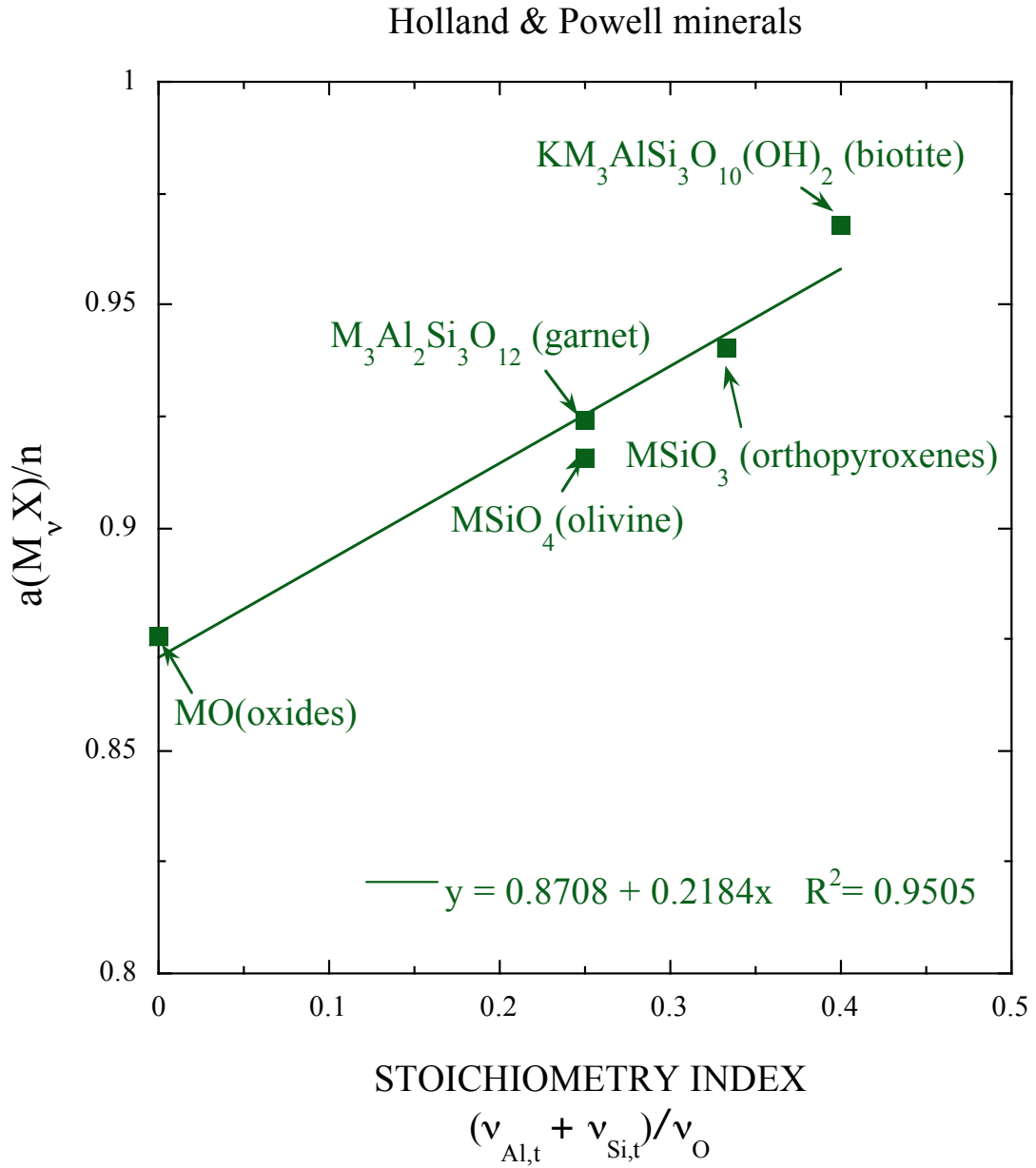


Figure 4. Linear correlation between normalized a (a values divided by number of metal atoms, a_{M_vX}/v) and stoichiometry index (total number of tetrahedral sites divided by total number of oxygen atoms, $(v_{Al,t} + v_{Si,t})/v_O$). Thermodynamic properties of mineral groups are from [Holland & Powell \(1998\)](#).

Chapter 4

A Model for Late Archean Chemical Weathering and World Average River Water

Interpretations of the geologic record of late Archean near-surface environments depend very strongly on an understanding of weathering and resultant riverine transport to the oceans. The late Archean atmosphere is widely recognized to be anoxic ($p\text{O}_{2,\text{g}} = 10^{-5}$ to 10^{-13} bars; $p\text{H}_{2,\text{g}} = 10^{-3}$ to 10^{-5} bars). Detrital siderite (FeCO_3), pyrite (FeS_2), and uraninite (UO_2) in late Archean sedimentary rocks also suggest anoxic conditions. However, whether the observed detrital minerals could have been thermodynamically stable during weathering and riverine transport under such an atmosphere remains untested. Similarly, interpretations of fluctuations recorded by trace metals and isotopes are hampered by a lack of knowledge of the chemical linkages between the atmosphere, weathering, riverine transport, and the mineralogical record.

In this study, we used theoretical reaction path models to simulate the chemistry involved in rainwater and weathering processes under present-day and hypothetical Archean atmospheric boundary conditions. We included new estimates of the thermodynamic properties of Fe(II)-smectites as well as smectite and calcite solid solutions. Simulation of present-day weathering of basalt + calcite by world-average rainwater produced

hematite, kaolinite, Na-Mg-saponite, and chalcedony after 10^{-4} moles of reactant minerals $\text{kg}^{-1} \text{H}_2\text{O}$ were destroyed. Combination of the resultant water chemistry with results for granitic weathering produced a water composition comparable to present-day world average river water (WARW). In contrast, under late Archean atmospheric conditions ($p\text{CO}_{2,\text{g}} = 10^{-1.5}$ and $p\text{H}_{2,\text{g}} = 10^{-5.0}$ bars), weathering of olivine basalt + calcite to the same degree of reaction produced kaolinite, chalcedony, and Na-Fe(II)-rich-saponite. Late Archean weathering of tonalite–trondhjemite–granodiorite (TTG) formed Fe(II)-rich beidellite and chalcedony. Combining the waters from olivine basalt and TTG weathering resulted in a model for late Archean WARW with the composition $\text{Na}^+ \text{-Ca}^{2+} \text{-Fe}^{2+} \text{-Mg}^{2+} \text{-Cl}^- \text{-HCO}_3^- \text{-SiO}_{2,\text{aq}}$. The pH of the water was 6.3 and it is much richer in HCO_3^- , and in Mg + Fe relative to Ca + Na, compared to present-day WARW. At higher $p\text{H}_{2,\text{g}}$ (e.g. $10^{-4.0}$ bars) organic acid anions could be metastable. Our results are consistent with the thermodynamic stability of Fe(II)-clays, pyrite, uraninite, and, under some conditions, siderite during weathering and riverine transport. Overall, our results provide a basis for assessing the formation of organic hazes and the mobility of trace elements and nutrients due to fluctuations of the late Archean atmosphere.

This paper has been published in Earth and Planetary Science Letters

Authors: Jihua Hao, Dimitri A. Sverjensky, and Robert M. Hazen

1. Introduction

Numerous studies have been carried out to attempt to unravel the nature of different parts of the near-surface early Earth system. Sulfur isotopic studies have established that the atmosphere was anoxic prior to 2.33 Ga (Farquhar et al., 2000; Luo et al., 2016). Based on non-equilibrium atmospheric models, the Archean atmosphere has been described as anoxic with high $p\text{CO}_{2,\text{g}}$ (Catling and Claire, 2005; Kasting, 2014), although considerable controversy surrounds the $\text{CO}_{2,\text{g}}$ content of the Archean atmosphere (Haqq-Misra et al., 2008; Hessler et al., 2004; Kasting, 2014; Ohmoto et al., 2004; Rosing et al., 2010; Rye et al., 1995; Sheldon, 2006; von Paris et al., 2008). Combined sulfur and carbon isotopic studies, and atmospheric models, have documented the likely importance of global organic-rich hazy atmospheres alternating with periods of no haze in the Neoarchean from 2.7-2.5 Ga (Izon et al., 2015; Zerkle et al., 2012).

It is also expected that many important aspects of surficial water chemistry in the late Archean were very different from the present-day. For example, it has been suggested that the oceans were probably rich in dissolved silica (Siever, 1992), low in sulfate (Crowe et al., 2014), and contained redox-sensitive elements in their reduced forms, for example $\text{H}_2\text{S}(\text{aq})$, Fe^{2+} and NH_4^+ (Catling and Claire, 2005; Holland, 1984; Lyons et al., 2014). On the late Archean continents, paleosol studies imply the mobility of aqueous Fe^{2+} -species in the near-surface weathering environment, detrital mineral records suggest preservation of uraninite, siderite, pyrite, and ferrous clay minerals (Frimmel, 2005; Hessler and Lowe, 2006; Johnson et al., 2014; Rasmussen and Buick, 1999), and mineral evolution studies are consistent with major changes in the near-surface environment (Hazen et al., 2014). Furthermore, numerous studies of the

sedimentary marine record (e.g. banded iron formations and shales) have suggested that trace metals were mobilized during oxidative weathering processes on the late Archean continents (Anbar et al., 2007; Frei et al., 2009; Gregory et al., 2015; Konhauser et al., 2015; Large et al., 2014; Stüeken et al., 2015). Whether or not these processes involved molecular $O_{2,g}$ is unclear. Finally, oscillation between hazy and non-hazy atmospheres proposed for the Neoproterozoic has been attributed to fluctuations in the production of trace nutrients (organic species or trace metals) in the weathering environment on the continents or in the oceanic hydrothermal environment (Izon et al., 2015). However, little is really known about the potential linkages between the atmosphere, the water chemistry during weathering and riverine transport, and the mineralogic record, which makes it difficult to interpret the causes of fluctuations in trace metal or nutrient availability during late Archean weathering.

Overall, the rich record of clues about the nature of the near-surface environment on early Earth offers a tantalizing, if not confusing, picture that is marked by numerous uncertainties and outright disagreements. However, the consistency of all these lines of evidence has not been examined with the aid of geochemical theory. Quantitative geochemical models of rainwater, river water, the oceans, and water-rock interactions could, in principle, be applied to early Earth, but have rarely been used (Alfimova et al., 2014; Fabre et al., 2011; González-Álvarez and Kerrich, 2012; Lafon and Mackenzie, 1974; Schmitt, 1999; Sverjensky and Lee, 2010). Nor has there been any attempt to link such models to the long literature on models of the early Earth atmosphere (e.g. Claire et al., 2014; Kurzweil et al., 2013). With one exception (Alfimova et al., 2014) involving paleosols on basalts, the application of quantitative models of chemical weathering that

include the chemical speciation of surface waters on the continents and the chemical speciation and state of saturation with respect to minerals in the shallow and deep oceans have not been addressed for the late Archean. The lack of quantitative chemistry prevents construction of an internally consistent, quantitative picture of the evolution of the near-surface environment of early Earth through deep time.

The present weathering study was designed to build a quantitative linkage between the results of atmospheric modeling of early Earth, the chemistry of surface waters on the continents, and the associated mineral weathering products that might be preserved in the geologic record. We focus here on water chemistry and the mineralogic record of change in the near-surface environment. In order to do this, we applied theoretical geochemical models of aqueous speciation, solubility, and chemical mass transfer to weathering on early Earth during the late Archean (3.0 - 2.5 Ga). This time period was chosen because of the reported occurrences of unusual detrital minerals in rocks interpreted to represent the sediments from riverine systems ([Frimmel, 2005](#); [Hessler and Lowe, 2006](#); [Johnson et al., 2014](#); [Rasmussen and Buick, 1999](#)) and the formation of major continents and therefore weathering and riverine transport ([Taylor & McLennan, 2009](#)). Similar approaches have focused previously on chemical weathering processes on Mars ([Catalano, 2013](#)) and on perturbations of early Earth's atmosphere that might affect weathering ([Sverjensky and Lee, 2010](#)), but these emphasized $p\text{O}_{2,\text{g}}$ in the early atmosphere. Here, we focus on the simulation of weathering processes with a steady-state atmosphere defined by atmospheric models in which the role of $\text{H}_{2,\text{g}}$ is emphasized. An overall goal in this project is to build a chemical model of the connection between weathering and late Archean world-average river water (WARW). This model

will serve as a framework for examining the potential mobility of trace metals and nutrients during weathering processes and is also a first step towards developing a geochemical model for the late Archean oceans.

2. Theoretical modeling approach and assumptions

2.1 Modeling approach

Detailed studies of individual riverine, soil zone, aquifer, and weathering systems have documented the many factors that can influence weathering rates. These factors include the effects of temperature, $p\text{CO}_{2,g}$ in the soil, vegetation, precipitation, and runoff (Bluth and Kump, 1994; Dessert et al., 2003; Gislason et al. 1996; Lasaga et al., 1994; Maher, 2010; West et al., 2005; White and Buss, 2014), as well as the kinetics of dissolution of primary minerals and the precipitation of secondary minerals (Bethke, 1996; Brantley and Olsen, 2014; Kump et al., 2000; Steinmann et al., 1994; Zhu, 2009). Complex weathering models that include chemistry, kinetics, hydrology, and climate change have addressed all these factors, but are still site-specific, primarily owing to the need to fit the thermodynamic properties of clay minerals or to test alternate kinetic models for mineral reactivity using measured weathering fluxes (Beaulieu et al., 2012; Dosseto et al., 2015; Dupré et al., 2003; Goddérís et al., 2006; Maher et al., 2009; Violette et al., 2010). For the Archean, this degree of constraint is clearly impossible. Consequently, a simpler approach is warranted.

Our focus is on the simulation of global late Archean weathering and its contribution to world average late Archean river water chemistry. One source of uncertainty in our simulations is the surficial temperature. Considering the wide range of

previously proposed Archean surface temperatures from mild, e.g., $T < 35^{\circ}\text{C}$ (Blake et al., 2010; Shields and Kasting, 2007) to hot e.g., $T \sim 80^{\circ}\text{C}$ (Knauth, 2005; Robert and Chaussidon, 2006), we carried out weathering calculations over a range of temperature conditions. For the purposes of this paper, we only show the results under 25°C conditions. We further assumed that during the late Archean, biological effects on weathering would have been small compared to those of the present-day. Soil cover may have been thinner, permitting greater chemical interaction between the $\text{CO}_{2,\text{g}}$ in the atmosphere, water, and rock. However, many other factors important at the present day are not known. Consequently, we applied purely chemical irreversible mass transfer models (Helgeson, 1979) to simulate reactions between rainwater and representative minerals in major crustal rocks. All the calculations were carried out with the aqueous speciation, solubility, and chemical mass transfer codes EQ3 & EQ6 (Wolery, 1992) using thermodynamic data files prepared as described in Sec. 2.2 and Chapter 3.

Recognizing the simplifications in the above approach, we applied the chemical mass transfer calculations to present day and late Archean rainwaters reacting with crustal rocks. The purely chemical model of present-day weathering was developed in order to calibrate the extent of silicate and carbonate weathering contributions to present-day world-average river water and provide a basis for taking a similar approach to predicting late Archean world-average river water. The irreversible reaction of the initial present-day and late Archean rainwaters with an excess of minerals approximating crustal rocks was computed. For simplicity, we assumed that the minerals react at relative rates of unity and that secondary minerals (i.e. weathering products) are precipitated at equilibrium with the evolving solution chemistry and may further precipitate or dissolve

as the aqueous solution continues to evolve chemically. Overall, this process simulates irreversible incongruent dissolution of the reactant minerals, as described in previous studies (Bethke, 1996; Helgeson, 1979; Sverjensky, 1984). We chose this approach instead of reaction with oxide components representing average crust. Using specific mineral solid-solutions imposes a more realistic constraint on the fluid evolution because, in the model, primary mineral species can actually reach zero chemical affinity for reaction. In order to simulate the kinetic inhibition of the precipitation of minerals such as pyrite and quartz under surficial conditions (Bjorlykke and Egeberg, 1993; Schoonen and Barnes, 1991), precipitation of these minerals was suppressed in the model. Similarly, in order to account for the likely lack of reactivity of aqueous hydrocarbons under surficial temperatures (Manning et al., 2013), they too were suppressed.

The conceptual model described above for reaction of rainwaters with rocks also raises the question of the extent of penetration of the atmosphere into the zone of weathering. At the present day, this penetration varies substantially in different parts of the world and is strongly affected by the biota in modern soil zones. For example, $p\text{CO}_{2,g}$ in modern soils is typically higher than in the atmosphere. However, by the time that waters from weathering zones have entered riverine systems, the $p\text{CO}_{2,g}$ affecting the waters is presumably similar to atmospheric. Therefore, in order to approximate the overall evolution of rainwater through weathering to river water at the present day, we used a fixed $p\text{CO}_{2,g}$ in the weathering zone set by the atmospheric value (see Sec. 3.1). For the late Archean, it might be expected that the atmosphere more readily interacted with the weathering zone compared to the present day, as only microbial life was present and thus, $p\text{CO}_{2,g}$ in the weathering zone was similar to the atmosphere (Berner, 1992). As

a first approximation therefore, the calculations modeling both the present day and Archean weathering processes were carried out at fixed temperature, $p\text{O}_{2,\text{g}}$, $p\text{H}_{2,\text{g}}$, and $p\text{CO}_{2,\text{g}}$ throughout all the reaction steps (see [Sec. 3.1](#)).

2.2 Thermodynamic data used in the calculations

Thermodynamic data files used in the calculations were built using data for aqueous species from [Shock et al. \(1997\)](#), for minerals from [Berman \(1988\)](#), [Berman and Aranovich \(1996\)](#), and [Sverjensky et al. \(1991\)](#). We also included the thermodynamic properties of the saponite and beidellite clay minerals ([Vidal and Dubacq, 2009](#)), which are consistent with [Berman \(1988\)](#). We used new estimates of the thermodynamic properties of Fe^{2+} -bearing clays based on a linear free energy method ([Sverjensky and Molling, 1992](#)) in which correlations are built for individual crystal structure types. Details of the estimation procedure for ferrous numerous minerals are given in the [Chapter 3](#).

3. Initial conditions for the modeling

3.1 Rainwater models: present-day and the late Archean

[Table 1](#) shows the compositions and the predicted predominant species in our present-day and late Archean rainwaters. For the present-day rainwater, we used $p\text{CO}_{2,\text{g}} = 10^{-3.5}$ bars and $p\text{O}_{2,\text{g}} = 10^{-0.68}$ bars. The concentrations of major species were adopted from an estimate of unpolluted, world-average rainwater ([Berner and Berner, 2012](#)). The concentrations of the minor elements Fe, Al, and Si were fixed by equilibrium with hematite, gibbsite, and kaolinite respectively, consistent with the possibility that the

sources of these elements might be soil dust in the atmosphere (Berner and Berner, 2012). A trace amount of dissolved N (0.56 μM) was added to explore the predicted redox state of N and the speciation during weathering.

For the late Archean rainwater composition (Table 1), we carried out trial calculations over the ranges given by atmospheric models: $p\text{CO}_{2,\text{g}} = 10^{-2.5 \text{ to } 1.0}$ bars and $p\text{H}_{2,\text{g}} = 10^{-3.0 \text{ to } -5.0}$ bars (Catling and Claire, 2005; Kasting, 2014). In the atmospheric models, $p\text{O}_{2,\text{g}}$ is at negligible values compared to $p\text{H}_{2,\text{g}}$. Furthermore, they are not at equilibrium. Consequently we chose to focus on $p\text{H}_{2,\text{g}}$ as the more meaningful measure of redox state in the Archean atmosphere. As a reference condition representative of these ranges, we chose $p\text{CO}_{2,\text{g}} = 10^{-1.5}$ bars and $p\text{H}_{2,\text{g}} = 10^{-5.0}$ bars. Results at other partial pressures were not significantly different except at higher $p\text{H}_{2,\text{g}}$ values, where an intriguing metastability of aqueous organic species was noted (see Table 2 and description below). The Archean rainwater was assumed to have the same concentrations of Na, K, Mg, and Ca as present-day rainwater. The concentrations of Al and Si were again calculated from equilibrium with gibbsite and kaolinite. However, the concentrations and speciation of the redox sensitive elements Fe and S must be very different to those in present-day rainwater. We assumed that in the reducing late Archean rainwater, Fe(II) has the same concentration as Mg(II) because of their similar geochemical properties and abundance in the crust. The concentration of S was estimated by assuming that all the S from volcanic outgassing rained out consistent with atmospheric model assumptions (Claire et al., 2014; Domagal-Goldman et al., 2008).

Although the total dissolved N contents of Archean rainwater are expected to be dominated by dissolved N_2 from the atmosphere, as at the present day, the equilibrium

speciation of N at $pH_{2,g} = 10^{-5.0}$ bars is expected to involve reduced N-species. Just as with carbon, if reduced N is somehow incorporated into Archean rainwater (e.g. through lightning), it should be stable in the rainwater. Consequently, we added a trace amount of reduced dissolved N (0.56 μ M) to track its predicted redox state during the weathering processes.

3.2 Initial rock types: present-day and the late Archean

The composition of the present-day upper continental crust was in part approximated by a combination of silicate and carbonate minerals. For the silicates, we used basalt consisting of the solid solutions plagioclase (albite₃₅anorthite₆₅) and augite (enstatite₂₂ferrosilite₈diopside₄₂hedenbergite₂₈) and granite consisting of plagioclase (albite₈₀anorthite₂₀), biotite (annite₇₅phlogopite₂₅), muscovite, and K-feldspar (Blatt et al., 2006). However, intensive studies of present-day river water chemistry have indicated a major influence from weathering of both silicate and carbonate rocks (Berner and Berner, 2012). River water chemistry ranges towards high Ca/Na, Mg/Na, and HCO_3^- /Na ratios because of the effect of carbonate rock weathering (Berner and Berner, 2012). Indeed, it is now widely recognized that the dissolution of trace amounts of carbonate rocks (or epidote or apatite-bearing hydrothermally altered rocks) can, in some cases, dominate the Ca^{2+} and HCO_3^- budgets of rivers (Beaulieu et al., 2012; Berner and Berner, 2012; Oliva et al., 2004). Consequently, we included a trace amount of calcite (0.001 moles, plus 1 mole of each silicate minerals) in the weathering models for basalt and granite. Considering that weathering reactions are limited in extent by water flow rate and soil

cover, we only showed model weathering results up to 10^{-3} moles of reactant minerals destroyed kg^{-1} of water (i.e. $\log \xi$ up to -3).

In contrast to the present-day upper crust, which is mainly granitic (Rudnick and Gao, 2003), the Archean upper crust had approximately equal amounts of basalt + komatiite and rocks of granitic affinity known as the tonalite–trondhjemite–granodiorite or TTG suite (Taylor and McLennan, 2009). Given that komatiite is essentially olivine, we used an olivine basalt and a granodiorite as representative of Archean crust. As in the case of the present-day crust, we included the same trace amounts of calcite as an additional reactant. Even though limestones and dolomites were probably much less abundant in the late Archean, calcite could have been weathered from metamorphic rocks and veins in altered igneous rocks.

4. Present-day weathering model results

4.1. Weathering of basalt + calcite

It can be seen in Fig. 1a that simulated weathering of basalt + calcite under present-day conditions initially produced a trace amount of gibbsite, followed by much greater amounts of kaolinite and hematite until $\log \xi \sim -4.0$, after which Na-Mg-saponite, chalcedony, and eventually calcite solid solution (almost pure calcite) were produced. Kaolinite, hematite, and smectite commonly form under present-day conditions (Gíslason et al., 1996). Previous field studies have suggested saponite as a low-temperature alteration and weathering product of mafic and ultramafic volcanic rocks (Huang et al., 2013; Treiman et al., 2014). It should be emphasized that the product minerals in the model refer to well-crystallized phases, which are not the initial minerals produced in

natural settings. Instead the model minerals represent what natural assemblages are evolving towards. In some instances this situation can be approximated directly. For example, instead of the thermodynamically stable quartz, microcrystalline silica such as chalcedony usually forms as a primary precipitate during weathering (Gíslason et al., 1997). In our model, this was approximated by suppressing the precipitation of quartz, which enabled some chalcedony to be produced at an advanced stage of basalt weathering.

The composition of the water also evolved during reaction progress (see Fig. 1b). World-average rainwater is a $\text{Na}^+\text{-Cl}^-$ -type water, but during reaction with basalt + calcite it evolved towards a predominantly $\text{Ca}^{2+}\text{-Na}^+\text{-HCO}_3^-\text{-SiO}_{2,\text{aq}}$ composition by $\log \xi \sim -4.0$, which is broadly consistent with present-day world-average river water (WARW) (Berner and Berner, 2012). The composition of the water at $\log \xi \sim -4.0$ can be compared with WARW in Table 2. At this value of $\log \xi$, with the exception of the low K and Mg concentrations, the model water is comparable in composition to WARW with respect to Na, Ca, Si, and C. In addition, the model pH = 8.0 at $\log \xi = -4.0$, which lies within the range for many present-day rivers (Gaillardet et al., 2014).

For values of $\log \xi \sim -4.0$ to -3.0 , it can be seen in Fig. 1b that the Mg content of the predicted waters drops significantly, but Ca, Na, C, and Si remain the major constituents. As expected, the trace N in the water during the weathering process was present in its most stable oxidized form, i.e. NO_3^- . In summary, our modeling results for weathering of basalt + calcite under present-day conditions are broadly consistent overall with natural water chemistry and an approximation to the major minerals in weathered basaltic rocks.

4.2 Weathering of granite + calcite

It can be seen in Fig. 2a that weathering of granite + calcite produced beidellite solid solution and hematite until $\log \xi \sim -4.0$, after which chalcedony and carbonate solid solution were produced. The proportions of the Ca, Mg, and Na end-members of beidellite are nearly constant during weathering (see Fig. 2b). For the carbonate solid solution (Fig. 2c) calcite is again the dominant component. Our modeling results are consistent with the geologic observation that beidellite commonly forms during granitic weathering under present-day conditions (Wilson, 2013).

It can be seen in Fig. 2d that the evolving water chemistry became enriched in the major species $\text{Na}^+ - \text{K}^+ - \text{Ca}^{2+} - \text{Mg}^{2+} - \text{HCO}_3^- - \text{SiO}_{2,\text{aq}}$. At $\log \xi \sim -4.0$, this composition differs from the predictions for weathering of basalt + calcite in the higher concentration of K and the lower concentration of Ca. The high K value is attributable to alteration of K-silicates present in granite model that are absent in basalt. The composition of the water at $\log \xi = -4.0$ is given in Table 2.

4.3 Comparison with present-day world-average river water (WARW)

The compositional evolution of the waters during weathering of basalt + calcite and granite + calcite can be more conveniently seen in Figs. 3a and b, which focus on the relative proportions of the dissolved constituents rather than the absolute concentrations. The reaction paths progressing from $\log \xi = -10.0$ to -3.0 are shown. The composition of WARW is also shown in Figs. 3a and b. It can be seen that for weathering of basalt +

calcite the closest match with WARW occurs at about $\log \xi = -4.0$. For weathering of granite + calcite the closest match is at about $\log \xi = -3.7$.

However, when the model waters from basalt and granite weathering are compared at the same value of $\log \xi$, e.g. at -4.0 in [Table 2](#) and in [Fig. 3a](#), it can be seen that the water from weathering of basalt is much closer to WARW with respect to the relative proportions of Na, Ca, and Mg than the water from granite. In [Fig. 3b](#), the evolution of the two waters at $\log \xi = -4.0$ is similar. As noted above, the major difference between the two waters is in the K concentration, which is too low for the basaltic water and too high for the granitic water at $\log \xi = -4.0$ compared with WARW ([Table 2](#)). Comparative studies of river water compositions for waters draining basaltic versus granitic terranes suggest that waters from basaltic areas represent a more advanced degree of weathering ([Dessert et al., 2003](#)). This is also reflected in global scale modeling, which has emphasized the importance of weathering of basaltic relative to granitic terranes ([Berner, 2006](#)) and the faster reaction rates (far from equilibrium) measured experimentally for mafic minerals compared with felsic minerals ([Brantley and Olsen, 2014](#)).

The value of $\xi = 10^{-4}$ corresponds to 10^{-4} moles of each reactant mineral destroyed $\text{kg}^{-1} \text{H}_2\text{O}$. This estimate is a theoretical value of ξ . It is possible to compare this value of ξ with empirical values obtained using studies of present-day rivers. For example, multiplying the dissolved silica concentrations for the 55 largest rivers with their runoff rates ([Gaillardet et al., 1999](#)) results in a range of calculated silicate weathering rates for these rivers ([Fig. 4](#)). Taking the rates with a 95% confidence interval about the mean results in a range of calculated rates of $10^{-9.2}$ to $10^{-8.8}$ $\text{moles.m}^{-2}.\text{sec}^{-1}$. Dividing this range

of rates by the global runoff rate for weathering in temperate climatic regions, $1.48 \times 10^{-8} \text{ m}\cdot\text{s}^{-1}$ (Meybeck, 1987), results in empirical values of ξ from $10^{-4.4}$ to $10^{-4.0}$ moles.kg⁻¹ H₂O, which overlaps with the theoretical value of $\xi = 10^{-4}$ moles.kg⁻¹ H₂O.

The above considerations, together with the model calculations summarized in Table 2, suggest that a mixture of water derived from a combination of weathering of basalt + calcite and granite + calcite results in a reasonable first approximation to WARW. We assumed that the upper crust is represented chemically by 1/4 basalt + 3/4 granite (Rudnick and Gao, 2003). Multiplying these proportions by the relative weathering rates of basalt versus granite in the ratio of 6:1 (Dessert et al., 2003), we obtained 2/3 basalt + 1/3 granite as the proportions contributing to the global weathering flux of silicates. Therefore, in the present study, we mixed 67% water from basalt + calcite weathering and 33% water from granite + calcite weathering to obtain a model river water composition from our calculations. It can be seen in Table 2 that our estimate of WARW corresponds quite closely to the actual WARW.

5. Late Archean weathering model results

5.1 Weathering of olivine basalt + calcite

The reference condition of $p\text{CO}_{2,\text{g}} = 10^{-1.5}$ and $p\text{H}_{2,\text{g}} = 10^{-5.0}$ bars assumed to prevail during the late Archean profoundly changed the mineral products during weathering compared with the present-day. Instead of the hematite, kaolinite, Na-Mg-saponite, and Ca-rich carbonate produced under present-day conditions, weathering of Archean olivine basalt + calcite generated kaolinite plus Na-Fe(II)-rich saponite, and (Ca,Mg,Fe(II))-carbonate solid solutions (Fig. 5a - c). To test the persistence of detrital

pyrite during Archean weathering, we also introduced a trace amount of pyrite (10^{-6} moles.kg⁻¹ H₂O) as a reactant. The result showed that pyrite saturated at $\log \xi \sim -6.3$. For values of $\log \xi > -6.3$ the aqueous solutions in our model became supersaturated with respect to pyrite. Such fluids could not dissolve pyrite during weathering and riverine transport. Therefore, our model is consistent with the preservation of pyrite as a detrital mineral during Archean weathering and sediment transport.

Ferrous-saponite is predicted to be the dominant end-member in our model of saponite solid solution (Fig. 5b) consistent with clay mineral evolution studies (Hazen et al., 2013). Moreover, both geologic observations (Huang et al., 2013; Treiman et al., 2014) and model simulations (Catalano, 2013) showed Mg- and Fe(II)-saponite as mineral products during weathering of ferromagnesian silicates in anoxic or reducing regimes. Overall, these results suggest that Na-Fe(II)-saponite may have formed during the late Archean because of the reducing atmosphere.

The predicted evolution of the water chemistry can be seen in Fig. 5d. Due to the reducing atmosphere, the initial rainwater contained a relatively high concentration of Fe²⁺, low S(II), and N is in the form of NH₄⁺. Moreover, HCO₃⁻ is high in Archean rainwater as a result of the much higher $p\text{CO}_{2,g}$ assumed in the model (Table 1). Considering the abundant precipitation of ferrous iron minerals and high concentration of Fe(II) in the water, iron is clearly mobile during basaltic weathering under Archean atmospheric conditions as anticipated from paleosol studies (Holland, 1984; Rye and Holland, 1998). Both geological and modeling studies have pointed out that the concentration of S(II) in surface environments should be much lower before the Great Oxidation Event (Claire et al., 2014; Domagal-Goldman et al., 2008; Rasmussen and

Buick, 1999), which is consistent with our results, even assuming all volcanic S was rained out as S(II).

5.2 Weathering of tonalite–trondhjemite–granodiorite (TTG) + calcite

In contrast to the modeling results for present-day weathering of granite, the late Archean weathering of TTG + calcite produced an Fe(II)-rich beidellite solid solution, along with chalcedony and an Fe(II)-rich carbonate solid solution (Figs. 6a - c). As in the case of the Archean olivine basalt weathering, we found that pyrite should persist during weathering. Our beidellite solid solution is predicted to contain Fe(II) as a major interlayer cation under the hypothetical Archean atmospheric conditions. The predicted carbonate solid solution is different from the olivine basaltic weathering with siderite as the major component, and magnesite and calcite as minor components (Fig. 6c), reflecting relative higher concentrations of Fe(II) in the water than during olivine basalt weathering.

It can be seen in Table 2 that at $\log \xi = -4.0$, the TTG + calcite weathering model resulted in a water with similar major species to the present-day granite + calcite weathering, except for the appearance of aqueous Fe(II) and S(II), the very high total dissolved C (HCO_3^- and CO_2), and the much lower pH values.

6. Implications for interpretations of the Archean near-surface environment

6.1 A model for late Archean world-average river water

We have shown above that model weathering calculations for basalt + calcite and granite + calcite together can provide a close approximation of present-day WARW. This

result can be used to provide the basis for a preliminary estimate of the composition of late Archean WARW. The fundamental assumption involved is that the results of the weathering models at $\log \xi = -4.0$ apply to the late Archean. The value of $\log \xi = -4.0$ corresponds to 10^{-4} moles of each reactant mineral destroyed $\text{kg}^{-1} \text{H}_2\text{O}$. For this value to apply to the late Archean, the ratio of the global average weathering rate to the global average runoff in the late Archean should be the same as at the present-day.

We suggest that the weathering rate in the Archean was faster than at present because of the higher $p\text{CO}_{2,\text{g}}$, which would lower the pH of the rainwater. Moreover, Fe in the anoxic environment would be mainly Fe(II) which is much more soluble and mobile than Fe(III). These considerations are confirmed by geological observations, such as Fe-leaching paleosols before the Great Oxidation Event ([Rye and Holland, 1998](#)). It is also possible that the global runoff was probably larger in the Archean than the present-day. There were no plants covering the Archean land surface, and there may have been a larger area of ocean and therefore a more intense hydrological cycle. If both weathering rates and runoff were higher in the Archean, the increases could have offset each other resulting in a similar ratio of the global average weathering rate to the global average runoff. Under these circumstances, it is a reasonable first step to approximate the overall reaction progress during late Archean weathering with the present-day value, i.e. $\log \xi = -4.0$ in the weathering models.

Many poorly quantifiable factors in the late Archean might influence the global ratio of weathering rate to runoff compared to the present day, including differences in temperature, land surface elevation, the nature of the soil cover when only microbial life was present, and differences in lithology that might influence reaction rates. For the

present-day, we showed above that WARW was closely approximated by combining 67% water from weathering of basalt + calcite and 33% from granite + calcite. Here we used a similar approach to generate a preliminary estimate of the late Archean WARW. As mentioned above, late Archean crust was assumed to be approximated by equal amounts of olivine basalt + TTG. If we assume that the relative weathering rates of those rock-types are the same as for basalt versus granite, i.e. that the weathering rate of olivine basalt is 6-times that of TTG, we derive the relative contribution of weathering fluxes to be 86% water from weathering of olivine basalt + calcite and 14% from TTG + calcite. The result is given in [Table 2](#) as Archean WARW at $p\text{H}_{2,\text{g}} = 10^{-5.0}$ bars.

In comparison with present-day WARW, late Archean WARW at $p\text{H}_{2,\text{g}} = 10^{-5.0}$ bars has similar Na, K, Ca, and Si concentrations, but much higher concentrations of HCO_3^- and $\text{Fe(II)} + \text{Mg}$ ([Table 2](#)). As a result, the late Archean WARW has a lower Ca/Na ratio and much higher Mg(Fe)/Na and HCO_3^-/Na ratios than present-day WARW ([Figs. 7a and b](#)). The values of the model pH for the waters from olivine basalt and TTGs ([Table 2](#)) suggest that the pH of late Archean WARW should be ~ 6.3 , substantially lower than present-day model values at the same extent of reaction progress ([Table 2](#)). Despite the assumptions and uncertainties involved, our model is a useful starting point for considering the speciation and mobility of trace elements released during weathering. It can also serve as a first step in quantifying the riverine input to the late Archean ocean.

As mentioned above, we also carried out calculations at higher $p\text{H}_{2,\text{g}} = 10^{-4.0}$ bars. [Table 2](#) shows a model WARW at this $p\text{H}_{2,\text{g}}$ for comparison with the reference late Archean WARW at $p\text{H}_{2,\text{g}} = 10^{-5.0}$ bars. It can be seen that the concentration of aqueous Fe increased by 50% and the total dissolved C increased by 40%. The large increase in C

content is due to the predicted metastability of organic acid anions such as CH_3COO^- and $\text{CH}_3\text{CH}_2\text{COO}^-$ (44.4% of total C). In the presence of these organic acids, the pH of the river water decreased from 6.3 to 6.0. We interpret the results at $p\text{H}_{2,g} = 10^{-4.0}$ bars as an indication of the potential for metastable aqueous organics to persist during weathering and riverine transport in the late Archean, as discussed further below.

6.2 Detrital mineral records

Studies of the apparent survival of pyrite during weathering and riverine transport in the late Archean have focused on the kinetics of pyrite dissolution ([Frimmel, 2005](#); [Johnson et al., 2014](#); [Rasmussen and Buick, 1999](#)). However, the state of saturation of weathering solutions or rivers with respect to pyrite has not previously been established. As discussed above, in our weathering models it was shown that the solutions easily become supersaturated with respect to pyrite ([Figs. 5a and 6a](#)). Kinetic inhibition may prevent precipitation of pyrite (without help from organisms), so it may remain supersaturated at near-surface conditions in the late Archean. Consequently, there will be no thermodynamic driving force for dissolution of pyrite. It should therefore be stably preserved during weathering and riverine transport in the late Archean, which is consistent with the detrital mineral record ([Johnson et al., 2014](#)).

Detrital siderite has been noted less frequently than detrital pyrite ([Hessler et al., 2004](#); [Rasmussen and Buick, 1999](#)). This difference is perhaps consistent with the fact that Fe(II)-carbonate solid solutions do not precipitate in our weathering models until advanced stages of weathering when carbonate solid solutions contain from about 20 to 100% siderite component ([Fig. 5c and 6c](#)). These results suggest that there are

circumstances in the late Archean where siderite could either form during weathering and/or be stable during weathering and riverine transport, consistent with the detrital mineral record from this period (Hessler and Lowe, 2006; Rasmussen and Buick, 1999).

Reasons for the apparent stability of uraninite during detrital mineral transport in the late Archean have also focused on the kinetics of uraninite dissolution during transport (Grandstaff, 1980; Johnson et al., 2014; Rasmussen and Buick, 1999). However, under the conditions of atmospheric $H_{2,g}$ considered in the present study, it is clear that uraninite is so insoluble that it is stable during riverine transport in the late Archean (Sverjensky and Lee, 2010). This result is consistent with the databases for U concentrations in shales and banded iron formations which show that U was immobile before the Great Oxidation Event (Partin et al., 2013a; Partin et al., 2013b). Overall, it should be emphasized here that we are not suggesting that minerals such as pyrite, siderite, and uraninite were actually in equilibrium with the Archean atmosphere, only that there was no thermodynamic driving force to destroy them during weathering and riverine transportation.

6.3 Paleosols

The depletion of Fe in paleosols was proposed to result from low $O_{2,g}$ levels ($<10^{-4}$ bars) during the Archean because Fe^{2+} is much more soluble than Fe^{3+} (Holland, 1984; Rye and Holland, 1998). This inference is consistent with our model for late Archean weathering (Figs. 5 and 6, and Table 2), which provides a preliminary quantification of the amounts of Fe(II) in aqueous solution and in the mineral weathering products. For the weathering of olivine basalt + calcite, it can be seen in Fig. 5 that most of the Fe(II) is

mobile in the aqueous phase until $\log \xi > -4.0$, after which Fe(II) will be retained in smectite. For the weathering of TTG + calcite, it can be seen in Fig. 6 that Fe(II) is mobile in the aqueous phase until $\log \xi > -4.0$ and simultaneously present as an exchangeable interlayer cation in beidellite. When $\log \xi > -4.0$, Fe(II) is predicted to be retained in siderite-rich carbonate solid solution. The maximum aqueous Fe(II) concentrations are predicted to be about 0.22 mM during weathering of TTG + calcite at $\log \xi = -4.0$ (Table 2).

Siderite, however, is characteristically absent from paleosols - a result that has been used to indicate an upper limit on $p\text{CO}_{2,g}$ of about $10^{-1.4}$ bars at 31 °C (Rye et al., 1995). As noted above, our results with $p\text{CO}_{2,g} = 10^{-1.5}$ bars at 25 °C indicate that siderite should not form until advanced stages of weathering, indicating that the formation of siderite is not just a simple reflection of $p\text{CO}_{2,g}$ values, but is also a function of the extent of weathering. Consequently, the absence of siderite is not particularly informative. Furthermore, Archean paleosols are all altered by diagenesis, metamorphism, and/or metasomatism, suggesting that the absence of siderite from paleosols might also be caused by these later processes, rendering the application of paleosols unpersuasive in constraining $p\text{CO}_{2,g}$ (Winter and Knauth, 1992). Finally, a recent study has suggested that siderite may not be stable at Earth's surface because of photo-oxidation to magnetite by UV radiation on early Earth (Kim et al., 2013).

6.4 Possible connections between haze formation and organic species in near-surface waters

Multiple episodes of organic haze formation in the Neoproterozoic atmosphere (2.7 to 2.5 Ga) have been inferred based on S and C isotopic analyses and atmospheric models (Izon et al., 2015; Zerkle et al., 2012). It has also been suggested that organic compounds could be deposited at the surface from hazes (Trainer et al., 2004; Trainer, 2013) or could form by photo-oxidation of Fe(II)-compounds in early waters (Joe et al., 1986). Our results for late Archean WARW at $p\text{H}_{2,\text{g}} = 10^{-4.0}$ bars (Table 2) suggest that if organic acids were deposited either from hazes or photo-oxidation processes, the aqueous aliphatic acid anions could persist metastably in near-surface waters.

Alternatively, if acetate was not deposited from hazes or photo-oxidation processes, it can be expected that its formation by abiotic processes in the near-surface environment would be kinetically inhibited. Under these circumstances, there would be a thermodynamic driving force for forming species such as acetate, which would have provided favorable conditions for acetogens in the late Archean. If such acetogens flourished, the acetate produced might have survived and been transported in surface waters, providing a food source for methanogens to contribute to the formation of organic hazes in the late Archean (Trainer et al., 2004).

7. Summary and concluding remarks

The present study has focused on using previously proposed Archean atmospheric boundary conditions to model the chemistry of weathering processes on the continents in the late Archean. This effort represents a preliminary step towards building an internally consistent, quantitative picture of the evolution of the near surface environment of early Earth. We carried out theoretical, reaction-path calculations to provide a predictive model

of the chemistry of present-day weathering processes and present-day world-average river water as well as late Archean world-average river water.

Our main conclusions are as follows:

(1) World-average present-day rainwater reacting with basalt + calcite and granite + calcite ($p\text{CO}_{2,g} = 10^{-3.5}$ bars, $p\text{O}_{2,g} = 10^{-0.68}$ bars) produced hematite, kaolinite, smectite, and chalcedony. Destruction of 10^{-4} moles minerals kg^{-1} H_2O resulted in Mg/Na, Ca/Na, and HCO_3^-/Na ratios, and pH values of 8.0 - 8.1 consistent with present-day world-average river water (WARW).

(2) World-average late Archean rainwater weathering olivine basalt + calcite and TTG + calcite ($p\text{CO}_{2,g} = 10^{-1.5}$ bars, $p\text{H}_{2,g} = 10^{-5.0}$ bars) produced kaolinite, Fe(II)-smectite, and chalcedony and waters with much higher concentrations of HCO_3^- and Fe(II) + Mg and a much lower pH of 6.3. The late Archean WARW is predicted to have a lower Ca/Na ratio and much higher Mg/Na and HCO_3^-/Na ratios than present-day WARW. Aqueous Fe(II) can reach concentrations of 0.2 mM during weathering, but can also be stored in clay minerals at advanced stages of weathering, consistent with the apparent mobility of Fe(II) in paleosols, but also suggesting that not all paleosols from the late Archean will record low total Fe contents after advanced stages of weathering.

(3) The late Archean weathering models were applied to further our understanding of the survival of the detrital minerals pyrite, siderite, and uraninite during weathering and riverine transport. Previous studies focused on the kinetics of mineral dissolution. Here we showed that the weathering solutions can easily become supersaturated with respect to pyrite so that there will be no thermodynamic driving force

for dissolution of pyrite in the late Archean, which is consistent with the detrital mineral record. Similar considerations apply to uraninite.

(4) Fe(II)-carbonate solid solutions (20 to 100% siderite component) only precipitate in our late Archean weathering models at fairly advanced stages of weathering. Under these conditions, siderite-rich carbonate might form during weathering or be stable during weathering and riverine transport, consistent with the detrital mineral record from this period. Overall, the formation of siderite reflects $p\text{CO}_{2,\text{g}}$ values and also the extent of weathering.

(5) Late Archean weathering at higher values of atmospheric hydrogen ($p\text{H}_{2,\text{g}} = 10^{-4.0}$ bars) may have favored the accumulation of aqueous organics, such as acetate, suggesting a potential link with recently documented occurrences of organic haze formation. If hazes produced acetate, our models indicate it could have accumulated and persisted in surface waters. Alternatively, the thermodynamic driving force for the formation of acetate indicated by our models may have facilitated the activity of acetogens, generating acetate which might have been used as a food source by methanogens to form organic hazes.

Acknowledgements

This research was supported by a Johns Hopkins Graduate Fellowship (J. H. H.) and the W.M. Keck Foundation (D. A. S. and R. M. H.). We thank the Associate Editor Michael J. Bickle, reviewer Gareth Izon, and an anonymous reviewer for their helpful comments on the manuscript. We gratefully acknowledge the help and support of the Johns Hopkins University and the Geophysical Laboratory of the Carnegie Institution for Science. We also thank R. Z. Tang for help with statistical analysis. We thank P. Heaney, S. D. Domagal-Goldman, M. W. Claire, G. N. Arney, B. Jelen, X. M. Liu, D. F. Strobel, A. Gnanadesikan, and C. Harman for discussions. The authors acknowledge W. Link for invaluable advice on science and life.

References:

- Alfimova, N.A., Novoselov, A.A., Matrenichev, V.A., Souza Filho, C.R. de, 2014. Conditions of subaerial weathering of basalts in the Neoarchean and Paleoproterozoic. *Precambrian Res.* 241, 1–16. doi: 10.1016/j.precamres.2013.09.013
- Anbar, A.D., Duan, Y., Lyons, T.W., Arnold, G.L., Kendall, B., Creaser, R.A., Kaufman, A.J., Gordon, G.W., Scott, C., Garvin, J., Buick, R., 2007. A whiff of oxygen before the Great Oxidation Event? *Science* 317, 1903–1906. doi: 10.1126/Science.1140325
- Beaulieu, E., Godderis, Y., Donnadieu, Y., Labat, D., Roelandt, C., 2012. High sensitivity of the continental-weathering carbon dioxide sink to future climate change. *Nat. Clim. Change.* 2, 346–349. doi: 10.1038/nclimate1419
- Berman, R.G., 1988. Internally-consistent thermodynamic data for minerals in the system $\text{Na}_2\text{O}-\text{K}_2\text{O}-\text{CaO}-\text{MgO}-\text{FeO}-\text{Fe}_2\text{O}_3-\text{Al}_2\text{O}_3-\text{SiO}_2-\text{TiO}_2-\text{H}_2\text{O}-\text{CO}_2$. *J. Petrol.* 29, 445–522. doi: 10.1093/petrology/29.2.445
- Berman, R.G., Aranovich, L.Y., 1996. Optimized standard state and solution properties of minerals. 1. Model calibration for olivine, orthopyroxene, cordierite, garnet, ilmenite in the system $\text{FeO}-\text{MgO}-\text{CaO}-\text{Al}_2\text{O}_3-\text{TiO}_2-\text{SiO}_2$. *Contrib. to Mineral. Petrol.* 126, 1–24. doi: 10.1007/S004100050232
- Berner, E.K., Berner, R.A., 2012. *Global environment: water, air, and geochemical cycles*. Princeton University Press.
- Berner, R.A., 1992. Weathering, plants, and the long-term carbon-cycle. *Geochim. Cosmochim. Acta* 56, 3225–3231. doi: 10.1016/0016-7037(92)90300-8

- Berner, R.A., 2006. Inclusion of the weathering of volcanic rocks in the GEOCARBSULF model. *Am. J. Sci.* 306, 295–302. doi:10.2475/05.2006.01
- Bethke, C., 1996. *Geochemical reaction modeling: concepts and applications*. Oxford University Press New York.
- Bjorlykke, K., Egeberg, P.K., 1993. Quartz cementation in sedimentary basins. *Am. Assoc. Pet. Geol. Bull.* 77, 1538–1548.
- Blake, R.E., Chang, S.J., Lepland, A., 2010. Phosphate oxygen isotopic evidence for a temperate and biologically active Archaean ocean. *Nature* 464, 1029–1032. doi: 10.1038/nature08952
- Blatt, H., Tracy, R.J., Owens, B.E., 2006. *Petrology: igneous, sedimentary, and metamorphic*. Macmillan.
- Bluth, G.J.S., Kump, L.R., 1994. Lithologic and climatologic controls of river chemistry. *Geochim. Cosmochim. Acta* 58, 2341–2359. doi: 10.1016/0016-7037(94)90015-9
- Brantley, S.L., Olsen, A.A., 2014. 7.3 - Reaction kinetics of primary rock-forming minerals under ambient conditions, in: Holland, H.D., Turekian, K.K. (Eds.), *Treatise on Geochemistry (Second Edition)*. Elsevier, Oxford, pp. 69–113. doi: 10.1016/B978-0-08-095975-7.00503-9
- Catalano, J.G., 2013. Thermodynamic and mass balance constraints on iron-bearing phyllosilicate formation and alteration pathways on early Mars. *J. Geophys. Res. Planets* 118, 2124–2136. doi: 10.1002/jgre.20161
- Catling, D.C., Claire, M.W., 2005. How Earth's atmosphere evolved to an oxic state: A status report. *Earth Planet. Sci. Lett.* 237, 1–20. doi: 10.1016/J.Epsl.2005.06.013

- Claire, M.W., Kasting, J.F., Domagal-Goldman, S.D., Stüeken, E.E., Buick, R., Meadows, V.S., 2014. Modeling the signature of sulfur mass-independent fractionation produced in the Archean atmosphere. *Geochim. Cosmochim. Acta* 141, 365–380. doi: 10.1016/j.gca.2014.06.032
- Crowe, S.A., Paris, G., Katsev, S., Jones, C., Kim, S.-T., Zerkle, A.L., Nomosatryo, S., Fowle, D.A., Adkins, J.F., Sessions, A.L., Farquhar, J., Canfield, D.E., 2014. Sulfate was a trace constituent of Archean seawater. *Science* 346, 735–739. doi:10.1126/science.1258966
- Dessert, C., Dupré, B., Gaillardet, J., François, L.M., Allègre, C.J., 2003. Basalt weathering laws and the impact of basalt weathering on the global carbon cycle. *Chem. Geol.* 202, 257–273. doi: 10.1016/j.chemgeo.2002.10.001
- Domagal-Goldman, S.D., Kasting, J.F., Johnston, D.T., Farquhar, J., 2008. Organic haze, glaciations and multiple sulfur isotopes in the Mid-Archean Era. *Earth Planet. Sci. Lett.* 269, 29–40. doi:10.1016/j.epsl.2008.01.040
- Dosseto, A., Vigier, N., Joannes-Boyau, R., Moffat, I., Singh, T., Srivastava, P., 2015. Rapid response of silicate weathering rates to climate change in the Himalaya. *Geochemical Perspect. Lett.* 1, 10–19. doi: 10.7185/geochemlet.1502
- Dupré, B., Dessert, C., Oliva, P., Goddérès, Y., Viers, J., François, L., Millot, R., Gaillardet, J., 2003. Rivers, chemical weathering and Earth's climate. *Comptes Rendus Geosci.* 335, 1141–1160. doi: 10.1016/j.crte.2003.09.015
- Fabre, S., Berger, G., Nédélec, A., 2011. Modeling of continental weathering under high- CO_2 atmospheres during Precambrian times. *Geochemistry, Geophys. Geosystems* 12, 1525–2027. doi:10.1029/2010GC003444

- Farquhar, J., Bao, H., Thiemens, M., 2000. Atmospheric influence of Earth's earliest sulfur cycle. *Science* 289, 756–758. doi:10.1126/science.289.5480.756
- Frei, R., Gaucher, C., Poulton, S.W., Canfield, D.E., 2009. Fluctuations in Precambrian atmospheric oxygenation recorded by chromium isotopes. *Nature* 461, 250–U125. doi: 10.1038/Nature08266
- Frimmel, H.E., 2005. Archaean atmospheric evolution: evidence from the Witwatersrand gold fields, South Africa. *Earth-Science Rev.* 70, 1–46. doi: 10.1016/J.Earscirev.2004.10.003
- Gaillardet, J., Dupré, B., Louvat, P., Allègre, C.J., 1999. Global silicate weathering and CO₂ consumption rates deduced from the chemistry of large rivers. *Chem. Geol.* 159, 3–30. doi: 10.1016/S0009-2541(99)00031-5
- Gaillardet, J., Viers, J., Dupré, B., 2014. 7.7 - Trace elements in river waters, in: *Treatise on Geochemistry (Second Edition)*. Elsevier, Oxford, pp. 195–235. doi: 10.1016/B978-0-08-095975-7.00507-6
- Gíslason, S. R., Arnórsson, S., and Ármannsson, H., 1996. Chemical weathering of basalt in Southwest Iceland: effects of runoff, age of rocks and vegetative/glacial cover. *Am. J. Sci.*, 296, pp. 837-907. doi: 10.2475/ajs.296.8.837
- Gíslason, S.R., Heaney, P.J., Oelkers, E.H., Schott, J., 1997. Kinetic and thermodynamic properties of moganite, a novel silica polymorph. *Geochim. Cosmochim. Acta* 61, 1193–1204. doi: 10.1016/S0016-7037(96)00409-7
- Goddéris, Y., François, L.M., Probst, A., Schott, J., Moncoulon, D., Labat, D., Viville, D., 2006. Modelling weathering processes at the catchment scale: the WITCH

- numerical model. *Geochim. Cosmochim. Acta* 70, 1128–1147. doi:
10.1016/j.gca.2005.11.018
- González-Álvarez, I., Kerrich, R., 2012. Weathering intensity in the Mesoproterozoic and modern large-river systems: a comparative study in the Belt-Purcell Supergroup, Canada and USA. *Precambrian Res.* 208–211, 174–196. doi:
10.1016/j.precamres.2012.04.008
- Grandstaff, D.E., 1980. Origin of uraniferous conglomerates at Elliot Lake, Canada and Witwatersrand, South Africa: implications for oxygen in the Precambrian atmosphere. *Precambrian Res.* 13, 1–26. doi: 10.1016/0301-9268(80)90056-X
- Gregory, D.D., Large, R.R., Halpin, J.A., Baturina, E.L., Lyons, T.W., Wu, S., Danyushevsky, L., Sack, P.J., Chappaz, A., Maslennikov, V. V, Bull, S.W., 2015. Trace element content of sedimentary pyrite in black shales. *Econ. Geol.* 110, 1389–1410. doi:10.2113/econgeo.110.6.1389
- Haqq-Misra, J.D., Domagal-Goldman, S.D., Kasting, P.J., Kasting, J.F., 2008. A revised, hazy methane greenhouse for the Archean Earth. *Astrobiology* 8, 1127–1137. doi:
10.1089/Ast.2007.0197
- Hazen, R.M., Sverjensky, D.A., Azzolini, D., Bish, D.L., Elmore, S.C., Hinnov, L., Milliken, R.E., 2013. Clay mineral evolution. *Am. Mineral.* 98, 2007–2029. doi:
10.2138/Am.2013.4425
- Hazen, R.M., Liu, X.-M., Downs, R.T., Golden, J., Pires, A.J., Grew, E.S., Hystad, G., Estrada, C., Sverjensky, D.A., 2014. Mineral evolution: episodic metallogenesis, the supercontinent cycle, and the coevolving geosphere and biosphere. *Soc. Econ. Geol. Spec. Publ.* 18, 1–15.

- Helgeson, H.C., 1979. Mass transfer among minerals and hydrothermal solutions, in:
Geochemistry of Hydrothermal Ore Deposits (Volume 2). Johns Wiley & Sons, Inc.,
pp. 568–610.
- Hessler, A.M., Lowe, D.R., 2006. Weathering and sediment generation in the Archean:
an integrated study of the evolution of siliciclastic sedimentary rocks of the 3.2 Ga
Moodies Group, Barberton greenstone belt, South Africa. *Precambrian Res.* 151,
185–210. doi: 10.1016/J.Precamres.2006.08.008
- Hessler, A.M., Lowe, D.R., Jones, R.L., Bird, D.K., 2004. A lower limit for atmospheric
carbon dioxide levels 3.2 billion years ago. *Nature* 428, 736–738. doi:
10.1038/Nature02471
- Holland, H.D., 1984. The chemical evolution of the atmosphere and oceans. Princeton
University Press.
- Huang, J., Chu, X., Lyons, T.W., Planavsky, N.J., Wen, H., 2013. A new look at saponite
formation and its implications for early animal records in the Ediacaran of South
China. *Geobiology* 11, 3–14. doi:10.1111/gbi.12018
- Izon, G., Zerkle, A.L., Zhelezinskaia, I., Farquhar, J., Newton, R.J., Poulton, S.W.,
Eigenbrode, J.L., Claire, M.W., 2015. Multiple oscillations in Neoarchaeon
atmospheric chemistry. *Earth Planet. Sci. Lett.* 431, 264–273. doi:
10.1016/j.epsl.2015.09.018
- Joe, H., Kuma, K., Paplawsky, W., Rea, B., Arrhenius, G., 1986. Abiotic photosynthesis
from ferrous carbonate (siderite) and water. *Orig. Life Evol. Biosph.* 16, 369–370.
doi: 10.1007/Bf02422078

- Johnson, J.E., Gerpheide, A., Lamb, M.P., Fischer, W.W., 2014. O₂ constraints from Paleoproterozoic detrital pyrite and uraninite. *Geol. Soc. Am. Bull.* doi:10.1130/B30949.1
- Kasting, J.F., 2014. 6.6 - Modeling the Archean atmosphere and climate, in: Holland, H.D., Turekian, K.K. (Eds.), *Treatise on Geochemistry (Second Edition)*. Elsevier, Oxford, pp. 157–175. doi: 10.1016/B978-0-08-095975-7.01306-1
- Kim, J.D., Yee, N., Nanda, V., Falkowski, P.G., 2013. Anoxic photochemical oxidation of siderite generates molecular hydrogen and iron oxides. *Proc. Natl. Acad. Sci.* 110, 10073–10077. doi: 10.1073/Pnas.1308958110
- Knauth, L.P., 2005. Temperature and salinity history of the Precambrian ocean: implications for the course of microbial evolution. *Palaeogeogr. Palaeoclimatol. Palaeoecol.* 219, 53-69. doi: 10.1016/j.palaeo.2004.10.014
- Konhauser, K.O., Robbins, L.J., Pecoits, E., Peacock, C., Kappler, A., Lalonde, S. V., 2015. The Archean nickel famine revisited. *Astrobiology* 15, 804–815. doi:10.1089/ast.2015.1301
- Kump, L.R., Brantley, S.L., Arthur, M.A., 2000. Chemical weathering, atmospheric CO₂, and climate. *Annu. Rev. Earth Planet. Sci.* 28, 611–667. doi:10.1146/annurev.earth.28.1.611
- Kurzweil, F., Claire, M., Thomazo, C., Peters, M., Hannington, M., Strauss, H., 2013. Atmospheric sulfur rearrangement 2.7 billion years ago: evidence for oxygenic photosynthesis. *Earth Planet. Sci. Lett.* 366, 17-26. doi: 10.1016/j.epsl.2013.01.028

- Lafon, G.M., Mackenzie, F.T., 1974. Early evolution of the oceans—a weathering model, in: *Studies in Paleo-Oceanography*. SEPM Society for Sedimentary Geology, pp. 205–218. doi:10.2110/pec.74.20.0205
- Large, R.R., Halpin, J.A., Danyushevsky, L. V, Maslennikov, V. V, Bull, S.W., Long, J.A., Gregory, D.D., Lounejeva, E., Lyons, T.W., Sack, P.J., McGoldrick, P.J., Calver, C.R., 2014. Trace element content of sedimentary pyrite as a new proxy for deep-time ocean–atmosphere evolution. *Earth Planet. Sci. Lett.* 389, 209–220. doi: 10.1016/j.epsl.2013.12.020
- Lasaga, A.C., Soler, J.M., Ganor, J., Burch, T.E., Nagy, K.L., 1994. Chemical weathering rate laws and global geochemical cycles. *Geochim. Cosmochim. Acta* 58, 2361–2386. doi: 10.1016/0016-7037(94)90016-7
- Luo, G., Ono, S., Beukes, N.J., Wang, D.T., Xie, S., Summons, R.E., 2016. Rapid oxygenation of Earth’s atmosphere 2.33 billion years ago. *Sci. Adv.* 2:. doi: 10.1126/sciadv
- Lyons, T.W., Reinhard, C.T., Planavsky, N.J., 2014. The rise of oxygen in Earth’s early ocean and atmosphere. *Nature* 506, 307–315. doi: 10.1038/Nature13068
- Maher, K., 2010. The dependence of chemical weathering rates on fluid residence time. *Earth Planet. Sci. Lett.* 294, 101–110. doi: 10.1016/j.epsl.2010.03.010
- Maher, K., Steefel, C.I., White, A.F., Stonestrom, D.A., 2009. The role of reaction affinity and secondary minerals in regulating chemical weathering rates at the Santa Cruz Soil Chronosequence, California. *Geochim. Cosmochim. Acta* 73, 2804–2831. doi: 10.1016/j.gca.2009.01.030

- Manning, C.E., Shock, E.L., Sverjensky, D.A., 2013. The chemistry of carbon in aqueous fluids at crustal and upper-mantle conditions: experimental and theoretical constraints. *Carbon in Earth* 75, 109–148. doi: 10.2138/Rmg.2013.75.5
- Meybeck, M., 1987. Global chemical weathering of surficial rocks estimated from river dissolved loads. *Am. J. Sci.* 287, 401–428. doi:10.2475/ajs.287.5.401
- Ohmoto, H., Watanabe, Y., Kumazawa, K., 2004. Evidence from massive siderite beds for a CO₂-rich atmosphere before, 1.8 billion years ago. *Nature* 429, 395–399. doi: 10.1038/Nature02573
- Oliva, P., Dupré, B., Martin, F., Viers, J., 2004. The role of trace minerals in chemical weathering in a high-elevation granitic watershed (Estibère, France): chemical and mineralogical evidence¹. *Geochim. Cosmochim. Acta* 68, 2223–2243. doi: 10.1016/j.gca.2003.10.043
- Partin, C.A., Bekker, A., Planavsky, N.J., Scott, C.T., Gill, B.C., Li, C., Podkovyrov, V., Maslov, A., Konhauser, K.O., Lalonde, S. V, Love, G.D., Poulton, S.W., Lyons, T.W., 2013. Large-scale fluctuations in Precambrian atmospheric and oceanic oxygen levels from the record of U in shales. *Earth Planet. Sci. Lett.* 369–370, 284–293. doi: 10.1016/j.epsl.2013.03.031
- Partin, C.A., Lalonde, S. V, Planavsky, N.J., Bekker, A., Rouxel, O.J., Lyons, T.W., Konhauser, K.O., 2013. Uranium in iron formations and the rise of atmospheric oxygen. *Chem. Geol.* 362, 82–90. doi: 10.1016/j.chemgeo.2013.09.005
- Rasmussen, B., Buick, R., 1999. Redox state of the Archean atmosphere: evidence from detrital heavy minerals in ca. 3250–2750 Ma sandstones from the Pilbara Craton,

- Australia. *Geology* 27, 115–118. doi:10.1130/0091-7613(1999)027<0115:rsotaa>2.3.co;2
- Robert, F., Chaussidon, M., 2006. A palaeotemperature curve for the Precambrian oceans based on silicon isotopes in cherts. *Nature* 443, 969–972. doi: 10.1038/nature05239
- Rosing, M.T., Bird, D.K., Sleep, N.H., Bjerrum, C.J., 2010. No climate paradox under the faint early Sun. *Nature* 464, 744–U117. doi: 10.1038/Nature08955
- Rudnick, R.L., Gao, S., 2003. 3.01 - Composition of the continental crust, in: *Treatise on Geochemistry*. Pergamon, Oxford, pp. 1–64. doi: 10.1016/B0-08-043751-6/03016-4
- Rye, R., Holland, H.D., 1998. Paleosols and the evolution of atmospheric oxygen: a critical review. *Am. J. Sci.* 298, 621–672. doi: 10.2475/ajs.298.8.621
- Rye, R., Kuo, P.H., Holland, H.D., 1995. Atmospheric carbon dioxide concentrations before 2.2-billion years ago. *Nature* 378, 603–605. doi: 10.1038/378603a0
- Schmitt, J.M., 1999. Weathering, rainwater and atmosphere chemistry: example and modelling of granite weathering in present conditions in a CO₂-rich, and in an anoxic palaeoatmosphere, in: *Palaeoweathering, Palaeosurfaces and Related Continental Deposits: Special Publication of the IAS. The International Association of Sedimentologists.*, pp. 21–41.
- Schoonen, M.A.A., Barnes, H.L., 1991. Reactions forming pyrite and marcasite from solution: I. Nucleation of FeS₂ below 100°C. *Geochim. Cosmochim. Acta* 55, 1495–1504. doi: 10.1016/0016-7037(91)90122-L
- Sheldon, N.D., 2006. Precambrian paleosols and atmospheric CO₂ levels. *Precambrian Res.* 147, 148–155. doi: 10.1016/J.Precamres.2006.02.004

- Shields, G.A., Kasting, J.F., 2007. Palaeoclimatology: evidence for hot early oceans? *Nature* 447, E1. doi: 10.1038/nature05830
- Shock, E.L., Sassani, D.C., Willis, M., Sverjensky, D.A., 1997. Inorganic species in geologic fluids: correlations among standard molal thermodynamic properties of aqueous ions and hydroxide complexes. *Geochim. Cosmochim. Acta* 61, 907–950. doi: 10.1016/S0016-7037(96)00339-0
- Siever, R., 1992. The silica cycle in the Precambrian. *Geochim. Cosmochim. Acta* 56, 3265–3272. doi: 10.1016/0016-7037(92)90303-Z
- Steinmann, P., Lichtner, P.C., Shotyk, W., 1994. Reaction-path approach to mineral weathering reactions. *Clays Clay Miner.* 42, 197–206. doi: 10.1346/Ccmn.1994.0420210
- Stüeken, E.E., Buick, R., Anbar, A.D., 2015. Selenium isotopes support free O₂ in the latest Archean. *Geology* 43, 259–263. doi: 10.1130/g36218.1
- Sverjensky, D.A., 1984. Oil-field brines as ore-forming solutions. *Econ. Geol.* 79, 23–37. doi: 10.2113/gsecongeo.79.1.23
- Sverjensky, D.A., Hemley, J.J., Dangelo, W.M., 1991. Thermodynamic assessment of hydrothermal alkali feldspar-mica-aluminosilicate equilibria. *Geochim. Cosmochim. Acta* 55, 989–1004. doi: 10.1016/0016-7037(91)90157-Z
- Sverjensky, D.A., Lee, N., 2010. The Great Oxidation Event and mineral diversification. *Elements* 6, 31–36. doi: 10.2113/Gselements.6.1.31
- Sverjensky, D.A., Molling, P.A., 1992. A linear free-energy relationship for crystalline solids and aqueous ions. *Nature* 356, 231–234. doi: 10.1038/356231a0

- Taylor, S.R., McLennan, S., 2009. Planetary crusts: their composition, origin and evolution. Cambridge University Press.
- Trainer, M.G., Pavlov, A.A., Curtis, D.B., McKay, C.P., Worsnop, D.R., Delia, A.E., Toohey, D.W., Toon, O.B., Tolbert, M.A., 2004. Haze aerosols in the atmosphere of early Earth: Manna from heaven. *Astrobiology* 4: 409-419.
doi:10.1089/ast.2004.4.409.
- Trainer, M.G., 2013. Atmospheric prebiotic chemistry and organic hazes. *Curr. Org. Chem.* 17, 1710–1723. doi: 10.2174/13852728113179990078
- Treiman, A.H., Morris, R. V, Agresti, D.G., Graff, T.G., Achilles, C.N., Rampe, E.B., Bristow, T.F., Ming, D.W., Blake, D.F., Vaniman, D.T., Bish, D.L., Chipera, S.J., Morrison, S.M., Downs, R.T., 2014. Ferrian saponite from the Santa Monica Mountains (California, U.S.A., Earth): characterization as an analog for clay minerals on Mars with application to Yellowknife Bay in Gale Crater. *Am. Mineral.* 99, 2234–2250. doi:10.2138/am-2014-4763
- Vidal, O., Dubacq, B., 2009. Thermodynamic modelling of clay dehydration, stability and compositional evolution with temperature, pressure and H₂O activity. *Geochim. Cosmochim. Acta* 73, 6544–6564. doi: 10.1016/J.Gca.2009.07.035
- Violette, A., Godd  ris, Y., Mar  chal, J.-C., Riotte, J., Oliva, P., Kumar, M.S.M., Sekhar, M., Braun, J.-J., 2010. Modelling the chemical weathering fluxes at the watershed scale in the Tropics (Mule Hole, South India): Relative contribution of the smectite/kaolinite assemblage versus primary minerals. *Chem. Geol.* 277, 42–60.
doi: 10.1016/j.chemgeo.2010.07.009

- von Paris, P., Rauer, H., Lee Grenfell, J., Patzer, B., Hedelt, P., Stracke, B., Trautmann, T., Schreier, F., 2008. Warming the early earth—CO₂ reconsidered. *Planet. Space Sci.* 56, 1244–1259. doi: 10.1016/j.pss.2008.04.008
- West, A.J., Galy, A., Bickle, M., 2005. Tectonic and climatic controls on silicate weathering. *Earth Planet. Sci. Lett.* 235, 211–228. doi: 10.1016/j.epsl.2005.03.020
- White, A.F., Buss, H.L., 2014. 7.4 - Natural weathering rates of silicate minerals, in: *Treatise on Geochemistry (Second Edition)*. Elsevier, Oxford, pp. 115–155. doi: 10.1016/B978-0-08-095975-7.00504-0
- Wilson, M.J., 2013. *Sheet Silicates: Clay Minerals*, 2nd ed, *GSL Rock-Forming Minerals*. The Geological Society.
- Winter, B.L., Knauth, L.P., 1992. Stable isotope geochemistry of cherts and carbonates from the 2.0 Ga gunflint iron formation: implications for the depositional setting, and the effects of diagenesis and metamorphism. *Precambrian Res.* 59, 283–313. doi: 10.1016/0301-9268(92)90061-R
- Wolery, T.J., 1992. EQ3/6: A software package for geochemical modeling of aqueous systems: package overview and installation guide (version 7.0). Lawrence Livermore National Laboratory Livermore, CA.
- Zerkle, A.L., Claire, M., Domagal-Goldman, S.D., Farquhar, J., Poulton, S.W., 2012. A bistable organic-rich atmosphere on the Neoarchaeon Earth. *Nat. Geosci.* 5, 359–363. doi:10.1038/ngeo1425
- Zhu, C., 2009. Geochemical modeling of reaction paths and geochemical reaction networks. *Rev. Mineral. Geochemistry* 70, 533–569. doi:10.2138/rmg.2009.70.12

Table 1. Summary of the compositions adopted for world-average present day rainwater (Berner and Berner, 2012) and late Archean rainwater (see text). Full details of the aqueous speciation of all the elements are given in the initial step of the model weathering results.

Present-day rainwater	Parameter value ^a	Most Abundant Species	Parameter value ^a
Na	0.15	Na ⁺	0.15
K	5.1×10^{-3}	K ⁺	5.1×10^{-3}
Mg	0.021	Mg ²⁺	0.019
Ca	7.5×10^{-3}	Ca ²⁺	7.4×10^{-3}
Fe	8.3×10^{-15}	Fe ³⁺	5.4×10^{-15}
Al	5.7×10^{-7}	Al(OH) ₄ ⁻	3.2×10^{-7}
Si	6.6×10^{-3}	SiO _{2,aq}	6.6×10^{-3}
Cl	0.17	Cl ⁻	0.17
S	0.021	SO ₄ ²⁻	0.021
C	0.015	CO _{2,aq}	0.011
N	5.5×10^{-4}	NO ₃ ⁻	5.5×10^{-4}
pH	5.85	H ⁺	1.4×10^{-3}
log <i>p</i> O _{2,g}	-0.68	O _{2,aq}	0.26
log <i>p</i> H _{2,g}	-41	H _{2,aq}	4.8×10^{-42}
log <i>p</i> CO _{2,g}	-3.5	CO _{2,aq}	0.011
Late Archean rainwater			
Na	0.15	Na ⁺	0.15
K	5.1×10^{-3}	K ⁺	5.1×10^{-3}
Mg	0.021	Mg ²⁺	0.021
Ca	7.5×10^{-3}	Ca ²⁺	7.5×10^{-3}
Fe	9.0×10^{-3}	Fe ²⁺	8.9×10^{-3}
Al	6.5×10^{-6}	Al(OH) ₃ ²⁺	3.5×10^{-7}
Si	6.6×10^{-3}	SiO _{2,aq}	6.6×10^{-3}
Cl	0.17	Cl ⁻	0.17
S	1.0×10^{-4}	H ₂ S _{aq}	1.0×10^{-4}
C	1.2	CO _{2,aq}	1.1
N	5.5×10^{-4}	NH ₄ ⁺	5.5×10^{-4}
pH	5.15	H ⁺	7.1×10^{-3}
log <i>p</i> H _{2,g}	-5.0	H _{2,aq}	7.8×10^{-6}
log <i>p</i> O _{2,g}	-73	O _{2,aq}	1.0×10^{-73}
log <i>p</i> CO _{2,g}	-1.5	CO _{2,aq}	1.1

^a. Concentrations of dissolved elements given in millimolar (mM).

Table 2. Major constituents of fluids from present-day weathering of basalt or granite plus calcite and Archean weathering of olivine basalt or TTG plus calcite (at $\log \xi = -4.0$) compared with modern and Archean world-average river water (WARW).

Present-day ^a	Basalt	Granite	Predicted WARW ^b	WARW ^c
Na	0.182	0.211	0.192	0.224
K	0.0051	0.305	0.105	0.033
Ca	0.242	0.107	0.197	0.335
Mg	0.053	0.086	0.064	0.136
Si	0.192	0.189	0.191	0.174
Total C	0.567	0.692	0.609	0.853
Cl-	0.169	0.169	0.169	0.162
Total S (SO ₄ ²⁻)	0.021	0.021	0.021	0.086
Mg/Na	0.29	0.41	0.33	0.61
Ca/Na	1.33	0.50	1.05	1.50
HCO ₃ ⁻ /Na	2.91	3.07	2.96	3.81
pH	8.04	8.13		6.5 to 8 ^d
Archean	Olivine Basalt	TTG	Archean WARW ^e , reference condition	Archean WARW ^e , higher $p\text{H}_{2,\text{g}}$ condition
$\log p\text{H}_{2,\text{g}}$	-5.0	-5.0	-5.0	-4.0
Na	0.182	0.216	0.187	0.191
K	0.0051	0.205	0.0331	0.0331
Ca	0.242	0.131	0.226	0.226
Mg	0.207	0.0929	0.191	0.191
Fe(II)	0.099	0.224	0.112	0.163
Si	0.187	0.187	0.187	0.187
Total C	2.24	2.27	2.24	3.19 ^f
Cl-	0.169	0.169	0.169	0.169
Mg/Na	1.14	0.43	1.04	1.00
Ca/Na	1.13	0.61	1.06	1.19
Fe(II)/Na	0.54	1.04	0.61	0.85
HCO ₃ ⁻ /Na	5.81	5.04	5.70	3.02
pH	6.34	6.35	6.34	6.04

^a All concentrations given in millimolar (mM).

^b Assuming 2/3 basalt + calcite water mixed with 1/3 granite + calcite water.

^c Berner and Berner (2012).

^d Gaillardet et al. (2014).

^e Mixing of waters derived from weathering of olivine basalt + calcite and TTG + calcite in the proportions of 5/6 and 1/6, respectively.

^f Includes: 1.12 mM CO_{2(aq)}, 0.577 mM HCO₃⁻, 0.509 mM CH₃COO⁻, 0.133 mM CH₃CH₂COO⁻.

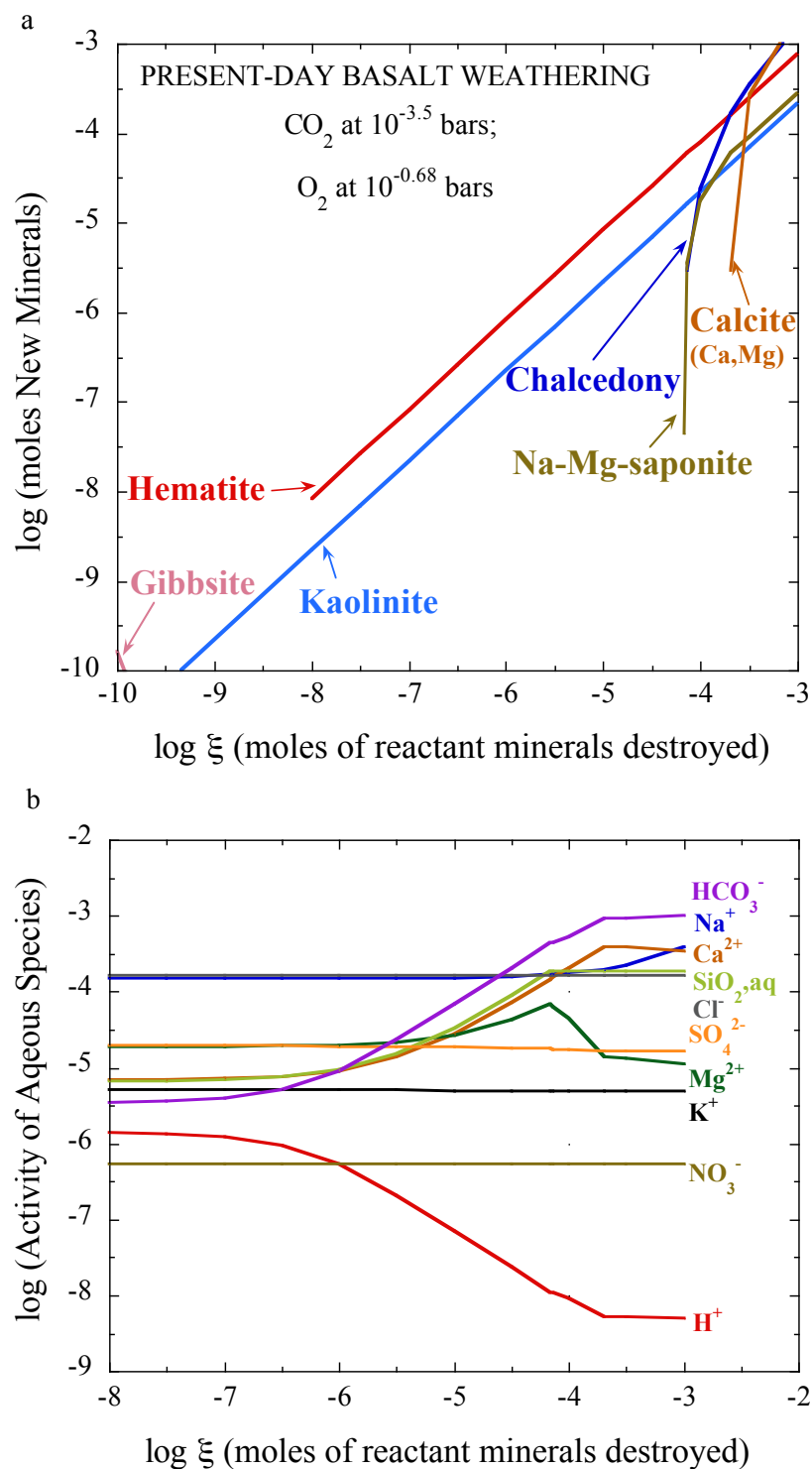


Figure 1. Modeling results of basaltic weathering under present-day atmospheric conditions. In (a) and (b), the logarithm of the number of moles of new minerals produced and the activity of the aqueous species during the weathering reactions are plotted as functions of the logarithm of reaction progress ξ (the number of moles of reactant minerals destroyed $\text{kg}^{-1} \text{H}_2\text{O}$).

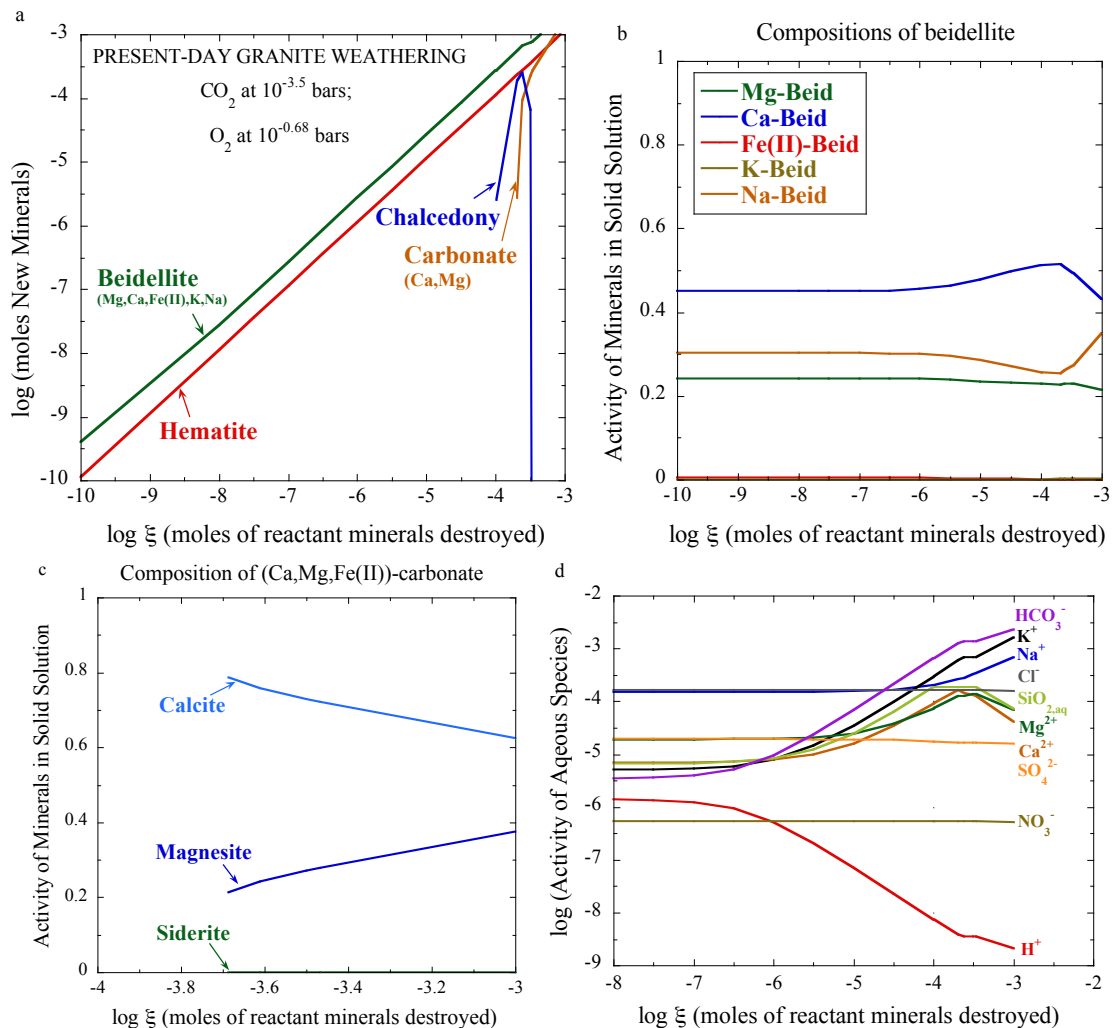


Figure 2. Modeling results of granitic weathering under present-day atmospheric conditions. In (a) and (d), the logarithm of the number of moles of new minerals produced and the activity of the aqueous species during the weathering reactions are plotted as functions of the logarithm of reaction progress ξ (the number of moles of reactant minerals destroyed $\text{kg}^{-1} \text{H}_2\text{O}$). In (b) and (c), the activity of end members in beidellite and carbonate solid solution is plotted as functions of the reaction progress.

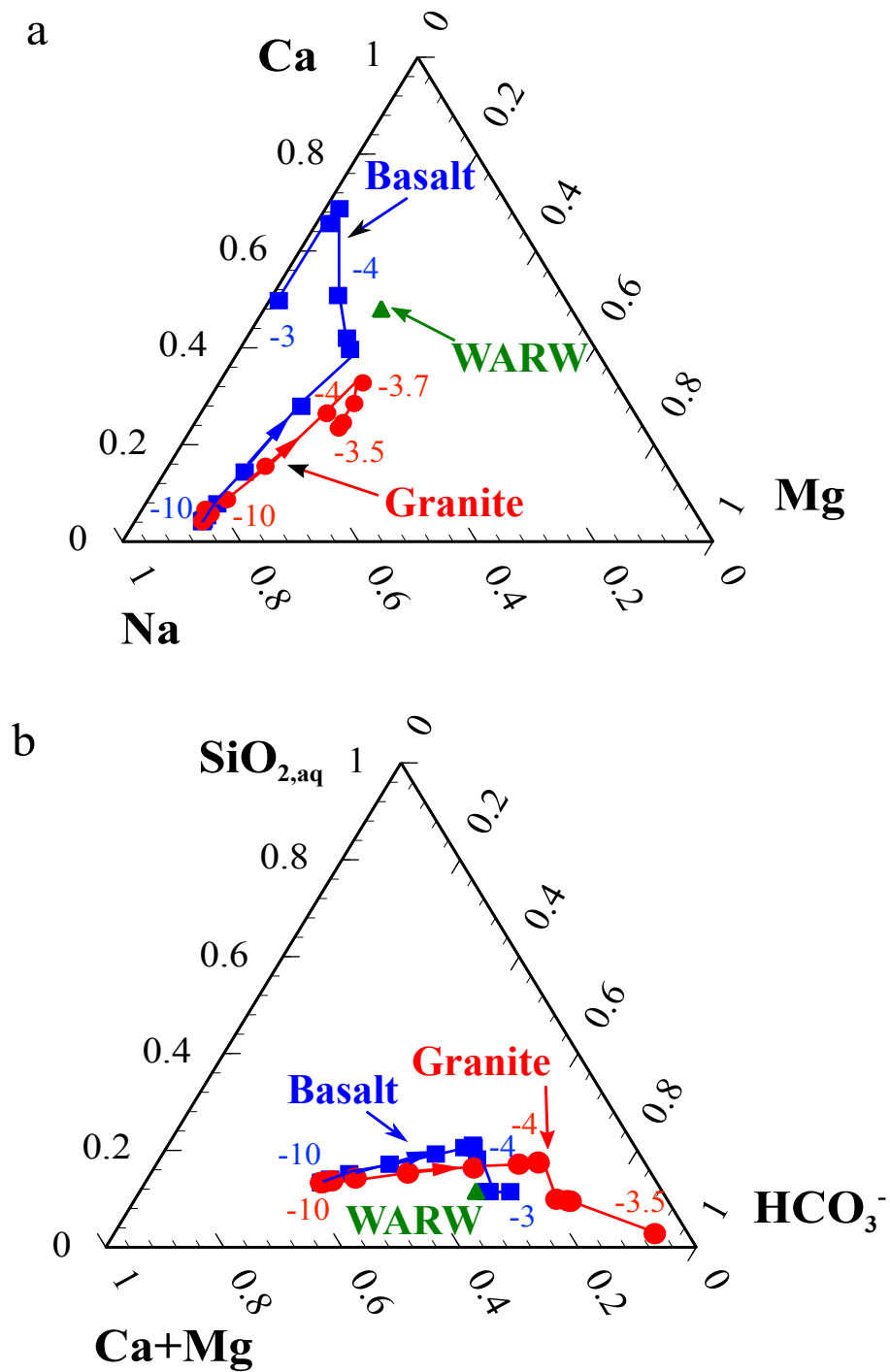


Figure 3. Predicted river water chemistry during present-day weathering of basalt and granite plus calcite compared with present-day world-average river water (WARW) composition.

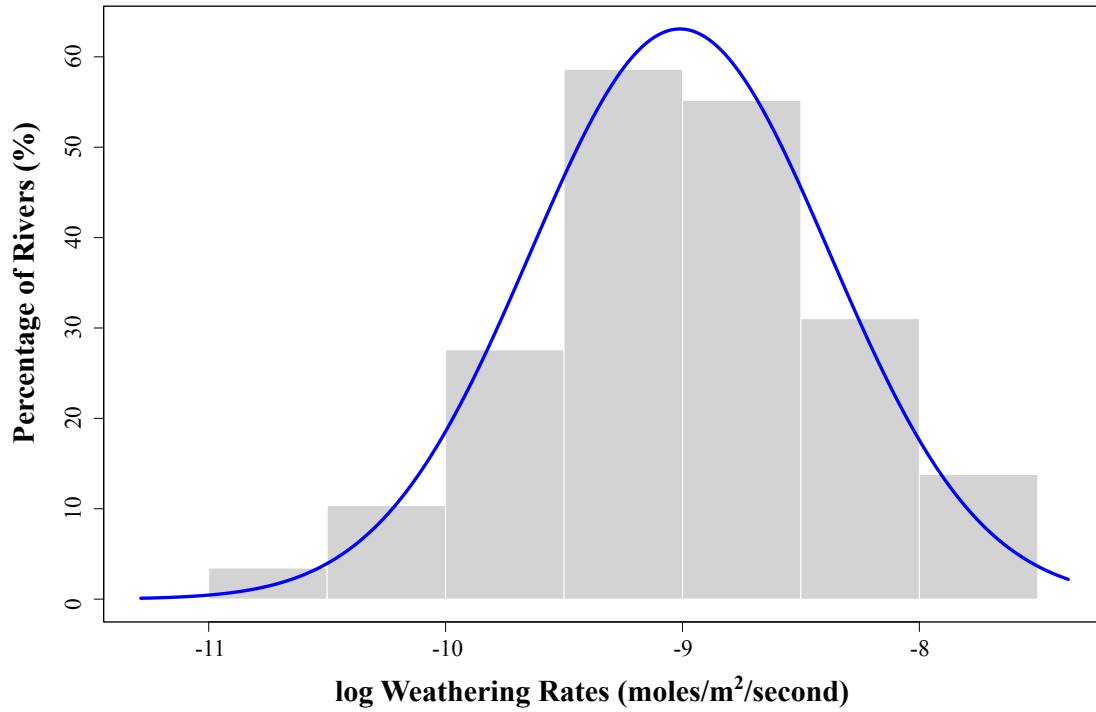


Figure 4. The distribution of weathering rates calculated with riverine runoff and dissolved Si concentration. Data are from 55 large globally distributed rivers, compiled by [Gaillardet et al. \(1999\)](#). The calculation assumed:

$$\text{Weathering rates (moles/(m}^2\text{*second))} = \text{Silica concentration (moles/l) * Runoff (l H}_2\text{O/(m}^2\text{*second))}$$

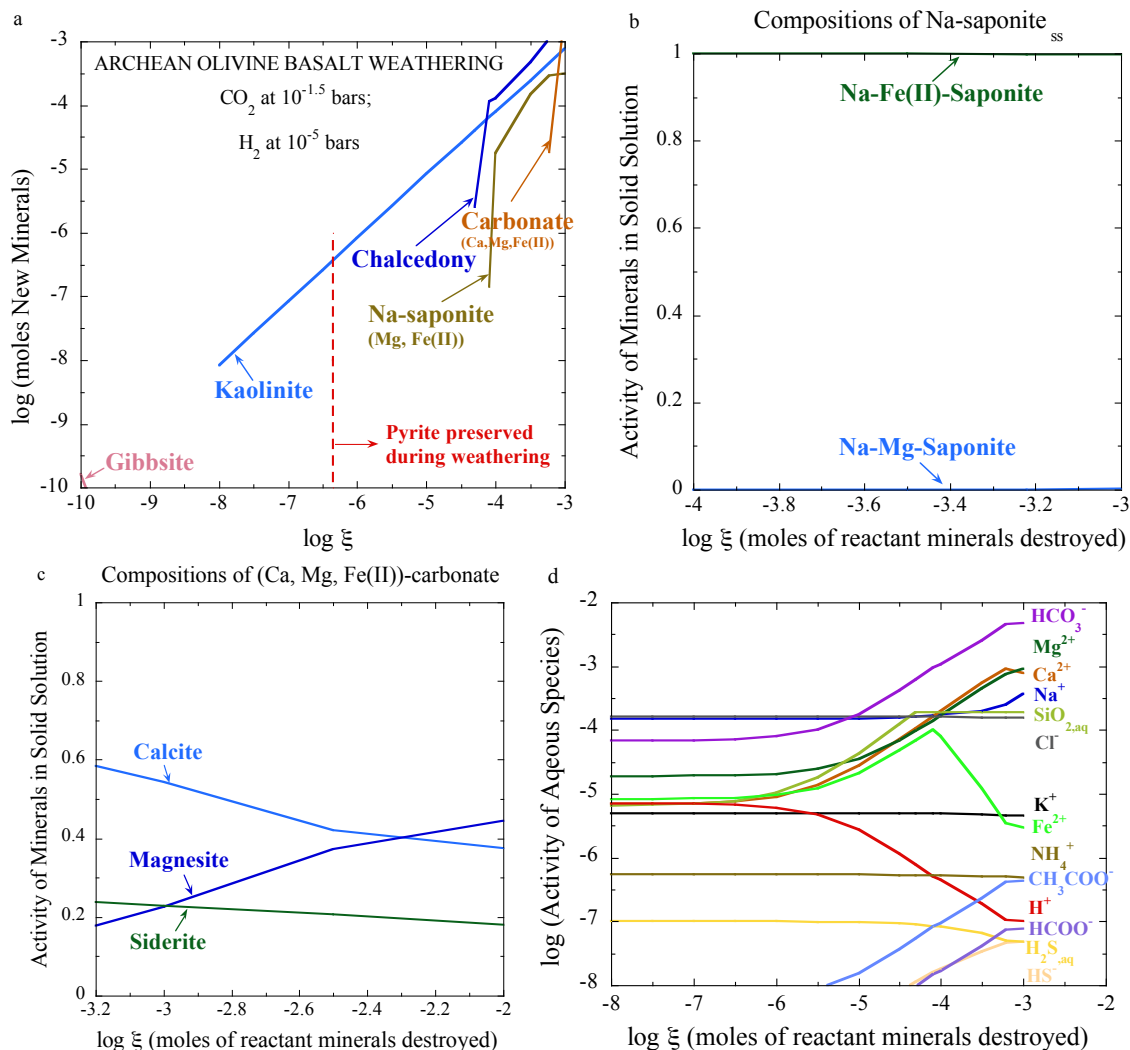


Figure 5. Modeling results of olivine-basaltic weathering under Archean atmospheric conditions. In (a) and (d), the logarithm of the number of moles of new minerals produced and the activity of the aqueous species during the weathering reactions are plotted as functions of the logarithm of reaction progress ξ (the number of moles of reactant minerals destroyed $\text{kg}^{-1} \text{H}_2\text{O}$). In (b) and (c), the activity of end members in solid solutions is plotted as functions of the reaction progress.

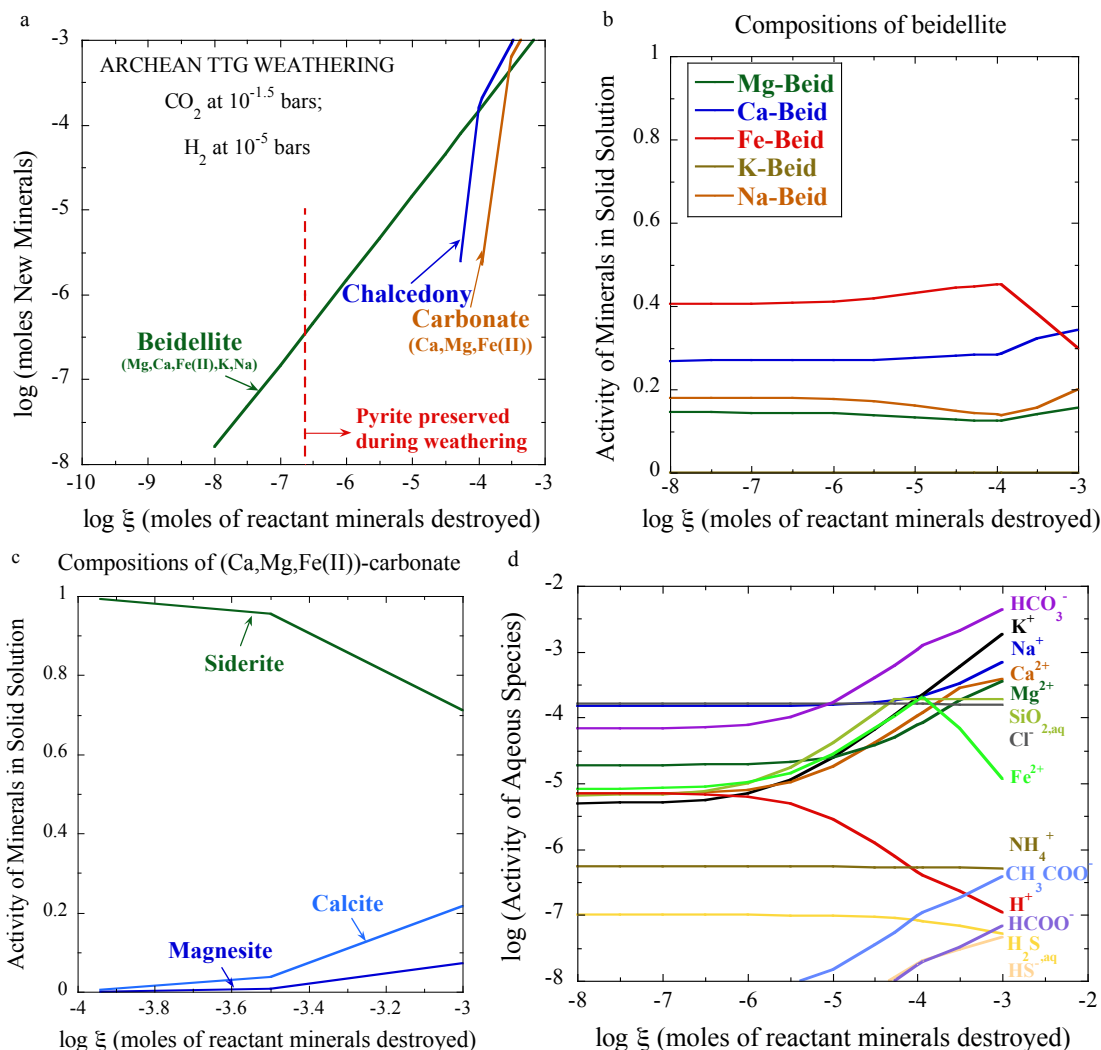


Figure 6. Modeling results of trondjemite-tonalite-granodiorite (TTG) weathering under Archean atmospheric conditions. In (a) and (d), the logarithm of the number of moles of new minerals produced and the activity of the aqueous species during the weathering reactions are plotted as functions of the logarithm of reaction progress ξ (the number of moles of reactant minerals destroyed $\text{kg}^{-1} \text{H}_2\text{O}$). In (b) and (c), the activity of end members in solid solutions is plotted as functions of the reaction progress. Notice the variation in the scale of the horizontal axis.

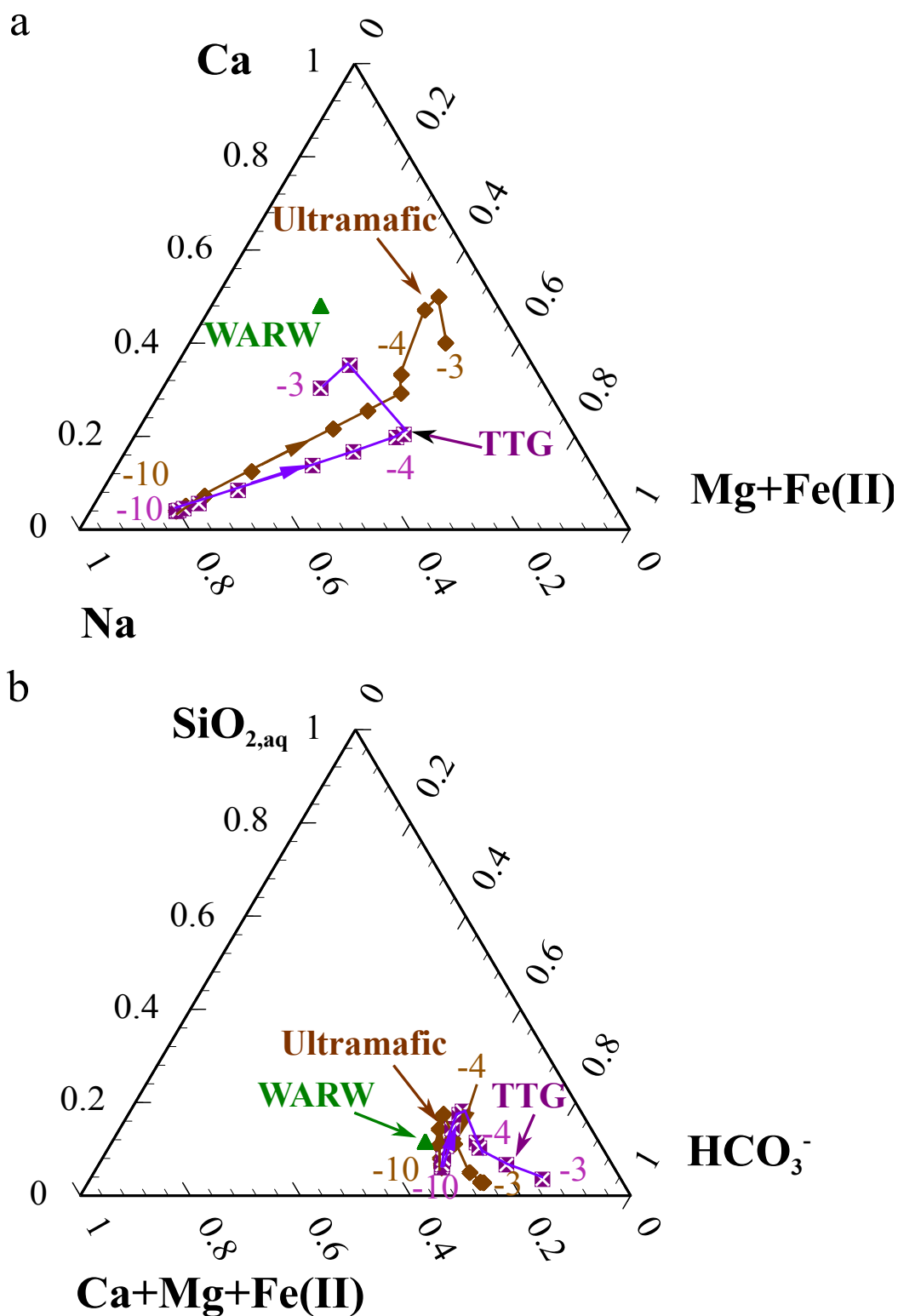


Figure 7. Predicted river water chemistry during Archean weathering of olivine basalt and TTG plus calcite compared with present-day world-average river water (WARW) composition.

Chapter 5

Mobility of nutrients and trace metals during weathering in the late Archean

The evolution of the geosphere and biosphere depends on the availability of bio-essential nutrients and trace metals. Consequently, the chemical and isotopic variability of trace elements in the sedimentary record have been widely used to infer the existence of early life and fluctuations in the near-surface environment on the early Earth, particularly fluctuations in the redox state of the atmosphere. In this study, we applied late Archean weathering models ([Hao et al., 2017](#)), developed to estimate the behavior of major elements and the composition of late Archean world average river water (WARW), to explore the behavior of nutrient and trace metals and their potential for riverine transport. We focused on P, Mn, Cr, and Cu during the weathering of olivine basalt.

In our standard late Archean weathering model ($p\text{CO}_{2,\text{g}} = 10^{-1.5}$ bars, $p\text{H}_{2,\text{g}} = 10^{-5.0}$ bars), crustal apatite was totally dissolved by the acidic rainwater during weathering. Our model quantitatively links the $p\text{CO}_{2,\text{g}}$ of the atmosphere to phosphate levels transported by rivers. The development of late Archean WARW (pH = 6.4) resulted in riverine phosphate of at least 1.7 μmolar , much higher than at the present-day. At the end of the early Proterozoic snowball Earth event when $p\text{CO}_{2,\text{g}}$ was at least 0.12 bars, WARW (pH = 5.7) may have transported up to 70 μmolar phosphate, depending on the availability of

apatite, thereby stimulating high levels of oxygenic photosynthesis in the marine environment.

Crustal levels of Mn in olivine dissolved completely during weathering, except at large extents of weathering where Mn was stored as a component of a secondary carbonate mineral. The corresponding Mn content of WARW, about 1.2 μmolar , is higher than in modern WARW. Whiff of 10^{-5} mole $\text{O}_{2,\text{g}}$ or $\text{HNO}_3 \text{ kg}^{-1} \text{ H}_2\text{O}$ resulted in the formation of $\text{MnO}_{2,\text{cr}}$ and abundant hematite and simultaneous dramatic decreases in the concentration of Mn(II) in the WARW.

Chromite dissolution resulted in negligible dissolved Cr in WARW. However, $\text{Cr}(\text{OH})_{3,\text{am}}$ representing easily weatherable Cr-bearing minerals dissolved totally during the weathering, resulting in concentrations of Cr(III) in the WARW of up to 0.14 μmolar , higher than at the present-day.

Late Archean weathering of accessory chalcopyrite produced chalcocite and bornite, and extremely low concentrations of Cu (about 3.2×10^{-16} molar) because of the low solubilities of the copper sulfides. However, pulses of either $\text{O}_{2,\text{g}}$ or HNO_3 produced native copper, chalcocite, and bornite, much more hematite, and WARW containing levels of dissolved Cu comparable to the present-day. Copper mineralogy predicted by weathering models might provide a new correlation with evidence from studies of copper mineral evolution.

Overall, our results implied that the redox state of the atmosphere, the pH of surface waters, and the availability of easily-weathered minerals are all important factors controlling the dissolution of trace elements in river water. Interpretation of the

sedimentary signatures of trace elements should consider not only the redox state but also the pH and availability of accessory minerals.

This paper will be submitted to Earth and Planetary Science Letters

Authors: Jihua Hao, Dimitri A. Sverjensky, and Robert M. Hazen

1. Introduction

The availability of bio-essential nutrients and trace metals in the surface environment were critical factors for the origin and evolution of life throughout Earth history (Anbar, 2008; Anbar & Knoll, 2002; Morel, 2008; Pasek et al., 2015; Saito et al., 2003; Williams et al., 2003; Zerkle et al., 2006). However, large uncertainties exist in estimation of the levels of nutrients and trace elements. For example, in the case of phosphate, Archean productivity was first thought to be limited by low dissolved phosphate in the seawater due to adsorption onto iron oxides deposited as banded iron formations (Bjerrum and Canfield, 2002), but in a subsequent study it was pointed out that the high concentration of dissolved silica expected in Archean seawater would effectively block phosphate adsorption sites on iron oxides and therefore dissolved phosphate might be higher than previously suggested (Konhauser et al., 2007; Planavsky et al., 2010). Such disputes mainly focused on the removal of phosphate from seawater and did not address the important role of weathering and riverine transport, which was the dominant influx of phosphate to the early oceans. The importance of this role has been emphasized for the Phanerozoic (Guidry and Mackenzie, 2000). Here we apply recent developments in the modeling of late Archean weathering and river water chemistry (Hao et al., 2017) that can be applied to simulate the dissolution of phosphate minerals and riverine transport of dissolved phosphate under late Archean atmospheric conditions.

In the case of trace metals, the redox-sensitive trace metals, such as Cr, Cu, U, Mo, and Re, and their isotopic fractionations recorded in various sedimentary records are now widely used to infer fluctuations in the redox history of Earth's surface environment

(Anbar and Rouxel, 2007; Farquhar et al., 2014; Tribovillard et al., 2006). The atmosphere before the Great Oxidation Event (GOE) is widely accepted to have been anoxic with a relatively high $p\text{H}_{2,\text{g}}$. Consequently, during normal weathering processes in the late Archean, elements such as Cr, Cu, U, Mo, and Re would have been immobile, and the solubilities of Fe and Mn would have been much higher than in present-day surface waters. However, recent studies reported enrichments of several trace metals (e.g. Mo, Re, Cr) and variability of isotopic fractionations in some sedimentary records that have been interpreted as evidence of “whiffs of molecular oxygen” in the Archean atmosphere (Anbar et al., 2007; Frei et al., 2009). This interpretation currently contradicts the overall picture of an anoxic Archean atmosphere suggested by the mass independent fractionation of S isotopes (Farquhar et al., 2000; Luo et al., 2016), the Fe-loss from paleosols (Rye and Holland, 1998), and the preservation of detrital minerals unstable in the presence of molecular oxygen (Hessler and Lowe, 2006; Johnson et al., 2014; Rasmussen and Buick, 1999). However, the exact conditions under which trace metals and their isotopes might have been mobilized have not been examined in a comprehensive framework of weathering simulations that link trace metals and their potential sources, major elements and rock-forming minerals, and perturbations of an anoxic late Archean environment. Here we address how trace nutrients and metals might have behaved by using a framework of thermodynamic weathering models (Hao et al., 2017). After the GOE, the atmosphere became oxic with $p\text{O}_{2,\text{g}}$ around 1% ~ 10% PAL (Kump, 2008; Lyons et al., 2014), resulting in oxidizing weathering and riverine transport of trace elements, similar to the present-day (Large et al., 2014).

Although researchers have relied largely on sedimentary records to probe paleoredox and paleoproductivity processes, the interpretation of sedimentary profiles depends strongly on a clear understanding of weathering, riverine transport, sedimentation, and preservation history. Trace elements are commonly hosted in accessory minerals and solid solutions in silicates, carbonates, or oxides in the crust. Dissolution of these host minerals during weathering is controlled by several factors including the mineral abundance and reactivity, the redox state, the pH of the water, and complexation with other species (Middelburg et al., 1988). After weathering, dissolved trace elements are transported by rivers to the ocean where they may be sequestered into sediments and preserved. Oxidation of several trace elements, e.g. Mn, Cr, Cu, Mo, and Re, can greatly enhance their solubility in surface waters, along with isotopic fractionation. Therefore, changes in the chemical profiles of these trace elements and their isotopic fractionation can be used as indicators of paleoredox. However, apart from the redox reactions, change of environmental pH, variation of weathering rates and the availability of easily weatherable accessory minerals, and/or complexation with possible ligands may also lead to fluctuations in the mobility of trace elements and their isotopic fractionation. Moreover, sedimentary records, especially Archean ones, are usually the result of low to medium-grade metamorphism and/or metasomatism. These post-depositional changes involving elevated temperature and pressure fluid-rock interactions can be expected to affect the original sedimentary records, confounding the interpretation of fluctuations in trace elements.

The present study was designed to simulate the dissolution of minerals that are hosting the nutrient P and the trace metals Mn, Cr, Cu during weathering of olivine basalt

and the mobility of these trace elements in late Archean (3.0-2.5 Ga) surface waters. This time period is selected because life probably have originated in the Archean (Arndt and Nisbet, 2012) and a supply of nutrients and trace metals is vitally important for the habitability and evolution of early life (Anbar, 2008). Geochemical modeling, which considers many environmental factors simultaneously, can approximate the major chemical reactions involved in weathering consistent with present-day world average river water (Hao et al., 2017). The goal of this project is to calculate the dissolution and speciation of these four elements during Archean weathering and riverine transport. Additionally, the influence of whiffs of oxidants, e.g. $O_{2,g}$ or HNO_3 , on the behaviors of trace elements will be investigated.

2. Factors affecting the dissolution of trace elements during the weathering

2.1 Redox level of the atmosphere

The chemical weathering of redox-sensitive minerals is greatly affected by the redox level of the surface environment (Aiuppa et al., 2000). Among the elements covered in this study, phosphorus only has one stable valence in the ambient environment, However, under modern reducing, diagenetic environments where Fe^{2+} occurs, PO_4^{3-} can precipitate as vivianite ($Fe_3(PO_4)_2 \cdot 8H_2O$) which controls the availability of phosphate (Ruttenberg, 2003). This scenario might also be true in the late Archean environment where high concentrations of Fe(II) could have occurred in surface waters (Hao et al., 2017). Consequently, the possible formation of vivianite in the near-surface Archean environment needs to be addressed. Other elements, namely Mn, Cr, and Cu, have

variable valences depending on the redox state of the environment and therefore their weathering is redox-sensitive.

The redox state of the Archean surface environment behaved as though it is controlled by $p\text{H}_{2,\text{g}}$ (10^{-3} to 10^{-5} bars) in the atmosphere (Hao et al., submitted). The $p\text{O}_{2,\text{g}}$ (10^{-11} to 10^{-17} bars or less) is not abundant enough to influence surface redox processes (Fig. 1a and b). In this environment, Fe^{2+} would have been mobile during weathering, and the stable redox states of S and N would also have been the reduced ones in surface waters (Fig. 1b). Fe(III)-(hydr)oxides are missing from paleosols and are not predicted to form during weathering in the late Archean (Hao et al., 2017). Under these circumstances, the surface adsorption of trace elements onto Fe(III)-(hydr)oxides might have been much less important for riverine transport than at the present-day. Based on this assumption, we didn't include the effect of surface adsorption on riverine transport of trace elements.

2.2 pH of near-surface waters

In addition to the redox state, the pH is another important factor controlling the dissolution and speciation of trace elements during weathering processes. Due to the limited biological activity on the Archean continents, it is reasonable to assume that the $p\text{CO}_{2,\text{g}}$ in the weathering zone is the same as in the atmosphere (Berner and Berner, 2012). A very wide range of values of $p\text{CO}_{2,\text{g}}$ has been suggested for the Archean atmosphere (Haqq-Misra et al., 2008; Hessler et al., 2004; Kasting, 2014; Ohmoto et al., 2004; Rosing et al., 2010; Rye et al., 1995; Sheldon, 2006; von Paris et al., 2008). However, the lowest part of this range, defined in part by the assumed stability of magnetite coexisting with hematite in the marine environment (Rosing et al., 2010), is not consistent with thermodynamic calculations when Fe-silicate is taken into account (Hao et al., submitted).

In the present day, we chose a narrower range of values for $p\text{CO}_{2,\text{g}}$ from $10^{-2.5}$ to 10 bars (Fig. 2). A corresponding range of pH values in rainwater can then be estimated. Furthermore, as weathering reactions proceed, the rainwater chemistry will gradually evolve towards river water, with increasing pH and alkalinity.

Utilizing the rainwater and weathering models proposed by Hao et al. (2017), we calculated the pH values of rainwater under the proposed range of Archean $p\text{CO}_{2,\text{g}}$. The results are represented by the lower dashed curve in Fig. 2. We then used the range of rainwater chemistries to model the weathering of olivine basalt. The resulting range of inferred WARW water pH and $p\text{CO}_{2,\text{g}}$ values is shown by the upper curve in Fig. 2. It should be emphasized that the results refer to the destruction of 10^{-4} moles of each basaltic mineral in order to compare with the pH and $p\text{CO}_{2,\text{g}}$ of the world average river water for the late Archean inferred previously (Hao et al., 2017). Overall, the results in Fig. 2 suggest that the pH of surface waters during the Archean could vary from 3.5 to 7.2 depending on the $p\text{CO}_{2,\text{g}}$ and the assumed extent of weathering.

Other geochemical processes could also have affected the pH of Archean surface waters. For example, the organic hazes proposed for the late Archean atmosphere (Izon et al., 2015; Zerkle et al., 2012) might have resulted in organic acids being incorporated into rainwater (Trainer et al., 2004), which would lower the pH of the rainwater (Hao et al., 2017). A similar result might have developed from the oxidation of sulfides due to an increasing oxidation state of the surface environment (Konhauser et al., 2011; Stüeken et al., 2012). Fluctuations of pH might also result in changes in the solubility of trace elements, although few studies have considered this possibility.

2.3 Accessory source minerals in the rocks

Trace elements are mainly hosted in accessory minerals, such as carbonates, oxides and sulfides but also as solid solutions in geologically abundant minerals such as silicates. The weathering rates of these host minerals vary considerably. For example, phosphorus commonly occurs as apatite, $\text{Ca}_5(\text{PO}_4)_3(\text{F}, \text{OH}, \text{Cl})$ which weathers at a rate comparable to or faster than silicate minerals (Brantley and Olsen, 2014). Under these circumstances, riverine transport of phosphorus could be partly limited by the availability of apatite in some environments. In contrast, chromite (FeCr_2O_4), as the principal bearing mineral of chromium in igneous rocks, weathers extremely slowly under ambient conditions and usually needs strong oxidants such as MnO_2 or H_2O_2 (Oze et al., 2007). Consequently, weathering of chromite contributes little to the riverine transport of Cr. Instead, the availability of easily weatherable Cr-bearing minerals such as Cr-silicates might control the concentration of aqueous Cr (Oze et al., 2004).

2.4 Formation of secondary minerals during weathering

Precipitation or adsorption of trace elements during weathering could conceivably strongly affect their mobility. For example, under Archean atmospheric conditions, S(-II) is likely to be thermodynamically stable in surface waters, which could lead to the supersaturation of some sulfide minerals and lower the affinity for destroying other sulfide minerals (Hao et al., 2017). A similar conclusion is also applicable to the weathering of chromite. The stability of Fe(II) in the Archean surface waters leads to an extremely low solubility for chromite. Other trace elements, for example Mn(II), which would be released during weathering of mafic silicates under anoxic conditions, could be incorporated into clays or carbonate minerals. However, as described above the expected lack of precipitation of Fe(III)-(hydr)oxides during the late Archean suggests that surface

adsorption on such minerals can be neglected. Consideration of all of these interrelated issues and their effects on water chemistry requires building a thermodynamic model simulating the dissolution potential of minerals in the Archean weathering environment.

3. Theoretical modeling approach and assumptions

3.1 Late Archean rainwater chemistry

Details of the Archean weathering model we used in this study were provided in our previous study ([Hao et al., 2017](#)). For the purposes of the present study, these results serve as a set of standard conditions ($p\text{H}_{2,\text{g}} = 10^{-5}$ bar and $p\text{CO}_{2,\text{g}} = 10^{-1.5}$ bars) against which perturbations can be compared. In summary, the major species in the Archean rainwater were assumed to be the same as in present-day rainwater ([Berner and Berner, 2012](#)) but different atmospheric values of $p\text{H}_{2,\text{g}}$ and $p\text{CO}_{2,\text{g}}$ prevailed. The pH of the rainwater was determined by the $p\text{CO}_{2,\text{g}}$. The concentration of Fe(II) in the rainwater was assumed to be the same as Mg^{2+} due to their similar geochemical properties under anoxic conditions. Trace amounts of S (10^{-7} mole/L) were introduced by assuming rainout of volcanic S outgassing, representing an upper limit of S concentrations ([Claire et al., 2014](#); [Hao et al., 2016](#); [Domagal-Goldman et al., 2008](#)). During the weathering we suppressed equilibration with aqueous methane because of the likely lack of reactivity of aqueous methane at low temperatures ([Manning et al., 2013](#)). However, if organic aqueous species such as acid anions were somehow incorporated into the surface waters, our calculations suggested that these species could be metastable ([Hao et al., 2017](#)). Consequently, surface waters in the late Archean are predicted to be able to have carried species such as formate and acetate.

3.2. Initial rock type: olivine basalt plus accessory minerals

The Archean crust is thought to be dominated by basalt and komatiite, and rocks of granitic affinity known as the tonalite-trondhjemite-granodiorite (TTG) suite (Taylor and McLennan, 2009). Due to the much faster weathering rate of mafic and ultramafic rocks than felsic rocks, river water from weathering of olivine basalt should dominate the global riverine transport during the Archean. Models for weathering of the two different rock types were described previously (Hao et al., 2017). Consequently, in the present study where the focus is on accessory minerals and trace species, we only present results for weathering of olivine basalt plus accessory minerals.

The amounts of accessory minerals added into the weathering calculations are summarized in Table 1. They were estimated by multiplying the concentrations of each trace element in the upper continental crust (Rudnick and Gao, 2003) with the amounts of olivine basalt rocks used in the weathering calculation. We used apatite solid solution as the source of phosphorus, (Fe, Mg, Mn)-olivine solid solution as the source of manganese, and chalcopyrite as the source of copper. With regard to chromium, previous studies have suggested that primary and secondary Cr-bearing minerals, e.g. olivine, pyroxene, serpentine and clays, are more important sources of chromium in soil solutions than chromite because of the sluggish dissolution of chromite (Oze et al., 2004). However, due to a lack of reliable thermodynamic properties of Cr-silicates, we cannot model their dissolution behavior in the Archean. Instead, we used the dissolution of $\text{Cr(OH)}_{3,\text{am}}$ which was assumed to represent the easily weatherable Cr in addition to chromite. Dissolution of $\text{Cr(OH)}_{3,\text{am}}$ also determines the solubility of weathered Cr(III) in the surface waters.

3.3 Model for trace element behavior during weathering

In the present study, we first used the model late Archean rainwater to react irreversibly with representative minerals of olivine basalt and a mineral source of a trace element under our standard set of late Archean atmospheric conditions: $p\text{H}_{2,\text{g}} = 10^{-5}$ bar and $p\text{CO}_{2,\text{g}} = 10^{-1.5}$ bar. The goal of this approach was to explore the behavior of the trace elements in the chemical environment established by the weathering of the major minerals and elements. For each trace element we then examined the influence of perturbations of the standard conditions. For example, we modeled the effects of whiffs of oxidants such as $\text{O}_{2,\text{g}}$ or HNO_3 on the mobility of trace metals during weathering. All the calculations were carried out with the aqueous speciation, solubility, and chemical mass transfer codes EQ3 & EQ6 (Wolery, 1992) using thermodynamic data as previously described (Hao et al., 2017). For the purpose of this study, we didn't include specific dissolution and precipitation rates of minerals into the model that might be important for specific drainage basins (Brantley and Olsen, 2014; Kump et al., 2000; Zhu et al., 2009). Instead, we assumed that all minerals react and precipitate at relative rates of unity. The major purpose of this model is to explore the weathering behavior of accessory minerals and riverine transport of trace elements on a global scale in the Archean.

The behavior of each trace element in the weathering model depends on the mineralogical source of the trace element (Table 1) and the uptake of the trace element in minerals produced during weathering. Clearly, in our model, minerals will be predicted to form during the weathering process only if there are thermodynamic characterizations of them in the data files used in the model. In the present study, the potential mineralogical

products that could form during weathering are listed in [Table 2](#) for each trace element. Apart from these listed minerals, there are many other minerals that could presumably form in the weathering zone, such as birnessite, digenite, and layered hydrous silicate/oxides as solid solutions. However, these minerals are not included in this study because either their thermodynamic properties are not experimentally measured or their composition is so complicated and variable that they cannot be represented in the chemical system we chosen. As a consequence, the secondary product minerals forming in our model represent an approximation to the potential complexity of mineral products.

4. Model results for late Archean weathering of olivine basalt and trace elements

4.1 Behavior of Phosphorus

[Figs. 3a](#) and [b](#) show the model results for weathering of olivine basalt plus apatite and the calculated concentrations of dissolved phosphate under the conditions adopted as standard late Archean atmospheric conditions, i.e. $p\text{H}_{2,\text{g}} = 10^{-5}$ bar and $p\text{CO}_{2,\text{g}} = 10^{-1.5}$ bar. As expected, the secondary minerals and their solid solutions formed during weathering are almost identical to the weathering results for olivine basalt without apatite ([Hao et al., 2017](#)). If we assume that the typical extent of weathering in the Archean was as established previously, i.e., 10^{-4} moles of primary silicate minerals weathered kg^{-1} H_2O ([Hao et al., 2017](#)), then primary apatite would be totally dissolved during weathering, without precipitation of any secondary phosphate minerals. Under these circumstances, we can infer that the phosphate content of river water during the late Archean was $1.7 \mu\text{molar}$ ([Fig. 3b](#)). Additional calculations show that if apatite were present in excess, the

maximum dissolved phosphate concentration in WARW under the standard conditions would be 10.5 μmolar .

However, if the weathering extent was larger, e.g. $10^{-3.5}$ moles of primary minerals weathered $\text{kg}^{-1} \text{H}_2\text{O}$, it can be seen in [Fig. 3a](#) that the fluid became saturated with respect to apatite and secondary apatite formed. Under these circumstances, the phosphate content of the river water during the late Archean could have been as high as 1.0 μmolar . The two late Archean values can be compared in [Fig. 3b](#) with the range of values for present-day WARW. They are clearly higher than the range of present-day values based on the crustal abundances of phosphorous we used as input apatite.

The main reason for the dissolution of the apatite is that the predicted pH values of the water in the weathering model increased from 5.2 in Archean rainwater to only 6.7 in the Archean WARW ([Hao et al., 2017](#)). As noted previously the latter pH value is significantly lower than most river water pH values at the present day. A limit for phosphate in Archean river water in our standard model is that at large extents of weathering, saturation with secondary apatite could be achieved, as shown in [Fig. 3a](#).

4.2 Behavior of Manganese

[Fig. 4a](#) shows the model results for weathering of olivine basalt that included a Mn_2SiO_4 component in the olivine, again under the conditions adopted as standard late Archean atmospheric conditions. As with the apatite example discussed above, the manganese component of olivine was totally destroyed during the weathering ([Fig. 4a](#)). The weathering products were again very similar to the results for olivine basalt ([Hao et](#)

al., 2017) except that the carbonate mineral formed at large extents of weathering contains Mn in addition to Ca, Mg, and Fe.

The effect of a whiff of oxidant, in this case $O_{2,g}$, in the Archean surface environment is shown in Fig. 4b. This model explores the formation of $MnO_{2,cr}$ during the weathering. $MnO_{2,cr}$ is itself a strong oxidant for Cr^{3+} in the environment (Oze et al., 2007) which has been suggested to be of importance for the mobility of chromium in the Archean and Proterozoic. Whether the formation of $MnO_{2,cr}$ was thermodynamically favorable because of whiffs of oxidants and how much oxidants were required are important parameters for the “whiffs of $O_{2,g}$ ” hypothesis. It can be seen in Fig. 4b that the redox state of the environment as monitored by $pH_{2,g}$ changed dramatically when 10^{-5} moles $O_{2,g}$ kg^{-1} H_2O were included as a reactant in the weathering model. $MnO_{2,cr}$ was predicted to form, although only under a narrow range of conditions. It should also be noted that the amount of hematite formed was more than 100 times greater than the amount of $MnO_{2,cr}$ that formed. It might even be expected that this hematite would coat the $MnO_{2,cr}$ greatly limiting its usefulness as an oxidant for other trace metals such as chromium.

The concentrations of Mn(II) in the waters during the weathering with and without the whiff of O_2 can be seen in Fig. 4c. Clearly, dissolved manganese eventually increased rapidly during weathering to levels a bit higher than the average for the present-day in river water (Gaillardet et al., 2014), both with and without the additional oxidant. However, during the whiff of oxidation, the concentration of aqueous Mn decreased dramatically because of the precipitation of $MnO_{2,cr}$. Moreover, at large extents of

weathering, the concentration would also decrease owing to the elevated pH and associated formation of Mn-rich carbonate solid solution.

Much attention in the literature has focused on whiffs of oxidation caused by non-steady state pulses of molecular O_2 in the late Archean (Anbar et al., 2007; Frei et al., 2009). Oxidants other than O_2 have rarely been considered (Sverjensky and Lee, 2010). In Fig. 4d, we present a model in which the whiff of oxidation comes from HNO_3 instead of O_2 as an added reactant in the weathering model. The results are similar to the simulation with $O_{2,g}$. Clearly, 10^{-5} mole of HNO_3 kg^{-1} H_2O could also oxidize Mn(II) to form $MnO_{2,cr}$.

4.3 Behavior of Chromium

Fig. 5a shows the model results for weathering of olivine basalt including chromite ($FeCr_2O_4$) and $Cr(OH)_{3,am}$ under the standard late Archean atmospheric conditions. Again the major secondary minerals and their solid solutions formed during weathering are almost identical to the weathering results of olivine basalt without chromium (Hao et al., 2017). Chromite is so insoluble (Fig. 5a) that it is an unimportant source of chromium in Archean near-surface environments. Chromite is also kinetically inhibited from reacting in modern weathering zones (Oze et al., 2007). Consequently, we suppressed chromite from the model and allowed $Cr(OH)_{3,am}$ to react during weathering as a source of chromium. It can be seen in Fig. 5a that the $Cr(OH)_{3,am}$ was totally dissolved in the water during weathering. Saturation with respect to $Cr(OH)_{3,am}$ was not reached. We already showed in the Mn weathering calculation that $MnO_{2,cr}$ is thermodynamically favored to form during a “whiff of $O_{2,g}$ ” (Fig. 4b). Given that $MnO_{2,cr}$

is an efficient oxidant for Cr(III), it can be expected that Cr(III) could also be oxidized to Cr(VI) if Mn(II) somehow was oxidized to Mn(IV).

In [Fig. 5b](#) it can be seen that $\text{Cr(OH)}_{3,\text{am}}$ was totally dissolved reaching 0.14 μmolar dissolved Cr, based on the mean crustal Cr abundance. However, with higher $\text{Cr(OH)}_{3,\text{am}}$ input, representing local enrichment of easily-weatherable Cr minerals, $\text{Cr(OH)}_{3,\text{am}}$ could precipitate during weathering. Under these circumstances, increases of pH during the weathering caused a decline of Cr(III) concentration in the water ([Fig. 5a](#)). At the pH value corresponding to the standard 10^{-4} moles of weathering of olivine basalt minerals, the Cr concentration in predicted late Archean WARW is about the same as the highest values associated with present-day rivers ([Gaillardet et al., 2014](#)).

4.4. Behavior of Copper

[Fig. 6a](#) shows the model results for weathering of olivine basalt including chalcopyrite (CuFeS_2) as a reactant mineral in the olivine basalt under the standard late Archean atmospheric conditions. The secondary minerals and their solid solutions formed during weathering are again almost identical to the weathering results of olivine basalt without copper ([Hao et al., 2017](#)). In contrast to the apatite example discussed above, the chalcopyrite was not totally destroyed during the weathering. The Archean weathering of chalcopyrite produced chalcocite (Cu_2S) followed by the precipitation of bornite (Cu_5FeS_4), after which the fluid became saturated with respect to chalcopyrite at a value of $\log \xi$ of about -5.3 ([Fig. 6a](#)). Consequently, chalcocite, bornite, and chalcopyrite are predicted to be stable under various stages of weathering in the near-surface late Archean environment.

The effect of a whiff of $O_{2,g}$ is shown in Fig. 6b. In contrast to the normal Archean weathering, two generations of chalcocite, bornite, and native copper were produced. Much more abundant hematite also formed, as in the case of the Mn-olivine with olivine basalt and a whiff of $O_{2,g}$.

The calculated aqueous concentrations of copper during the weathering can be seen in Fig 6c. Without a whiff of oxidant, very low concentrations of Cu (about 3.2×10^{-16} molar) are to be expected in Archean surface waters because of the consistent occurrences of low solubility of secondary copper sulfides. However, after adding 10^{-6} mole $O_{2,g}$ kg^{-1} H_2O , the reactant chalcopyrite was totally dissolved during weathering at log ξ values where no secondary Cu minerals precipitated (Fig. 6c). The total dissolved Cu(II) concentrations increased to a level typical of modern river water. After consumption of $O_{2,g}$ in the system, the oxidation state declined, native Cu and chalcocite formed again, and the total dissolved Cu(II) concentrations in the water decreased dramatically.

5. Discussion and Implications for the Late Archean Environment

5.1 Riverine transport of phosphorus and the Great Oxidation Event

Phosphorus has been suggested as the limiting nutrient for early life in the Archean ocean as revealed by the low phosphorus content in banded iron formations (Bjerrum & Canfield, 2002). However, more recent studies (Planavsky et al., 2010) have concluded that the phosphate content of the late Archean oceans was significantly higher than at the present day. Our results for late Archean WARW described above also suggest that dissolved phosphate levels were much higher than at the present-day. The

high phosphate results primarily from the fact that the $p\text{CO}_{2,g}$ is $10^{-1.5}$ bars in our standard rainwater model, a value much higher than at the present day. The surface waters in the late Archean are predicted to have been too acidic for the stability of apatite and possible secondary minerals such as vivianite. Consequently, the phosphate levels in late Archean river water were probably not controlled by the solubility of apatite or vivianite.

Previous experimental studies have shown a high dissolution rate of apatite, especially in low pH waters ([Brantley and Olsen, 2014](#)); therefore, the weathering rate of apatite in the Archean surface environments should be the same or even higher than that of olivine basalt. Given the fast weathering rate of apatite, our model results suggest that amounts of phosphate in Archean river water would have been limited by the availability of apatite rather than by the weathering rate and/or precipitation of secondary minerals. Furthermore high levels of riverine transport of phosphate might have been facilitated by the massive increase of continental crust in the late Archean ([Taylor & McLennan, 2009](#)). A large supply of phosphate from acidic rivers may have facilitated photosynthesis in the marine environment and contributed to the irreversible oxidation of the surface environment known as the Great Oxidation Event (GOE).

Overall, our model results suggest, perhaps surprisingly, that a high $p\text{CO}_{2,g}$ level in the late Archean could, indirectly, be a contributing factor to the GOE. In other words, we can now consider the interesting possibility that a prolonged spike in atmospheric $p\text{CO}_{2,g}$ values could have resulted in a large pulse of phosphate transported by rivers in the late Archean. Worldwide spikes in $p\text{CO}_{2,g}$ were likely to have occurred immediately after snowball Earth events through Earth history ([Hoffman et al., 1998](#)). The very high $p\text{CO}_{2,g}$ associated with these events was drawn down through intensive weathering as the

continents were deglaciated. If the $p\text{CO}_{2,g}$ levels were at least 0.12 bars (Hoffman et al, 1998), reference to Fig. 2 suggests that the rainwater could have had pH values of 4.7 or lower. Under these acidic conditions, our calculations suggest that the maximum solubility of apatite was 70 μmolar . Consequently, the phosphate concentrations in river water could have been anomalously high, depending only on the availability of apatite for weathering, further implying that phosphorus may have been readily available to stimulate high photosynthetic activity in the marine environment. In turn, the high biologic activity could have helped drive up the $\text{O}_{2,g}$ levels in the atmosphere.

The stimulation of biologic activity by increased availability of phosphate after snowball events has previously been suggested (Papineau et al., 2013). However, our weathering model indicates a specific mechanism for the increased availability of phosphate in the marine environment: the acidic rainwater associated with the high atmospheric $p\text{CO}_2$ was probably able to dissolve any apatite available to weathering at that time. It should be noted that the Paleoproterozoic snowball event occurred at about 2,200 Ma, some time after the actual beginning of the GOE at about 2,400 Ma. Consequently, the phosphate stimulation of biologic activity is unlikely to have been the initial cause of the GOE. Instead, it seems likely that the stimulation of the biologic activity might have been a contributing cause of the persistence of molecular O_2 in the atmosphere after 2,200 Ma. High levels of phosphate in the early Proterozoic oceans may have finally been removed during the formation of the first major phosphorite rocks at about 2,000 Ma (Papineau, 2010). This inference suggests a significant change in ocean chemistry by about 2,000 Ma, possibly a higher Ca concentration and/or a higher pH value.

5.2 Manganese and chromium during weathering: whiffs of oxidant or not?

Recently, many studies have suggested that whiffs of molecular $O_{2,g}$ occurred in Archean surface environments based on the anomalous enrichments of trace elements and isotopic fractionations in the sedimentary records (Anbar et al., 2007; Crowe et al., 2013; Frei et al., 2009; Garvin et al., 2009; Godfrey and Falkowski, 2009; Golden et al., 2013; Gregory et al., 2015; Kaufman et al., 2007; Kendall et al., 2010; Large et al., 2014; Reinhard et al., 2009; Stüeken et al., 2015).

Here, our weathering model that included Mn showed that “whiffs of $O_{2,g}$ ” could potentially produce MnO_2 which has been suggested to have catalyzed oxidation of Cr(III) during weathering. In the model, we needed 10^{-5} to 10^{-6} moles $O_{2,g}$ kg^{-1} H_2O or more to oxidize Mn. This amount of $O_{2,g}$ is equivalent to a transitory pulse of 10^{-4} to 10^{-3} bars of $O_{2,g}$. In turn this implies a non-steady state of regional and transient pulse of $O_{2,g}$ in the Archean aqueous environment could favor the occasional formation of $MnO_{2,cr}$. However, we also carried out calculations using HNO_3 as an oxidant in order to demonstrate that, apart from $O_{2,g}$, there are other potential oxidants. A non-steady state pulse of HNO_3 could conceivably have arisen as a by-product of the formation of NO_x during periods of excessive lightning occurrence. As an additional example, the formation of Mn-oxides in the 2.415 Ga sedimentary record revealed that if thermodynamically favorable, microbes could oxidize Mn(II) during photosynthesis and form $MnO_{2,g}$ without the appearance of free $O_{2,g}$ (Johnson et al., 2013).

The traditional scenario used to interpret the anomalous enrichment of trace metals and their isotopic fractionations recorded in sediments in the late Archean (Frei et

al, 2009) involves multiple steps. For example, in the case of Cr isotopes, the first step involved oxidation of Mn(II) to Mn(IV) during fluctuations of redox states as discussed above. Second, Mn-oxides catalyzed oxidation of Cr(III) to CrO_4^{2-} , mobilizing the Cr in surface waters. Third, dissolved CrO_4^{2-} was transported by rivers to the ocean where reduction took place and Cr was incorporated into sediments. One vital step in this chain of events is the riverine transport of metal-oxyanions. Both paleosols and our modeling studies pointed out that Fe(II) was likely to have been a significant species in the late Archean river water (Hao et al., 2016; Rye and Holland, 1998). Experimental studies have suggested that the reduction of metal oxyanions by Fe^{2+} is very efficient and fast (Eary and Rai, 1989; Fendorf and Li, 1996; Døssing et al., 2011). Consequently, stable riverine transport of metal oxyanions seems unlikely (Hao et al., submitted). Further modeling work incorporating weathering and riverine transport is needed to explore this issue.

In addition to a dependence on the redox state of the water, the solubilities of trace metals also depend strongly on the pH of the water. For example, our weathering calculation that included chromium showed that saturation with respect to $\text{Cr}(\text{OH})_{3,\text{am}}$ was not achieved in the Archean acidic surface waters given a reasonable estimate of the abundance of easily weatherable Cr-bearing minerals. Experimental dissolution studies have also suggested high solubilities of $\text{Cr}(\text{OH})_{3,\text{am}}$ in low pH waters and/or at high $p\text{CO}_{2,\text{g}}$ (Rai et al., 2007). Consequently, acidic dissolution of easily weatherable Cr-bearing minerals might be the dominant source of Cr in Archean surface waters. Examples of easily weatherable Cr minerals include Cr-bearing igneous and metamorphic silicates in the protolith and clay minerals in the soil (Morrison et al., 2015; Oze et al.,

2004). Weathering and riverine transport of Cr during the Archean might be limited by the availability of easily weatherable Cr-bearing minerals. Furthermore, preferential dissolution of some secondary Cr-bearing minerals with Cr isotopic compositions different from the mantle source (Babechuk et al., 2016; Farkaš et al., 2013; Wang et al., 2016) might cause noticeable isotopic fractionation, which complicates the interpretation of small chromium isotopic fractionations as “whiffs of O_{2,g}” in the Archean (Frei et al., 2009).

5.3 Trace Cu-minerals as signatures of the surface environment and mineral evolution

As discussed above, some of the most widely used indicators of fluctuations in Earth’s near surface environment during the late Archean include anomalous concentrations or isotopic ratios of trace metals in the sedimentary record. In addition, attention has long focused on a few detrital minerals, e.g. pyrite, siderite, and uraninite, whose abundances seem anomalous compared with younger sedimentary records. Our calculations suggest another potential line of evidence: perturbations in the near-surface mineralogic environment which might be traceable in the geologic record. We base this discussion on copper mobility in the late Archean surface environment because copper has three oxidation states under ambient temperatures and pressures in nature. Furthermore, it is an element of importance in the biogeochemistry of early enzymes (Dupont et al., 2010), stable isotopic studies of copper have been linked to fluctuating redox conditions (Balistrieri et al., 2008; Chi Fru et al., 2016). Finally, because copper minerals are readily identified in the geologic record and could potentially become an

important part of mineral evolution studies that link the coevolution of Earth and life ([Hazen et al., 2014](#)).

Our model calculations of the behavior of copper during late Archean weathering indicated that product minerals predicted to occur during the weathering could be potentially used to indicate the redox evolution of the environment. For example, weathering of chalcopyrite under the standard late Archean atmospheric conditions produced chalcocite and bornite ([Fig. 6a](#)). However, when there were fluctuations in the oxidation state of the atmosphere, native copper could form ([Fig. 6b](#)). If there were geological observations in Archean weathering profiles showing the occurrence of native Cu, they might be relatable to fluctuations of the near surface oxidation state. Compared with the chemical profiles of trace elements preserved in marine sedimentary rocks, the occurrence of minerals in terrestrial records doesn't necessarily involve riverine transport, which may preserve the *in situ* weathering signatures. Therefore, we want to emphasize here the potential application of mineral assemblages formed during weathering as an aid to understanding the evolution of Earth's surface redox state, especially before the GOE. Our results could be used in combination with copper mineral evolution studies to provide a new, thermodynamically interpretable level of detail within the overall framework derived in previous studies of the supercontinent cycle and the development of the biosphere ([Hazen et al., 2014](#)).

6. Conclusions

This study has applied a recently developed chemical framework for late Archean weathering to study the behaviors of phosphorus, manganese, chromium, and copper

during weathering of olivine basalt plus trace element-bearing accessory minerals under a set of standard Archean atmospheric boundary conditions. Moreover, whiffs of oxidants, such as $O_{2,g}$ and HNO_3 , were included as reactants to explore their influences on the mobility and speciation of Mn and Cu during the weathering.

Our main conclusions are as follows:

(1) The set of standard late Archean atmospheric conditions we adopted, i.e. $pH_{2,g} = 10^{-5}$ bar and $pCO_{2,g} = 10^{-1.5}$ bar, resulted in late Archean WARW with a pH of 6.4. Excursions of $pCO_{2,g}$ away from the standard conditions may have resulted in pH values of Archean surface waters ranging from 3.5 to 7.2 depending also on the extent of weathering. The metastability of organic acids deposited from organic hazes, or the oxidation of sulfides caused by fluctuations of the near-surface redox state, could also have influenced the pH of late Archean surface waters.

(2) Our model quantitatively links the pCO_2 of the atmosphere to the level of phosphate transported by rivers. When pCO_2 was $10^{-1.5}$ bars, accessory apatite was totally dissolved during weathering and the development of late Archean WARW (pH = 6.4) resulted in riverine phosphate of at least 1.7 μ molar, much higher than at the present-day. This result is consistent with the high levels of phosphate in late Archean seawater inferred from the P/Fe ratios of banded iron formations ([Planavsky et al., 2010](#)).

(3) At the end of the early Proterozoic snowball Earth event when pCO_2 was at least 0.12 bars, the pH of WARW may have been as low as about 5.7, which would have corresponded to a solubility of 70 μ molar phosphate. The amount transported by WARW would have depended on the availability of apatite. In this way, our model provides a specific mechanism for the previously suggested high levels of phosphate in the marine

environment that may have influenced O₂ levels in the atmosphere by stimulating high levels of oxygenic photosynthesis (Papineau et al., 2013).

(4) Crustal levels of Mn housed in Mn-olivine were predicted to dissolve completely without producing any secondary minerals except Mn-bearing carbonate at large extents of weathering. The corresponding Mn content of WARW reached about 1.2 μ molar, higher than in the modern WARW. Whiffs of 10^{-5} mole O_{2,g} or HNO₃ kg⁻¹ H₂O in the weathering model resulted in the formation of MnO_{2,cr} together with about 100 times more hematite. The concentrations of Mn(II) in the WARW would have decreased dramatically during the precipitation of MnO_{2,cr}.

(5) Chromite was too insoluble to dissolve during the late Archean weathering of olivine basalt, resulting in negligible dissolved Cr in the WARW. However, Cr(OH)_{3,am}, representing easily weatherable Cr-bearing minerals dissolved totally during the weathering, resulting in concentrations of Cr(III) in the late Archean river water of up to 0.14 μ molar, higher than at the present-day.

(6) Late Archean weathering of accessory chalcopyrite in olivine basalt under our standard conditions produced chalcocite and bornite, along with other secondary minerals. The predicted concentrations of Cu in the resultant river water would have been extremely low (about 5.9×10^{-11} nmolar) because of the low solubilities of the copper sulfides. However, during a pulse of either 10^{-6} mole O_{2,g} kg⁻¹ H₂O or 10^{-6} mole HNO₃ kg⁻¹ H₂O, weathering of chalcopyrite produced two generations of native copper, chalcocite and bornite, together with about 100 times more hematite. The resultant WARW contained comparable level of dissolved Cu as the modern river water.

(7) The copper mineralogy recorded in weathering profiles might be useful as a signature of the surface redox environment. The thermodynamically interpretable signals may provide a new correlation with evidence from studies of copper mineral evolution. Preliminary results suggest that native copper occurrences in the late Archean might indicate fluctuations in the oxidation state of the weathering zone.

(8) In addition to redox variations, fluctuations in pH and the availability of easily weatherable accessory minerals could also affect the mobility and speciation of trace elements in the late Archean. These results suggest that the abnormal enrichment of trace elements and their isotopic fractionations do not necessarily suggest the appearance of oxygenic photosynthesis and accumulation of free $O_{2,g}$ in the early atmosphere. Besides traditional sedimentary records, secondary mineral assemblages of trace elements can be potentially useful to understand the evolution of surface environment, especially before the GOE.

Acknowledgements:

This research was supported by a Johns Hopkins Graduate Fellowship (J. H. H.) and the W.M. Keck Foundation (D. A. S. and R. M. H.). We gratefully acknowledge the help and support of the Johns Hopkins University and the Geophysical Laboratory of the Carnegie Institution for Science. We thank E. Smith, J. Golden, S. M. Morrison, C. Liu, D. Hummer, S. D. Domagal-Goldman, M. W. Claire, G. N. Arney, B. Jelen, X. M. Liu, and A. Gnanadesikan for discussions.

References:

- Aiuppa, A., Allard, P., D'Alessandro, W., Michel, A., Parello, F., Treuil, M., Valenza, M., 2000. Mobility and fluxes of major, minor and trace metals during basalt weathering and groundwater transport at Mt. Etna volcano (Sicily). *Geochim. Cosmochim. Acta* 64, 1827–1841. doi:10.1016/S0016-7037(00)00345-8
- Anbar, A.D., 2008. Oceans. Elements and evolution. *Science* 322, 1481–1483. doi:10.1126/science.1163100
- Anbar, A.D., Duan, Y., Lyons, T.W., Arnold, G.L., Kendall, B., Creaser, R.A., Kaufman, A.J., Gordon, G.W., Scott, C., Garvin, J., Buick, R., 2007. A whiff of oxygen before the great oxidation event? *Science* 317, 1903–1906. doi:10.1126/science.1140325
- Anbar, A.D., Knoll, A.H., 2002. Proterozoic ocean chemistry and evolution: a bioinorganic bridge? *Science* 297, 1137–1142. doi:10.1126/science.1069651
- Anbar, A.D., Rouxel, O., 2007. Metal stable isotopes in paleoceanography. *Annu. Rev. Earth Planet. Sci.* 35, 717–746. doi:10.1146/annurev.earth.34.031405.125029
- Arndt, N.T., Nisbet, E.G., 2012. Processes on the Young Earth and the Habitats of Early Life. *Annu. Rev. Earth Planet. Sci.* 40, 521–549. doi:10.1146/annurev-earth-042711-105316
- Babechuk, M.G., Kleinhanns, I.C., Schoenberg, R., 2016. Chromium geochemistry of the ca. 1.85 Ga Flin Flon paleosol. *Geobiology* n/a-n/a. doi:10.1111/gbi.12203
- Balistrieri, L.S., Borrok, D.M., Wanty, R.B., Ridley, W.I., 2008. Fractionation of Cu and Zn isotopes during adsorption onto amorphous Fe(III) oxyhydroxide: Experimental mixing of acid rock drainage and ambient river water. *Geochim. Cosmochim. Acta* 72, 311–328. doi: 10.1016/j.gca.2007.11.013

- Berner, E.K., Berner, R.A., 2012. Global environment: water, air, and geochemical cycles. Princeton University Press.
- Bjerrum, C.J., Canfield, D.E., 2002. Ocean productivity before about 1.9 Gyr ago limited by phosphorus adsorption onto iron oxides. *Nature* 417, 159–162.
doi:10.1038/417159a
- Brantley, S.L., Olsen, A.A., 2014. 7.3 - Reaction Kinetics of Primary Rock-Forming Minerals under Ambient Conditions, in: Holland, H.D., Turekian, K.K. (Eds.), *Treatise on Geochemistry (Second Edition)*. Elsevier, Oxford, pp. 69–113. doi: 10.1016/B978-0-08-095975-7.00503-9
- Chi Fru, E., Hemmingsson, C., Holm, M., Chiu, B., Iñiguez, E., 2016. Arsenic-induced phosphate limitation under experimental Early Proterozoic oceanic conditions. *Earth Planet. Sci. Lett.* 434, 52–63. doi: 10.1016/j.epsl.2015.11.009
- Claire, M.W., Kasting, J.F., Domagal-Goldman, S.D., Stueken, E.E., Buick, R., Meadows, V.S., 2014. Modeling the signature of sulfur mass-independent fractionation produced in the Archean atmosphere. *Geochim. Cosmochim. Acta* 141, 365–380.
doi:10.1016/j.gca.2014.06.032
- Crowe, S.A., Dossing, L.N., Beukes, N.J., Bau, M., Kruger, S.J., Frei, R., Canfield, D.E., 2013. Atmospheric oxygenation three billion years ago. *Nature* 501, 535–538.
doi:10.1038/nature12426
- Domagal-Goldman, S.D., Kasting, J.F., Johnston, D.T., Farquhar, J., 2008. Organic haze, glaciations and multiple sulfur isotopes in the Mid-Archean Era. *Earth Planet. Sci. Lett.* 269, 29–40. doi:10.1016/j.epsl.2008.01.040

- Døssing, L.N., Dideriksen, K., Stipp, S.L.S., Frei, R., 2011. Reduction of hexavalent chromium by ferrous iron: A process of chromium isotope fractionation and its relevance to natural environments. *Chem. Geol.* 285, 157–166.
doi:10.1016/j.chemgeo.2011.04.005
- Dupont, C.L., Butcher, A., Valas, R.E., Bourne, P.E., Caetano-Anollés, G., 2010. History of biological metal utilization inferred through phylogenomic analysis of protein structures. *Proc. Natl. Acad. Sci.* 107, 10567–10572. doi:10.1073/pnas.0912491107
- Eary, L.E., Rai, D., 1989. Kinetics of chromate reduction by ferrous-ions derived from hematite and biotite at 25 °C. *Am. J. Sci.* 289, 180–213. doi:10.2475/ajs.289.2.180
- Farkaš, J., Chrástný, V., Novák, M., Čadkova, E., Pašava, J., Chakrabarti, R., Jacobsen, S.B., Ackerman, L., Bullen, T.D., 2013. Chromium isotope variations ($\delta^{53/52}\text{Cr}$) in mantle-derived sources and their weathering products: Implications for environmental studies and the evolution of $\delta^{53/52}\text{Cr}$ in the Earth's mantle over geologic time. *Geochim. Cosmochim. Acta* 123, 74–92.
doi:10.1016/j.gca.2013.08.016
- Farquhar, J., Bao, H., Thiemens, M., 2000. Atmospheric influence of Earth's earliest sulfur cycle. *Science* 289, 756–759. doi: 10.1126/Science.289.5480.756
- Farquhar, J., Zerkle, A.L., Bekker, A., 2014. 6.4 - Geologic and Geochemical Constraints on Earth's Early Atmosphere A2 - Holland, Heinrich D, in: Turekian, K.K. (Ed.), *Treatise on Geochemistry (Second Edition)*. Elsevier, Oxford, pp. 91–138. doi: 10.1016/B978-0-08-095975-7.01304-8
- Fendorf, S.E., Li, G.C., 1996. Kinetics of chromate reduction by ferrous iron. *Environ. Sci. Technol.* 30, 1614–1617. doi: 10.1021/es950618m

- Frei, R., Gaucher, C., Poulton, S.W., Canfield, D.E., 2009. Fluctuations in Precambrian atmospheric oxygenation recorded by chromium isotopes. *Nature* 461, 250–253.
doi:10.1038/nature08266
- Gaillardet, J., Viers, J., Dupré, B., 2014. 7.7 - Trace Elements in River Waters A2 - Turekian, Heinrich D. HollandKarl K, in: *Treatise on Geochemistry* (Second Edition). Elsevier, Oxford, pp. 195–235. doi:10.1016/B978-0-08-095975-7.00507-6
- Garvin, J., Buick, R., Anbar, A.D., Arnold, G.L., Kaufman, A.J., 2009. Isotopic evidence for an aerobic nitrogen cycle in the latest Archean. *Science* 323, 1045–1048.
doi:10.1126/science.1165675
- Godfrey, L. V, Falkowski, P.G., 2009. The cycling and redox state of nitrogen in the Archaean ocean. *Nat. Geosci.* 2, 725–729. doi:10.1038/ngeo633
- Golden, J., McMillan, M., Downs, R.T., Hystad, G., Goldstein, I., Stein, H.J., Zimmerman, A., Sverjensky, D.A., Armstrong, J.T., Hazen, R.M., 2013. Rhenium variations in molybdenite (MoS₂): Evidence for progressive subsurface oxidation. *Earth Planet. Sci. Lett.* 366, 1–5. doi:10.1016/j.epsl.2013.01.034
- Gregory, D.D., Large, R.R., Halpin, J.A., Baturina, E.L., Lyons, T.W., Wu, S., Danyushevsky, L., Sack, P.J., Chappaz, A., Maslennikov, V. V, Bull, S.W., 2015. Trace Element Content of Sedimentary Pyrite in Black Shales. *Econ. Geol.* 110, 1389–1410. doi:10.2113/econgeo.110.6.1389
- Guidry, M.W., Mackenzie, F.T., 2000. Apatite weathering and the Phanerozoic phosphorus cycle. *Geology* 28, 631–634. doi:10.1130/0091-7613(2000)028<0631:Awatpp>2.3.Co;2

- Hao, J., Sverjensky, D.A., Hazen, R.M., 2017. A model for late Archean chemical weathering and world average river water. *Earth Planet. Sci. Lett.* 457, 191-203.
doi:10.1016/j.epsl.2016.10.021
- Hao, J., Sverjensky, D.A., Hazen, R.M. (under review). Importance of Atmospheric H_{2,g} in Surficial Environments of the Archean.
- Haqq-Misra, J.D., Domagal-Goldman, S.D., Kasting, P.J., Kasting, J.F., 2008. A revised, hazy methane greenhouse for the Archean Earth. *Astrobiology* 8, 1127–1137.
doi:10.1089/ast.2007.0197
- Hazen, R.M., Liu, X.M., Downs, R.T., Golden, J., Pires, A.J., Grew, E.S., Hystad, G., Estrada, C., Sverjensky, D.A., 2014. Mineral Evolution: Episodic Metallogenesis, the Supercontinent Cycle, and the Coevolving Geosphere and Biosphere. *Soc. Econ. Geol. Spec. P.* 18, 1–15.
- Hessler, A.M., Lowe, D.R., 2006. Weathering and sediment generation in the Archean: An integrated study of the evolution of siliciclastic sedimentary rocks of the 3.2 Ga Moodies Group, Barberton greenstone belt, South Africa. *Precambrian Res.* 151, 185–210. doi:10.1016/j.precamres.2006.08.008
- Hessler, A.M., Lowe, D.R., Jones, R.L., Bird, D.K., 2004. A lower limit for atmospheric carbon dioxide levels 3.2 billion years ago. *Nature* 428, 736–738.
doi:10.1038/Nature02471
- Hoffman, P.F., Kaufman, A.J., Halverson, G.P., Schrag, D.P., 1998. A Neoproterozoic Snowball Earth. *Science* 281, 1342–1346. doi:10.1126/science.281.5381.1342
- Izon, G., Zerkle, A.L., Zhelezinskaia, I., Farquhar, J., Newton, R.J., Poulton, S.W., Eigenbrode, J.L., Claire, M.W., 2015. Multiple oscillations in Neoarchaeon

- atmospheric chemistry. *Earth Planet. Sci. Lett.* 431, 264–273.
doi:10.1016/j.epsl.2015.09.018
- Johnson, J.E., Webb, S.M., Ma, C., Fischer, W.W., 2016. Manganese mineralogy and diagenesis in the sedimentary rock record. *Geochim. Cosmochim. Acta* 173, 210–231. doi:10.1016/j.gca.2015.10.027
- Johnson, J.E., Webb, S.M., Thomas, K., Ono, S., Kirschvink, J.L., Fischer, W.W., 2013. Manganese-oxidizing photosynthesis before the rise of cyanobacteria. *Proc. Natl. Acad. Sci.* 110, 11238–11243. doi:10.1073/pnas.1305530110
- Johnson, J.E., Gerpheide, A., Lamb, M.P., Fischer, W.W., 2014. O₂ constraints from Paleoproterozoic detrital pyrite and uraninite. *Geol. Soc. Am. Bull.* 126, 813–830. doi: 10.1130/B30949.1
- Kasting, J.F., 2014. 6.6 - Modeling the Archean Atmosphere and Climate, in: Holland, H.D., Turekian, K.K. (Eds.), *Treatise on Geochemistry (Second Edition)*. Elsevier, Oxford, pp. 157–175. doi:10.1016/B978-0-08-095975-7.01306-1
- Kaufman, A.J., Johnston, D.T., Farquhar, J., Masterson, A.L., Lyons, T.W., Bates, S., Anbar, A.D., Arnold, G.L., Garvin, J., Buick, R., 2007. Late Archean biospheric oxygenation and atmospheric evolution. *Science* 317, 1900–1903.
doi:10.1126/science.1138700
- Kendall, B., Reinhard, C.T., Lyons, T., Kaufman, A.J., Poulton, S.W., Anbar, A.D., 2010. Pervasive oxygenation along late Archaean ocean margins. *Nat. Geosci.* 3, 647–652.
doi:10.1038/Ngeo942
- Konhauser, K.O., Lalonde, S. V, Amskold, L., Holland, H.D., 2007. Was there really an Archean phosphate crisis? *Science* 315, 1234. doi:10.1126/science.1136328

- Konhauser, K.O., Lalonde, S. V, Planavsky, N.J., Pecoits, E., Lyons, T.W., Mojzsis, S.J., Rouxel, O.J., Barley, M.E., Rosiere, C., Fralick, P.W., Kump, L.R., Bekker, A., 2011. Aerobic bacterial pyrite oxidation and acid rock drainage during the Great Oxidation Event. *Nature* 478, 369–373. doi:10.1038/nature10511
- Kump, L.R., 2008. The rise of atmospheric oxygen. *Nature* 451, 277–278. doi:10.1038/nature06587
- Kump, L.R., Brantley, S.L., Arthur, M.A., 2000. Chemical, weathering, atmospheric CO₂, and climate. *Annu. Rev. Earth Planet. Sci.* 28, 611–667. doi:10.1146/annurev.earth.28.1.611
- Large, R.R., Halpin, J.A., Danyushevsky, L. V, Maslennikov, V. V, Bull, S.W., Long, J.A., Gregory, D.D., Lounejeva, E., Lyons, T.W., Sack, P.J., McGoldrick, P.J., Calver, C.R., 2014. Trace element content of sedimentary pyrite as a new proxy for deep-time ocean-atmosphere evolution. *Earth Planet. Sci. Lett.* 389, 209–220. doi:10.1016/j.epsl.2013.12.020
- Luo, G., Ono, S., Beukes, N.J., Wang, D.T., Xie, S., Summons, R.E., 2016. Rapid oxygenation of Earth’s atmosphere 2.33 billion years ago. *Sci. Adv.* 2, e1600134. doi:10.1126/sciadv.1600134
- Lyons, T.W., Reinhard, C.T., Planavsky, N.J., 2014. The rise of oxygen in Earth’s early ocean and atmosphere. *Nature* 506, 307–315. doi:10.1038/nature13068
- Manning, C.E., Shock, E.L., Sverjensky, D.A., 2013. The Chemistry of Carbon in Aqueous Fluids at Crustal and Upper-Mantle Conditions: Experimental and Theoretical Constraints. *Carbon in Earth* 75, 109–148. doi:10.2138/rmg.2013.75.5

- Middelburg, J.J., Vanderweijden, C.H., Woittiez, J.R.W., 1988. Chemical Processes Affecting the Mobility of Major, Minor and Trace-Elements during Weathering of Granitic-Rocks. *Chem. Geol.* 68, 253–273. doi:10.1016/0009-2541(88)90025-3
- Morel, F.M., 2008. The co-evolution of phytoplankton and trace element cycles in the oceans. *Geobiology* 6, 318–324. doi:10.1111/j.1472-4669.2008.00144.x
- Morrison, J.M., Goldhaber, M.B., Mills, C.T., Breit, G.N., Hooper, R.L., Holloway, J.M., Diehl, S.F., Ranville, J.F., 2015. Weathering and transport of chromium and nickel from serpentinite in the Coast Range ophiolite to the Sacramento Valley, California, USA. *Appl. Geochemistry* 61, 72–86. doi:10.1016/j.apgeochem.2015.05.018
- Ohmoto, H., Watanabe, Y., Kumazawa, K., 2004. Evidence from massive siderite beds for a CO₂-rich atmosphere before, 1.8 billion years ago. *Nature* 429, 395–399. doi:10.1038/Nature02573
- Oze, C., Bird, D.K., Fendorf, S., 2007. Genesis of hexavalent chromium from natural sources in soil and groundwater. *Proc. Natl. Acad. Sci.* 104, 6544–6549. doi:10.1073/pnas.0701085104
- Oze, C., Fendorf, S., Bird, D.K., Coleman, R.G., 2004. Chromium geochemistry in serpentinized ultramafic rocks and serpentine soils from the Franciscan complex of California. *Am. J. Sci.* 304, 67–101. doi:10.2475/ajs.304.1.67
- Papineau, D., 2010. Global Biogeochemical Changes at Both Ends of the Proterozoic: Insights from Phosphorites. *Astrobiology* 10, 165–181. doi:10.1089/ast.2009.0360
- Papineau, D., Purohit, R., Fogel, M.L., Shields-Zhou, G.A., 2013. High phosphate availability as a possible cause for massive cyanobacterial production of oxygen in

- the Paleoproterozoic atmosphere. *Earth Planet. Sci. Lett.* 362, 225–236.
doi:10.1016/j.epsl.2012.11.050
- Pasek, M., Herschy, B., Kee, T.P., 2015. Phosphorus: a case for mineral-organic reactions in prebiotic chemistry. *Orig. Life Evol. Biosph.* 45, 207–218.
doi:10.1007/s11084-015-9420-y
- Planavsky, N.J., Rouxel, O.J., Bekker, A., Lalonde, S. V, Konhauser, K.O., Reinhard, C.T., Lyons, T.W., 2010. The evolution of the marine phosphate reservoir. *Nature* 467, 1088–1090. doi: 10.1038-nature09485
- Rai, D., Moore, D.A., Hess, N.J., Rosso, K.M., Rao, L., Heald, S.M., 2007. Chromium(III) Hydroxide Solubility in the Aqueous $K^+ - H^+ - OH^- - CO_2 - HCO_3^- - CO_3^{2-} - H_2O$ System: A Thermodynamic Model. *J. Solution Chem.* 36, 1261–1285.
doi:10.1007/s10953-007-9179-5
- Rasmussen, B., Buick, R., 1999. Redox state of the Archean atmosphere: Evidence from detrital heavy minerals in ca. 3250-2750 Ma sandstones from the Pilbara Craton, Australia. *Geology* 27, 115. doi:10.1130/0091-7613(1999)027<0115:rsotaa>2.3.co;2
- Reinhard, C.T., Raiswell, R., Scott, C., Anbar, A.D., Lyons, T.W., 2009. A late Archean sulfidic sea stimulated by early oxidative weathering of the continents. *Science* 326, 713–716. doi:10.1126/science.1176711
- Rosing, M.T., Bird, D.K., Sleep, N.H., Bjerrum, C.J., 2010. No climate paradox under the faint early Sun. *Nature* 464, 744–747. doi:10.1038/Nature08955
- Rudnick, R.L., Gao, S., 2003. 3.01 - Composition of the Continental Crust A2 - Turekian, Heinrich D. HollandKarl K, in: *Treatise on Geochemistry*. Pergamon, Oxford, pp. 1–64. doi:10.1016/B0-08-043751-6/03016-4

- Ruttenberg, K.C., 2003. 8.13 - The Global Phosphorus Cycle, in: Turekian, H.D.H.K. (Ed.), *Treatise on Geochemistry*. Pergamon, Oxford, pp. 585–643.
doi:<http://dx.doi.org/10.1016/B0-08-043751-6/08153-6>
- Rye, R., Holland, H.D., 1998. Paleosols and the evolution of atmospheric oxygen: a critical review. *Am. J. Sci.* 298, 621–672.
- Rye, R., Kuo, P.H., Holland, H.D., 1995. Atmospheric carbon dioxide concentrations before 2.2 billion years ago. *Nature* 378, 603–605. doi:10.1038/378603a0
- Saito, M.A., Sigman, D.M., Morel, F.M.M., 2003. The bioinorganic chemistry of the ancient ocean: the co-evolution of cyanobacterial metal requirements and biogeochemical cycles at the Archean–Proterozoic boundary? *Inorganica Chim. Acta* 356, 308–318. doi:10.1016/s0020-1693(03)00442-0
- Sheldon, N.D., 2006. Precambrian paleosols and atmospheric CO₂ levels. *Precambrian Res.* 147, 148–155. doi:10.1016/J.Precamres.2006.02.004
- Stüeken, E.E., Catling, D.C., Buick, R., 2012. Contributions to late Archaean sulphur cycling by life on land. *Nat. Geosci.* 5, 722–725. doi:10.1038/ngeo1585
- Sverjensky, D.A., Lee, N., 2010. The Great Oxidation Event and Mineral Diversification. *Elements* 6, 31–36. doi:10.2113/gselements.6.1.31
- Taylor, S.R., McLennan, S., 2009. *Planetary crusts: their composition, origin and evolution*. Cambridge University Press.
- Trainer, M.G., Pavlov, A.A., Curtis, D.B., McKay, C.P., Worsnop, D.R., Delia, A.E., Toohey, D.W., Toon, O.B., Tolbert, M.A., 2004. Haze aerosols in the atmosphere of early Earth: manna from heaven. *Astrobiology* 4, 409–419.
doi:10.1089/ast.2004.4.409

- Tribovillard, N., Algeo, T.J., Lyons, T., Riboulleau, A., 2006. Trace metals as paleoredox and paleoproductivity proxies: An update. *Chem. Geol.* 232, 12–32.
doi:10.1016/j.chemgeo.2006.02.012
- von Paris, P., Rauer, H., Lee Grenfell, J., Patzer, B., Hedelt, P., Stracke, B., Trautmann, T., Schreier, F., 2008. Warming the early earth—CO₂ reconsidered. *Planet. Space Sci.* 56, 1244–1259. doi:10.1016/j.pss.2008.04.008
- Wang, X.L., Planavsky, N.J., Reinhard, C.T., Zou, H.J., Ague, J.J., Wu, Y.B., Gill, B.C., Schwarzenbach, E.M., Peucker-Ehrenbrink, B., 2016. Chromium isotope fractionation during subduction-related metamorphism, black shale weathering, and hydrothermal alteration. *Chem. Geol.* 423, 19–33.
doi:10.1016/j.chemgeo.2016.01.003
- Williams, R.J.P., Da Silva, J.J.R.F., 2003. Evolution was chemically constrained. *J. Theor. Biol.* 220, 323–343. doi:10.1006/jtbi.2003.3152
- Wolery, T.J., 1992. EQ3/6: A software package for geochemical modeling of aqueous systems: package overview and installation guide (version 7.0). Lawrence Livermore National Laboratory Livermore, CA.
- Zerkle, A.L., Claire, M., Domagal-Goldman, S.D., Farquhar, J., Poulton, S.W., 2012. A bistable organic-rich atmosphere on the Neoproterozoic Earth. *Nat. Geosci.* 5, 359–363.
- Zerkle, A.L., House, C.H., Cox, R.P., Canfield, D.E., 2006. Metal limitation of cyanobacterial N₂fixation and implications for the Precambrian nitrogen cycle. *Geobiology* 4, 285–297. doi:10.1111/j.1472-4669.2006.00082.x

Zhu, C., 2009. Geochemical Modeling of Reaction Paths and Geochemical Reaction Networks. *Thermodyn. Kinet. Water-Rock Interact.* 70, 533–569.
doi:10.2138/rmg.2009.70.12

Table 1. Sources of trace elements in the weathering model expressed as amounts of accessory minerals in olivine basalt estimated from elemental upper continental crust abundances.

Trace element	Abundance ¹ (ppm)	Mineral Source	Amount used in the model ² ($\mu\text{moles.kg}^{-1} \text{H}_2\text{O}$)
P	1310	Apatite (0.45 F-apatite; 0.45 OH-apatite; 0.10 Cl-apatite)	0.55
Mn	775	Mn ₂ SiO ₄ (0.006) in olivine solid solution	0.36
Cr	92	Chromite or Amorphous Cr(OH) ₃	0.14
Cu	28	Chalcopyrite	0.017

¹ Concentrations in the upper continental crust ([Rudnick and Gao, 2003](#)).

² Values correspond to 10^{-4} moles of primary minerals destroyed per kg H₂O.

Table 2 Potential mineral products that might form during weathering and that were in the thermodynamic data file used for the modeling.

Trace element	Possible secondary minerals	Formula
P	Apatite	$\text{Ca}_5(\text{PO}_4)_3(\text{OH}, \text{F}, \text{Cl})$
	Vivianite	$\text{Fe}_3(\text{PO}_4)_2 \cdot 8\text{H}_2\text{O}$
Mn	Hausmanite	Mn_3O_4
	Pyrolusite	MnO_2
	Bixbyite	Mn_2O_3
	Alabandite	MnS
	Manganosite	MnO
	Rhodochrosite	MnCO_3
Cr	Amorphous $\text{Cr}(\text{OH})_3$	$\text{Cr}(\text{OH})_3$
Cu	Native copper	Cu
	Covellite	CuS
	Chalcocite	Cu_2S
	Bornite	FeCu_5S_4
	Cuprite	Cu_2O
	Tenorite	CuO
	Malachite	$\text{Cu}_2\text{CO}_3(\text{OH})_2$
	Azurite	$\text{Cu}_3(\text{CO}_3)_2(\text{OH})_2$

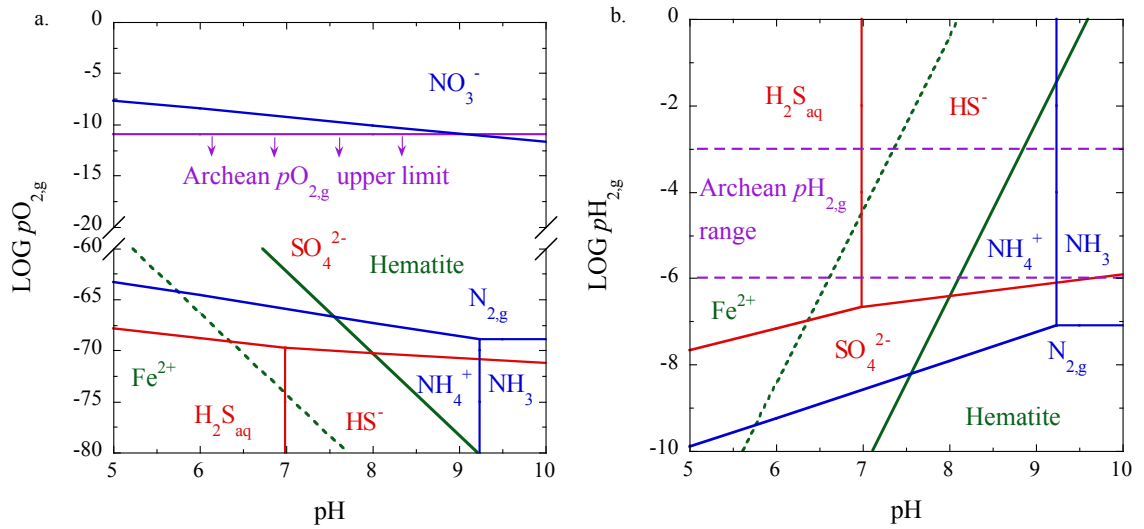


Figure 1. Equilibrium diagrams in the Fe-S-N-O-H system as a function of pH and a. $pO_{2,g}$ or b. $pH_{2,g}$. Solid lines represent equilibrium boundaries between aqueous species, gases, and minerals by assuming $a(NH_4^+) = a(NH_{3,aq}) = a(NO_3^-) = 10^{-6}$, $a(Fe^{2+}) = 10^{-6}$ (solid green line) or 10^{-3} (dashed green line), and $pN_{2,g} = 0.78$. Purple dashed lines show the constraints suggested from atmospheric models (Catling and Claire, 2005; Kasting, 1991, 2014; Kasting et al. 2001).

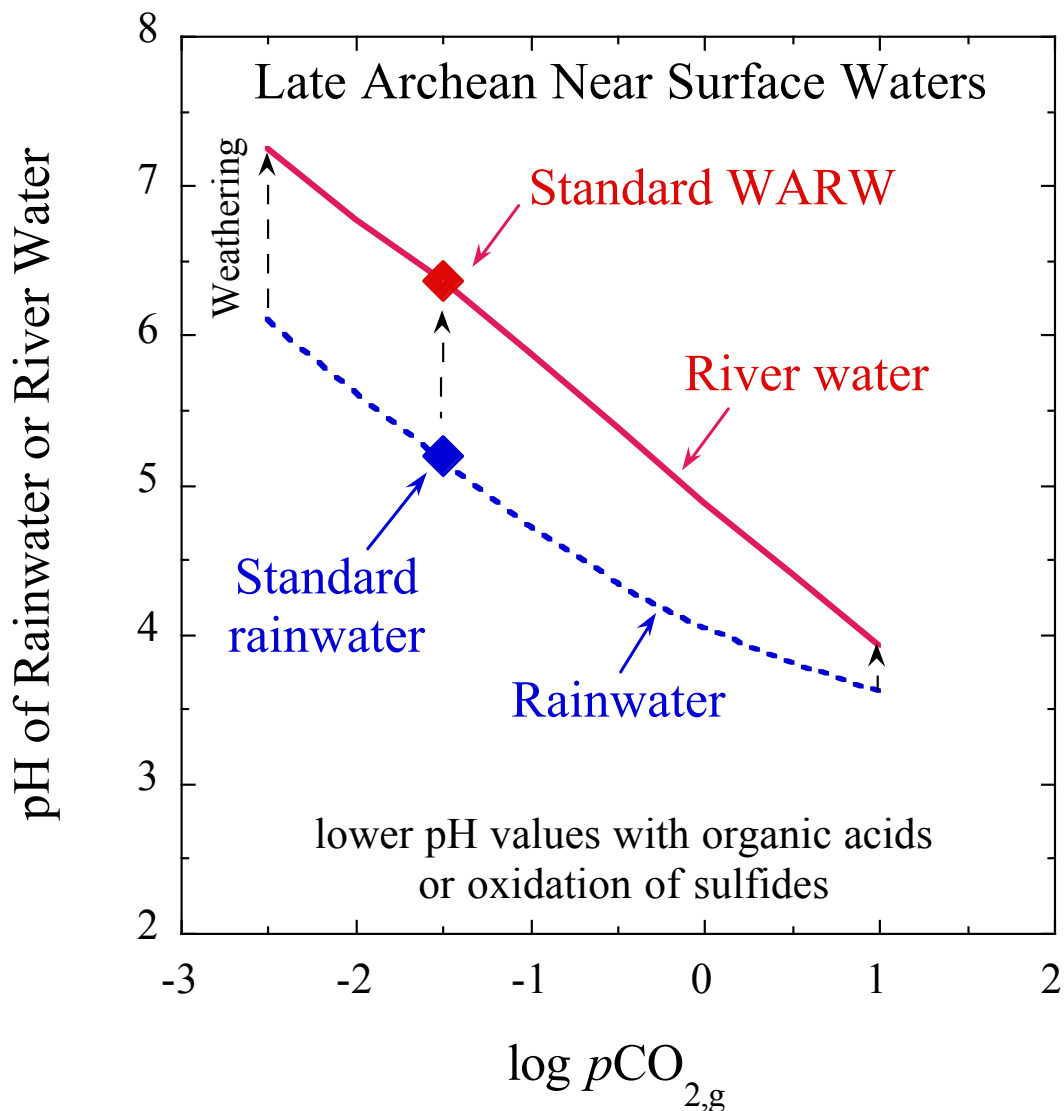


Figure 2. Proposed ranges of pH values of late Archean rainwater and river water as a function of atmospheric $p\text{CO}_{2,g}$. The upward arrows show changes of pH from rainwater to river water during weathering (Hao *et al.*, 2017). The solid diamonds refers to the pH values of our standard rainwater and world-average river water (WARW) when $p\text{H}_{2,g} = 10^{-5}$ bar and $p\text{CO}_{2,g} = 10^{-1.5}$ bar (Hao *et al.*, 2017). Even lower pH values could result from organic acids when $p\text{H}_{2,g}$ increases (Hao *et al.*, under review), or the oxidation of sulfides by aerobic bacteria when $p\text{H}_{2,g}$ decreases (Konhauser *et al.* 2011).

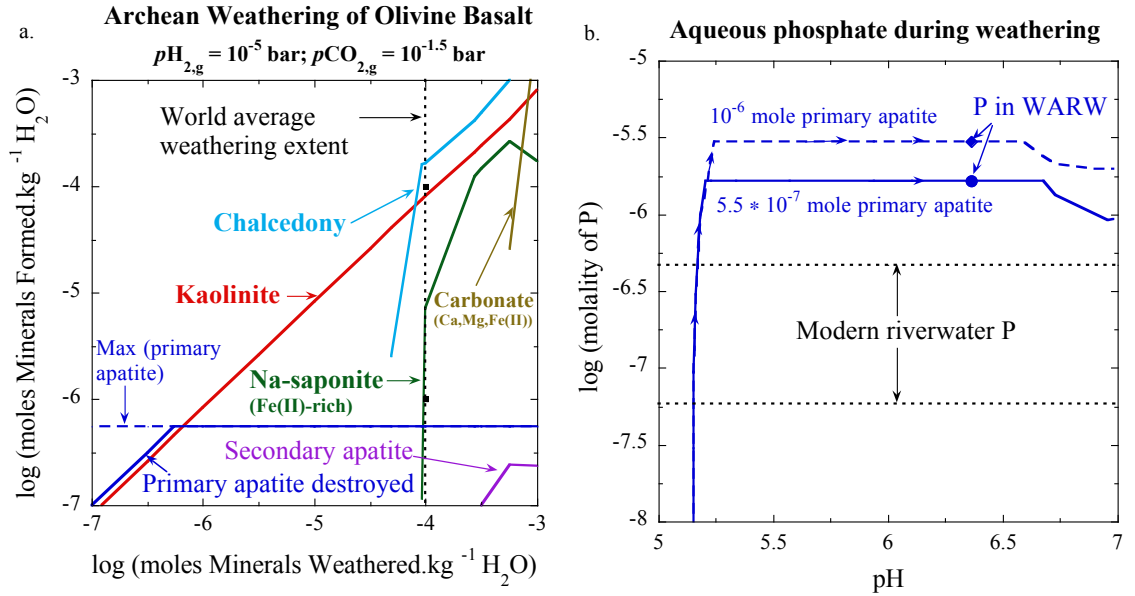


Figure 3. a. Destruction of 5.5×10^{-7} moles primary apatite during weathering of olivine basalt under the standard Archean atmospheric conditions. b. Evolution of aqueous phosphate during the weathering. Arrows along the lines show the evolving water chemistry in the direction of increasing reaction extent during the weathering of 5.5×10^{-7} mole (blue solid line) or 10^{-6} mole (blue dashed line) of apatite. Round and square points suggest the concentrations of dissolved phosphate in the Archean world average riverwater (WARW) corresponding to the different initial amounts of apatite. Black dashed lines show the range of dissolved phosphate in the present-day river water (data from Gaillardet et al., 2014).

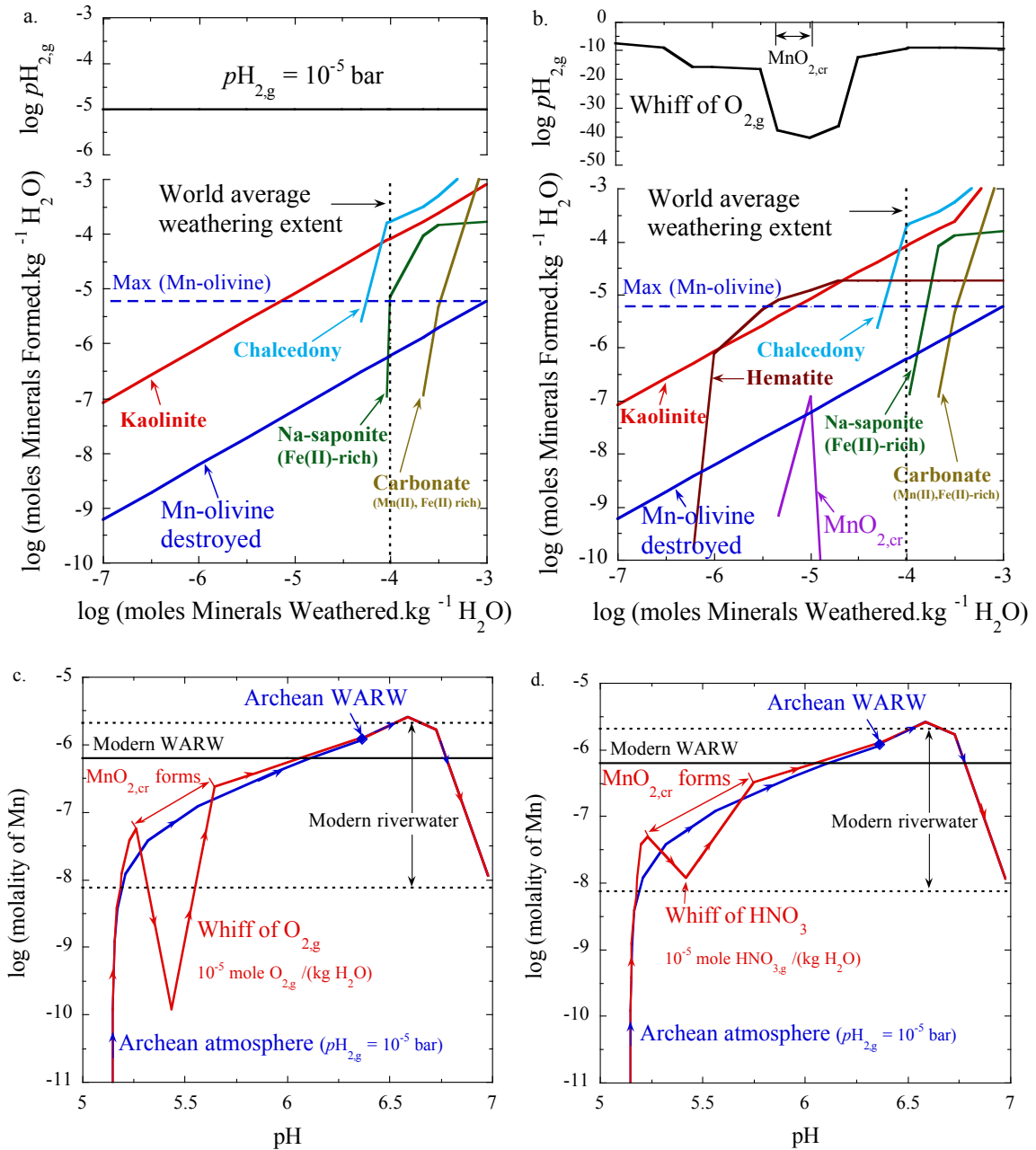


Figure 4. a. & b. Destruction of Mn-bearing olivine during the weathering of olivine basalt: (a) The standard Archean atmospheric conditions; (b) Whiff of $O_{2,g}$. The upper parts of the figures show the changes of $\log pH_{2,g}$ during the weathering; (c) & (d) Evolution of dissolved manganese during weathering during the addition of O_2 or HNO_3 , respectively. Arrows along the lines show the evolving water chemistry in the direction of increasing reaction extent during the weathering. Blue diamonds suggest the concentrations of dissolved Mn in Archean world average river water under the standard conditions. Black solid line and dashed lines show the average value and the range of dissolved Mn in the present-day riverwater (data from Gaillardet et al., 2014).

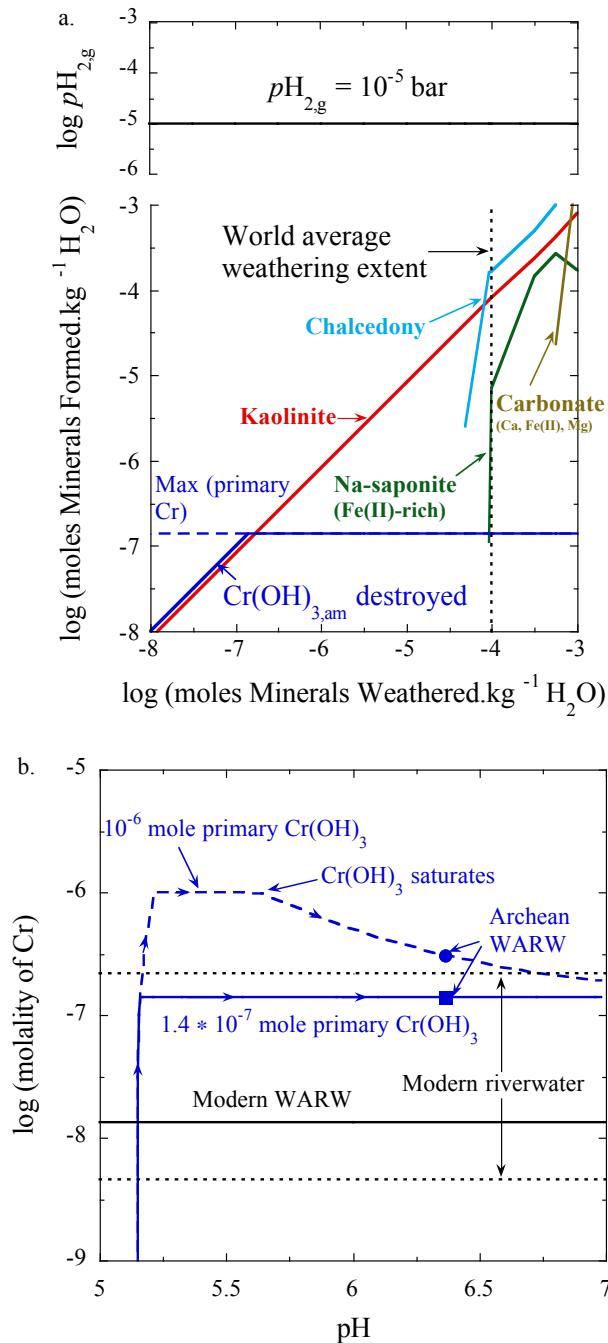


Figure 5. a. Destruction of $\text{Cr(OH)}_{3,\text{am}}$, stability of chromite (FeCr_2O_4) and formation of secondary minerals during the weathering of olivine basalt under the Archean atmospheric conditions. b. Evolution of dissolved chromium during weathering. Arrows along the lines show the evolving water chemistry in the direction of increasing reaction extent during the weathering of $1.4 \times 10^{-7} \text{ mole}$ (blue solid line) or 10^{-6} mole Cr(OH)_3 . The solid circle and square points suggest the concentrations of dissolved Cr in the Archean WARW corresponding to different amounts of Cr(OH)_3 . Black solid line and dashed lines show the average value and the range of dissolved Cr in the present-day riverwater (Gaillardet et al., 2014).

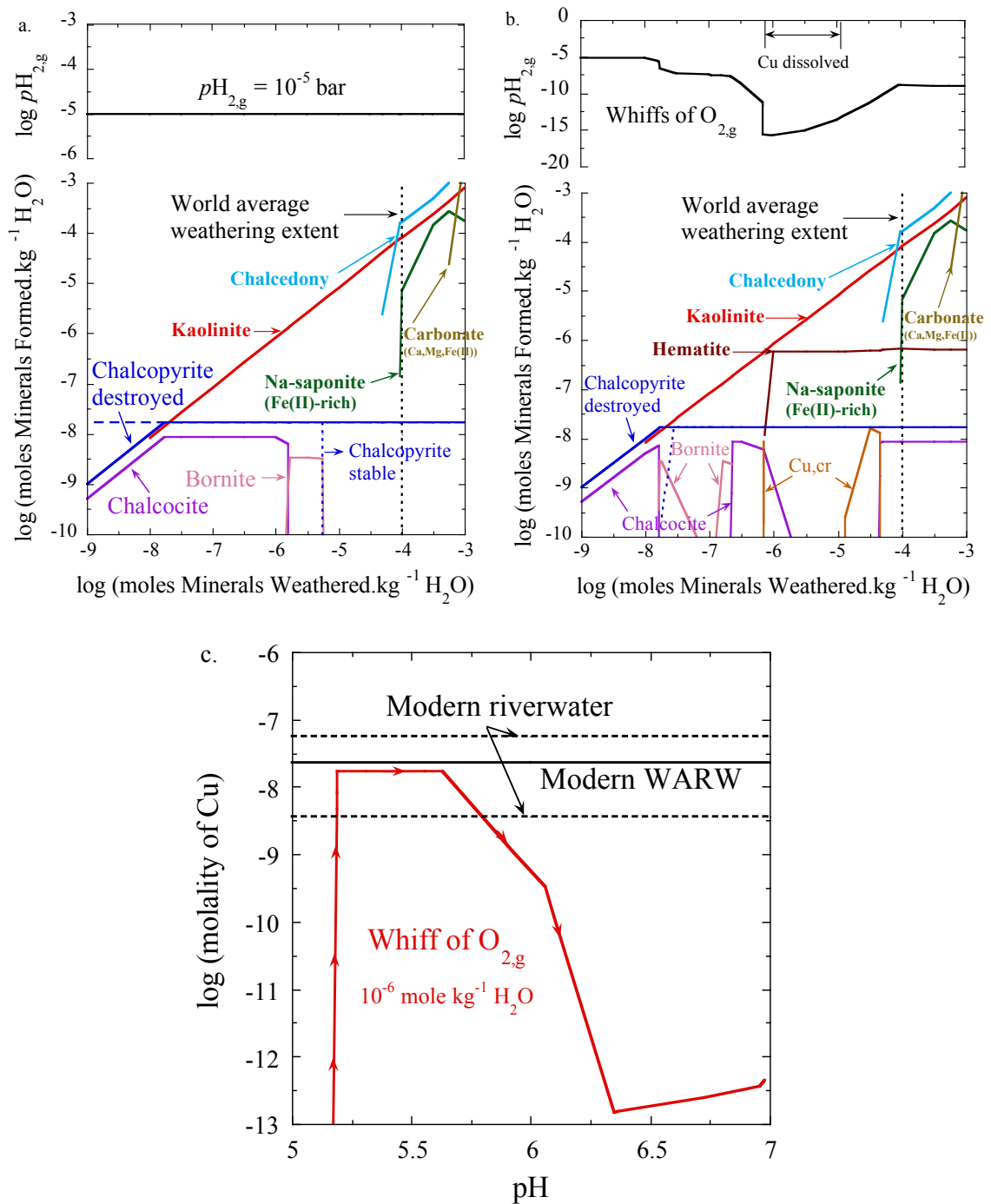


Figure 6. Destruction of chalcopyrite (CuFeS_2) and formation of secondary minerals during the weathering of olivine basalt under (a) the standard Archean atmospheric conditions and (b) Whiff of $\text{O}_{2,\text{g}}$ (10^{-6} mole $\text{O}_{2,\text{g}}$ $\text{kg}^{-1} \text{H}_2\text{O}$). c. Evolution of dissolved copper during weathering. Arrows along the lines show the evolving water chemistry in the direction of increasing reaction extent during the weathering. The black solid line and dashed lines show the average value and the range of dissolved Cu in the present-day riverwater (Gaillardet et al., 2014).

Chapter 6

Chromium Redox Equilibria in Aqueous Fluids Under Hydrothermal and Subduction-zone Conditions

Chemical profiles of chromium and its isotopes in sedimentary archives have been widely used as a paleo-redox proxy. However, sedimentary rocks from early Earth have all experienced variable degrees of diagenesis and/or low to middle grades metamorphism. Consequently, the behavior of chromium at temperatures and pressures greater than the original depositional conditions is potentially very important for the interpretation of the chromium signature but has rarely been reported. In this study, we applied the recently developed Deep Earth Water (DEW) Model ([Sverjensky et al., 2014](#)) to simulate the speciation and solubility of chromium in aqueous solutions over a wide range of temperatures and pressures including diagenetic, hydrothermal, and subduction-zone conditions. Moreover, the effects of redox state, pH, and complexation with Cl^- on the behavior of chromium were also investigated.

In low-pressure diagenetic and hydrothermal environments, our calculations showed that Cr^{2+} could be a dominant species together with Cr^{3+} within geologically reasonable ranges of pH and $\log f\text{O}_{2,\text{g}}$ at 100 °C and $P_{\text{sat.}}$. Cr^{2+} is stable at high pH and low $f\text{O}_{2,\text{g}}$ and Cr^{3+} is stable at low pH and high $f\text{O}_{2,\text{g}}$. Cr(VI) species are not important

under these conditions. However, if temperature increases to 250 °C, Cr^{2+} becomes the only dominant Cr species in aqueous fluids within the reasonable ranges of pH and $\log f\text{O}_{2,\text{g}}$, suggesting that increasing temperature favors the stability of Cr(II) relative to Cr(III). Further calculation suggested that although Cr(III)- Cl^- complexation could promote the stability of Cr^{3+} relative to Cr^{2+} , Cr^{2+} is still a dominant species even with extremely high concentration of Cl^- , and Cr^{2+} is further favored if it too forms complexes.

In high-pressure subduction-zone environments, prediction of the oxidation reaction of Cr^{2+} to Cr^{3+} suggested increasing stability of Cr^{2+} versus Cr^{3+} with increasing temperature but increasing pressure favors stability of Cr^{3+} versus Cr^{2+} . Specifically, at 1 GPa and 200 °C, Cr^{2+} is the only dominant aqueous Cr species within geologically reasonable ranges of pH and $\log f\text{O}_{2,\text{g}}$. Cr^{3+} could be stable at low pH with $\log f\text{O}_{2,\text{g}}$ close to QFM. The stability of Cr(VI) species requires high $f\text{O}_{2,\text{g}}$ and pH conditions. Similarly, at 1 GPa and 600 °C, Cr^{2+} is still the only dominant species within ranges of pH and $\log f\text{O}_{2,\text{g}}$ constrained by mineral buffers. Cr^{3+} is not stable under these conditions but HCrO_4^- could be stable at $\log f\text{O}_{2,\text{g}}$ close to QFM and high pH. At 5 GPa and 600 °C, Cr^{3+} is the only dominant aqueous Cr within the ranges of pH and $\log f\text{O}_{2,\text{g}}$ constrained by mineral buffers. At $\log f\text{O}_{2,\text{g}}$ close to QFM, Cr^{2+} and CrO_4^{2-} could be stable at moderately high pH and higher pH respectively. At 5 GPa and 1000 °C, the results are similar to the case at 1 GPa and 600 °C.

Complexation between Cr and Cl^- could conceivably promote the solubility of $\text{Cr}_2\text{O}_{3,\text{cr}}$ at 0.5 GPa, 600 °C or 6 GPa, 1000 °C, but all of the dissolved species should be Cr(II). HCrO_4^- could be stable at high pH but Cr(III) was predicted to not be stable. Our calculation results suggested that metamorphism involving aqueous fluids could

solubilize chromium as Cr(II) or Cr(VI) and modify the original sedimentary signatures. This process also could cause isotopic fractionation of Cr. High-temperature fluids carrying high concentrations of Cr(II) might also cause the formation of the hydrothermal mineral crocoite, chromite ore deposits, and Cr-rich garnets associated with diamond formation.

Authors: Jihua Hao, Dimitri A. Sverjensky, and Robert M. Hazen

1. Introduction

Chromium is a trace element in the continental crust but enriched in ultramafic and mafic rocks. Chromium has three common redox states: Cr(II), Cr(III), and Cr(VI). Under ambient conditions, Cr(II) requires very reducing conditions and is not stable in water as shown in [Figure 1](#). Instead, Cr(III) and Cr(VI) can be stable depending on the pH and $\log f\text{O}_{2,\text{g}}$. Specifically, under anoxic to reducing conditions, Cr(III) is stable. If the surface water is acidic ($\text{pH} < 5.5$), the solubility of Cr(III) is high and Cr^{3+} is the major aqueous species; otherwise, $\text{Cr}(\text{OH})_{3,\text{am}}$ will precipitate and limit the solubility of chromium. Oxidation of Cr(III) to form Cr(VI) is thermodynamically favorable under moderately oxidizing conditions even without the existence of molecular $\text{O}_{2,\text{g}}$ ([Fig. 1](#)). However, the oxidation of Cr(III) in the surface environment relies on the catalysis of strong oxidants, e.g. $\text{MnO}_{2,\text{cr}}$ or H_2O_2 ([Oze et al., 2007](#)). If somehow these oxidants are present, Cr(III) can be oxidized to Cr(VI) which greatly increases the solubility of chromium. These processes facilitate riverine transport of chromium to the ocean where Cr(VI) can again be reduced and sequestered into sediments.

Based on the above understanding of chromium weathering and riverine transport, recent studies have utilized the chemical profiles of chromium recorded in ancient marine sediments to reconstruct the evolutionary history of atmosphere $\text{O}_{2,\text{g}}$. For example, high concentrations of chromium in banded iron formations were interpreted to indicate the appearance of molecular $\text{O}_{2,\text{g}}$ in the early atmosphere before the Great Oxidation Event ([Frei et al., 2009](#)). However, all early sedimentary records have experienced diagenesis and low to high-grade metamorphism which might potentially modify the original geochemical signatures. At elevated temperature and pressure, previous studies have

suggested that low valence states of trace metals such as Fe(II), Eu(II), and Cu(I) are thermodynamically favorable to form in aqueous solutions due to the large difference of entropy among valences (e.g. [Sverjensky, 1984](#)). If this principle also applies to chromium, then Cr(II) might be expected in aqueous fluids once the temperature is increased during advanced diagenesis or low to high-grade metamorphism. Reduction of Cr(III) to Cr(II) would be expected to increase the solubility of chromium in aqueous fluids. In this case, the original depositional isotopic signature of chromium may not be preserved.

A limited number of geological observations and experimental studies present a complicated picture of chromium behaviors to be expected in hydrothermal fluids. For example, onboard-ship analysis of dissolved Cr in diffuse hydrothermal fluids has been used to calculate the total chromium concentration in the hydrothermal end-member ([Sander and Koschinsky, 2002](#)) of about 1200 nM without considering any fluid-rock interactions during the transport of the hydrothermal fluid. Given the likelihood of possible scavenging processes of aqueous Cr by Fe-Mn oxides along with cooling of the fluid ([German et al., 1991](#)), the concentrations of dissolved Cr in the hydrothermal fluid end-member might be even higher than the suggested value.

Experimental studies suggest a limited solubility of chromium in low pressure hydrothermal fluids ([Hiroishi et al., 1998](#); [Ziemniak et al., 1998](#)). Specifically, [Hiroishi et al. \(1998\)](#) measured the solubility of $\text{Cr}_2\text{O}_{3,\text{cr}}$ in pure water at 200 °C and reported 22.4 nM dissolved Cr with pH of the solution as around 4.5 at room temperature. Other experiments reported less than 1 nM dissolved Cr in alkaline solutions in equilibrium with $\text{Cr}_2\text{O}_{3,\text{cr}}$ at temperatures ranging from 25 °C to 300 °C ([Ziemniak et al., 1998](#)). In

order to solve the contradiction between the reported solubilities between geological observations and laboratory experiments, a better understanding of the speciation of aqueous chromium is required together with considerations of constraints on the pH and redox in geological settings.

As in the case of hydrothermal systems, the mobility of chromium under subduction-zone and upper mantle conditions are rarely addressed and poorly understood. Evidence from various diamond inclusions showed up to 2.5 wt% Cr, implying high concentrations of chromium in upper mantle fluids (Klein-BenDavid et al. 2009; Sobolev et al., 2009). It has been proposed that such high concentrations of chromium were the result of transport in high salinity fluids, especially with high concentrations of chloride (Sobolev et al., 2009). Cr-rich veins with up to 4 wt% chromium in eclogite (~600 °C and ~ 2.0 GPa) have been interpreted to represent an external Cr-rich fluid probably derived from serpentine dehydration (Spandler et al., 2011).

Experiments on the solubility of $\text{Cr}_2\text{O}_{3,\text{cr}}$ with a range of KCl concentrations at 1,000 °C and 4 GPa reported concentrations of dissolved chromium as high as 0.06 molal (Klein-BenDavid et al., 2011). Similar experiments at lower temperatures and pressures (Watenphul et al., 2014) showed that solubilities of $\text{Cr}_2\text{O}_{3,\text{cr}}$ in Na_2CO_3 and $\text{Na}_2\text{Si}_3\text{O}_7$ solutions are below the detection limit, whereas the solubility of $\text{Cr}_2\text{O}_{3,\text{cr}}$ in HCl_{aq} could be up to 0.29 M. Various lines of evidence point to the fact that chromium could be very mobile in fluids at high temperature and pressure. In addition, complexation with ligands, such as Cl^- and/or low pH might be expected to increase the solubility of chromium minerals. However, none of the experimental studies determined the valence of aqueous chromium during the experiments. The possibility that reduction of Cr(III) to Cr(II)

increases the solubility of chromium at high temperature and pressure cannot be ruled out experimentally unless the redox state of the system is well controlled and the valence information of aqueous chromium is analyzed.

The present study was designed to apply the recently developed Deep Earth Water (DEW) Model (Sverjensky et al., 2014) to calculate the speciation and solubility of chromium in aqueous solutions over a wide range of temperatures and pressures covering hydrothermal, subduction-zone, and upper mantle conditions. In addition, the effects of redox state, pH, and complexation with possible ligands on the behavior of chromium were investigated. The goal of this project is to use theoretical thermodynamic calculations to explore the possible behavior of chromium in aqueous fluids as a guide to future experiments and as an aid to the interpretation of the chromium concentrations in minerals.

2. Theoretical calculation approach and assumptions

2.1 Calculation approach

The thermodynamic properties of aqueous and solid chromium species used in the calculations are listed in Table 1. For the aqueous chromium species, we used the Helgeson-Kirkham-Flowers equations and predictive correlations to calculate the standard Gibbs free energies of formation at high temperatures and pressures ranging from hydrothermal to subduction-zone conditions (Helgeson et al., 1981; Shock et al., 1997; Sverjensky et al., 1997). The calculations were conducted with the Deep Earth Water (DEW) Model (Sverjensky et al., 2014) which has recently applied to explore the behaviors of C and N in upper mantle and subduction-zone fluids (Mikhail and

Sverjensky, 2014; Sverjensky et al., 2014). The Gibbs free energies of formation of Cr-bearing solids at high temperatures and pressures were calculated using the SUPCRT92b code, an adaption of SUPCRT92 (Johnson et al., 1992) that we use to compute the thermodynamic properties of minerals consistent with Berman (1988), Berman and Aranovich (1996), Sverjensky et al. (1991).

Owing to the lack of stability of Cr(II) in surface waters the thermodynamic properties of Cr(II)-complexes are not known. In this study, we examined the potential role of Cr(II)-Cl complexes on the solubility of chromium minerals by considering a range of values for the dissociation constant of CrCl^+ . With regard to simple Cr-bearing solids, we used $\text{Cr}_2\text{O}_{3,\text{cr}}$ even though it is a rare mineral in nature. Chromium occurs mainly as chromite or as solid solutions in silicate minerals, suggesting that $\text{Cr}_2\text{O}_{3,\text{cr}}$ is not stable in multicomponent rocks. We considered it because the thermodynamic properties have been measured and experiments have mainly used $\text{Cr}_2\text{O}_{3,\text{cr}}$ to study the solubility of chromium at high temperatures and pressures. In this way, our calculations can be compared with experimental results even though $\text{Cr}_2\text{O}_{3,\text{cr}}$ has little relevance to the occurrence of chromium in nature.

2.2 Assumptions for hydrothermal and subduction-zone conditions

The temperatures of low-pressure hydrothermal fluids can range from about 50 °C in the shallow subsurface of the seafloor to at least 400 °C and pressures from a few hundred bars to several kilobars (Vanko, 1988; Shock, 1992). The oxidation states of hydrothermal fluids could be in principle constrained by several mineral redox buffers (Shock 1992; Seewald, 1996). In our study, we chose quartz-fayalite-magnetite (QFM)

and magnetite-hematite (MH) to represent a wide range of redox states under hydrothermal conditions. As in the case of the oxygen fugacity, mineral buffers can be used to indicate the likely ranges of pH of hydrothermal. One common example is the feldspar-muscovite-quartz assemblage because the equilibrium constant is the activity ratio of K^+ and H^+ (Sverjensky et al., 1991). At a given temperature and pressure, the pH values of hydrothermal fluids are determined by a given $a(K^+)$ value (Hemley and Jones, 1964).

In subduction zones, the appropriate temperatures and pressures vary a lot among different subduction-zones (Syracuse et al., 2010; van Keken et al., 2011). In this study, we didn't investigate speciation of aqueous chromium in one specific subduction-zone setting; instead, we selected four P-T boundary conditions to explore most of the likely ranges. The redox states of subduction-zone fluids are thought to be indicated by the QFM redox buffer, specifically between QFM and QFM - 2 (Parkinson and Arculus, 1999; Kelley and Cottrell, 2009). In order to simulate possible variations of redox states among tectonic settings, we also calculated the $\log fO_{2,g}$ values represented by HM and iron-wüstite. In contrast to the hydrothermal fluids, few studies have considered the possible pH ranges of subduction-zone fluids (Galvez et al., 2016; Sverjensky et al., 2014). Given that forsterite and enstatite are two abundant minerals in the ultramafic oceanic lithosphere, we adopted these minerals to indicate the potential ranges of pH of subduction-zone fluids in the present study.

3. Predicted behavior of aqueous chromium at elevated temperatures and pressures

3.1 Chromium redox equilibria in low-pressure hydrothermal systems

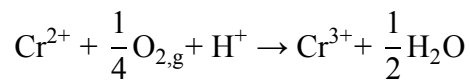
Figure 2 shows the predicted relative stabilities of aqueous chromium species in hydrothermal fluids as functions of pH and $\log fO_{2,g}$. It can be seen in Fig. 2a that at 100 °C and the saturation pressure of water vapor ($P_{sat.}$), the speciation of chromium varies greatly depending on the pH and redox states of the fluid. Specifically, at $\log fO_{2,g}$ between QFM and magnetite-hematite and pH constrained by KMQ, Cr^{2+} and Cr^{3+} are the dominant aqueous species of chromium. The results indicate that Cr^{2+} , which is not stable under ambient conditions (Fig. 1), could be thermodynamically stable in water as temperature increases. Moreover, the stability of Cr^{2+} is favored by low $\log fO_{2,g}$ and high pH, as suggested by Fig. 2a, whereas formation of Cr^{3+} is favored by high $\log fO_{2,g}$ and low pH. The diagram also indicates that within $HCrO_4^-$ and CrO_4^{2-} do not have stability fields unless both $\log fO_{2,g}$ and pH are much higher than the geochemically reasonable ranges considered here. Speciation results in the sulfur system suggested H_2S_{aq} to be the dominant aqueous sulfur species in hydrothermal fluids within the ranges of $\log fO_{2,g}$ and pH constrained by the mineral assemblages in Fig. 2a.

The increased stability of aqueous Cr^{2+} with increasing temperature is shown even more dramatically in Fig. 2b. Here it can be seen that the stability field of Cr^{3+} retreats to geochemically unreasonable pH and $\log fO_{2,g}$ conditions, leaving Cr^{2+} as the predicted dominant aqueous chromium species. This result confirms the hypothesis that high temperatures favor the stability of the lower valence of chromium in aqueous solution. Moreover, Fig. 2b suggests an expansion of the stability field of $HCrO_4^-$ relative to CrO_4^{2-} . Nevertheless, $HCrO_4^-$ is still not an important species within the ranges of pH and $\log fO_{2,g}$ constrained by the mineral assemblages in Fig. 2b. H_2S_{aq} is again the dominant aqueous species of sulfur under these conditions.

The speciation of trace metals such as chromium can be greatly affected by complexation with anions such as Cl^- , HS^- , SO_4^{2-} , and organics (Sander and Koschinsky, 2000). In this study, we estimated the thermodynamic properties of CrCl^{2+} and explored its behavior in our calculations at 250 °C and $P_{\text{sat.}}$. The results shown in Fig. 3 indicate that, as expected, the stability field of Cr(III) increases with elevated concentrations of Cl^- , meaning that complexation between Cr^{3+} and Cl^- could promote the stability of aqueous Cr(III) versus Cr(II). However, even with $a(\text{Cl}^-) = 1$, Cr^{2+} remains a major Cr aqueous species. The role of Cr(III)-Cl complexation does not effectively cancel the effect of increasing temperature on the stability of Cr(II) versus Cr(III). In addition, Cr(II) might be expected to have a similar ability to complex with Cl^- , similar to the behaviors of Fe(II) and Fe(III) (Shock and Koretsky, 1995; Sverjensky et al., 1997). In this case, the complexation of both Cr(II) and Cr(III) would oppose each other and tend to cancel, which would favor the enhanced stability field of Cr(II) at elevated temperatures.

3.2 Chromium redox equilibria in high pressure-temperature fluids

The key equilibrium between Cr^{2+} and Cr^{3+} can be expressed as



The predicted behavior of this equilibrium constant at both elevated temperatures and pressures can be seen in Fig. 4. As expected, the strong decrease in log K with increasing temperature favors the relative stability of Cr^{2+} compared with Cr^{3+} in the fluid. However, it can also be seen in Fig. 4 that log K increases with increasing pressure, which opposes the trend with increasing temperature. In order to explore the relative effects of

temperature and pressure, in the following discussion, we show four representative cases covering a large range of temperatures and pressures (Fig. 5).

The results at 1 GPa and 200 °C (Fig. 5a) are similar to those obtained for the low pressure hydrothermal systems discussed previously: Cr^{3+} is stable at low pH whereas Cr^{2+} is stable at high pH at $\log f\text{O}_{2,g}$ close to QFM. The most oxidized species, HCrO_4^- and CrO_4^{2-} , require $\log f\text{O}_{2,g}$ values much higher than QFM. Under conditions with $\log f\text{O}_{2,g}$ between QFM and QFM - 2 and pH values set by the forsterite-enstatite buffer, Cr^{2+} is suggested to be the dominant aqueous species. Under these circumstances, the formation of a Cr^{3+} mineral from an aqueous fluid containing Cr^{2+} will necessarily involve a redox reaction.

At the same pressure of 1 GPa and the higher temperature of 600 °C, it can clearly be seen in Fig. 5b that Cr^{2+} and HCrO_4^- are predicted to be the dominant aqueous species over the whole $\log f\text{O}_{2,g}$ and pH range. At this pressure and temperature, Cr^{3+} and CrO_4^{2-} have no stability fields. Consequently, even at 1 GPa, high temperature favors the stability of Cr^{2+} versus Cr^{3+} . Neutral pH doesn't change much with the increasing temperature from Fig. 5a to b, however the pH levels of the forsterite-enstatite buffer drop dramatically from alkaline at 1 GPa and 200 °C to acidic at 1 GPa and 600 °C. The level of $\log f\text{O}_{2,g}$ indicated by the QFM buffer increases greatly from 200 °C to 600 °C. Within the ranges of $\log f\text{O}_{2,g}$ and pH constrained by these mineral buffers for pH and $\log f\text{O}_2$, Cr^{2+} is the only dominant aqueous species in the fluids. Moreover, our calculation also shows that aqueous HCrO_4^- could be stable at high $\log f\text{O}_{2,g}$ but also at high pH when $\log f\text{O}_{2,g}$ is around QFM. This result indicates that HCrO_4^- might form in highly alkaline fluid (pH > 6) without any changes of oxidation states at this temperature and

pressure, although whether this level of high pH is geologically sensible or not is unknown.

Much higher pressures are depicted in Fig. 5c and d. In Fig. 5c, it can be seen that at 5 GPa and 600 °C when $\log fO_{2,g}$ is between QFM and QFM-2, Cr^{3+} is thermodynamically stable at low pH, Cr^{2+} at moderate pH, and CrO_4^{2-} at high pH. Within the pH range constrained by the forsterite-enstatite assemblage, Cr^{3+} is the dominant aqueous species, in contrast to the results at 1 GPa, 600 °C which show that Cr^{2+} is the dominant aqueous species. This result confirms the preliminary conclusion (Fig. 4) that increasing pressure favors the oxidation of Cr^{2+} to form Cr^{3+} . In addition, the calculation also suggests that Cr(VI) could form in highly alkaline fluids (pH > 6) with $\log fO_{2,g}$ of approximately QFM.

At both high pressure and high temperature, i.e. 5 GPa and 1000 °C, it can be seen in Fig. 5d that the results are similar to those at 1 GPa and 600 °C. Specifically, only Cr^{2+} and $HCrO_4^-$ are stable species in the fluids. Within the ranges of $\log fO_{2,g}$ and pH constrained by mineral assemblages, Cr^{2+} is the only dominant aqueous Cr species. Obviously, $HCrO_4^-$ could form at high $\log fO_{2,g}$, but also form at pH > 4 even when $\log fO_{2,g}$ is close to or lower than QFM (Fig. 5d).

Overall, the calculation results at different temperatures and pressures as shown in Figs. 4 and 5 suggest a complicated picture of the speciation of aqueous chromium strongly depending on both redox and pH. Although high temperature favors the stability of Cr^{2+} , high pressure favors the stability of Cr^{3+} . Considering the large coupled variations of temperature and pressure inferred for subduction-zone systems (Syracuse et al., 2010; van Keken et al., 2011), the chromium in the subduction-zone fluids can be

expected to experience repeated redox reactions, especially between Cr^{2+} and Cr^{3+} -species, including their complexes. According to our calculations, the formation of Cr(VI) would require unusually high $\log f\text{O}_{2,\text{g}}$ or high pH. As mentioned above, if the redox states of subduction-zone mainly lies between QFM and QFM-2, there is little possibility of forming Cr(VI) via oxidation of Cr(II) or Cr(III). Whether there could be large enough pH changes during water-rock interaction that could enable the formation of Cr(VI) without redox changes remains an open question. Previous work has suggested the effect of pH change due to water-rock interactions in the formation of diamond in eclogitic environments (Sverjensky et al., 2015). A similar modeling approach could now be applied to include the behavior of chromium during water-rock interactions in the future.

3.3 Solubility of $\text{Cr}_2\text{O}_{3,\text{cr}}$ at high temperature and pressure

Figure 6 shows equilibrium diagrams for the $\text{Cr}_2\text{O}_3\text{-H}_2\text{O-HCl}$ system that include $\text{Cr}_2\text{O}_{3,\text{cr}}$ at two settings of temperature and pressure. At 0.5 GPa and 600 °C, our calculation suggests that Cr(II) and HCrO_4^- are dominant aqueous species in equilibrium with $\text{Cr}_2\text{O}_{3,\text{cr}}$. There is no stability field for aqueous Cr(III), implying that aqueous Cr(III) is not thermodynamically stable in this environment in the fluid. This result might appear to contradict suggestions that the dissolved chromium is Cr(III) under similar temperature and pressure conditions (Watenphul et al., 2014). However, it should be emphasized that the Watenphul et al. (2014) study involved the solubility of $\text{Cr}_2\text{O}_{3,\text{cr}}$ in very strongly acidic HCl solutions for which we do not currently have an aqueous speciation model. Our equilibrium constant calculations reported in Fig. 6 do show a strong dependence of the solubility of $\text{Cr}_2\text{O}_{3,\text{cr}}$ on the pH as well as the $\log f\text{O}_{2,\text{g}}$ in the water. Specifically,

under low pH and low $\log f_{\text{O}_{2,\text{g}}}$ conditions, aqueous Cr(II) is thermodynamically favored to form. Given the high solubility of Cr(II) in the water, the solubility of Cr(III)-minerals will be promoted as long as the reduction of Cr(III) to Cr(II) proceeds. This process may partly explain the high solubility of $\text{Cr}_2\text{O}_{3,\text{cr}}$ in high $\text{HCl}(\text{aq})$ -rich solutions (Watenphul et al., 2014).

Apart from the pH and redox, another important factor affecting the solubility of minerals is the complexation with ligands. In the case of hydrothermal and subduction-zone fluids, one of the most abundant species is Cl^- (Manning, 2004; Von Damm, 1990). As we mentioned above, due to the limitation of thermodynamic properties for Cr(II)-Cl, we simply calculated the effects of complexation by giving a range for the stability constant ($\log \beta$). Larger $\log \beta$ values represent stronger complexation. It can be seen in Fig. 6 that strong complexation between Cr^{2+} and Cl^- could expand the stability field of aqueous Cr(II) toward that of $\text{Cr}_2\text{O}_{3,\text{cr}}$, implying an increase of solubility of $\text{Cr}_2\text{O}_{3,\text{cr}}$. Our results presumably show that complexation of Cr(II) with Cl^- could increase the solubility of $\text{Cr}_2\text{O}_{3,\text{cr}}$, as also suggested by Watenphul et al. (2014). However, to quantitatively examine the complexation effect, a reliable estimation of the thermodynamic properties of Cr(II)-Cl complexes will be required.

At 5 GPa, 1000 °C it can be seen in Fig. 6b that aqueous Cr(III) is not stable in the supercritical fluid. However, unlike the case at 0.5 GPa, 600 °C, CrCl^+ is the dominant species rather than $\text{Cr}_2\text{O}_{3,\text{cr}}$ at the redox states close to QFM and neutral pH. This indicates a moderate or high solubility of $\text{Cr}_2\text{O}_{3,\text{cr}}$ in the hydrous fluid under these conditions, consistent with the high solubility of $\text{Cr}_2\text{O}_{3,\text{cr}}$ in neutral and KCl fluids at similar temperatures and pressures reported by Klein-BenDavid et al. (2011). However,

our calculation suggests that Cr(II) is the dominant aqueous species instead of Cr(III) proposed by Klein-BenDavid et al. (2011). It was also observed that the solubility of $\text{Cr}_2\text{O}_{3,\text{cr}}$ would increase as the concentration of KCl increased (Klein-BenDavid et al., 2011), indicating potential effects of complexation between aqueous Cr and Cl^- . Here, our results showed an expansion of the stability field of CrCl^+ in response to the stronger complexation, although we changed the stability constant of CrCl^+ instead of concentration of Cl^- due to a lack of reliable thermodynamic properties of CrCl^+ . In addition, our results imply a strong dependence of speciation and solubility of chromium on the pH of the fluids at 5 GPa and 1000 °C. For example, HCrO_4^- could form at $\text{pH} > 6$ when the redox state is close to QFM. As we mentioned above, formation of HCrO_4^- would greatly elevate the solubility of chromium minerals.

4. Discussions and implications

Our results overall indicate a perhaps surprising stability for Cr(II) species in aqueous solution at temperature of greater than about 100 °C. Increase of pressure oppose this trend, but Cr(III) can only compete with Cr(II) when the pressure becomes very high, of the order of 5 GPa at temperatures of about 600 °C or less. These results have important implications for the geochemistry of chromium and its stable isotopes over a wide range of geologic environments from diagenetic to low pressure hydrothermal environments, and to subduction-zone conditions. We now discuss examples of the implications for chromium in these different environments.

4.1 The sedimentary banded iron formation record of chromium geochemistry

The chemical profiles of chromium and its isotopes recorded in various kinds of sedimentary records have been used to reconstruct the evolution of atmosphere $pO_{2,g}$ (Crowe et al., 2013; Frei et al., 2009 & 2016). One of the fundamental assumption behind these interpretations is that chromium can only be mobile when it is in its oxidized form, i.e. Cr(VI) ions, although recent studies also pointed out the role of fluctuations of pH in solubilizing Cr(III)-minerals without any $O_{2,g}$ (Hao et al., in preparation; Konhauser et al., 2011). In addition to all the factors affecting the weathering of chromium at ambient conditions, our study has revealed that even at modest elevations of temperature, Cr(II) instead of Cr(III) could be the dominant aqueous species at reasonable ranges of $\log fO_{2,g}$ and pH constrained by mineral buffers (Fig. 2). Cr(II) has a higher solubility than Cr(III) which will enable mobility of chromium. This process might conceivably have been very important in the geologic record considering that all of the reported Archean sedimentary archives have experienced at least low- to medium-grade metamorphism.

As with the the reduction of Fe(III), the reduction of Cr(III) to Cr(II) might also involve isotopic fractionation. If this is the case, Cr(II) should be isotopically lighter than Cr(III). It can be expected that during the interaction of water and Cr(III)-minerals at temperatures and pressures where the aqueous phase contains mainly Cr(II), the light chromium isotope will be enriched in the Cr(II) and any secondary minerals containing mainly Cr(III) will be enriched in the heavy chromium isotope. Moreover, at high temperature and pH, our calculation suggested that $HCrO_4^-$ could form by oxidation of Cr(II)/Cr(III) at $\log fO_{2,g}$ close to QFM (Fig. 6 & 7). This also implies that highly alkaline fluid could mobilize chromium in the form of $HCrO_4^-$ without $\log fO_{2,g}$ much higher than QFM. During this process, $HCrO_4^-$ will become isotopically heavier and solid residues as

mainly Cr(III) become isotopically lighter (Schauble et al., 2004). Under these circumstances, fluid-rock interactions occurring during the diagenesis and metamorphism of the sediments might generate small but noticeable isotope fractionations, which would confuse the interpretation of small anomalies of chromium isotopes. Therefore, further investigation of Archean sedimentary records should consider the influence of metamorphism especially processes involving hydrous fluids on the chemical profiles of chromium and its isotopes.

4.2 Behavior of chromium in hydrothermal and subduction-zone fluids

Examples of the involvement of aqueous chromium in hydrothermal and subduction-zone fluids include serpentinization environments, hydrothermal crocoite deposits, podiform chromium deposits, and fluids associated with diamond formation. It has been documented that serpentinites have heavy chromium isotopes compared to the mantle inventory (Farkaš et al., 2013; Wang et al., 2016). This result supports our inferences discussed above. In the relatively low pressure, high temperature environment of hydrothermal serpentine formation, aqueous Cr(II) species should predominate. When ultramafic rocks are altered by hydrothermal fluids the isotopically light Cr(II) in the fluids should be associated with isotopically heavier Cr(III) in the serpentine that forms in equilibrium with the fluid.

A second example involves the formation of the chromate mineral crocoite (PbCrO_4). According to our predictions, crocoite must form from a hydrothermal fluid containing Cr(II) species by a redox reaction. The oxidation of aqueous Cr(II) to Cr(VI) in alkaline hydrous fluids should result in very large isotopic fractionations because of

the difference of four redox units. This prediction provides a mechanism to explain the extremely heavy isotope compositions of hydrothermal crocoite from a variety of locations (Schoenberg et al., 2008).

Recent studies have also emphasized an important role for hydrothermal fluids in the formation of chromium ore deposits (Arai and Akizawa, 2014; Borisova et al., 2012; Matveev and Ballhaus, 2002). It is necessary to have a high solubility of chromium in the water in order to form ore-bodies of enormous volumes. As mentioned above, investigations of the complexation of Cr^{3+} and Cl^- have emphasized its role in increasing the solubility of chromium. However, as indicated in the experimental settings, it generally requires remarkably high concentrations of Cl^- or extreme conditions to have considerable solubility of chromium. In this study, we found that Cr(II) rather than Cr(III) is the dominant aqueous species under the redox and pH constrained by geologically abundant mineral assemblages. The solubility of Cr(II) should be much higher than Cr(III). Complexation of Cr(II) with ligands like Cl^- could further increase the solubility of chromium in the fluid. At high temperature and pressure, these processes should enable transport of high levels of chromium in aqueous fluids. However, aqueous Cr(II) might become less stable as the fluids cool and get oxidized to form Cr(III)-bearing minerals. Conceivably, the lower solubility of Cr(III) in the fluids would cause the precipitation of Cr-(hydro)oxides or chromite if Fe(II) is present in the system, forming chromium ore deposits. Direct precipitation of chromite from hydrothermal fluids has been suggested during metasomatic activity in peridotite rocks (Arai et al., 2014), consistent with our suggestions.

A final example of the potential importance of aqueous Cr(II) species involves the numerous lines of evidence for Cr transport by fluids associated with diamond formation and mantle metasomatism. The fluids recorded in diamond fluid and solid inclusions indicate dissolved chromium concentrations of the order of 1 wt. % (Klein Ben-David et al., 2009). Furthermore, garnets associated with diamond formation and mantle metasomatism typically are Cr-rich and low in Ca (Stachel and Harris, 2008). However, this association depends on the environment of diamond formation. Garnet inclusions in diamonds with eclogitic affinity typically have a low Cr content (much less than 1 wt% Cr₂O₃), whereas diamonds with a peridotitic affinity have high Cr contents (typically 7 - 10 % Cr₂O₃). The very high Cr concentrations in such garnets have often interpreted to reflect transport in Cl-bearing fluids (Wang et al., 2011; Stachel and Harris, 2008; Klein Ben-David et al., 2011).

5. Concluding remarks

This study has predicted the speciation of chromium in aqueous fluids as functions of log $f_{O_{2,g}}$ and pH at elevated temperatures and pressures using the recently developed Deep Earth Water (DEW) model. It has also investigated the effects of complexation between Cr(II)/Cr(III) and Cl⁻ on the relative stability of aqueous species and the solubility of Cr₂O_{3,cr}.

Our main conclusions are as follows:

(1) At 100 °C and $P_{sat.}$, Cr²⁺ and Cr³⁺ are the dominant aqueous Cr species given the ranges of pH and log $f_{O_{2,g}}$ constrained by mineral buffers. Low pH and high log $f_{O_{2,g}}$ favors the stability of Cr³⁺ and high pH and low log $f_{O_{2,g}}$ favors the stability of Cr²⁺.

Cr(VI) species are not thermodynamically stable unless at much higher $\log f\text{O}_{2,g}$ than QFM and very high pH.

(2) At 250 °C and $P_{\text{sat.}}$, Cr^{2+} becomes the only dominant aqueous Cr species whereas Cr^{3+} is not stable within ranges of pH and $\log f\text{O}_{2,g}$ constrained by mineral buffers. HCrO_4^- becomes more stable compared with the case at 100 °C, $P_{\text{sat.}}$, but is still unlikely to form under normal hydrothermal conditions.

(3) Complexation between Cr(III) and Cl^- could promote the stability of Cr^{3+} relative to Cr^{2+} at 250 °C and $P_{\text{sat.}}$. However, Cr(II) might have similar complexation behavior to Cr(III) and that would tend to cancel out the stabilization of Cr(III).

(4) At 1 GPa and 200 °C, Cr^{2+} is the only dominant aqueous Cr species within ranges of pH and $\log f\text{O}_{2,g}$ constrained by mineral buffers. At $\log f\text{O}_{2,g}$ values close to QFM, Cr^{3+} could be stable at low pH. Again, the stability of Cr(VI) species requires high $f\text{O}_{2,g}$ and pH conditions.

(5) At 1 GPa and 600 °C, Cr^{2+} is still the only dominant aqueous Cr species within ranges of pH and $\log f\text{O}_{2,g}$ constrained by mineral buffers. Cr^{3+} is not thermodynamically stable over a wide range of pH and $\log f\text{O}_{2,g}$. Instead, HCrO_4^- could be stable at $\log f\text{O}_{2,g}$ close to QFM and high pH.

(6) At 5 GPa and 600 °C, Cr^{3+} is the only dominant aqueous Cr species within ranges of pH and $\log f\text{O}_{2,g}$ constrained by mineral buffers. At $\log f\text{O}_{2,g}$ values close to QFM, Cr^{2+} could be stable at moderately high pH and CrO_4^{2-} could form at higher pH.

(7) At 5 GPa and 1000 °C, the speciation is similar to the case at 1 GPa and 600 °C, i.e. Cr^{2+} as the dominant aqueous Cr species and the stability of HCrO_4^- at high pH.

(9) Cr^{2+} and its complexes are dominant aqueous species during dissolution of $\text{Cr}_2\text{O}_{3,\text{cr}}$ at 0.5 GPa, 600 °C or 6 GPa, 1000 °C. The solubility of $\text{Cr}_2\text{O}_{3,\text{cr}}$ could be promoted by complexation with Cl^- . HCrO_4^- could be stable at high pH and its relative abundance could also increase the solubility of $\text{Cr}_2\text{O}_{3,\text{cr}}$ at high temperatures and pressures.

(10) Metamorphism involving hydrous fluids could modify the original sedimentary signatures of chromium by solubilizing chromium as Cr(II) or Cr(VI). Fluid-rock interactions under even mild diagenetic temperatures and pressures could cause isotopic fractionations of Cr under some circumstances, potentially confusing the interpretation of chemical profiles of Cr isotopes.

(11) Fluids carrying high concentrations of Cr(II) at elevated temperature and pressure might play an important role in the formation of the hydrothermal mineral crocoite, the formation of chromite ore deposits, and the formation of Cr-rich garnets associated with diamond formation. As all of the minerals involved contain Cr(III), redox reactions from aqueous Cr(II) to Cr(III) in the minerals would be necessary.

References:

- Arai, S., Akizawa, N., 2014. Precipitation and dissolution of chromite by hydrothermal solutions in the Oman ophiolite: New behavior of Cr and chromite. *Am. Mineral.* 99, 28–34. doi:10.2138/am.2014.4473
- Berman, R.G., 1988. Internally-Consistent Thermodynamic Data for Minerals in the System $\text{Na}_2\text{O}-\text{K}_2\text{O}-\text{CaO}-\text{MgO}-\text{FeO}-\text{Fe}_2\text{O}_3-\text{Al}_2\text{O}_3-\text{SiO}_2-\text{TiO}_2-\text{H}_2\text{O}-\text{CO}_2$. *J. Petrol.* 29, 445–522.
- Berman, R.G., Aranovich, L.Y., 1996. Optimized standard state and solution properties of minerals .1. Model calibration for olivine, orthopyroxene, cordierite, garnet, ilmenite in the system $\text{FeO}-\text{MgO}-\text{CaO}-\text{Al}_2\text{O}_3-\text{TiO}_2-\text{SiO}_2$. *Contrib. to Mineral. Petrol.* 126, 1–24. doi:10.1007/S004100050232
- Chase Jr, M.W., Davies, C.A., Downey Jr, J.R., Frurip, D.J., McDonald, R.A., Syverud, A.N., 1985. JANAF Thermodynamical tables 3rd Edition. *J. Phys. Chem. Ref. Data* 14.
- Crerar, D., Wood, S., Brantley, S., Bocarsly, A., 1985. Chemical controls on solubility of ore-forming minerals in hydrothermal solutions. *Can. Mineral.* 23, 333–352.
- Crowe, S.A., Dossing, L.N., Beukes, N.J., Bau, M., Kruger, S.J., Frei, R., Canfield, D.E., 2013. Atmospheric oxygenation three billion years ago. *Nature* 501, 535–538. doi:10.1038/nature12426
- Delano, J.W., 2001. Redox History of the Earth's Interior since 3900 Ma: Implications for Prebiotic Molecules. *Orig. Life Evol. Biosph.* 31, 311–341. doi:10.1023/A:1011895600380

- Farkaš, J., Chrastný, V., Novák, M., Čadkova, E., Pašava, J., Chakrabarti, R., Jacobsen, S.B., Ackerman, L., Bullen, T.D., 2013. Chromium isotope variations ($\delta^{53/52}\text{Cr}$) in mantle-derived sources and their weathering products: Implications for environmental studies and the evolution of $\delta^{53/52}\text{Cr}$ in the Earth's mantle over geologic time. *Geochim. Cosmochim. Acta* 123, 74–92.
doi:10.1016/j.gca.2013.08.016
- Frei, R., Crowe, S.A., Bau, M., Polat, A., Fowle, D.A., Dossing, L.N., 2016. Oxidative elemental cycling under the low O_2 Eoarchean atmosphere. *Sci Rep* 6, 21058.
doi:10.1038/srep21058
- Galvez, M.E., Connolly, J.A.D., Manning, C.E., 2016. Implications for metal and volatile cycles from the pH of subduction zone fluids. *Nature* 539, 420–424.
doi:10.1038/nature20103
- German, C.R., Campbell, A.C., Edmond, J.M., 1991. Hydrothermal scavenging at the Mid-Atlantic Ridge: Modification of trace element dissolved fluxes. *Earth Planet. Sci. Lett.* 107, 101–114. doi:10.1016/0012-821X(91)90047-L
- Gloyna, E.F., Li, L., 1993. Supercritical water oxidation model development for selected EPA priority pollutants. Center for Research in Water Resources, Bureau of Engineering Research, University of Texas at Austin.
- Gurevich, V.M., Kuskov, O.L., Smirnova, N.N., Gavrichev, K.S., Markin, A. V, 2009. Thermodynamic functions of eskolaite $\text{Cr}_2\text{O}_3(\text{c})$ at 0–1800 K. *Geochemistry Int.* 47, 1170. doi:10.1134/S0016702909120027
- Hao, J., Sverjensky, D.A., Hazen, R.M. (in preparation). Mobility of nutrients and trace metals during weathering in the late Archean.

- Helgeson, H.C., Kirkham, D.H., Flowers, G.C., 1981. Theoretical prediction of the thermodynamic behavior of aqueous electrolytes by high pressures and temperatures; IV, Calculation of activity coefficients, osmotic coefficients, and apparent molal and standard and relative partial molal properties to 600 °C and 5kb. *Am. J. Sci.* 281, 1249–1516. doi:10.2475/ajs.281.10.1249
- Hemley, J.J., Jones, W.R., 1964. Chemical aspects of hydrothermal alteration with emphasis on hydrogen metasomatism. *Econ. Geol.* 59, 538–569. doi:10.2113/gsecongeo.59.4.538
- Hiroishi, D., Matsuura, C., Ishiguro, K., 1998. Hydrolysis of chromium (III) ion and solubility of chromium (III) oxide in high temperature water. *Mineral. Mag.* 62 A, 626–627.
- Johnson, D.A., Nelson, P.G., 2012. Improvements in Estimated Entropies and Related Thermodynamic Data for Aqueous Metal Ions. *Inorg. Chem.* 51, 6116–6128. doi:10.1021/ic3000334
- Johnson, J.W., Oelkers, E.H., Helgeson, H.C., 1992. Supcrt92 - a Software Package for Calculating the Standard Molal Thermodynamic Properties of Minerals, Gases, Aqueous Species, and Reactions from 1 Bar to 5000 Bar and 0 °C to 1000 °C. *Comput. Geosci.* 18, 899–947. doi:10.1016/0098-3004(92)90029-Q
- Kelley, K.A., Cottrell, E., 2009. Water and the Oxidation State of Subduction Zone Magmas. *Science* 325, 605–607. doi:10.1126/science.1174156
- Klein-BenDavid, O., Logvinova, A.M., Schrauder, M., Spetius, Z. V, Weiss, Y., Hauri, E.H., Kaminsky, F. V, Sobolev, N. V, Navon, O., 2009. High-Mg carbonatitic

- microinclusions in some Yakutian diamonds—a new type of diamond-forming fluid. *Lithos* 112, Supplement 2, 648–659. doi:10.1016/j.lithos.2009.03.015
- Klein-BenDavid, O., Pettke, T., Kessel, R., 2011. Chromium mobility in hydrous fluids at upper mantle conditions. *Lithos* 125, 122–130. doi:10.1016/j.lithos.2011.02.002
- Mah, A.D., 1954. Heats of Formation of Chromium Oxide and Cadmium Oxide from Combustion Calorimetry. *J. Am. Chem. Soc.* 76, 3363–3365. doi:10.1021/ja01642a002
- Manning, C.E., 2004. The chemistry of subduction-zone fluids. *Earth Planet. Sci. Lett.* 223, 1–16. doi:10.1016/j.epsl.2004.04.030
- Matveev, S., Ballhaus, C., 2002. Role of water in the origin of podiform chromitite deposits. *Earth Planet. Sci. Lett.* 203, 235–243. doi:10.1016/S0012-821X(02)00860-9
- Mikhail, S., Sverjensky, D.A., 2014. Nitrogen speciation in upper mantle fluids and the origin of Earth's nitrogen-rich atmosphere. *Nat. Geosci* 7, 816–819. doi:10.1038/ngeo2271
- Oze, C., Bird, D.K., Fendorf, S., 2007. Genesis of hexavalent chromium from natural sources in soil and groundwater. *Proc Natl Acad Sci U S A* 104, 6544–6549. doi:10.1073/Pnas.0701085104
- Parkinson, I.J., Arculus, R.J., 1999. The redox state of subduction zones: insights from arc-peridotites. *Chem. Geol.* 160, 409–423. doi:10.1016/S0009-2541(99)00110-2
- Rai, D., Moore, D.A., Hess, N.J., Rosso, K.M., Rao, L., Heald, S.M., 2007. Chromium(III) Hydroxide Solubility in the Aqueous K^+ - H^+ - OH^- - CO_2 - HCO_3^- - CO_3^{2-} -

- H₂O System: A Thermodynamic Model. *J. Solution Chem.* 36, 1261–1285.
doi:10.1007/s10953-007-9179-5
- Rekhi, S., Dubrovinsky, L.S., Ahuja, R., Saxena, S.K., Johansson, B., 2000.
Experimental and theoretical investigations on eskolaite (Cr₂O₃) at high pressures. *J. Alloys Compd.* 302, 16–20. doi:10.1016/S0925-8388(00)00613-7
- Sander, S., Koschinsky, A., 2000. Onboard-ship redox speciation of chromium in diffuse hydrothermal fluids from the North Fiji Basin. *Mar. Chem.* 71, 83–102.
doi:10.1016/S0304-4203(00)00042-6
- Schauble, E., Rossman, G.R., Taylor Jr, H.P., 2004. Theoretical estimates of equilibrium chromium-isotope fractionations. *Chem. Geol.* 205, 99–114.
doi:10.1016/j.chemgeo.2003.12.015
- Seewald, J.S., 1996. Mineral Redox Buffers and The Stability of Organic Compounds Under Hydrothermal Conditions. *MRS Proc.* 432. doi:10.1557/PROC-432-317
- Shock, E.L., Koretsky, C.M., 1995. Metal-Organic Complexes in Geochemical Processes - Estimation of Standard Partial Molal Thermodynamic Properties of Aqueous Complexes between Metal-Cations and Monovalent Organic-Acid Ligands at High-Pressures and Temperatures. *Geochim. Cosmochim. Acta* 59, 1497–1532.
doi:10.1016/0016-7037(95)00058-8
- Shock, E.L., Sassani, D.C., Willis, M., Sverjensky, D.A., 1997. Inorganic species in geologic fluids: Correlations among standard molal thermodynamic properties of aqueous ions and hydroxide complexes. *Geochim. Cosmochim. Acta* 61, 907–950.
doi:10.1016/S0016-7037(96)00339-0

- Shock, E.L., 1992. Chemical Environments of Submarine Hydrothermal Systems, in: Holm, N.G. (Ed.), *Marine Hydrothermal Systems and the Origin of Life: Report of SCOR Working Group 91*. Springer Netherlands, Dordrecht, pp. 67–107.
doi:10.1007/978-94-011-2741-7_5
- Sobolev, N. V, Logvinova, A.M., Efimova, E.S., 2009. Syngenetic phlogopite inclusions in kimberlite-hosted diamonds: implications for role of volatiles in diamond formation. *Russ. Geol. Geophys.* 50, 1234–1248. doi:10.1016/j.rgg.2009.11.021
- Spandler, C., Pettke, T., Rubatto, D., 2011. Internal and External Fluid Sources for Eclogite-facies Veins in the Monviso Meta-ophiolite, Western Alps: Implications for Fluid Flow in Subduction Zones. *J. Petrol.* doi:10.1093/petrology/egr025
- Stachel, T., Harris, J.W., 2008. The origin of cratonic diamonds — Constraints from mineral inclusions. *Ore Geol. Rev.* 34, 5–32. doi:10.1016/j.oregeorev.2007.05.002
- Sverjensky, D.A., 1984. Europium Redox Equilibria in Aqueous-Solution. *Earth Planet. Sci. Lett.* 67, 70–78. doi:10.1016/0012-821x(84)90039-6
- Sverjensky, D.A., Shock, E.L., Helgeson, H.C., 1997. Prediction of the thermodynamic properties of aqueous metal complexes to 1000 °C and 5 kb. *Geochim. Cosmochim. Acta* 61, 1359–1412. doi:10.1016/S0016-7037(97)00009-4
- Sverjensky, D.A., Harrison, B., Azzolini, D., 2014. Water in the deep Earth: The dielectric constant and the solubilities of quartz and corundum to 60 kb and 1200 °C. *Geochim. Cosmochim. Acta* 129, 125–145. doi:10.1016/j.gca.2013.12.019
- Sverjensky, D.A., Hemley, J.J., D'Angelo, W.M., 1991. Thermodynamic assessment of hydrothermal alkali feldspar-mica-aluminosilicate equilibria. *Geochim. Cosmochim. Acta* 55, 989–1004. doi:10.1016/0016-7037(91)90157-Z

- Sverjensky, D.A., Stagno, V., Huang, F., 2014. Important role for organic carbon in subduction-zone fluids in the deep carbon cycle. *Nat. Geosci* 7, 909–913.
doi:10.1038/ngeo2291
- Syracuse, E.M., van Keken, P.E., Abers, G.A., 2010. The global range of subduction zone thermal models. *Phys. Earth Planet. Inter.* 183, 73–90.
doi:10.1016/j.pepi.2010.02.004
- van Keken, P.E., Hacker, B.R., Syracuse, E.M., Abers, G.A., 2011. Subduction factory: 4. Depth-dependent flux of H₂O from subducting slabs worldwide. *J. Geophys. Res. Solid Earth* 116, B01401. doi:10.1029/2010JB007922
- Vanko, D.A., 1988. Temperature, pressure, and composition of hydrothermal fluids, with their bearing on the magnitude of tectonic uplift at mid-ocean ridges, inferred from fluid inclusions in oceanic layer 3 rocks. *J. Geophys. Res. Solid Earth* 93, 4595–4611. doi:10.1029/JB093iB05p04595
- Von Damm, K.L., 1990. Seafloor Hydrothermal Activity: Black Smoker Chemistry and Chimneys. *Annu. Rev. Earth Planet. Sci.* 18, 173–204.
doi:10.1146/annurev.ea.18.050190.001133
- Wang, X.L., Planavsky, N.J., Reinhard, C.T., Zou, H.J., Ague, J.J., Wu, Y.B., Gill, B.C., Schwarzenbach, E.M., Peucker-Ehrenbrink, B., 2016. Chromium isotope fractionation during subduction-related metamorphism, black shale weathering, and hydrothermal alteration. *Chem. Geol.* 423, 19–33.
doi:10.1016/j.chemgeo.2016.01.003

- Wang, Z., Bucholz, C., Skinner, B., Shimizu, N., Eiler, J., 2011. Oxygen isotope constraints on the origin of high-Cr garnets from kimberlites. *Earth Planet. Sci. Lett.* 312, 337–347. doi:10.1016/j.epsl.2011.09.061
- Watenphul, A., Schmidt, C., Jahn, S., 2014. Cr(III) solubility in aqueous fluids at high pressures and temperatures. *Geochim. Cosmochim. Acta* 126, 212–227. doi:10.1016/j.gca.2013.10.054
- Ziemniak, S.E., Jones, M.E., Combs, K.E.S., 1998. Solubility and Phase Behavior of Cr(III) Oxides in Alkaline Media at Elevated Temperatures. *J. Solution Chem.* 27, 33–66. doi:10.1023/A:1022688528380

Table 1 Thermodynamic properties of chromium aqueous species and minerals used in this study. All equation of state parameters were computed by the Deep Earth Water (DEW) model using correlations with the partial molal properties (Shock and Helgeson, 1988; Shock et al., 1989; and Sverjensky et al., 2014) unless otherwise noted.

AQUEOUS SPECIES	$\Delta G_f^{0\text{ a}}$	$\Delta H_f^{0\text{ a}}$	$S^{0\text{ b}}$	$C_P^{0\text{ b}}$	$V^{0\text{ c}}$	$a_1 \times 10^{\text{ d}}$	$a_2 \times 10^{-2\text{ a}}$	$a_3^{\text{ e}}$	$a_4 \times 10^{-4\text{ f}}$	$c_1^{\text{ b}}$	$c_2 \times 10^{-4\text{ f}}$	$\omega \times 10^{-5\text{ a}}$	
Cr ²⁺	-36,570 ^g	-34,420 ^g	-19.0 ^g	-4.4 ^h	-17.2 ^h	0.028	-8.50	8.87	-2.43	16.0	-3.93	1.35 ⁱ	
Cr ³⁺	-45,650 ^g	-54,970 ^g	-71.9 ^g	-23.8 ^h	-40.0 ^h	-7.15	-3.31	13.3	-2.64	16.8	-7.88	2.67	
CrCl ²⁺	-76,824 ⁱ	-88,614 ⁱ	-37.97 ^j	-1.2 ^j	-17.8	-1.16	-5.38	9.35	-2.56	20.5	-3.28	1.63	
HCrO ₄ ⁻	-181,980 ^k	-208,650 ^l	45.51 ^l	1.5 ^m	44.9 ^m	10.7	5.90	-0.106	-3.02	15.7	-2.73	-0.940	
CrO ₄ ²⁻	-173,090 ^k	-209,610 ^k	12.45 ^k	-62.6 ⁿ	19.8 ^m	9.24	-4.09	1.99	-2.61	-2.66	-15.8	3.02	
Cr ₂ O ₇ ²⁻	-309,530 ^k	-352,690 ^k	69.26 ^k	-29.1 ^m	72.7 ^m	20.6	1.34	-6.51	-2.83	9.05	-8.96	2.16	
MINERALS	$\Delta G_f^{0\text{ a}}$	$\Delta H_f^{0\text{ a}}$	$S^{0\text{ b}}$	$C_P^{0\text{ b}}$	$V^{0\text{ c}}$	$k_1^{\text{ o}}$	$k_2^{\text{ o}}$	$k_3^{\text{ o}}$	$k_4^{\text{ o}}$	$v_1 \times 10^6\text{ p}$	$v_2 \times 10^{12}\text{ p}$	$v_3 \times 10^6\text{ q}$	$v_4 \times 10^{12}\text{ q}$
Cr ₂ O _{3,cr}	-253,180 ^k	-272,710 ^r	19.40 ^s	28.76 ^s	29.09 ^t	152.9 ^u	-789.5 ^u	-0.002 ^u	1 ^u	-0.413 ^v	0.2569 ^v	38.310 ^w	1.650 ^w

^a cal.mole⁻¹; ^b cal.mole⁻¹.K⁻¹; ^c cm³.mole⁻¹; ^d cal.mole⁻¹.bar⁻¹; ^e cal.K.mole⁻¹.bar⁻¹; ^f cal.K.mole⁻¹; ^g Johnson and Nelson (2012); ^h Calculated from the given values of S (Johnson and Nelson, 2012) with the equations proposed by Shock et al., (1997); ⁱ Calculated from enthalpy of the complexation reaction by Dellien and Hepler (1976); ^j Estimated with equations from Sverjensky et al. (1997); ^k Ball and Nordstrom (1998); ^l Retrieved with experimental data from Palmer et al. (1987); ^m Shock et al. (1997); ⁿ Adjusted value from Shock et al. (1997) with experimental data from Hovey and Helper (1990); ^o J.mole⁻¹.K⁻¹; ^p bar-1; ^q K⁻¹; ^r Mah (1954); ^s Chase et al. (1985); ^t Holland and Powell (2011); ^u Extrapolated with data from Gurevich et al. (2009) and NIST-JANAF data base (1998) with Berman-Brown Cp equation from Berman (1988); ^v Extrapolated with data from Rekhi et al. (2000); ^w Assume same with the parameters of hematite from Berman (1988).

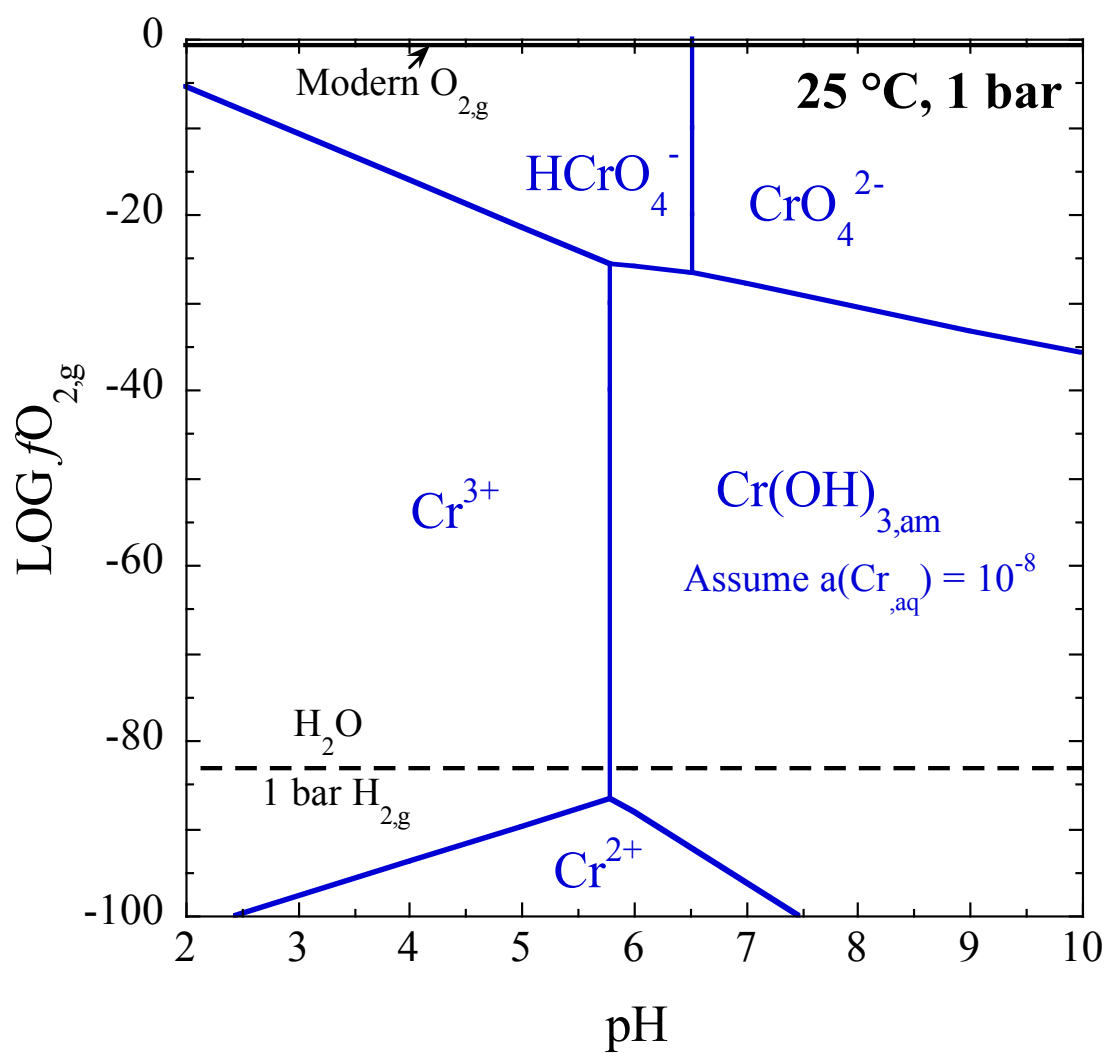


Figure 1. Equilibrium diagram of Cr-O-H system at 25 °C and 1 bar. Equal activities of aqueous species or activities of Cr(aq) equal to 10^{-8} define the stability boundaries.

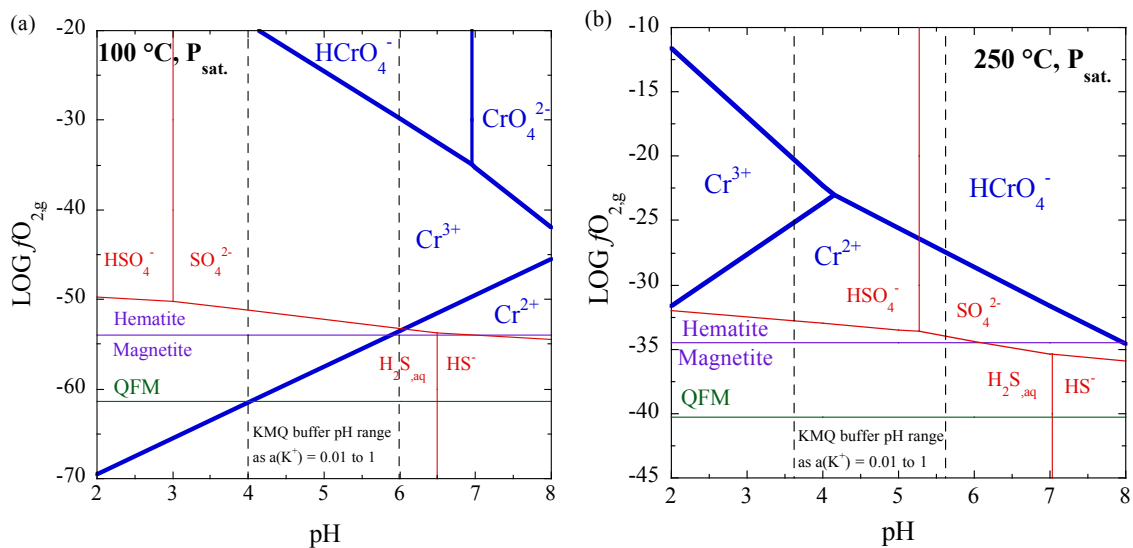


Figure 2. Predicted speciation of aqueous Cr under hydrothermal conditions: (a) 100 °C, $P_{\text{sat.}}$; (b) 250 °C, $P_{\text{sat.}}$. Blue solid lines show the equilibrium boundaries between Cr aqueous species defined by equal activities. The red lines show analogous boundaries for aqueous sulfur species. The purple and green solid lines indicate the equilibrium boundaries for magnetite-hematite, and quartz-fayalite-magnetite respectively. Black dashed lines show the range of pH defined by the assemblage K-feldspar-muscovite-quartz with activities of K^+ ranging from 0.01 to unity.

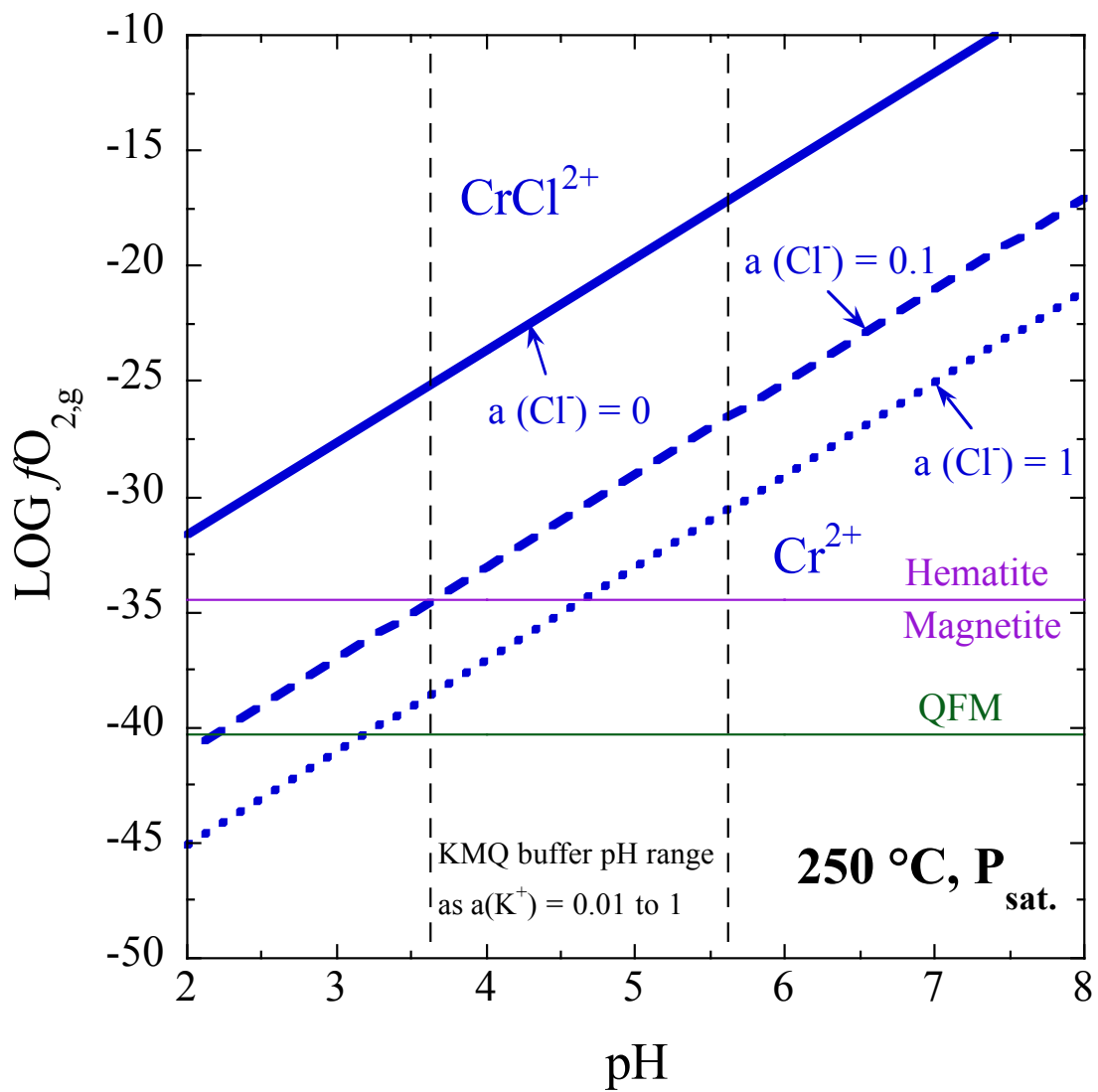


Figure 3. Equilibrium boundaries for equal activities between Cr^{2+} and CrCl^{2+} at $250\text{ }^{\circ}\text{C}$, $P_{\text{sat.}}$. The dashed lines correspond to boundaries of Cr^{2+} and CrCl^{2+} when $a(\text{Cl}^-) = 0.1$ or unity.

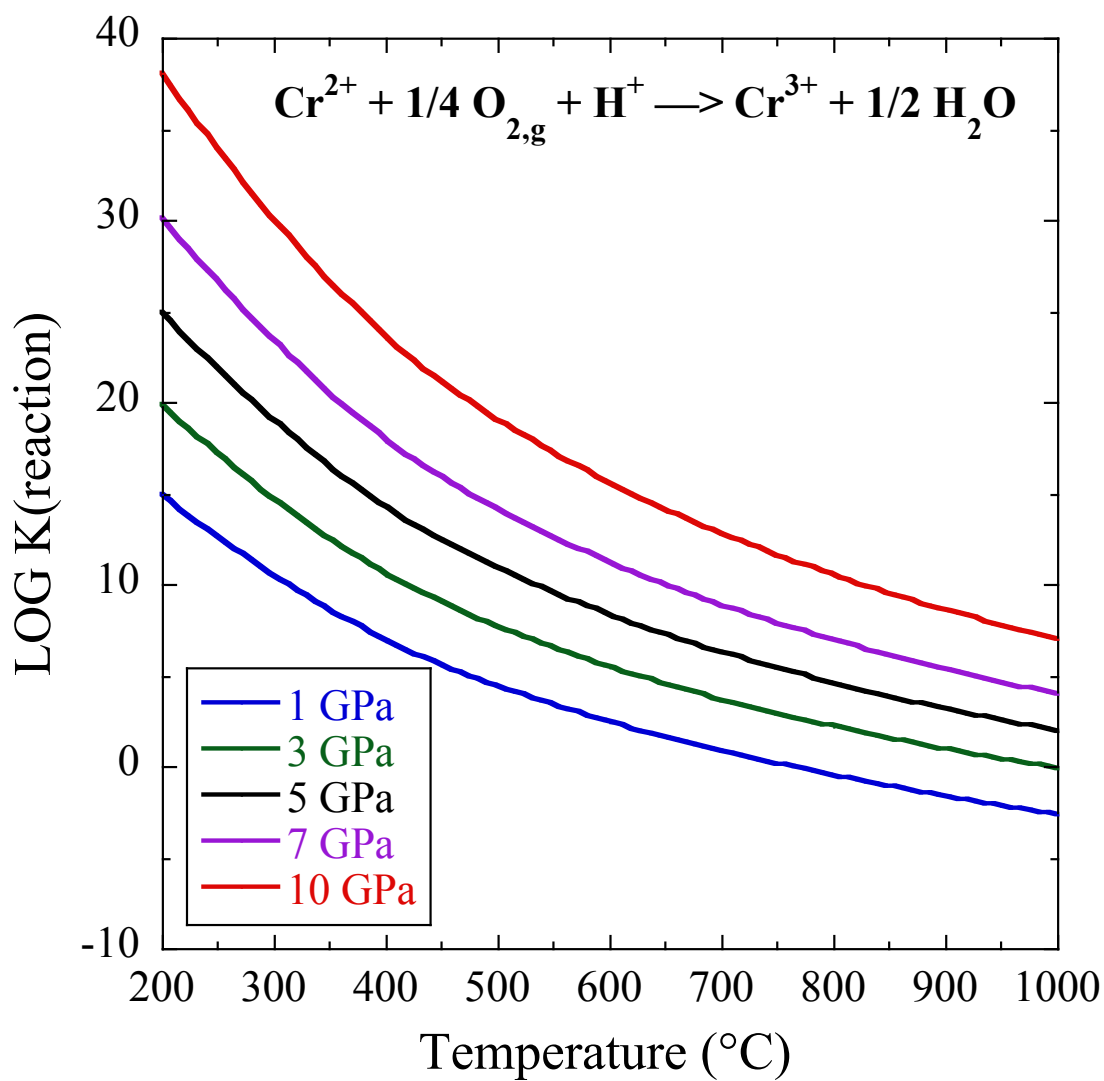


Figure 4. Effects of temperature and pressure on the equilibrium constant relating aqueous Cr^{2+} to Cr^{3+} . These results were calculated with the Deep Earth Water (DEW) model (Sverjensky et al., 2014).

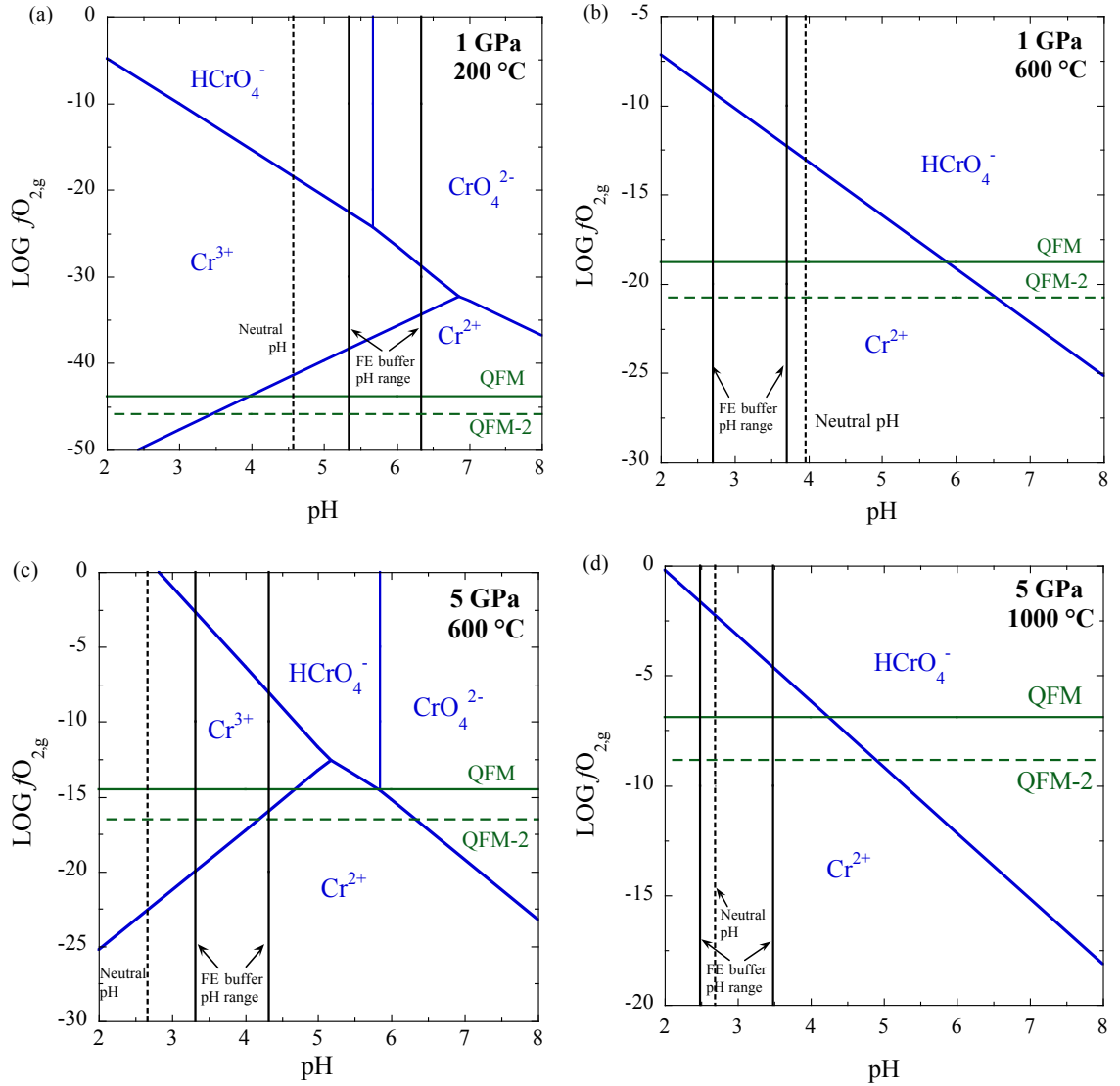


Figure 5. Predicted speciation of aqueous chromium under conditions relevant to subduction-zones: (a) 1 GPa, 200 °C; (b) 1 GPa, 600 °C; (c) 5 GPa, 600 °C; (d) 5 GPa, 1000 °C. The green lines refer to the oxygen fugacity values corresponding to QFM and QFM-2. The black lines refer to the neutral pH and pH range of the forsterite-enstatite buffer at the given temperature and pressure.

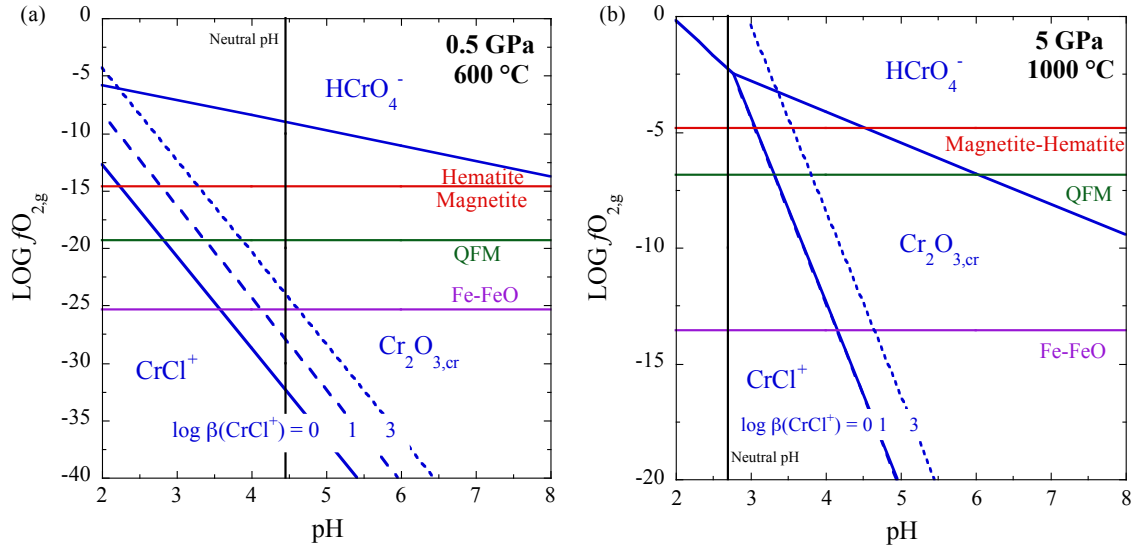


Figure 6. Effect of Cr-Cl complexation on the solubility of $\text{Cr}_2\text{O}_{3,\text{cr}}$ at conditions relevant to subduction-zone environments: (a) 600 °C, 0.5 GPa; (b) 1000 °C, 5 GPa. Activities of aqueous chromium species are assumed to be equal to 10^{-8} . The $a(\text{Cl}^-) = 4$ is the same as the value used in [Watenphul et al. \(2014\)](#) at 0.5 GPa and 600 °C and $a(\text{Cl}^-) = 0.304$ is same as the value used in [Klein-BenDavid et al. \(2011\)](#) at 5 GPa and 1000 °C. The dashed blue lines refer to the boundary of CrCl^+ and $\text{Cr}_2\text{O}_{3,\text{cr}}$ when the dissociation constant of CrCl^+ is equal to -1 or -3. The red solid line refers to the oxygen fugacity of the Fe-FeO mineral redox buffer.

Chapter 7

Conclusions

In this study, I have examined the quantification of $O_{2,g}$ and $H_{2,g}$ as redox indicators of Archean surficial environments based on evidence from atmospheric models, detrital mineral records, isotopic signals, and abnormal enrichment of trace metals in sediments. I carried out aqueous speciation and mineral solubility calculations to provide insights into the preservation of detrital minerals, the mobility of trace elements, and the metastable presence of simple organic compounds in surface waters during the Archean. I found that using $pH_{2,g}$ as the redox indicator can provide consistent results with detrital minerals and therefore is a more sensible and practical redox indicator of Archean surface environments compared with $pO_{2,g}$. Volcanic outgassing of $H_{2,g}$ is significantly affected by the tectonic settings and temperatures of the volcanoes. Before subduction began, $pH_{2,g}$ might be much higher than previous estimates, which is very favorable for the origin of life. After life appeared and prospered on the Earth, early metabolisms would use $H_{2,g}$ as an important electron donor and therefore draw down $pH_{2,g}$ probably to $< 10^{-5}$ bar in the atmosphere. Fluctuations of $pH_{2,g}$ and/or pH in the Archean surface environments might be the major reasons for the abnormal enrichment of trace elements and their isotopic fractionations recorded in the sediments before the GOE. This study

also found that simple organic compounds such as acetate and formate could be metastable in the Archean rainwater and river water at high $p\text{H}_{2,\text{g}}$ ($10^{-3.5}$ bar or higher). Increasing $p\text{H}_{2,\text{g}}$ during intense pulses of volcanic activity might form riverine transport of organic acids and provide food for early methanogens to form hazy atmospheres. Under the Archean $p\text{H}_{2,\text{g}}$ conditions, it is predicted that magnetite does not have a stability field in high-silica seawater; instead, either greenalite or siderite should form, depending on the $p\text{CO}_{2,\text{g}}$. Overall, this effort represents a first step towards a more fundamental understanding of the redox history of Archean surface environments.

For the purpose of geochemically simulating water-rock interactions, this study proposed an extended linear free energy relationship for predicting ΔG_f° of crystalline solids with the same crystal structure. Specifically, it is now possible to estimate the parameters necessary to estimate the ΔG_f° values of all the divalent cation end-members of a given crystal structure, based on knowing only the ΔG_f° value of the Mg end-member solid. Key parameters characteristic of each structure ([Sverjensky and Molling, 1992](#)) were shown to be predictable from correlations with the stoichiometry and cation coordination properties of each silicate mineral family.

Using the LFER approach, the thermodynamic properties of the end-member solids for eighteen different divalent cations were predicted for crystal structures corresponding to those of common silicates, including orthopyroxene, olivine, garnet, biotite, serpentine, chlorite, talc, saponite and beidellite. These predicted standard Gibbs free energies of formation can be used to predict trace element distribution between silicates and aqueous solutions at 25 °C and 1 bar. Together with predicted values of the entropies, volumes, and heat capacities, the results of the present study could also be

applied to predict trace element distribution at elevated temperatures and pressures. The results of our study should have considerable practical application to modeling the behavior of trace during water-rock interactions in geological processes.

By focusing on the previously proposed Archean atmospheric boundary conditions to model the chemistry of weathering processes on the continents in the late Archean, this study has carried out theoretical, reaction-path calculations to provide a predictive model of the chemistry of present-day weathering processes and present-day world-average river water as well as late Archean world-average river water. The predicted thermodynamic properties of possible ferrous-clay minerals, i.e. saponite and beidellite, were also included in the models. This effort represents a preliminary step towards building an internally consistent, quantitative picture of the evolution of the near surface environment of early Earth.

Under the present-day atmospheric conditions ($p\text{CO}_{2,g} = 10^{-3.5}$ bars, $p\text{O}_{2,g} = 10^{-0.68}$ bars), the simulation showed that weathering of basalt + calcite and granite + calcite produced hematite, kaolinite, smectite, and chalcedony. Destruction of 10^{-4} moles of reactant minerals kg^{-1} H_2O resulted in Mg/Na, Ca/Na, and HCO_3^-/Na ratios, and pH values of 8.0 - 8.1 consistent with present-day world-average river water (WARW).

Under the late Archean atmospheric conditions ($p\text{CO}_{2,g} = 10^{-1.5}$ bars, $p\text{H}_{2,g} = 10^{-5.0}$ bars), weathering of olivine basalt + calcite and TTG + calcite produced kaolinite, Fe(II)-smectite, and chalcedony and waters with much higher concentrations of HCO_3^- and Fe(II) + Mg and a much lower pH of 6.3. The late Archean WARW is predicted to have a lower Ca/Na ratio and much higher Mg/Na and HCO_3^-/Na ratios than present-day WARW. Aqueous Fe(II) can reach concentrations of 0.2 mM during weathering, but can

also be stored in clay minerals at advanced stages of weathering, consistent with the apparent mobility of Fe(II) in paleosols.

The late Archean weathering solutions can easily become supersaturated with respect to pyrite so that there will be no thermodynamic driving force for dissolution of pyrite in the late Archean, which is consistent with the detrital mineral record. Similar considerations apply to uraninite. Fe(II)-carbonate solid solutions (20 to 100% siderite component) only precipitate at fairly advanced stages of weathering. Under these conditions, siderite-rich carbonate might form during weathering or be stable during weathering and riverine transport, consistent with the detrital mineral record from this period. Overall, the occurrence of siderite in the geologic record might reflect $p\text{CO}_{2,g}$ values but also the extent of weathering.

After building the chemical framework for late Archean weathering, this study has applied it to predict the behaviors of phosphorus, manganese, chromium, and copper during weathering of olivine basalt plus trace element-bearing accessory minerals under a set of standard Archean atmospheric boundary conditions. Moreover, whiffs of oxidants, such as $\text{O}_{2,g}$ and HNO_3 , were included as reactants to explore their influences on the mobility and speciation of Mn and Cu during the weathering.

The set of standard late Archean atmospheric conditions we adopted, i.e. $p\text{H}_{2,g} = 10^{-5}$ bar and $p\text{CO}_{2,g} = 10^{-1.5}$ bar, resulted in late Archean WARW with a pH of 6.4. Excursions of $p\text{CO}_{2,g}$ away from the standard conditions may have resulted in pH values of Archean surface waters ranging from 3.5 to 7.2 depending also on the extent of weathering. The metastability of organic acids deposited from organic hazes, or the

oxidation of sulfides caused by fluctuations of the near-surface redox state, could also have influenced the pH of late Archean surface waters.

When $p\text{CO}_2$ was $10^{-1.5}$ bars, accessory apatite was totally dissolved during weathering and the development of late Archean WARW (pH = 6.4) resulted in riverine phosphate of at least 1.7 μmolar , much higher than at the present-day. This result is consistent with the high levels of phosphate in late Archean seawater inferred from the P/Fe ratios of banded iron formations (Planavsky et al., 2010). At the end of the early Proterozoic snowball Earth event when $p\text{CO}_2$ was at least 0.12 bars, the pH of WARW may have been as low as about 5.7, which would have corresponded to a solubility of 70 μmolar phosphate. The amount transported by WARW would have depended on the availability of apatite. In this way, the model proposed here provides a specific mechanism for the previously suggested high levels of phosphate in the marine environment that may have influenced O_2 levels in the atmosphere by stimulating high levels of oxygenic photosynthesis (Papineau et al., 2013).

Crustal levels of Mn housed in Mn-olivine were predicted to dissolve completely without producing any secondary minerals except Mn-bearing carbonate at large extents of weathering. The corresponding Mn content of WARW reached about 1.2 μmolar , higher than in the modern WARW. Whiffs of 10^{-5} mole $\text{O}_{2,\text{g}}$ or $\text{HNO}_3 \text{ kg}^{-1} \text{H}_2\text{O}$ in the weathering model resulted in the formation of $\text{MnO}_{2,\text{cr}}$ together with about 100 times more hematite. The concentrations of Mn(II) in the WARW would have decreased dramatically during the precipitation of $\text{MnO}_{2,\text{cr}}$.

Chromite was too insoluble to dissolve during the late Archean weathering of olivine basalt, resulting in negligible dissolved Cr in the WARW. However, $\text{Cr}(\text{OH})_{3,\text{am}}$,

representing easily weatherable Cr-bearing minerals dissolved totally during the weathering, resulting in concentrations of Cr(III) in the late Archean river water of up to 0.14 μ molar, higher than at the present-day.

Late Archean weathering of accessory chalcopyrite in olivine basalt under our standard conditions produced chalcocite and bornite, along with other secondary minerals. The predicted concentrations of Cu in the resultant river water would have been extremely low (about 5.9×10^{-11} nmolar) because of the low solubilities of the copper sulfides. However, during a pulse of either 10^{-6} mole $O_{2,g}$ kg^{-1} H_2O or 10^{-6} mole HNO_3 kg^{-1} H_2O , weathering of chalcopyrite produced two generations of native copper, chalcocite and bornite, together with about 100 times more hematite. The resultant WARW contained comparable level of dissolved Cu as the modern river water.

The copper mineralogy recorded in weathering profiles might be useful as a signature of the surface redox environment. The thermodynamically interpretable signals may provide a new correlation with evidence from studies of copper mineral evolution. Preliminary results suggest that native copper occurrences in the late Archean might indicate fluctuations in the oxidation state of the weathering zone.

In addition to redox variations, fluctuations in pH and the availability of easily weatherable accessory minerals could also affect the mobility and speciation of trace elements in the late Archean. These results suggest that the abnormal enrichment of trace elements and their isotopic fractionations do not necessarily suggest the appearance of oxygenic photosynthesis and accumulation of free $O_{2,g}$ in the early atmosphere. Besides traditional sedimentary records, secondary mineral assemblages of trace elements can be

potentially useful to understand the evolution of the surface environment, especially before the GOE.

To assess the effects of diagenesis and metamorphism on the behavior of chromium in the sedimentary archives, this study has predicted the speciation of chromium in aqueous fluids as functions of $\log fO_{2,g}$ and pH at elevated temperatures and pressures using the recently developed Deep Earth Water (DEW) model. It has also investigated the effects of complexation between Cr(II)/Cr(III) and Cl^- on the relative stability of aqueous species and the solubility of $Cr_2O_{3,cr}$.

Under hydrothermal conditions, at 100 °C and $P_{sat.}$, Cr^{2+} and Cr^{3+} are the dominant aqueous Cr species given the ranges of pH and $\log fO_{2,g}$ constrained by mineral buffers. Low pH and high $\log fO_{2,g}$ favors the stability of Cr^{3+} and high pH and low $\log fO_{2,g}$ favors the stability of Cr^{2+} . Cr(VI) species are not thermodynamically stable unless at much higher $\log fO_{2,g}$ than QFM and very high pH. At 250 °C and $P_{sat.}$, Cr^{2+} becomes the only dominant aqueous Cr species whereas Cr^{3+} is not stable within ranges of pH and $\log fO_{2,g}$ constrained by mineral buffers. $HCrO_4^-$ becomes more stable compared with the case at 100 °C and $P_{sat.}$, but is still unlikely to form under normal hydrothermal conditions. Complexation between Cr(III) and Cl^- could promote the stability of Cr^{3+} relative to Cr^{2+} at 250 °C and $P_{sat.}$. However, Cr(II) might have similar complexation behavior to Cr(III) and that would tend to cancel out the stabilization of Cr(III).

Under subduction-zone conditions, at 1 GPa and 200 °C, Cr^{2+} is the only dominant aqueous Cr species within ranges of pH and $\log fO_{2,g}$ constrained by mineral buffers. At $\log fO_{2,g}$ values close to QFM, Cr^{3+} could be stable at low pH. Again, the stability of Cr(VI) species requires high $fO_{2,g}$ and pH conditions. At 1 GPa and 600 °C,

Cr^{2+} is still the only dominant aqueous Cr species within ranges of pH and $\log f\text{O}_{2,\text{g}}$ constrained by mineral buffers. Cr^{3+} is not thermodynamically stable over a wide range of pH and $\log f\text{O}_{2,\text{g}}$. Instead, HCrO_4^- could be stable at $\log f\text{O}_{2,\text{g}}$ close to QFM and high pH. At 5 GPa and 600 °C, Cr^{3+} is the only dominant aqueous Cr species within ranges of pH and $\log f\text{O}_{2,\text{g}}$ constrained by mineral buffers. At $\log f\text{O}_{2,\text{g}}$ values close to QFM, Cr^{2+} could be stable at moderately high pH and CrO_4^{2-} could form at higher pH. At 5 GPa and 1000 °C, the speciation is similar to the case at 1 GPa and 600 °C, i.e. Cr^{2+} as the dominant aqueous Cr species and the stability of HCrO_4^- at high pH.

Cr^{2+} and its complexes are dominant aqueous species during dissolution of $\text{Cr}_2\text{O}_{3,\text{cr}}$ at 0.5 GPa, 600 °C or 6 GPa, 1000 °C. The solubility of $\text{Cr}_2\text{O}_{3,\text{cr}}$ could be promoted by complexation with Cl^- . HCrO_4^- could be stable at high pH and its relative abundance could also increase the solubility of $\text{Cr}_2\text{O}_{3,\text{cr}}$ at high temperatures and pressures. My results indicate that advanced diagenesis or low-grade metamorphism involving aqueous fluids could modify the original sedimentary signatures of chromium by solubilizing chromium as Cr(II) or Cr(VI). Fluid-rock interactions under even mild diagenetic temperatures and pressures could cause isotopic fractionation of Cr under some circumstances, potentially confusing the interpretation of chemical profiles of Cr isotopes. Moreover, fluids carrying high concentrations of Cr(II) at elevated temperature and pressure might play an important role in the formation of the hydrothermal mineral crocoite, the formation of chromite ore deposits, and the formation of Cr-rich garnets associated with diamond formation. As all of the minerals involved contain Cr(III), redox reactions from aqueous Cr(II) to Cr(III) in the minerals would be necessary.

References:

- Papineau, D., Purohit, R., Fogel, M.L., Shields-Zhou, G.A., 2013. High phosphate availability as a possible cause for massive cyanobacterial production of oxygen in the Paleoproterozoic atmosphere. *Earth Planet. Sci. Lett.* 362, 225–236. doi:10.1016/j.epsl.2012.11.050
- Planavsky, N.J., Rouxel, O.J., Bekker, A., Lalonde, S. V, Konhauser, K.O., Reinhard, C.T., Lyons, T.W., 2010. The evolution of the marine phosphate reservoir. *Nature* 467, 1088–1090. doi:10.1038-nature09485
- Sverjensky, D.A., Molling, P.A., 1992. A Linear Free-Energy Relationship for Crystalline Solids and Aqueous Ions. *Nature* 356, 231–234. doi:10.1038/356231a0

Curriculum Vitae

DOB: 1991/07/07 at Liaocheng
Dept. of Earth & Planetary Sciences,
Johns Hopkins University
3400 N Charles St., Baltimore, MD-21218, USA
Mobile: +1(443) 240-3582
E-mail: jhao3@jhu.edu
Homepage: <http://haojihua.org/>

Education

- **Ph.D.** candidate in Geochemistry, Johns Hopkins University, Baltimore, Maryland, USA, August, 2012 – December, 2016 (Expected completion)
- **M.A.** in Geochemistry, Johns Hopkins University, Baltimore, Maryland, USA, August 2012 - March, 2014
- **B.Eng.** in Environmental Science, University of Science & Technology (USTC), Hefei, Anhui, China, August, 2008 - July, 2012

Research Interests

- Evolution of Early Earth Atmosphere
- Archean Weathering and Riverine Transport
- Mineral Evolution & Ecology
- Coevolution of the Biosphere and Geosphere
- Formation and Diagenesis of Banded Iron Formations
- Interfacial Geochemistry between Water and Minerals
- Stability of Biomolecules in Hydrothermal Systems
- High Temperature and Pressure Aqueous Geochemistry

Research Experience

- Research Assistant, Dept. of Earth & Planetary Sciences, Johns Hopkins University, 2013, summer - Present. Advisor: Prof. Dimitri A. Sverjensky
- Pre-doctoral Associate, Geophysical Lab, Carnegie Institution of Washington, DC, USA, 2013, summer - Present. Mentor: Dr. Robert M. Hazen.
- Undergraduate Graduation Thesis, “*Holocene Climate and extreme environment events deciphered from the sedimentary records of Southern Yellow Sea, China*”, 2012. Advisor: Prof. Liguang Sun, USTC
- Undergraduate Research Project, “*The Historical Record of Pb in the Mud Sediments of Southern Yellow Sea and its Paleoenvironmental Meaning*”, 2011. Advisor: Prof. Liguang Sun, USTC
- Research Assistant, “*Deposition History of Black Carbon in Past 400 Years in*

Xisha Islands of South China Sea”, 2009. Supervisor: Prof. Xiaodong Liu, USTC

Presentations

- Poster (Co-author), ***“THE CO-EVOLUTION OF THE GEO- AND BIOSPHERES: AN INTEGRATED PROGRAM FOR DATA-DRIVEN, ABDUCTIVE DISCOVERY IN THE EARTH SCIENCES”***, GSA Annual Meeting in Denver, Colorado, USA, 2016.
- Poster, ***“Importance of Atmospheric H₂ in Surficial Environments of the Archean”***, Second DCO Yellowstone Summer School, USA, 2016.
- Oral, ***“Weathering and late Archean riverine transport”***, Australasian Astrobiology Meeting in Perth, Australia, 2016
- Poster (Co-author), ***“Lithium adsorption on kaolinite, gibbsite, goethite, and hematite”***, Goldschmidt Conference in Yokohama, Japan, 2016.
- Oral, ***“Weathering and Late Archean World Average River Water”***, Goldschmidt Conference in Yokohama, Japan, 2016
- Oral, ***“Chromium Redox Equilibria in Fluids and Minerals under Hydrothermal and Subduction-zone Conditions”***, AGU Fall Conference, San Francisco, USA, 2015.
- Oral, ***“Protection of Amino Acids by Magnetite in Hydrothermal Systems”***, Dept. of Earth & Planetary Sciences, Johns Hopkins University, Baltimore, USA, 2015.
- Oral (INVITED), ***“Earth Prebiotic Environment & the Origin of Life”***, Dept. of Earth & Space Sciences, USTC, Hefei, China, 2015.
- Poster, ***“Equilibrium Chromium Isotopic Fractionation as Functions of Redox and pH on the Early Earth”***, Goldschmidt Conference in Prague, Czech Republic, 2015
- Poster (Co-author), ***“Aspartate Transformation Under Hydrothermal Conditions with Brucite [Mg(OH)₂]”***, Goldschmidt Conference, Prague, Czech Republic, 2015.
- Poster, ***“Limits on the Partial Pressure of H₂ in the Archean Atmosphere during Weathering of Basaltic Minerals”***, Goldschmidt Conference, Sacramento, California, USA, 2014
- Oral, ***“Basaltic and Granitic Weathering During the Archean: including thermodynamic properties of ferrous-clay minerals”***, Geophysical Laboratory, Carnegie Institution of Washington, USA, 2014
- Oral, ***“Constraints on the Archean atmospheric composition and the weathering of basaltic minerals”***, Dept. of Earth & Planetary Sciences, Johns Hopkins University, USA, 2014
- Poster, ***“Sedimentary Record of Pb in the Mud Region of Southern Yellow Sea and its Paleoenvironmental Meaning”***, 1st SUCOS Academic Forum Meeting in Qingdao, China, 2012

Manuscripts

- **Hao, J.**, Sverjensky, D.A. and Hazen, R.M., 2017. A Model for Late Archean Chemical Weathering and World Average River Water. *Earth and Planetary Science Letters* 457, 191-203. doi: 10.1016/j.epsl.2016.10.021
- **Hao, J.**, Sverjensky, D.A., and Hazen, R.M. Importance of Atmospheric H₂ in Surficial Environments of the Archean. *Geobiology* (**submitted**)
- Estrada, C.F., Mamajov, I., **Hao, J.**, Sverjensky, D.A., Cody, G.D., Hazen, R.M. Aspartate transformation at 200 °C with brucite [Mg(OH)₂], NH₃, and H₂: Implications for prebiotic molecules in hydrothermal vents. *Chemical Geology* (**submitted**).
- **Hao, J.**, Sverjensky, D.A., and Hazen, R.M. Mobility of nutrients and trace elements during weathering on the Archean (**in preparation**)
- **Hao, J.**, Sverjensky, D.A., and Hazen, R.M. Chromium Redox Equilibria in Fluids and under Hydrothermal and Subduction-zone Conditions (**in preparation**)

Honors and Awards

- Predoctoral Fellowship, Geophysical Laboratory, Carnegie Institution of Washington, USA, 2013, summer-Present.
- Ph.D. Fellowship, Johns Hopkins University, USA, 2012
- Zhao JIUTZHANG Scholarship, Chinese Academy of Sciences, China, 2011
- National Scholarship, Ministry of Education, China, 2010

Field Experience

- The most convincing evidence of the oldest life on Earth in the Pilbara Craton, astrobiology field trip led by Prof. Martin Van Kranendonk and Ms Tara Djokic (UNSW). July 13 - 17 2016.
- Geology and geochemistry of Yellowstone hydrothermal vents, Second DCO Yellowstone Summer School fieldtrip led by Prof. Lisa Morgan, Prof. Pat Shanks, and Prof. Anna-Louise Reysenbach. July 23 - 30, 2016.
- East Shore Field Trip to Assateague National Park, Department field study of JHU, led by Prof. Kevin Lewis, April 15-17, 2016.

Short-courses or Workshops

- EPS Software Carpentry Coding Workshop by D. Wheeler and M. Sadjadi about Unix shell, Python, Git, Aug 22 -23, 2016, Johns Hopkins University, USA.
- “Keck-RPI Science Day” by Prof. P. Fox and others, about visualizing big data, June 8 - 10, 2016, Rensselaer Polytechnic Institute, USA.
- “Keck-Rutgers Protein Boot Camp” by Prof. P. Falkowski and others, about protein structure and data resources, Jan 28 2016, Rutgers University, USA.
- “Hydrothermal experimental techniques” short-course by Dr. D. Foustoukos, Oct 28 - 30 2015, Geophysical Laboratory, USA.

Teaching Activities

- AS.271.107.01.SP15 Introduction to Sustainability, Johns Hopkins University, 2015 Spring. Teaching assistant, with Prof. Cindy Parker.
- AS.270.114.01.SP14 Guided Tour: The Planets, Johns Hopkins University, 2014 Spring. Teaching assistant, with Prof. Bruce Marsh and Prof. Darrell Strobel.
- AS.270.102.01/02.FA13 Conversations with the Earth, Johns Hopkins University, 2013 Fall. Teaching assistant, with Prof. Bruce Marsh and Prof. Darrell Strobel.

Employment

- Research Assistant, Dept. of Earth & Planetary Sciences, Johns Hopkins University, June, 2014 - Now
- Teaching Assistant, Dept. of Earth & Planetary Sciences, Johns Hopkins University, 2013 - 2014
- Research Assistant, Prof. Liguang Sun, USTC, 2010 - 2012
- Research Assistant, Prof. Xiaodong Liu, USTC, 2009 summer

Languages

- Mandarin Chinese (native); English (highly proficient); French (beginner).

Computer Skills

- C, Python, JMP11, KaleidaGraph, DeltaGraph, Matlab, SPSS, ChemBioDraw, CrystalMaker, Inkscape, Endnote
- **Aqueous speciation & water-rock interaction modeling:** SUPCRT92b, EQ3/6 codes, EQPT, Deep Earth Water Calculator
- **Surface chemistry:** Geosurf.

Laboratory Skills

- **Batch adsorption experiment:** X-ray Diffraction (XRD), Scanning Electron Microscope (SEM), Transmission Electron Microscope (TEM), Ion Chromatography with Dionex ICS-5000 DP dual pump system.
- **Hydrothermal experiments:** PUK 3S Plus Professional Precision Welder, gold tubes/gold bag hydrothermal techniques, Teflon autoclave reactors, Gas Chromatography-Mass Spectrometry (GCMS), High-Performance Liquid Chromatography (HPLC), Metrohm 850 Ion Chromatography System.

Related Experience

- Participant in the Keck project “The Co-Evolution of the Geo- and Biospheres: An Integrated Program for Data-Driven, Abductive Discovery in the Earth Sciences”, 2015-Present
- Supervisor in charge of living affairs of the School of Earth & Space Sciences, USTC, 2008-2012
- Volunteer for the Summer Practice of USTC in undeveloped areas of Anhui Province, 2009

- Volunteer for the Sci-Tech Week of USTC, 2009 & 2012
- Volleyball team leader, School of Earth & Space Sciences, USTC, 2009-2010.